

***Production of pharmaceutical and
nutraceutical formulations for
bioavailability improvement using
Supercritical Assisted Atomization***

Alessia Di Capua

UNIVERSITY OF SALERNO



DEPARTMENT OF INDUSTRIAL ENGINEERING

*Ph.D. Course in Industrial Engineering
Curriculum in Chemical Engineering - XXXI Cycle*

PRODUCTION OF PHARMACEUTICAL AND NUTRACEUTICAL FORMULATIONS FOR BIOAVAILABILITY IMPROVEMENT USING SUPERCRITICAL ASSISTED ATOMIZATION

Supervisor

Prof. Ernesto Reverchon

Ph.D. student

Alessia Di Capua

Scientific Referees

Ing. Renata Adami

Dr. Fausto Vellani

Ph.D. Course Coordinator

Prof. Ernesto Reverchon

*I dedicate this thesis to the most
important persons in my life.
I love you!*

to my irreplaceable sister
for her pure and limitless love,
her patience and total support.
Thank you for being my sister, my lead!

to mum & dad
for their unconditional love,
and confidence in me.
Thank you for everything!

to my dear Agostino
for his encouragement,
dedication, and love.
Thank you for being by my side!

List of Publications

International Journal Papers

- 1) R. Adami, **A. Di Capua**, E. Reverchon, Supercritical Assisted Atomization for the production of curcumin-biopolymer microspheres, *Powder Technology*, 305 (2017), 455-461.
(<https://doi.org/10.1016/j.powtec.2016.10.020>)
- 2) **A. Di Capua**, R. Adami, E. Reverchon, Production of Luteolin-biopolymer microspheres by Supercritical Assisted Atomization, *Industrial & Engineering Chemistry Research*, 56 (2017), 4334-4340.
(<https://doi.org/10.1021/acs.iecr.7b00211>)
- 3) **A. Di Capua**, R. Adami, L. Izzo, E. Reverchon, Luteolin/dextran-FITC fluorescent microspheres produced by supercritical assisted atomization, *The Journal of Supercritical Fluids*, 130 (2017), 97-104.
(<https://doi.org/10.1016/j.supflu.2017.07.034>)
- 4) M.C. Barrella, **A. Di Capua**, R. Adami, E. Reverchon, M. Mella, L. Izzo, Impact of intermolecular drug-copolymer interactions on size and drug release kinetics from pH-responsive polymersomes, *Supramolecular Chemistry*, 29 (2017), 796-807.
(<http://www.tandfonline.com/doi/abs/10.1080/10610278.2017.1377836>)
- 5) **A. Di Capua**, A. Bejarano, R. Adami, E. Reverchon, Preparation and characterization of Chilean propolis coprecipitates using Supercritical Assisted Atomization, *Chemical Engineering Research and Design*, 136 (2018), 776-785.
(<https://doi.org/10.1016/j.cherd.2018.06.037>)
- 6) R. Adami, S. Liparoti, **A. Di Capua**, M. Scognamiglio, E. Reverchon, Production of PEA nanostructured coprecipitates using Supercritical Assisted Atomization, *The Journal of Supercritical Fluids*, 143 (2019), 82-89.
(<https://doi.org/10.1016/j.supflu.2018.07.020>)
- 7) **A. Di Capua**, R. Adami, E. Cosenza, V. Jalaber, C. Crampon, E. Badens, E. Reverchon, β -carotene/PVP microspheres produced by Supercritical Assisted Atomization, *Powder Technology*, 346 (2019), 228-236.
(<https://doi.org/10.1016/j.powtec.2019.01.069>)

International Conference Proceedings

- 1) R. Adami, **A. Di Capua**, L. Sesti Osséo, E. Reverchon, Supercritical Assisted Atomization process for the production of antitumoral active principle- biopolymer nanostructured microspheres, *11th International Symposium on Supercritical Fluids*, October 11-14 2015, Seoul, Republic of Korea.
- 2) **A. Di Capua**, R. Adami, E. Reverchon, Supercritical Assisted Atomization for the production of curcumin-biopolymer microspheres, *CONVEGNO GRICU*, September 12-14 2016, Anacapri (Na), Italy.
- 3) **A. Di Capua**, R. Adami, E. Reverchon, Supercritical Assisted Atomization for the stabilization of active compounds, *12th International Symposium on Supercritical Fluids*, April 22-25 2018, Antibes-Juan-Les-Pins, France.
- 4) **A. Di Capua**, R. Adami, E. Cosenza, V. Jalaber, C. Crampon, E. Badens, E. Reverchon, Production of β -carotene/PVP coprecipitates using Supercritical Assisted Atomization, *12th International Symposium on Supercritical Fluids*, April 22-25 2018, Antibes-Juan-Les-Pins, France.

Presentations

- 1) **A. Di Capua**, R. Adami, E. Reverchon, Production of pharmaceutical and nutraceutical formulations for bioavailability improvement using Supercritical Assisted Atomization, *GRICU 2017*, September 24-29 2017, Palermo, Italy.
- 2) **A. Di Capua**, R. Adami, E. Reverchon, Production of nutraceutical and pharmaceutical formulations using Supercritical Assisted Atomization, *GRICU 2018*, May 16-19 2018, Pisa, Italy. (*Best Poster Award*)

Contents

Contents	I
Figure Index.....	V
Table Index	XI
Abstract.....	XIII
Introduction	XVII
<i>Bioavailability of pharmaceuticals</i>	<i>XVII</i>
<i>Bioavailability of nutraceuticals</i>	<i>XXI</i>
<i>Aim of the thesis</i>	<i>XXIII</i>
<i>Outline of the thesis</i>	<i>XXIV</i>
Chapter I Micronization and coprecipitation processes.....	1
I.1 Introduction	1
<i>I.1.1 Conventional techniques</i>	<i>2</i>
<i>I.1.2 Supercritical techniques</i>	<i>4</i>
I.2 Supercritical Assisted Atomization	7
<i>I.2.1 Apparatus</i>	<i>7</i>
<i>I.2.2 Process parameters</i>	<i>8</i>
<i>I.2.3 State of the Art of SAA process</i>	<i>10</i>
Chapter II Analytical methods.....	17
II.1 Analyses on morphology	17
<i>II.1.1 Field Emission Scanning Electron Microscope</i>	<i>17</i>
<i>II.1.2 Fluorescent microscope</i>	<i>17</i>
II.2 Particle size distribution (PSD)	17
II.3 Analyses on solid state	18
<i>II.3.1 Differential Scanning Calorimetry</i>	<i>18</i>
<i>II.3.2 X-Ray Diffraction</i>	<i>18</i>
<i>II.3.3 Fourier Transform Infrared (FTIR)</i>	<i>18</i>
II.4 Loading efficiency and dissolution tests	18
<i>II.4.1 Spectrophotometer UV-vis</i>	<i>18</i>

II.4.2	<i>High Performance Liquid Chromatography</i>	19
II.5	Antioxidant activity	19
II.5.1	<i>DPPH method</i>	19
II.5.2	<i>Total polyphenol content</i>	20
II.6	Synthesis of FITC-labeled dextran	20
Chapter III Pharmaceutical formulations for Cerbios Pharma		21
III.1	Agreement with Cerbios Pharma	21
III.2	Compound #1: BRI	22
III.2.1	<i>Experimental results on BRI</i>	22
III.2.2	<i>Characterization of BRI particles</i>	25
III.3	Compound #2: FUL	26
III.3.1	<i>Experimental results on FUL</i>	27
III.3.2	<i>Dissolution tests</i>	30
III.4	Compound #3: DAS	31
III.4.1	<i>Experimental results on DAS</i>	31
III.4.2	<i>Characterization of DAS-PVP particles</i>	35
III.5	Compound #4: NAP	36
III.5.1	<i>Experimental results on NAP</i>	36
III.6	Compound #5: GPB	42
III.6.1	<i>Experimental results on GPB</i>	42
III.7	Conclusions on drugs proposed by Cerbios Pharma	53
Chapter IV Coprecipitation of pharmaceutical compounds using SAA technique		55
IV.1	Introduction	55
IV.2	PEA stabilization	56
IV.2.1	<i>Experimental results</i>	57
IV.2.2	<i>Characterization of coprecipitates PEA-PVP</i>	58
IV.2.3	<i>Characterization of coprecipitates PEA-LUT</i>	61
IV.2.4	<i>Conclusions on PEA-PVP and PEA-LUT systems</i>	66
IV.3	Improvement of CUR bioavailability	67

IV.3.1	<i>Experimental results</i>	69
IV.3.2	<i>Characterization of coprecipitates</i>	72
IV.3.3	<i>Conclusions on CUR-PVP system</i>	77
IV.4	Improvement of LUT bioavailability	77
IV.4.1	<i>Experimental results</i>	78
IV.4.2	<i>Characterization of particles</i>	80
IV.4.3	<i>Conclusions on LUT-PVP system</i>	85
IV.5	Fluorescent microspheres based on DEX, FITC and LUT	85
IV.5.1	<i>Experimental results</i>	86
IV.5.2	<i>Characterization of particles</i>	91
IV.5.3	<i>Conclusions on LUT-DEX-FITC system</i>	96
IV.6	Improvement of NIF bioavailability	96
IV.6.1	<i>Experimental results</i>	97
IV.6.2	<i>Characterization of particles</i>	101
IV.6.3	<i>Conclusions on HPβCD-NIF system</i>	104
Chapter V Coprecipitation of nutraceutical compounds using SAA technique		105
V.1	Introduction	105
V.2	Stabilization and protection of Chilean propolis	106
V.2.1	<i>Experimental results</i>	108
V.2.2	<i>Characterization of particles</i>	114
V.2.3	<i>Antioxidant activity</i>	117
V.2.4	<i>Conclusions on EEP solid dispersions</i>	118
V.3	Stabilization and protection of beta-carotene	119
V.3.1	<i>Experimental results</i>	120
V.3.2	<i>Characterization of BC-PVP coprecipitates</i>	124
V.3.3	<i>Antioxidant activity</i>	129
V.3.4	<i>Conclusions on BC-PVP system</i>	130
Chapter VI Recovery and protection of antioxidants from bio-residues		131

VI.1	Saffron petals as sources of antioxidants	131
VI.1.1	<i>Extraction from saffron petals</i>	134
VI.1.2	<i>SAA coprecipitation experiments</i>	141
VI.1.3	<i>Characterization of extract-PVP coprecipitates</i>	146
VI.1.4	<i>Conclusions on extract-PVP systems</i>	149
Conclusions		151
References		153
List of Symbols.....		175

Figure Index

Figure I.1 a) SAA plant in laboratory T8 at UNISA; b) GMP industrial plant (Cerbios Pharma, Lugano).	7
Figure I.2 Schematic representation of a SAA apparatus. S, saturator; P, precipitator; H, heat exchanger; C, liquid condenser.	8
Figure III.1 FESEM image of untreated BRI.	22
Figure III.2 FESEM image of SAA BRI powders produced using methanol as solvent at $T_s=60^\circ\text{C}$, $T_p=70^\circ\text{C}$	23
Figure III.3 FESEM images of SAA BRI powders produced at: a) $T_s=T_p=60^\circ\text{C}$; b) $T_s=60^\circ\text{C}$, $T_p=70^\circ\text{C}$; c) $T_s=60^\circ\text{C}$, $T_p=80^\circ\text{C}$; d) $T_s=T_p=80^\circ\text{C}$	24
Figure III.4 XRPD spectra related to SAA particles and untreated BRI. ...	25
Figure III.5 DSC thermograms related to untreated BRI and SAA particles.	26
Figure III.6 FESEM images of micronized FUL using SAS technique (article not cited for secrecy agreements).....	27
Figure III.7 FESEM image of untreated FUL.....	27
Figure III.8 FESEM images of micronized FUL using SAA technique at a) 20 mg/mL, b) 40 mg/mL and c) 60 mg/mL.	29
Figure III.9 PSDs of FUL particles obtained at different concentrations. ...	30
Figure III.10 Dissolution profiles of FUL in physiological solution at 37°C	31
Figure III.11 FESEM image of untreated DAS.	32
Figure III.12 FESEM images of PVP micronized at a) $T_s=60^\circ\text{C}$, $T_p=70^\circ\text{C}$, GLR=2.5, 10 mg/mL; b) $T_s=80^\circ\text{C}$, $T_p=80^\circ\text{C}$, GLR=1.8, 20 mg/mL.	33
Figure III.13 FESEM images of DAS-PVP particles produced at $T_s=80^\circ\text{C}$, $T_p=80^\circ\text{C}$, GLR=1.8, and at a) R=1/20, b) R=1/5.	34
Figure III.14 Cumulative volumetric particle size distribution of DAS-PVP powder obtained by SAA at different R (see Table III.6).	35
Figure III.15 EDX analyses related to DAS-PVP particles produced at R=1/20.....	36
Figure III.16 FESEM image of untreated NAP.	37
Figure III.17 Photographs of foaming materials in the saturator.....	38
Figure III.18 FESEM images of micronized NAP at a) $T_s=85^\circ\text{C}$, $T_p=100^\circ\text{C}$, GLR=2.5, 30 mg/mL; b) $T_s=85^\circ\text{C}$, $T_p=100^\circ\text{C}$, GLR=1.8, 15 mg/mL; c) $T_s=85^\circ\text{C}$, $T_p=100^\circ\text{C}$, GLR=1, 15 mg/mL.....	38
Figure III.19 FESEM images of NAP micronized using ethanol at 20 mg/mL and a) $T_s=T_p=80^\circ\text{C}$, GLR=1.8; b) $T_s=T_p=80^\circ\text{C}$, GLR=1.3; c) $T_s=T_p=80^\circ\text{C}$, GLR=1; d) $T_s=60^\circ\text{C}$, $T_p=70^\circ\text{C}$, GLR=1.8.....	40
Figure III.20 Comparison of cumulative volumetric PSDs of NAP particles obtained by SAA at different concentrations.	41
Figure III.21 X-ray traces of untreated NAP and SAA processed NAP.....	42
Figure III.22 FESEM image of untreated GPB.	43
Figure III.23 DSC thermogram related to untreated GPB.	43

Figure III.24 FESEM images of GPB-PVP particles (R=1/5), using a PVP concentration in ethanol of: a) 10 mg/mL; b) 20 mg/mL; c) 40 mg/mL.....	45
Figure III.25 FESEM images of GPB-PVP particles produced using ethanol and a PVP concentration of 10 mg/mL and: a) R=1/3, b) R=1/2.	46
Figure III.26 FESEM images of GPB-DEX particles produced using water:ethanol (70:30 v/v) at R=1/5 and a DEX concentration of: a) 10 mg/mL; b) 20 mg/mL; c) 40 mg/mL.	47
Figure III.27 Comparison of cumulative volumetric PSDs of GPB-DEX particles obtained by SAA at different DEX concentrations in water:ethanol (70:30 v/v).	48
Figure III.28 FESEM images of GPB-DEX particles produced using water:ethanol at DEX concentration of 40 mg/mL and: a) R=1/4, [GPB]=10 mg/mL, b) R=1/2, [GPB]=20 mg/mL.	49
Figure III.29 FESEM images of GPB-DEX particles produced using water at: a) [DEX]=10 mg/mL, R=1/5; b) [DEX]=20 mg/mL, R=1/5; c) [DEX]=40 mg/mL, R=1/4; d) [DEX]=40 mg/mL, R=1/2.	50
Figure III.30 FESEM images of coprecipitates after 4 months; a) GPB/PVP=1/5; using [DEX]=40 mg/mL in water:ethanol (70:30 v/v) b), GPB/DEX=1/4; c) GPB/DEX=1/2; d) [DEX]=40 mg/mL, GPB/DEX=1/4, using water.	52
Figure IV.1 FESEM images of SAA powders produced at different weight ratios (R=PEA/PVP w/w): a) R=1/3; b) R=1/5 and c) R=1/8.	58
Figure IV.2 XRPD spectra: comparison among SAA coprecipitates PEA-PVP, PEA micronized by SAA and PEA untreated.	59
Figure IV.3 FESEM image of LUT micronized by SAA at 81°C and 93 bar in the saturator, 65°C in the precipitator.	60
Figure IV.4 FESEM image of SAA PEA-LUT coprecipitate, produced at PEA/LUT=10:1 (w:w) ratio.	61
Figure IV.5 XRPD spectra: comparison among a) LUT, untreated and micronized by SAA and b) SAA coprecipitates PEA-LUT and untreated PEA.	62
Figure IV.6 FTIR spectra in the 3700-2500 cm ⁻¹ range: comparison among SAA PEA-LUT coprecipitate (10:1 w:w), untreated LUT and pure PEA. ...	63
Figure IV.7 DSC thermograms related to PEA, LUT and SAA PEA-LUT coprecipitates.....	64
Figure IV.8 FESEM image of PEA-LUT particles (10:1 w/w) coprecipitated by SAA after 10 days of storage.....	65
Figure IV.9 Operative points in the phase equilibrium diagram CO ₂ -ethanol at 80°C.....	69
Figure IV.10 FESEM images (Mag=20 KX) of CUR/PVP microparticles, obtained by SAA at different mass ratios R: a) 1/8, b) 1/6, c) 1/4, d) 1/2....	70
Figure IV.11 PSDs in terms of particles number of CUR/PVP particles at different drug/polymer weight ratios.....	71

Figure IV.12 XRPD related to the PVP and CUR untreated and all coprecipitates produced by SAA.....	73
Figure IV.13 DSC analysis related to the PVP and CUR untreated and all coprecipitates produced by SAA.....	73
Figure IV.14 FTIR analyses of raw material and SAA coprecipitates.....	74
Figure IV.15 Dissolution profiles of CUR in PBS at 37 °C and pH 6.5.	75
Figure IV.16 Dissolution profiles of CUR in PBS at 37 °C and pH 7.4.	76
Figure IV.17 FESEM image (Mag= 35 KX) of SAA LUT particles.....	78
Figure IV.18 FESEM images (Mag=30 KX) of LUT/PVP microparticles produced at a) R=1/4 and b) R=1/8.....	79
Figure IV.19 PSDs of LUT/PVP composite particles produced by SAA at different drug/polymer weight ratios.....	80
Figure IV.20 XRPD related to the PVP and LUT untreated and SAA coprecipitates.....	81
Figure IV.21 FTIR analyses of raw materials and SAA coprecipitates.	81
Figure IV.22 DSC analyses of untreated materials and SAA coprecipitates.	83
Figure IV.23 Dissolution profiles of LUT in PBS at 37°C and pH 7.4.	84
Figure IV.24 a) FESEM image of DF particles at concentration of 8 mg/mL; b) PSDs of DF particles obtained at different DEX concentration.	87
Figure IV.25 FESEM images of LUT/DEX+FITC coprecipitates at R=1/8 w/w and DEX concentration of 10 mg/mL; PSDs of LUT/DEX R=1/8 w/w coprecipitates obtained at different DEX concentration.	88
Figure IV.26 FESEM images of coprecipitates produced at a) R=1/6 (DLF05), b) R=1/6 (DFL*, using DEX labeled FITC).	89
Figure IV.27 PSDs of LUT/DEX micronized by SAA, in terms of number of particle percentage; *: DEX labeled FITC.....	89
Figure IV.28 FM images related to a) R=1/6 DLF05; b) R=1/6 DFL*, test using DEX labeled with FITC.....	90
Figure IV.29 a) SAA powder under visible light; b) SAA powder under UV lamp.....	90
Figure IV.30 XRPD spectra: comparison among untreated compound and microspheres produced by SAA; *test using DEX labeled FITC+LUT (DFL*).....	91
Figure IV.31 DSC thermographs related to DEX, LUT and SAA coprecipitates; DF: DEX+FITC; * test using DEX labeled FITC (DFL*). .	92
Figure IV.32 FTIR spectra of untreated compounds and SAA coprecipitates; *test using DEX labeled FITC (DFL*).	94
Figure IV.33 Release profiles of LUT in PBS at pH 7.4 and 37°C; * test using DEX labeled FITC (DFL*).....	95
Figure IV.34. FESEM images of NIF micronized by SAA technique, using acetone as solvent at: a) 10 mg/mL, b) 40 mg/mL.....	98
Figure IV.35. FESEM image of HP β CD micronized by SAA technique. ..	99

Figure IV.36. FESEM images of NIF-HP β CD precipitated, at different weight ratios R: a) 1/4, b) 1/2.....	100
Figure IV.37 Volumetric cumulative particle size distributions of NIF/HP β CD, at different weight ratios R.....	100
Figure IV.38 X-Ray spectra of NIF/HP β CD: comparison among raw materials and SAA coprecipitated microspheres.....	101
Figure IV.39 FT-IR spectra of NIF/HP β CD: comparison among raw materials and SAA coprecipitated microspheres.....	102
Figure IV.40 Release profiles of NIF in PBS at 37°C and pH 7.4.	103
Figure V.1 FESEM images related to a) HP β CD and b) PVP, micronized by SAA alone at 20 mg/mL in water:ethanol 30:70 (v/v) solution.	109
Figure V.2 A simple representation of the whole process and SAA precipitator.....	109
Figure V.3 FESEM images related to SAA test a) #01 (R=1/2), b) #03 (R=1/5).	111
Figure V.4 Comparison of PSDs related to EEP-HP β CD particles precipitated at a concentration of 30 mg/mL (tests #02, #03, #04).	111
Figure V.5 FESEM images related to SAA test a) #07 (R=1/3 w/w), b) #09 (R=1/8 w/w).	112
Figure V.6 Comparison of PSDs related to EEP-PVP particles precipitated at a concentration of 30 mg/mL (tests #07, #08, #09).....	113
Figure V.7 DSC analyses of a) HP β CD, EEP and EEP-HP β CD coprecipitates b) PVP, EEP and EEP-PVP coprecipitates.	115
Figure V.8 XPRD related to a) HP β CD and EEP-HP β CD coprecipitates b) PVP and EEP-PVP coprecipitates.	116
Figure V.9 FESEM images of PVP precipitated from a) ethanol and b) acetone/ethanol 70/30 (v/v) (#06).	121
Figure V.10 a) Picture of the filter covered by coprecipitated powder; SEM image of BC-PVP precipitated from ethanol at R=1/6 (#03).	122
Figure V.11 Volumetric cumulative PSD of BC-PVP in ethanol, at different weight ratios R (w/w).....	122
Figure V.12 FESEM images of BC-PVP precipitated from acetone/ethanol 70/30 (v/v) at different R, a) 1/20 and b) 1/6 (#08).....	123
Figure V.13 Volumetric cumulative particle size distribution of BC-PVP in the mixture acetone:ethanol, at different R.	123
Figure V.14 DSC thermograms of BC-PVP: comparison among raw materials and SAA coprecipitates.	125
Figure V.15 X-Ray spectra of BC/PVP: comparison among raw materials and SAA coprecipitated microspheres.	125
Figure V.16 FT-IR spectra: comparison among raw materials and SAA coprecipitated microspheres.	126
Figure V.17 Release profiles of BC in PBS at 37°C and pH 7.4: BC-PVP particles obtained using a) EtOH and b) Ac:EtOH (70:30 v/v) as solvent.	128

Figure VI.1 SEM images of samples produced using: SG) β -glucan and SC) β -cyclodextrin (Ahmad et al., 2018).	133
Figure VI.2 Saffron petals.....	134
Figure VI.3 Extracts obtained using ethanol as solvent at room temperature after a) 3 h; b) 6h; c) 24h.....	135
Figure VI.4 Extracts obtained using water:ethanol (41:59 v/v) as solvent at room temperature after a) 3 h; b) 6h; c) 24h.	136
Figure VI.5 Extracts obtained at room temperature after 6 hours of flower maceration, using a) ethanol at pH=2; b) water:ethanol (41:59 v/v) at pH=2.	136
Figure VI.6 Areas under peaks related to the glycosides of kaempferol and quercetin in the HPLC chromatograms of the extracts obtained in ethanol, at 25°C and different times of flower maceration.	137
Figure VI.7 Areas under peaks related to the glycosides of kaempferol and quercetin in the HPLC chromatograms of the extracts obtained in water:ethanol (41:59 v/v), at 25°C and different times of flower maceration.	138
Figure VI.8 Areas under peaks related to the glycosides of kaempferol and quercetin in the HPLC chromatograms of the extracts obtained in ethanol and water:ethanol (41:59 v/v) at pH=2 and 6 hours of flower maceration.	139
Figure VI.9 a) SAA powder obtained from EtOH extract with PVP; FESEM images related to SAA tests performed at b) R=1/5, c) R=1/3.....	143
Figure VI.10 a) SAA powders from EtOH extract at pH=2 with PVP; FESEM images related to SAA tests performed at b) R=1/5, c) R=1/3.....	143
Figure VI.11 Comparison of PSDs related to extract-PVP particles precipitated from ethanol extract (pink) and from ethanol extract at pH=2 (blue) at different R (w/w).	144
Figure VI.12 a) SAA powder from H ₂ O:EtOH (41:59 v/v) extract with PVP; FESEM images of samples obtained at: b) R=1/5, c) R=1/3.	145
Figure VI.13 a) SAA powder from H ₂ O:EtOH (41:59 v/v) extract at pH=2 with PVP; FESEM images of samples obtained at b) R=1/5, c) R=1/3.	145
Figure VI.14 DSC thermograms of extract-PVP coprecipitates.	147
Figure VI.15 XPRD related to coprecipitates obtained from ethanol extract and from water:ethanol (41:59 v/v) with PVP, at different R (extract/PVP w/w).....	147

Table Index

Table III.1 BRI solubilities in different solvents.	23
Table III.2 PSD data of BRI particles produced by SAA.	25
Table III.3 FUL solubilities in solvents.	28
Table III.4 PSDs data of FUL particles produced by SAA.	30
Table III.5 Operating conditions used SAA micronization experiments. (T_s : saturator temperature; T_p : precipitator temperature; P_s : saturator pressure; P_p : precipitator pressure; GLR: gas to liquid ratio).....	32
Table III.6 Operating conditions used for SAA coprecipitation experiments; PSD data in terms of volume of particles (T_s : saturator temperature; T_p : precipitator temperature; P_s : saturator pressure; P_p : precipitator pressure; GLR: gas to liquid ratio).	33
Table III.7 Operating conditions used for SAA experiments on NAP using water; PSD data in terms of volume of particles (C: NAP concentration; GLR: gas to liquid ratio).	37
Table III.8 Operating conditions used for NAP micronization using ethanol; (C: NAP concentration; T_s : saturator temperature; T_p : precipitator temperature; GLR: gas to liquid ratio).	39
Table III.9 Concentrations used for GPB-PVP coprecipitation using ethanol; PSD data in terms of volume of particles (C_{PVP} : PVP concentration; C_{GPB} : GPB concentration; R: GPB/PVP weight ratio w/w).	45
Table III.10 Operating conditions used SAA coprecipitation experiments for GPB-DEX particles produced in water:ethanol (70:30 v/v); PSD data in terms of volume of particles (C_{DEX} : DEX concentration; C_{GPB} : GPB concentration; R: GPB/DEX w/w).	47
Table III.11 PSD data in terms of volume of particles (C_{DEX} :DEX concentration; C_{GPB} :GPB concentration; R: GPB/DEX w/w); *:no powder produced.	49
Table III.12 PSD data in terms of volume of particles (C_{DEX} : DEX concentration; C_{GPB} :GPB concentration; R:GPB/DEX w/w).	50
Table IV.1 Operating conditions used for PEA-PVP coprecipitation experiments. (C: total concentration; Q_{CO_2} : CO ₂ flow rate; T_p : precipitator temperature).	57
Table IV.2 Compositions and operating conditions used to perform PEA-LUT coprecipitation experiments. (C: total concentration; Q_{CO_2} : CO ₂ flow rate; P_{sat} : saturator pressure; T_p : precipitator temperature).	60
Table IV.3 Solvent residues in the tested materials.	64
Table IV.4 Stability analysis of SAA coprecipitates of PEA/LUT 10:1 w/w during 23 days.	65
Table IV.5 Operative conditions used to produce CUR and PVP particles by SAA technique.	69
Table IV.6 PSDs data based on number and volume of CUR-PVP particles.	71

Table IV.7 PSDs data based on the volume of CUR/PVP particles at different GLR values, for R=1/8 w/w.	72
Table IV.8 Ratios and concentrations of LUT and PVP used for SAA experiments. (C_{pol} : PVP concentration; C: total concentration; R=LUT/PVP w/w; * superposition of amorphous and crystalline product).....	79
Table IV.9 Composition and PSD data of LUT/DEX microparticles produced by SAA (C_{FITC} : FITC concentration; C_{tot} : total concentration; C_{DEX} : carrier concentration; C_{LUT} : LUT concentration; R= LUT/DEX w/w, w_{LUT} = LUT weight, w_{DEX} = DEX weight; DF: DEX+FITC; DF*: DEX labeled FITC; DLF: DEX+LUT+FITC; DFL*: DEX labeled FITC + LUT).	87
Table IV.10 Composition and PSD data of NIF/HP β CD particles produced by SAA (R=NIF/HP β CD w/w; C_{NIF} : NIF concentration; C_{tot} : total concentration; *loss of carrier into the saturator).....	99
Table V.1 Composition and PSD data of EEP-carrier microparticles produced by SAA (R=EPP/carrier w/w; C_{tot} : total concentration; C_{EEP} : EEP concentration; C_{car} : carrier concentration).....	110
Table V.2 Antioxidant activity of propolis coprecipitates: total polyphenol content; scavenging activity (IC_{50}) by DPPH method (R: EEP/carrier w/w; GA: Gallic Acid; Eff: polyphenol loading efficiency).	117
Table V.3 Composition and PSD data of BC-PVP SAA particles (R=BC/polymer w/w; C_{tot} : total concentration; C_{PVP} : PVP concentration).121	
Table V.4 BC loading efficiency in SAA coprecipitates; antioxidant activity of SAA powders by DPPH method. R= BC/PVP w/w.	127
Table VI.1 Extraction results obtained after 6 hours using ethanol and water:ethanol (41:59 v/v); (C_{ext} : extract concentration; C_K : kaempferol concentration; C_Q : quercetin concentration; SA: Scavenging Activity).....	140
Table VI.2 Composition and PSD data of extract-PVP particles produced by SAA (R=extract/PVP w/w; C_{ext} : total extract concentration; C_{PVP} : PVP concentration; T_s = saturator temperature; T_p = precipitator temperature)...	142
Table VI.3 Loading efficiencies of quercetin and kaempferol glycosides and antioxidant activity of powders (R: extract/PVP w/w; C_{ext} : extract concentration; Q: quercetin glycoside; K: kaempferol glycoside; SA reduction: Scavenging Activity reduction after 3 months).....	148

Abstract

Industrial interest is focused on the development of new pharmaceutical and nutraceutical formulations aimed at the enhancement of bioavailability of poorly water-soluble active compounds. Various factors influence the bioavailability of an active principle in a solid formulation, such as the particle size distribution, the solid state and the morphology. In order to enhance bioavailability, two different approaches were investigated in this thesis: particle size reduction of pure ingredients and production of amorphous formulations consisting of the dispersion of the hydrophobic molecule into a hydrophilic matrix (*carrier*). Supercritical fluid (SCFs) based techniques demonstrated to be a valid alternative to traditional processes, given the SCFs specific properties, such as liquid-like density, very fast mass transfer similar to gas, near-zero surface tension, effective solvent elimination. Among SCFs techniques, Supercritical Assisted Atomization (SAA) was successfully used to produce controlled micro and sub-microparticles of pure compounds, but also composite systems. The enhancement of bioavailability of active ingredients is still poorly investigated in the SAA literature. The ability of the SAA process in crystallinity control and particle size reduction is investigated in order to enhance the bioavailability of new active principles, often not feasible through conventional methods. This Ph.D. work is the most recent advance in the application of this supercritical fluid technology for the production of new and stable pharmaceutical and nutraceutical formulations.

Industrial companies are very interested in the development of these feasible formulation technologies. In fact, this Ph.D. work was supported and granted by Cerbios Pharma, a Swiss pharmaceutical company located in Lugano and specialized in the development and production of chemical and biological active principles. In the frame of the research collaboration between Cerbios Pharma and the Department of Industrial Engineering (DIIN) of the University of Salerno, a part of this thesis concerned the development of pharmaceutical formulations based on active principles suggested by the Company for its world-wide partners, in order to scale up this process for industrialization purposes. Due to secrecy agreements, the proposed active substances were presented using acronyms and no further detailed information was herein reported. Different kinds of active principles were tested on behalf of Cerbios Pharma: BRI (an alpha adrenergic agonists drug), FUL (an anti-estrogen drug), DAS (an anticancer drug), NAP (a non-steroidal anti-inflammatory drug) and GPB (an anticholinergic agent). These drugs were previously unsuccessfully tested using traditional techniques. For each active principle, during this Ph.D. work, a series of SAA experiments was performed in laboratory scale to optimize process conditions, in order to

reach the targets requested by the Company. BRI, FUL and NAP were micronized alone, whereas DAS and GPB were dispersed in different carrier matrices producing coprecipitates (Chapter III). In particular, the study performed on NAP compound allowed to validate the SAA industrial plant in Cerbios Pharma and obtain the SwissMedic authorization for *Good Manufacturing Practice* (GMP) production, on January 2017.

To investigate in depth the applicability of the SAA process in the development of new and stable pharmaceutical formulations, *curcumin*, *luteolin*, *palmitoylethanolamide* and *nifedipine* were selected as active principles, for their therapeutic and healing properties. All these substances showed low water-solubility and remarkably fast crystallization rates, interfering with the micronization processes; therefore, they were difficult to handle in an industrial perspective. *Polyvinylpyrrolidone*, *hydroxypropyl- β -cyclodextrin* and *dextran* were investigated as *carrier* since they are non-toxic, water-soluble, biodegradable, biocompatible, *Food & Drug Administration*-approved and crystal growth inhibitors. The study was focused on the role of the *carrier* in influencing particle size distribution, morphology, solid state, and mostly in inhibiting recrystallization of the active principles and enhancing their bioavailability. In particular, the selected carriers demonstrated to be very efficient in controlling the tendency of active principles to crystallize and agglomerate, by producing SAA stable particles over time. Indeed, well-separated and amorphous microspheres were obtained by SAA process with diameters lower than 1.8 μm and high active principle loading efficiencies, up to 100% in most of the experiments performed. Dissolution tests confirmed improvements of bioavailability up to 12 times, due to the coprecipitation of the pharmaceutical compounds and carrier: the produced composite particles showed active principle dissolution rates much faster compared to the physical mixtures. The active principle/carrier weight ratio and chemical interactions in the coprecipitates revealed to be controlling parameters for dissolution rates (Chapter IV).

The production of composite microspheres loaded with bioactive compounds has been another important challenge handled in this Ph.D. work. In particular, *beta-carotene* and extracts obtained from *propolis* and *saffron petals* (normally considered as industrial wastes) were selected in this framework for their nutraceutical properties. The main outcome of this investigation was not only the improvement of the bioavailability, but also the protection of the antioxidant activity of the bioactive compound. Defined and spherical particles were produced by means of the SAA technique using *polyvinylpyrrolidone* and *hydroxypropyl- β -cyclodextrin* as carriers, with mean diameters influenced by the concentrations under test. The UV-vis analyses confirmed high loading efficiencies (up to 94-100%) and preserved

antioxidant activity against light, heat and oxygen. In particular, the study on saffron petals extracts demonstrated that SAA produced particles, using *polyvinylpyrrolidone* as carrier, were able to preserve the antioxidant power over time. After three months, the values of scavenging activity were practically confirmed for SAA coprecipitates and reduced by 35% for crude saffron extracts. As result, the antioxidant-rich particles produced can be used as natural sources of antioxidants and for food supplements, thus proving that it is possible to enlarge the application field of the SAA process to the production of nutraceutical formulations (Chapter V and Chapter VI).

In conclusion, the SAA technique was successfully applied both in pharmaceutical and nutraceutical fields, demonstrating to be an attractive and available process from an industrial point of view.

Introduction

Bioavailability of pharmaceuticals

Many of the newly developed pharmaceuticals, as well as a significant proportion of the drugs on the market, are classified as *poorly water-soluble*, according to the Biopharmaceutics Classification System (Lipinski et al., 2001, Merisko-Liversidge and Liversidge, 2011, Baghel et al., 2016, Sigfridsson et al., 2009, Rodriguez-Aller et al., 2015). Since approximately 65% of the human body consists of water, a drug must have a good water solubility and an acceptable bioavailability level. The bioavailability is defined as the rate at which the relative amount of an administered dose of an active principle is absorbed from a pharmaceutical form and becomes available at the site of action (Chow, 2014). Generally, the rate-limiting step for absorption of drug poorly water-soluble is the liberation that corresponds to the release of drug from pharmaceutical formulation and its dissolution (Junyaprasert and Morakul, 2015). A limited absorption of these active principles leads to slow onset of action, beyond excessive and frequent dosage of drugs to reach the therapeutic concentration in blood. These increased dosages may cause several negative effects including inefficient treatment, higher patient costs, undesirable side effects on human health, poor patient compliance and more risks of toxicity or even death (Kawabata et al., 2011). The improvement of active principle bioavailability is one of the most challenging features of the drug development process, especially for oral drug delivery systems.

Several approaches have been proposed to overcome these limitations and to improve the dissolution rate of pharmaceutical compounds in aqueous media (Fu et al., 2017, Gupta et al., 2013). These approaches can be classified as chemical and physical modifications. Among the chemical modifications, for example, the synthesis of soluble pro-drugs and salts starting from the pure active principle is one of the most used. However, these approaches cannot be used for neutral molecules and the improvement of dissolution in water of the salt than free drug is not always guaranteed (Kalepu and Nekkanti, 2015, Junyaprasert and Morakul, 2015). On the other hand, physical modifications include: complexation or solubilization (using

cyclodextrins, surfactants, conjugation with dendrimers), particle size reduction (micronization and nanonization techniques), changes of the crystal habit (polymorphs) and preparation of drug solid dispersions in different type of carriers (for examples, polymeric and polysaccharide matrices, liposomes, micelles) (Sharma et al., 2016, Stella and He, 2008, Savjani et al., 2012, Merisko-Liversidge and Liversidge, 2011, Chen et al., 2011). As reported in several works in the literature, the time of dissolution, hence, the dissolution rate may change due to several factors, such as the solid state, the particle size, the type of formulation, etcetera (Merisko-Liversidge and Liversidge, 2011, Kalepu and Nekkanti, 2015, Junyaprasert and Morakul, 2015).

According to the Noyes-Whitney equation, the dissolution rate is directly proportional to the drug solubility and its interfacial surface area (Hancock and Parks, 2000, Savjani et al., 2012, Mosharraf and Nyström, 1995, Khadka et al., 2014).

$$dm/dt = DA*(C_s - C_{bulk})/h \quad (1)$$

where dm/dt is the dissolution rate of drug, D is its diffusion coefficient, A is its surface area, C_s is its saturation concentration in the solvent, C_{bulk} is its concentration in the bulk, and h is the thickness of the hydrodynamic boundary layer.

Nevertheless, the drug solubility fundamentally depends on the solvent used as well as on temperature and pressure. It is an equilibrium parameter and it is almost the same for all sizes of a drug, in crystalline or amorphous state: given enough time, even large particles eventually dissolve up to the saturation concentration in the specific solvent (Sun et al., 2012, Savjani et al., 2012). In addition, the solid state of the drug can affect the dissolution rate of an active principle. A crystalline and poorly water-soluble drug, when in the amorphous state tends to have higher release rate, since no energy is required to break up the crystal lattice during the dissolution process. Therefore, the amorphous pharmaceuticals show markedly higher dissolution rate than their crystalline counterparts (Sun et al., 2012, Savjani et al., 2012, DiNunzio et al., 2008, Alonzo et al., 2010). Some thermodynamic aspects explain the reason: unlike crystalline material, an amorphous solid is characterized as having a molecular arrangement that lacks long-range order. Consequently, the entropy (ΔS) and the free energy (ΔG) of an amorphous solid is higher than that of its crystalline arrangement. This energy difference explains the reason why significantly faster dissolution can be obtained for amorphous formulations compared to their crystalline equivalents. By manipulating the solid state and producing *polymorphs* (thanks to the use of different solvents and/or operating conditions during the production), it is possible to develop the best stable arrangement of the drug to assure an improved bioavailability and a long shelf-life. When a solid is in an amorphous state, it exhibits only molecular

vibrations; therefore, amorphous one-phase formulations can be used to improve dissolution rates of poorly water-soluble drug, and, at the same time, to produce long-term stability of dried powders (Hancock and Parks, 2000, Savjani et al., 2012, Baghel et al., 2016, Kalepu and Nekkanti, 2015).

The particle size reduction approaches to prepare stable micro and nanoparticles have emerged to increase the bioavailability of poorly water-soluble compounds. Indeed, the micronization method increases the surface area to volume ratios of drug powders allowing greater interactions with the solvent and, hence, enhancing the dissolution rates (absorption) (Chen et al., 2011). The surface area of a drug, indeed, increases as the size of the active principle particles is decreased from bulk to a micro to a nano scale. The smaller particle size results in a large surface area that is proportional to the dissolution rate, as described by the Noyes-Whitney equation (Kogermann et al., 2013, Mosharraf and Nyström, 1995, Sun et al., 2012). Although the particle size reduction is one of the oldest strategies for improving the dissolution rate, micro and nanoparticles of active substances may be affected by aggregation or recrystallization phenomena; therefore, they are difficult to handle in an industrial perspective. For this reason, the pharmaceutical companies have long recognized the advantages of multi-composite systems in order to improve the pharmacokinetic behavior and enhance the bioavailability of the active principles in the formulations (Junyaprasert and Morakul, 2015, Savjani et al., 2012, Khadka et al., 2014). Solid dispersions represent a useful pharmaceutical technique and consist of at least two different compounds, generally a hydrophobic drug and a hydrophilic matrix that acts as a *carrier*. The composite system can be produced in form of microspheres or microcapsules. In the first case, the carrier and the active compounds are uniformly dispersed within the same particle (*composites*), whereas in the second case, the compound of interest is surrounded by a carrier shell (core-shell systems or *encapsulates*) (Cocero et al., 2009). The carrier has to be soluble in water, biocompatible, biodegradable, non-toxic, FDA (*Food and Drug Administration*)-approved; furthermore, it has to protect the active principle, to inhibit its recrystallization and to improve its dissolution. The most widely used carriers for solid dispersions include hydroxypropylmethyl cellulose, polyvinylpyrrolidone, hydroxypropylmethyl cellulose acetate succinate, sugars and polyethylene glycols. These carriers have high glass temperature transitions (T_g), thus they are in glassy state at room temperature (Merisko-Liversidge and Liversidge, 2011, Savjani et al., 2012, Sinha et al., 2010, Vasconcelos et al., 2007, Alonzo et al., 2010). Carriers capable of interacting with some active principles, such as through hydrogen bonding or steric hindrance, have been demonstrated to inhibit crystallization at very low concentrations. These physical or chemical interactions can restrict the molecular mobility of the drug molecules and provide stability to the system (Baghel et al., 2016).

Conventional methods, including emulsion/solvent evaporation, thermal gelation, hot homogenization technique, coacervation, spray drying, freeze-drying, antisolvent precipitation, jet milling have been used to obtain particle size reduction and solid dispersions of poorly water-soluble active principles in different carriers. However, these strategies are not always suitable or feasible and may show some drawbacks (Campardelli et al., 2015), such as the production of coarse and large particles with broad particle size distribution, the degradation of the product due to mechanical or thermal stresses, or its contamination with organic solvents or other toxic substances, low loading efficiencies and difficulty in scale up (Martín and Cocero, 2008, Temelli, 2018). In particular, emulsification and solvent evaporation need a large use of heavy and toxic organic solvents; furthermore, to reduce the residual organic solvent below the safety limits, many downstream processes, such as additional drying step, have to be performed. Even spray drying has some limitations: uses of large amount of toxic organic solvents, high temperatures to remove solvents, possible degradation of the active product due to the thermal stress and production of large particles with wide particle size distribution. Furthermore, some drugs result to be difficult processed by conventional methods, due to their fast tendency to crystallize and to agglomerate.

In recent years, the application of supercritical-carbon dioxide (SC-CO₂) based processes has attracted great attention as a valid alternative to traditional techniques (Cocero et al., 2009, Campardelli et al., 2015). These SC-CO₂ based techniques have been successfully applied in several fields: among them, micronization, membranes, scaffold production (Cocero et al., 2009, Campardelli et al., 2015, Baldino et al., 2014a, Baldino et al., 2014b, Reverchon and Della Porta, 2003, Prosapio et al., 2015, Franceschi et al., 2008, Adami et al., 2017b, Adami et al., 2012, Adami and Reverchon, 2012, Martin et al., 2013, Meneses et al., 2015, Reverchon et al., 2015, Wu et al., 2009). Among the SC-CO₂ based processes, Supercritical Assisted Atomization (SAA) is an efficient technique that has been used until now to produce micro and sub-microparticles of several kinds of compounds: active molecules, salts, catalysts, proteins and polymers (Reverchon et al., 2003, Adami and Reverchon, 2012, Della Porta et al., 2006, Reverchon and Spada, 2004a, Adami et al., 2011, Liparoti et al., 2012, Adami et al., 2012, Martin et al., 2013). In SAA process, SC-CO₂ is solubilized in a solution containing the compound to be micronized forming an expanded liquid, characterized by reduced viscosity and surface tension that is subsequently atomized. SAA produces controlled micro and submicro-droplets that, upon drying, produce submicroparticles.

Bioavailability of nutraceuticals

Nowadays, a significant interest in incorporating micronutrients (bioactive compounds) into functional food and beverage products has increased to benefit human health and wellness through the diet (Handford et al., 2014). These micronutrients include vitamins, minerals, flavors, antioxidants, antimicrobials, polyphenols, probiotics, prebiotics and preservatives. Some of these micronutrients are essential for human well-being (such as vitamins), whereas other substances derived from food sources provide health benefits in addition to diet (*nutraceuticals*) (Joye et al., 2014, Handford et al., 2014). Various bioactive compounds have been obtained from natural sources, for examples vegetables, fruits, legumes, oil and have shown beneficial effects on human health including antioxidant, anti-inflammatory, and antibacterial activities (Recharla et al., 2017). A recent tendency is the recovery of these bioactive compounds also from wastes derived by food industry. Indeed, the processing of plant foods results in the production of a large volume of by-products that is still rich in bioactive compounds that can be recovered. These residues could be an alternative source for obtaining natural antioxidants, which are considered completely safe in comparison with synthetic ones (Murthy and Naidu, 2012, Lafka et al., 2007, Balasundram et al., 2006, Guamán-Balcázar et al., 2019, Meneses et al., 2015).

However, bioactive compounds cannot be incorporated in their pure state into commercial food products, due to their susceptibility to physical, chemical and enzymatic degradation (Coronel-Aguilera and San Martín-González, 2015). Furthermore, the performance of these substances can be affected by light, heat, water and oxygen exposure, compromising their activity and shelf-life (Handford et al., 2014). Moreover, some bioactive compounds have strong taste and aroma, such as propolis (Nori et al., 2011, Kalogeropoulos et al., 2009), and show low water solubility and, hence, limited oral bioavailability (de Souza Simões et al., 2017).

In order to improve bioavailability of these micronutrients, the production and the use of nanoparticles of pure compounds is rare for food applications; whereas, several advantages are associated with the production of composite delivery systems and, particularly, with microencapsulation or dispersion of the bioactive compounds in a wide variety of food-grade materials (Joye and McClements, 2013, Puligundla et al., 2017, Franceschi et al., 2008, Priamo et al., 2011). First, these strategies allow the easier incorporation of functional components into food systems; second, it may preserve the activity of micronutrients from chemical reactions and degradations (oxidation, hydrolysis); third, the delivery systems may release the active substances in a particular site of action, and protect them to the various stresses for food during its production, storage, transport and consumption (Joye and McClements, 2013, Joye et al., 2014). Therefore, one important

application of nanotechnology in food and nutrition is to design and develop novel functional food ingredients with improved oral bioavailability, and thermal and mechanical stability (Huang et al., 2010). Engineered materials, for a variety of agro-food applications such as food additives, are developed using polymers, polysaccharides, micelles, liposomes, polyelectrolyte complexes and hydrogel particles (Puligundla et al., 2017, Priamo et al., 2011, Temelli, 2018, Joye et al., 2014).

Solid formulations consisted of the incorporation of bioactive compounds in polymeric matrices are gaining increasing interest by food industry, representing a suitable method to stabilize and protect the bioactive compound from environmental conditions (Champagne and Fustier, 2007, Franceschi et al., 2008, Janiszewska-Turak, 2017, de Paz et al., 2012, Priamo et al., 2011, Guamán-Balcázar et al., 2019). Different processes are being applied in order to produce micro- and nanosystems for functional foods using “top down” and “bottom up” approaches or the combination of both strategies. The wide range of available techniques that can be employed for food application includes spray drying, emulsion, coacervation, antisolvent precipitation (Guamán-Balcázar et al., 2019, de Souza Simões et al., 2017). These traditional processes suffer from several well-known drawbacks, such as excessive use of solvent, thermal and chemical solute degradation, high residual solvent concentration and difficulty in controlling the particle size distribution during processing, low loading efficiencies and in some cases difficulty in scale up the process (Temelli, 2018). In recent years, the encapsulation of bioactive compounds by supercritical technology using SC-CO₂ is considered as a suitable technique for natural products encapsulation (Temelli, 2018, Janiszewska-Turak, 2017). According to Cocero et al. (Cocero et al., 2009), the application of SC-CO₂ based processes is a promising alternative to conventional techniques since they can eliminate or reduce the use of organic solvents, the separation of supercritical fluid can be easily accomplished by depressurization, hence obtaining solvent-free products. Furthermore, SC-CO₂ based processes allow working at lower temperatures compared to the conventional ones, avoiding degradation of bioactive compounds that are thermo-sensitive.

In this field, the SAA process may be an efficient alternative for the production of formulations based on bioactive compounds loaded in different carrier matrix in order to develop novel functional food ingredients with improved bioavailability, thermal stability and preserved antioxidant activity. The challenge is to apply the SAA process in a very poorly explored domain, as nutraceutical one.

Aim of the thesis

The aim of this work is to adopt SCF-based process, able to enhance the bioavailability and the stability of some active principles. Up to now, the Supercritical Assisted Atomization (SAA) process has been successfully used to produce controlled micro and submicroparticles of pure compounds, but also composite systems. The enhancement of bioavailability of active ingredients is, instead, poorly investigated and discussed in the SAA literature. Therefore, this Ph.D. work regards the recent advances in the application of this supercritical fluid technology for the production of new solid formulations to improve active principle dissolution rates. Two approaches are investigated to reach such a goal: the particle size reduction of pure ingredients and the production of amorphous formulations consisting of the dispersion of the hydrophobic molecules into a hydrophilic matrix (*carrier*), named coprecipitates. The ability of the SAA process in crystallinity control and particle size reduction is investigated in order to enhance the bioavailability of new active principles, often not reachable with conventional methods.

This Ph.D. work has been supported and granted by Cerbios Pharma, a Swiss pharmaceutical company located in Lugano and specialized in the development and production of chemical and biological active principles. Cerbios Pharma has funded this research project with the aim to invest in an atomization plant for particle engineering using SCFs. In the frame of the research collaboration between Cerbios Pharma and the Department of Industrial Engineering (DIIN) of the University of Salerno, a part of this work of thesis has concerned the development of pharmaceutical formulations based on active principles proposed by the Company, in order to scale up SAA process for industrialization purposes. Due to secrecy agreements, these active substances are presented using acronyms and no further detailed information is reported. Different kinds of active principles are tested on behalf of Cerbios Pharma: BRI (an alpha adrenergic agonists drug), FUL (a antiestrogen drug), DAS (an anticancer drug), NAP (a non-steroidal anti-inflammatory drug), GPB (an anticholinergic agent). For each of these drugs, a systematic study is performed to optimize SAA process conditions aimed at the specific targets requested by the Company. In particular, the Chapter IV of this work of thesis presents the results achieved in the frame of this research collaboration, which are aimed to validate the SAA industrial plant in Cerbios Pharma and obtain the SwissMedic authorization for *Good Manufacturing Practice* production.

To investigate in depth the applicability of SAA process in the development of new and stable pharmaceutical formulations, *curcumin* (CUR), *luteolin* (LUT), *palmitoylethanolamide* (PEA) and *nifedipine* (NIF)

are selected as active principles, for their therapeutic and pharmacological properties. All these active principles show fast tendency to crystallize and low dissolution rates in aqueous media. A series of coprecipitation tests is performed to study the role of the *carrier* in influencing PSD, morphology, solid state, and, particularly, in inhibiting recrystallization of the selected active principles and enhancing their bioavailability. Three different carriers are investigated: *polyvinylpyrrolidone* (PVP), *hydroxypropyl- β -cyclodextrin* (HP β CD) and *dextran* (DEX), since they are water-soluble, biodegradable, biocompatible, *Food & Drug Administration*-approved and crystal growth inhibitors.

Another aspect still poorly explored in SAA literature regards the application of this well-known technology in a new research field, like the nutraceutical one. Therefore, the aim of this part of Ph.D. work has been to test the applicability of the SAA process in the production of nutraceutical formulations based on the dispersion of bioactive compounds, such as *beta-carotene* and extracts obtained from *propolis* or *saffron petals*, in matrices like PVP and HP β CD. For these systems, in addition to the improvement of bioavailability, the most important aspect has concerned the role of the *carrier* in protecting the antioxidant activity of the bioactive compound.

Outline of the thesis

The dissertation is organized as follows.

In Chapter I, a brief review on micronization and coprecipitation technologies is followed by an introduction on the scientific relevance and the innovative aspects of SAA process and, in particular, by an in-depth review of the SAA literature.

The description of the analytical methodologies used to study the characteristics of the SAA produced particles and raw materials (including size, solid state, morphology, dissolution behavior, loading efficiency and antioxidant activity) are described in Chapter II.

In Chapter III, the results achieved in the frame of the research collaboration between Cerbios Pharma and the Department of Industrial Engineering (DIIN) of the University of Salerno are discussed. These scientific results are not published due to secrecy agreements.

In Chapter IV, several applications concerning SAA laboratory scale production of composite systems, loaded with hydrophobic and crystalline compounds with pharmacological properties, are proposed and investigated to reach an improved bioavailability and control of the crystalline behavior of the active principle tested in this work.

In Chapter V and Chapter VI, the application of the SAA process in the still poorly-investigated field of the nutraceutical compounds is presented and discussed, thus endorsing the SAA technique as a reliable alternative to conventional processes.

Finally, some conclusions are drawn on the main results achieved by this Ph.D. work.

The dissertation contains three chapters (IV-VI) presenting results published in journal and conference proceedings. The complete citations for these papers are provided in the Publication List.

Fruitful cooperations contributed to validate the results discussed in this work of thesis, including the scientific collaboration with Italian and foreign research groups (like the Italian Departments of Pharmacy and of Chemistry & Biology of the University of Salerno, the Chilean Institute of Fraunhofer and the French Laboratory of Mechanics, Modeling & Clean Processes of the University of Marseille) and pharmaceutical companies (like the Swiss Cerbios Pharma and the Italian Epitech Group).

Chapter I

Micronization and coprecipitation processes

I.1 Introduction

The bioavailability of pharmaceuticals and nutraceuticals in solid formulation strongly depends on the size, particles size distribution and solid state of materials. Due to this, there is an increasing interest in the development of efficient micronization technologies (Martín and Cocero, 2008). There are different micronization techniques proposed in literature, classified in two classes: *top down* and *bottom up*. The “top down” processes provide the reduction of the original materials by involving a physical or chemical process of breaking down larger particles into smaller ones, for examples grinding or milling. The “bottom up” techniques can create more complex molecular structures of compounds, for examples the precipitation of particles from a liquid phase, crystallization process, self-assembly method (Reverchon and Adami, 2006, Chiou et al., 2006, Handford et al., 2014). An important current alternative to the micronization of a pure compound is based on the production of composite systems consisted of the active principle and a carrier system. There are different kinds of carrier: biopolymer matrices, polysaccharides, cyclodextrins, lipids, micelles, liposomes (Handford et al., 2014). The composite system can be produced in form of microspheres or microcapsules. In the first case, the carrier and the active compounds are uniformly dispersed within the same particle (*composites*), whereas in the second case, the compound of interest is surrounded by a carrier shell (core-shell systems or *encapsulates*) (Cocero et al., 2009). These kinds of particles have demonstrated to be very useful in both nutraceutical and pharmaceutical field. In particular, these solid formulations are easier to handle than the pure particle of an active principle that may be affected by crystallization or oxidation phenomena with a possible loss of activity. Furthermore, the carriers used can allow achieving a controlled delivery of the active compound on time and in the site of action,

protecting it against degradation/oxidation and loss of activity, enhancing its dissolution rate and inhibiting its recrystallization. Moreover, some active substances can have a distinct off-flavor or a strong and unpleasant taste and aroma, thus their application as a food ingredient or in pharmaceutical industries can be limited. The loading/encapsulation of these compounds in a carrier can be an option to overcome these negative aspects (Joye et al., 2014, Handford et al., 2014, Temelli, 2018).

1.1.1 Conventional techniques

Spray drying

This process consists of the atomization of a liquid solution containing the substrate to be micronized. The spray formed is then dried using a heated gas flow (compressed air or nitrogen) in order to remove the solvent. Using cyclones or filter it is possible to recover the final product from the gaseous stream. The main limitations of spray drying are the difficulty in controlling the particle size distribution (which are very wide), the high tendency to agglomerate, low loading efficiencies and possible degradation of active principle due to high temperatures used to remove the solvent (Martín and Cocero, 2008, Ishwarya et al., 2015, Vandana et al., 2014).

Spray freeze drying

In this process, the solution containing the substrate to be micronized is sprayed directly in a cryogenic liquid (liquid nitrogen or a cold gaseous stream). The frozen droplets are thus lyophilized and fine particles are produced. The low temperatures used allow to process also thermal sensitive compounds avoiding possible degradation. The limitations are comparable to those of conventional spray drying (Ishwarya et al., 2015, Vandana et al., 2014).

Anti-solvent precipitation

In this process, the precipitation of particles proceeds in steps of mixing of solution and anti-solvent, generation of supersaturation, nucleation, and growth by coagulation and condensation, followed by agglomeration in case of uncontrolled growth. The solution containing the compound to be micronized is mixed with an anti-solvent; the solute has to be insoluble in this mixture and, consequently, it precipitates. The drawbacks of this technique are the high residual solvent in particles produced, the wide particle size distribution obtained and the longtime of process (Betancourt et al., 2007, Alshamsan, 2014).

High pressure homogenization

The production of drug nanoparticles via the top-down approach of disintegration mechanism involves the high pressure homogenization (Chen et al., 2011). This process is performed in water or in a non-aqueous media in the case of water sensitive drugs. A suspension of crystalline drug and stabilizers is passed through the narrow gap of a homogenizer at high pressure (500-2000 bar). The high pressures create some disruptive forces, such as collision and shearing that cause the disintegration of the starting material. The particles produced show size depending of the number of cycles and the pressure reached during the homogenization process (Chen et al., 2011).

Jet milling

This technique is applied to physically break down coarse particles to finer ones due to mechanical energy applied to the system; hence, it is a “top-down” method (Loh et al., 2015). Generally, milling may be conducted in different conditions: dry state (dry milling) or in a liquid medium (wet milling). In particular, in the *jet milling* method, a high velocity medium gas (nitrogen or air) passing through a nozzle carries coarse particles into the jet mill causing their disintegration due to the impact and the collision against the wall of the vessel. By this technique, particles of 1-20 μm can be produced (Hoyer et al., 2008, Nykamp et al., 2002, Chen et al., 2011). The lack of control over particle size distribution and the possible chemical degradation of material due to the mechanical energy applied to the system represent the main limitations of the application of this type of micronization technique in pharmaceutical fields.

Emulsion/Solvent evaporation

This process is mainly used to produce composite particles starting from an emulsion. The polymer is dissolved in a suitable water immiscible solvent and the drug is dispersed or dissolved in this polymeric solution. The resultant solution is then emulsified in an aqueous phase to form droplets. The emulsion is continuously stirred and heated (at a fixed temperature) to remove the organic solvent for evaporation. At the end, microspheres can be recovered as a cake. This technique, however, generally provide limited control over the particles size and particle size distribution. Furthermore, to reduce the residual organic solvent, many downstream processes, such as additional drying step, have to be performed (O'Donnell and McGinity, 1997).

1.1.2 Supercritical techniques

Conventional micronization processes reported show several drawbacks: high process temperatures, possible degradation of the active product due to mechanical and thermal stresses, production of irregular particles with broad PSD, low encapsulation efficiencies, large use of heavy and toxic organic solvents with further treatments required to reduce solvent residues below the safety limits. Furthermore, some molecules are often difficult to be processed using conventional techniques, due to their high crystallization rates or fast tendency to agglomerate (Martín and Cocero, 2008). Supercritical fluids (SCFs) based processes for the precipitation of pharmaceutical and natural compounds have demonstrated to be a valid alternative to traditional processes, given the SCFs hybrid liquid-like gas-like properties: very fast mass transfer, near zero surface tension and effective solvents elimination. Therefore, SCFs technologies can play a relevant role in micronization and coprecipitation fields. The most commonly used supercritical fluid is carbon dioxide thanks to the more accessible critical point ($P_c=73.8$ bar and $T_c=304.25$ K), furthermore it is non-combustible, non-toxic, ecofriendly and cheap; it is also easily available as it occurs naturally as well as being the by-product of many industrial processes.

These techniques can be classified according to the role of SCF in the process: solvent (RESS, PGSS, RESOLV), solute (SAA) and anti-solvent (SAS, ASES, SEDS, GAS) (Martín and Cocero, 2008, Campardelli et al., 2015, Reverchon and Adami, 2006, Reverchon et al., 2009, Fahim et al., 2014).

Precipitation from Gas Saturated Solution

In this process, well known as PGSS, the supercritical fluid is dissolved in a melted solute to create a saturated solution that is then expanded to atmospheric pressure. This expansion causes a fast release of the dissolved gas producing a fast solidification of the solute in form of particles avoiding the use of organic solvents. In order to apply this technology, solids have to be immiscible in the supercritical fluid and no thermal sensitive (Martín and Cocero, 2008, Reverchon et al., 2009).

Rapid Expansion of Supercritical Solution

This process, well known as RESS, consists of the saturation of the supercritical fluid with a solid solute; then, this solution is sprayed through a heated injector into a low pressure vessel producing a rapid nucleation of the substrate in form of very small particles that are collected from the gaseous stream. Depending of process parameters, such as temperature, pressure drop, type of nozzle etc., different kind of morphology can be obtained.

When the supercritical solution is expanded directly in a liquid, the process is named RESOLV. These processes show some drawbacks: difficulty in controlling the particle size of the precipitates, possible coalescence of particles produced. However, the main limitation is that the application of this technique requires high solubility of the compound in the supercritical fluid to be processed (Martín and Cocero, 2008, Campardelli et al., 2015).

Supercritical Emulsion Extraction

This technique, well known as SEE, uses supercritical fluid for the extraction of the organic phase from a single or double emulsion producing nano and microparticles and microcapsules. A solute is dissolved in a suitable solvent to form a solution; the solution is then dispersed into an immiscible or partially miscible liquid to form an emulsion. Extracting selectively the solvent from the oil phase of the emulsion, the SEE process produces an aqueous colloidal suspension of particles. SC-CO₂ extraction has a relatively faster extraction rate compared to extraction rates of other conventional techniques (processing in minutes instead of several hours), and this allows the formation of relatively smaller particles, with narrow size distributions, and very small solvent residues. SEE process has been applied to produce nanocarriers, such as polycaprolactone, poly(L-lactide) and polylactic-co-glycolic acid, but, also, to prepare particles encapsulating magnetite, proteins, peptides and drugs (Campardelli et al., 2015, Reverchon et al., 2015, Reverchon et al., 2009).

Supercritical Antisolvent precipitation

The Supercritical Anti-solvent (SAS) has been proposed using various acronyms (SEDS, ASES); but, the process is substantially the same in all cases. In SAS, the supercritical fluid is used as an anti-solvent that causes the precipitation of the solute in a liquid solvent in form of empty shells (balloons), micro and nanoparticles depending of the operating conditions investigated. The key phenomena of SAS process are the jet break-up at the exit of the nozzle, the high-pressure vapor-liquid equilibrium and mass transfer in and out of the droplet. If the precipitation occurs from a supercritical phase, nanoparticles are obtained since droplets do not form and the material precipitates from the gas. In subcritical single-phase conditions, the droplets are formed and the competition between surface tension and jet break-up is responsible of the process evolution. The droplet expansion followed by the solute precipitation leads to the production of empty particles (ballons). At intermediate conditions (near critical critical point), microparticles can be produced (Campardelli et al., 2015, Reverchon et al., 2015).

Supercritical Assisted Liposome formation

The Supercritical Assisted Liposome formation (SuperLip) has used to create lipid nanovesicles, starting from the production of water nanodroplets and, then, nanosomes are formed around them. For this reason, the process consists of a first step of atomization of water based solutions directly in a supercritical solution in which phospholipids are dissolved. Then generally, ethanol is added to increase solubility of phospholipids in SC-CO₂. Since micelle formation is a fast and spontaneous process, the lipids contained in the expanded liquid formed tend to organize themselves in a layer around the water nanodroplets. Studies have demonstrated that different drugs and antioxidants can be encapsulated with efficiencies around 80% (Campardelli et al., 2015).

I.2 Supercritical Assisted Atomization

SAA technique is a micronization process patented by Reverchon (Reverchon, 2002) in 2002, in which the supercritical fluid is used as an atomizing medium enhancing the atomization process. The process is based on the solubilization of the SC-CO₂ in a liquid solution, where one/or more compounds to be micronized are previously dissolved, forming an expanded liquid in a saturator. The subsequent atomization of this expanded liquid through a thin wall nozzle allows the production of droplets smaller than those produced using traditional similar micronization techniques and, after drying, smaller particles (Reverchon, 2002). The typical solvents used in this process are water and organic solvents, such as ethanol, methanol, and acetone. The possibility to use water as solvent makes the process clearly environmental friendly. SAA process allows obtaining microparticles and sub-microparticles ranging between 0.2 and 5 μm , with narrow particle size distribution and no residual solvent. Moreover, composite systems formed by two or more compounds can be produced with high loading efficiencies.

I.2.1 Apparatus

The homemade equipment used for the experimentation is shown in Figure I.1a, whereas the GMP industrial plant owned by Cerbios Pharma is reported in Figure I.1b.

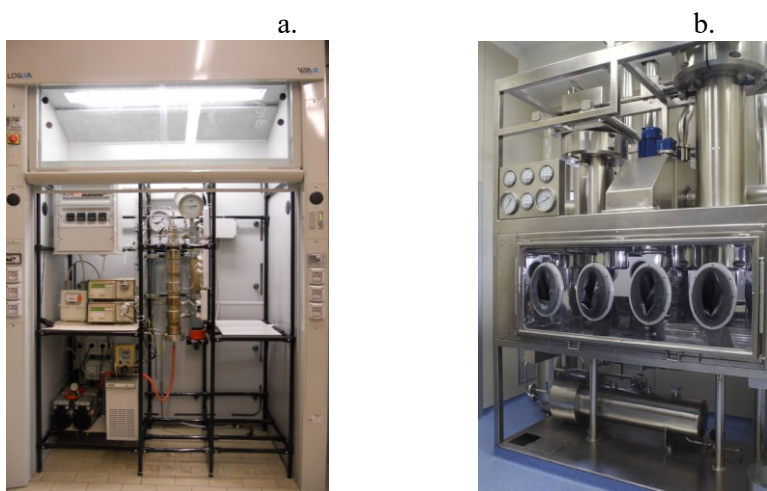


Figure I.1 a) SAA plant in laboratory T8 at UNISA; b) GMP industrial plant (Cerbios Pharma, Lugano).

In Figure I.2, a scheme of the SAA laboratory plant used for the experiments is reported.

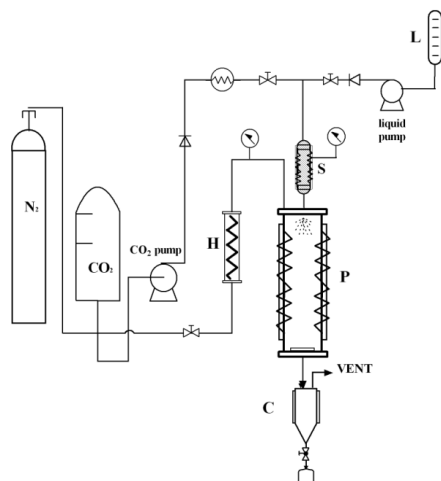


Figure I.2 Schematic representation of a SAA apparatus. *S*, saturator; *P*, precipitator; *H*, heat exchanger; *C*, liquid condenser.

SAA plant consists of two high-pressure pumps (mod. 305, Gilson) delivering liquid solution and CO₂ to the saturator. The saturator is a high-pressure vessel (50 cm³ internal volume) loaded with stainless steel perforated saddles, that assures a large contact surface between the liquid solution and CO₂. The expanded liquid obtained in the saturator is sprayed through a thin wall injection nozzle (80 μm internal diameter) into the precipitator (3 dm³ internal volume). A controlled flow of N₂ is taken from a cylinder, heated in an electric heat exchanger (mod. CBEN 24G6, Watlow) and sent to the precipitator to induce droplets evaporation. The saturator and the precipitator are electrically heated using thin band heaters (Watlow, mod. STB3EA10). A stainless steel filter, located at the bottom of the precipitator, allows powder collection and the gaseous stream flow out. A condenser that separates liquids from the gas stream completes the system.

I.2.2 Process parameters

The process parameters influencing the efficiency of the atomization process, the particle size (PS) and particle size distribution (PSD) are:

- ❖ the mass flow ratio (GLR) between CO₂ and liquid solution,
- ❖ the operating pressure (P_{mix}) and temperature (T_s) in the saturator,
- ❖ the solute concentration in the liquid solution (C),
- ❖ the temperature in the precipitator (T_p),
- ❖ the nozzle diameter,
- ❖ the active principle/carrier ratio in the liquid solution.

The operating conditions are selected considering the binary vapor-liquid equilibrium (VLE) diagram solvent-CO₂. The molar fraction of CO₂, the temperature and the pressure selected at the saturator ensure large CO₂ solubility in the liquid. The solubilization of CO₂ in the liquid solution reduces the viscosity and the surface tension allowing an increased jet breakup efficiency and, hence, a more effective atomization. In particular, CO₂ shows good solubility in solvents like ethanol, therefore, it is possible to operate in the one-phase region in the saturator. Whereas CO₂ is not completely soluble in water and, in this case, a discontinuous region is formed. The no dissolved CO₂ reduces the section for the passage of the liquid improving the efficacy of the atomization. Therefore, the particles obtained in ethanol are smaller than those produced using water as solvent, since the largest decrease of cohesive forces due to the viscosity and the surface tension (Caputo et al., 2012). The SAA literature has demonstrated the key role of dissolved CO₂ in reducing the cohesive forces that have the most influence on particle size (Liparoti et al., 2015). Therefore, the atomization strongly depends on the GLR. At low value of GLR (lower than 2) larger droplets are obtained, whereas at higher GLR droplets size rapidly decreases. For GLR values higher than 3, the droplets size is not more sensitive to further increments.

Moreover, the droplet sizes slightly decrease with a decrease in injector diameter (Caputo et al., 2012, Adami et al., 2013). However, the particle size is also influenced by the solute concentration; larger particles are produced when high solute concentrations are processed. Typically, this effect can be related to the increase of viscosity of the starting solution due to a higher concentration. Since viscosity is a cohesive force, its increase tends to produce larger droplets below the nozzle and an overall result of enlargement of particle size (Reverchon and Antonacci, 2007b).

The injection of the solution (solvent+solute+SC-CO₂) through the nozzle allows the formation of the droplets that are dried in the precipitation vessel. After the formation of the droplets, the drying of the solvent takes place thanks to the nitrogen flow (N₂). It is possible to apply the theory proposed by Vicente and Vehring (Vehring, 2008, Vicente et al., 2013) on the drying process in the spray drying. The evaporation of the droplets involves mass and heat transfer mechanisms, influenced by the drying temperature and the solute concentration. During drying, the precipitation of the solid starts from the droplet surface and a thin layer is formed through which the solvent can diffuse. If this diffusion is fast (when high temperatures are used), particles with internal void space can be obtained; these thin layers can be sometimes fragile, depending on the material, and the particles can collapse (*shrinking effect*). When the drying is not too fast, the solutes tend to precipitate homogeneously inside the droplets and the produced particles show no void spaces (Vehring, 2008, Vicente et al., 2013).

The nitrogen flow and the temperature fixed in the precipitator do not affect the atomization process in the nozzle. However, these two parameters can influence the spray shape, removing the solvent and avoiding the recondensation of the liquid in the precipitator. The particle sizes can be influenced by the temperature in the precipitator because of the *shrinking effect* above mentioned.

Furthermore, the presence of the solutes could modify the VLE diagram solvent-CO₂; consequently, there will be the possibility that the solutes could precipitate in the saturator because of the *anti-solvent effect*. The *anti-solvent effect* occurs when the solvent, in which the compound to be micronized is solubilized, has very high solubility in SC-CO₂. Consequently, when the solute reaches the supersaturation in the mixture liquid solvent- SC-CO₂, it is possible to observe an undesired precipitation of the compound on the packings in the saturator. This condition must be avoided in order to have a successful SAA micronization or coprecipitation (Reverchon et al., 2009).

1.2.3 State of the Art of SAA process

Micronization

Different kinds of materials have been successfully micronized by SAA, such as pharmaceutical compounds, superconductors and catalyst precursors, dyes, polymers, enzymes, etc (Della Porta et al., 2006, Reverchon, 2002, Reverchon and Adami, 2006, Reverchon et al., 2005, Reverchon and Antonacci, 2006b, Reverchon and Della Porta, 2003, Wu et al., 2015, Wu and Yang, 2011, Wu et al., 2014).

Among polymers processed by SAA process, Reverchon and Antonacci (Reverchon and Antonacci, 2007b) micronized polymethylmethacrylate (PMMA) and poly-L-lactide (PLLA) testing the effect of process parameters (such as GLR, precipitation temperature and solute concentration). PMMA and PLLA size-controlled microparticles were produced ranging between 0.05 and 1.6 μm and between 0.1 and 3.5 μm , respectively. Particle size distribution of PMMA and PLLA microparticles showed a dependence on the GLR and the solute concentration. Increasing the GLR, smaller polymer particles were produced; whereas, an increase of the solute concentration produced larger particles due to an increase of viscosity and surface tension of the liquid solution processed. Also Wu and Yang (Wu and Yang, 2011) processed PMMA in order to prepare nanoparticles (mean diameters of about 250 nm) using acetone as solvent. The hydroxypropyl methylcellulose (HPMC) was micronized using water as solvent; particles produced were spherical and well-defined. A significant increase in particles size was observed when C varied from 0.5 to 5 mg/mL, with particles ranging between 0.1 and 1 μm at C=0.5 μm and between 0.3 and 3 μm at C=5

mg/mL. A less marked increase in particle size was obtained increasing C up to 10 mg/mL; in this case, indeed, the larger particles are collapsed losing the spherical shape (Reverchon et al., 2008). Chitosan in 1% acetic acid aqueous solutions was successfully micronized producing non-coalescing spherical microparticles with diameters ranging between 0.1 and 1.5 μm . A decrease in chitosan crystallinity was observed when higher precipitation temperatures were used (Reverchon and Antonacci, 2006a). Also Wu et al. (Wu et al., 2015) studied the SAA micronization of chitosan hydrochloride using 50% (v/v) ethanol aqueous solution as the solvent. Produced particles were regular and spherical varying chitosan concentration from 1 and 7 mg/mL with diameters lower than 1 μm . Liparoti et al. (Liparoti et al., 2015) studied the influence of the solvent and process parameters, such as temperature and pressure inside the saturator, on the micronization of polyvinylpyrrolidone (PVP) using SAA. Spherical and non-coalescing PVP microparticles were produced using different kind of solvents: ethanol, water, and mixture water–acetone. The experimental evidences demonstrated that the amount of solubilized CO_2 is one of the main factor that influences the particle size distribution. The smallest PVP particles were obtained when ethanol was used as solvent and they showed a mean diameter of 0.5 μm and a standard deviation of 0.2 μm (Liparoti et al., 2015).

Adami and Reverchon (Adami and Reverchon, 2012) investigated the application of SAA process to the formation of polymer microparticles loaded with magnetite nanoparticles, starting from suspensions of nanoparticles in polymer–solvent solutions. Dextran and chitosan were used as dispersing matrix. The encapsulation in a polymeric coating makes the nanoparticles biocompatible. Nanostructured chitosan microspheres were successfully obtained, with mean diameters ranging between 1.2 and 2 μm and with nanoparticle loading up to 24.4% w/w (nanoparticles/polymer).

SAA was used to micronize also pharmaceutical compounds, such as griseofulvin (GF) using acetone as solvent. GF spherical particles with mean diameters ranging from 0.5 to 2.5 μm were produced with crystalline nature. No drug degradation was observed after SAA process and a solvent residue less than 800 ppm was measured. Dissolution tests demonstrated that SAA GF showed a faster dissolution rates compared to GF particles obtained by jet milling technique (Reverchon et al., 2004). Ampicillin particles suitable for aerosol delivery in the size range 1–5 μm were obtained using buffered water by SAA process (Reverchon et al., 2003). Tetracycline and rifampicin microparticles were produced using water and methanol as solvent, respectively. Spherical particles with controlled particle size ranging between 0.5 and 3 μm were obtained for both drugs operating at 97 bar and 85°C in the saturator and at 60 °C in the precipitator. The X-ray traces revealed that all the SAA micronized powders were amorphous whereas the untreated material were crystalline (Reverchon and Della Porta, 2003). SAA process was used to micronize also Erythromycin using different solvents.

Spherical micrometric and non-coalescing particles of the drug were obtained with diameters smaller than 3 μm using methanol and ethanol. No degradation of SAA erythromycin and a maximum solvent residue in the processed material of 90 ppb were obtained (Reverchon and Spada, 2004b). Dexamethasone and dexamethasone acetate microparticles were obtained using SAA technique by Della Porta et al. (Della Porta et al., 2006). Spherical corticosteroid particles with mean diameters ranging from 0.5 to 1.2 μm were produced with no drug degradation and solvent residues of 300 and 500 ppm for acetone and methanol, respectively. SAA-glucocorticoids retained the activity of the untreated compounds and, particularly in the case of dexamethasone, SAA processing improved drug performance (Della Porta et al., 2006). Cromolyn sodium (CS) micrometric particles for aerosol delivery were micronized using SAA technique. The CS particles obtained were spherical, with a volumetric percentage of particles with a diameter ranging between 1 and 5 μm of 50% to 66%. The micronized product was stable after 12 months of storage, and no modifications in structure, morphology, or crystallinity were detected (Reverchon et al., 2007). Beclomethasone dipropionate (BDP) was micronized by SAA using methanol, acetone, acetone + water 9% v/v, and methanol + water 4% v/v as liquid solvents. Particles with narrow size distributions (PSD) were obtained by changing the SAA process operating conditions. In particular, using acetone + water 9% v/v with a BDP concentration of 90 mg/mL, crystalline particles ranging between 0.2 and 4.7 μm were produced and 70% by volume of these particles ranged between 1 and 3 μm . The results obtained on the laboratory scale plant were successfully reproduced on a pilot plant and a further refinement of the operating conditions was performed. About 30 g of BDP microparticles were produced per batch and a recovery of about 93 w % of the micronized powder with respect to the injected quantity was obtained (Reverchon et al., 2010). Reverchon et al. (Reverchon et al., 2015) tested SAA process in the attempt of reducing palmitoylethanolamide (PEA) particle size and crystallization. The best results in terms of powder morphology were obtained using ethanol and isopropanol as liquid solvent; but, irregular particles were produced in the micrometric range, due to the high PEA tendency to crystallize forming flat particles (Reverchon et al., 2015).

SAA technique was performed to produce lysozyme microparticles by Adami et al. (Adami et al., 2009) using water, buffered water at pH 6.2 and water-ethanol mixtures at different volume percentages. Precipitated lysozyme particles were spherical, with a narrow particle size distribution ranging between 0.1 and 4 μm . No degradation and lysozyme activity were verified; depending on the process conditions, lysozyme retained from 95% to 100% of the biological activity compared to the untreated enzyme.

Composite systems by SAA coprecipitation

SAA was proposed to produce HPMC based composite microparticles using ampicillin trihydrate as model drug (Reverchon et al., 2008). Amorphous and spherical or “doughnut-like” HPMC-drug microparticles with particle sizes ranging between 0.05 and 5.45 μm were produced. Ampicillin was released in more than 72 h from tablet formulation based on HPMP-drug particle allowing a slower drug release compared to the untreated material (Reverchon et al., 2008). Ampicillin trihydrate and chitosan were selected as model drug and carrier, respectively, and 1% v/v acetic acid aqueous solution was used as solvent, to produce a drug-prolonged delivery system using SAA by Reverchon and Antonacci (Reverchon and Antonacci, 2007a). Non-coalescing and spherical microparticles formed by chitosan-ampicillin were produced with sharp particle distribution (diameters ranging between about 0.1 and 6 μm). A prolonged release from SAA coprecipitates with respect to raw drug and physical mixtures of chitosan and ampicillin was obtained; moreover, the polymer/drug ratio revealed to be a controlling parameter for drug release (Reverchon and Antonacci, 2007a). Della Porta et al. (Della Porta et al., 2010) produced bovine serum albumin (BSA) microspheres charged with Gentamicin sulfate (GS). SAA precipitation temperature was selected in the range 100-130°C to generate protein coagulation and to recover micronized BSA in form of hydrophobic aggregates with GS encapsulation efficiency in SAA powders reached 100%. In all cases, spherical and non-coalescing particles were successfully produced with a mean particle size of 2 μm . The release profiles of the entrapped drug were monitored using Franz cells to evaluate the possible application of the produced microspheres in wound dressing formulations. Particularly, the microspheres with a BSA/GS ratio of 4:1 after the first burst effect (of 40% of GS loaded) were able to release the GS continuously over 10 days. Aquino et al. (Aquino et al., 2013) proposed SAA process for the production of topic carrier microsystems based on alginate-pectin blends. GS was loaded as high soluble and hygroscopic antibiotic. The micronized particles showed spherical shape and narrow particle size distribution (mean diameter about 2 μm). GS loading efficiencies were up to 100% with a burst release of 6 h followed by a GS release continuous for 6 days. De Cicco et al. (De Cicco et al., 2014) used SAA process to prepare microparticulate carriers based on high-mannuronic alginate and amidated pectin blend loaded with GS, able to move rapidly from dry to soft hydrogel. Particles with very high loading efficiencies (up to 100%) and small diameters (less than 2 μm) were obtained. Release tests demonstrated a first burst release of GS followed by prolonged release up to 10 days. Reverchon and Adami (Reverchon and Adami, 2013) produced coprecipitates formed by hydroxyapatite nanometric particles and chitosan by SAA process. The best operating conditions for particle diameter and coprecipitate stability were: precipitation temperature 110 °C, chitosan

concentration in the starting solution 10 mg/mL, that produced spherical composite microparticles with a mean diameter of 0.6 μm and a loading efficiency of about 91%. Liparoti et al. (Liparoti et al., 2013) produced SAA coprecipitates dispersing a corticosteroid (dexamethasone) in a PVP matrix with the aim to enhance the dissolution rate of the drug. The experiments were performed using ethanol as solvent, operating at 40°C and 76 bar in the saturator and 70°C and 1.6 bar in the precipitator. Produced composite particles were amorphous and showed a regular, spherical shape and a mean diameter ranging from about 0.8 to 1 μm , with loading efficiencies up to 95%. Dissolution analyses demonstrated that microparticles show a higher dissolution rate compared to the untreated drug (Liparoti et al., 2013). Nanostructured microparticles of BSA loaded with lincomycin hydrochloride (lincoHCl) were prepared by Adami et al. (Adami et al., 2017b). SAA precipitation temperature was set as 100°C to obtain BSA coagulation and efficient entrapping of lincoHCl. Spherical microparticles showed no coalescence and were produced in all cases studied, with a mean particle size in the range 1–2 μm and loading efficiencies between 87 and 90%. The microspheres produced by SAA showed a controlled release of the drug over about 6 days.

Aliakbarian et al. (Aliakbarian et al., 2017) proposed for the first time the application of SAA process for the encapsulation of phenolic compounds extracted from olive pomace in maltodextrins. Spherical particles with average diameter of 712 nm with high total polyphenol content (105.0 ± 0.1 mg of caffeic acid equivalent/g dry powder) and antiradical power (98.8 ± 3.0 mg of DPPH/ mL of extract) were obtained (Aliakbarian et al., 2017).

Modification of SAA apparatus

Cai et al. (Cai et al., 2008) introduced a hydrodynamic cavitation mixer (HCM) in SAA process (SAA-HCM) to improve mass transfer. Levofloxacin hydrochloride was selected as a model drug to investigate the effects of cavitation generator on morphology, size and distribution of precipitated particles. Spherical and amorphous microparticles were obtained with diameters smaller than 2.1 μm . Wang et al. (Wang et al., 2010) investigated the same technique to produce sodium cellulose sulfate (NaCS) microparticles. Spherical NaCS particles with mean diameters ranging from 0.3 to 3.0 μm were produced. No changes in the primary structure and stability of the NaCS processed by SAA-HCM were verified by Fourier transform infrared spectroscopy, whereas X-ray and thermo-gravimetric analyses demonstrated a slight change in crystalline state with higher thermal stability. Using the same process, insulin microparticles were produced from acidic solution with mean diameters increasing from 1.4 μm to 2.7 μm when protein concentration increased from 3 g/L to 50 g/L. HPLC chromatograms showed no degradation of insulin after SAA-HCM

processing (Du et al., 2013). Shen et al. (Shen et al., 2014) used SAA-HCM to prepare chitosan microparticles with diameters ranging between 0.2 and 5 μm . Analyses demonstrated a decrease in crystallinity and no changes of the original structure of polymer. Furthermore, Shen et al. (Shen et al., 2015) studied the micronization of trypsin and the production of chitosan-trypsin particles from aqueous solutions. Various morphologies were found for precipitated trypsin particles (spherical and pseudo-spherical, deflated particles) with diameter ranging between 0.2 and 4 μm . Looking at the coprecipitation of trypsin with chitosan, amorphous, non-coalescing and spherical composite microparticles with particle sizes ranging between 0.2 and 3 μm and loading efficiencies up to 90% were obtained (Shen et al., 2015). SAA-HCM was also used to prepare BSA microparticles using water as solvent by Wang et al. (Wang et al., 2011). Under the different conditions investigated, the prepared BSA particles showed various morphologies, such as corrugated particles, smooth hollow spherical particles and cup particles, with particle diameters ranging from 0.3 to 5 μm .

In order to improve the processability of the thermolable compounds such as BSA, Adami et al. (Adami et al., 2011) proposed a modified process configuration of SAA apparatus to operate the precipitation process below the atmospheric pressure, and to perform the drying process at lower temperatures without any damage to thermal sensitive materials. Two model thermolable compounds were investigated: PLLA and BSA producing well-defined spherical particles. PLLA microparticles coalescence was avoided using a precipitation pressure from 0.65 to 0.5 bar producing particles with a mean diameter between 1 and 1.5 μm , and a standard deviation of about 0.4. BSA spherical particles with a mean diameter of about 1 μm , and a standard deviation of about 0.7, were obtained operating at 0.8 bar in the precipitator. Fourier transform infrared analysis on BSA microparticles revealed that no modification on protein secondary structure took place during SAA process, thus, protein denaturation was avoided. In this new SAA arrangement, also two types of polyethylene glycol (PEG10000 and PEG6000, thermo-sensitive polymers) were micronized at reduced pressure and precipitation temperatures as low as 5°C. When PEG6000 was processed particles tended to collapse; however, when PEG10000 was processed spherical and not aggregated particles were obtained with mean diameters ranging between 2 and 3.3 μm and characterized by sharp particle size distribution. X-ray powder diffraction analysis showed that SAA processed PEG retained the same crystalline structure of the unprocessed material (Liparoti et al., 2012). Also well-defined and sub-microparticles of PEG-PLA copolymers were produced using SAA under reduced pressure by Adami et al. (Adami et al., 2012). The microparticles obtained showed a lower degree of crystallinity compared to the untreated materials, with no modifications of the original structures (Adami et al., 2012). This SAA configuration was successfully used also for the encapsulation of rotenone in different carriers (PEG, PVP

and sodium alginate) (Martin et al., 2013). The best results, in terms of encapsulation efficiency, were obtained for the system alginate/rotenone (close to 100%) and for the system PEG/rotenone (98%). PVP-rotenone composite microparticles showed the lowest coprecipitation efficiency ranged between 30% and 50%. The particles obtained were spherical with the mean diameters ranging between 0.6 and 1.5 μm (Martin et al., 2013). Labuschagne et al. (Labuschagne et al., 2014) used the same technique for the coprecipitation of poly(D,L-lactide) (PDLLA) and rifampicin for sustained release applications. Spherical PDLLA/rifampicin nanoparticles with mean diameter ranging from 123 to 148 nm and with rifampicin loadings up to 50.5% were produced. X-ray diffraction revealed that the encapsulated rifampicin is in an amorphous state, while NMR spectra indicated no structural modifications after SAA process. In-vitro release studies showed an initial burst release of 80–87% of total rifampicin loaded, necessary to suppress the generation of resistance by the microorganism, followed by first-order sustained release between 0.4 and 0.8 mg/L rifampicin per day over a period of 17 days (Labuschagne et al., 2014).

Hijazi et al. (Hijazi et al., 2014) proposed a SC-CO₂ assisted solubilization and atomization process (SCASA) that did not use any organic solvent. In the process, the acidifying strength of pressurized CO₂ enabled the dissolution of chitosan, and the atomization process generated spherical chitosan particles (Hijazi et al., 2014).

Chapter II

Analytical methods

II.1 Analyses on morphology

II.1.1 Field Emission Scanning Electron Microscope

The morphology of the powder was observed by a field emission-scanning electron microscope (FESEM, mod. LEO 1525, Carl Zeiss SMT AG). SAA powders were dispersed on a carbon tab previously stuck to an aluminum stub (Agar Scientific, Stansted) and coated with gold (layer thickness 250Å) using a sputter coater (mod. B7341, Agar Scientific Stansted). Approximate composition of particles was observed using FESEM coupled with an energy dispersive X-ray spectroscopy (EDX, INCA Energy 350).

II.1.2 Fluorescent microscope

Fluorescent microscopy (FM) were performed to analyze produced powders with a Zeiss Axiophot fluorescence microscope, equipped with a 20×1.4 NA no-oil immersion plan Apochroma objective (Carl Zeiss Vision, München-Hallbergmoos). DAPI (4', 6-diamidino-2-phenylindole) optics absorbing violet radiation (λ_{\max} 372 nm) and emitting a blue fluorescence (λ_{\max} 456 nm) was used.

II.2 Particle size distribution (PSD)

PSD was calculated also by FESEM photomicrographs using Sigma Scan Pro Software (release 5.0 Aspire Software international, Ashburn, VA, USA). The diameters of about 1000 particles were measured for each particle size distribution calculation. The obtained histograms represented the particle size distribution and were fitted using Microcal Origin Software to compare well the results (release 8.0, Microcal Software, Inc.,

Northampton, MA). PSDs values are expressed as d_{10} , d_{50} and d_{90} indicating the diameters at 10th, 50th and 90th percentile; these percentiles indicate the amount of particles with diameters smaller than d_{10} , d_{50} and d_{90} .

II.3 Analyses on solid state

II.3.1 Differential Scanning Calorimetry

The thermal behavior of powders was measured by a Differential Scanning Calorimeter (DSC, model TC11, Mettler Toledo, Inc., Columbus, USA), using Mettler STARe system. Fusion temperature and enthalpy were calibrated with an indium standard (melting point, 156.6°C, enthalpy of fusion 28.52 J/g). 3 mg of the sample were accurately weighed, crimped into an aluminum pan that was heated from 25 to 350°C under a nitrogen purge (flow rate 50 mL/min), at 10°C/min.

II.3.2 X-Ray Diffraction

Solid state analysis of the samples (XRPD=X-ray powder diffraction) was performed using an X-ray diffractometer (mod. D8 Discover, Bruker AXS, Inc., Madison, WI) with a Cu sealed tube source. Samples were placed in the holder and flattened with a glass slide, to assure a good surface texture. The measuring conditions were as follows: Ni-filtered CuK α radiation, $\lambda=1.54$ Å, 2θ angle ranging from 3 to 50° with a scan rate of 3 s/step and a step size of 0.02°.

II.3.3 Fourier Transform Infrared (FTIR)

The measurement of FTIR spectra was carried out with a FTIR spectrophotometer (IR-Tracer100, Shimadzu). The powder samples were ground and mixed thoroughly with small amount of potassium bromide (KBr) and pressed to 10 tons for 10 minutes in a manual press. The scan analysis was performed at 25°C, in a scan wavenumber ranging between 4000 and 450 cm^{-1} at a resolution of 1 cm^{-1} ; 32 scan signals were averaged to reduce the noise of measurements.

II.4 Loading efficiency and dissolution tests

II.4.1 Spectrophotometer UV-vis

Active principle (API) loading in SAA particles was evaluated by UV-vis spectrophotometer (model Cary 50, Varian, Palo Alto, CA), measuring the

absorbance in correspondence of API characteristic wavelength. The carriers used for SAA coprecipitation experiments is not visible at these wavelengths by spectrophotometer. Then the absorbance was converted into API concentration, using a calibration curve. Each analysis was performed in triplicate and the results were expressed as the mean value. The loading efficiency is calculated as the ratio of the effective loading to the theoretical loading. The theoretical loading is the mass ratio of active principle/carrier (w/w) in the solution injected into the SAA plant. The effective loading is the actual mass ratio of active principle/carrier (w/w) in the SAA particles.

The same instrument was used to perform *in vitro* dissolution tests in order to study the properties of SAA microparticles as drug delivery system. API release experiments were conducted in a 0.1 M Phosphate Buffer Solution (PBS) at pH 7.4, as dissolution medium. Accurately weighted samples containing an equivalent amount of drug (5 mg/L) were suspended in 1.5 mL of PBS and placed into a dialysis membrane that was immersed in 400 mL of PBS continuously stirred at 200 rpm and 37°C. Each dissolution test was carried out in triplicate and the proposed dissolution curves are the mean profiles.

II.4.2 High Performance Liquid Chromatography

The separation and the identification of extracted compounds from saffron petals was performed in an Agilent HPLC-UV/vis (High Performance Liquid Chromatography, Hewlett-Packard model G131-132). The column used is a reverse phase C₁₈ column (4.6 mm x 100 mm, 3.5 μm). The eluents were: 0.1% (v/v) formic acid in water (A) and 0.1% (v/v) formic acid in methanol (B) with the following gradient: 20% B, 1 min; 80% B, 13 min; and 20% B, 20 min. The flow rate was 0.8 mL/min and the detector was set at 270 nm. All of the analyses were performed in duplicate.

II.5 Antioxidant activity

II.5.1 DPPH method

DPPH[•] (2,2-diphenyl-1-picrylhydrazyl) is a stable free radical that assumes a purple color in solution, with an absorption band around 517 nm. When this radical reacts with a hydrogen donor, the reduced form of DPPH is formed and a discoloration of the violet color is obtained. The spectrophotometric method described in literature (Brand-Williams et al., 1995) with minor modifications was used to study the reduction of DPPH and, hence, the antioxidant capacity. 1 mL of the tested sample at a fixed concentration was placed in 3 mL of 10⁻⁴ M of DPPH solution (9.9 mg of DPPH in 250 mL of MeOH) and left under dark at room temperature. The

discoloration of the solutions from purple to yellow is clearly visible and the absorbance reduction was measured at 517 nm using an UV/vis spectrophotometer (model Cary 50, Varian). The scavenging activity (SA, %) was expressed according to the equation:

$$SA = (1 - A_s/A_b) * 100 \quad (2)$$

where:

- A_s : sample absorbance;
- A_b : blank absorbance.

The antioxidant capacity were also expressed in terms of Trolox equivalent (TE) by gram of powder, where higher value means higher antioxidant power.

II.5.2 Total polyphenol content

Total phenolic content was determined in triplicate with the Folin Ciocalteu method, as described by Singleton and Rossi (Singleton and Rossi, 1965) with minor modifications. Approximately 10 mg of each propolis powder sample was dissolved in 5 mL of ethanol (70% v/v), an aliquot of 100 μ L of this solution was mixed with 4900 μ L of distilled water, 0.5 mL of the Folin Ciocalteu reagent and 1700 μ L of a 20% carbonate solution (prepared 24 h before). The mixture was filled with distilled water to a 10 mL graduated volumetric flask, shaken for 30 min under dark, and then transferred 225 μ L to a 96-well microplate for the determination of its absorbance in a Tecan (Infinite PRO200R) microplate reader at 760 nm. Calibration was performed using Gallic Acid as reference compound and the results were expressed in mg of Gallic Acid Equivalents (GAE) per gram of powder.

II.6 Synthesis of FITC-labeled dextran

In a 50 mL reaction flask, FITC (9.2×10^{-5} mol) and N,N'-carbonyldiimidazole (9.2×10^{-5} mol) were dissolved in 15 mL of THF and stirred at room temperature under N_2 atmosphere over night. Then, 1 g of DEX (43 kDa, 2.33×10^{-5} mol) and 1.38 mL of triethylamine (9.95×10^{-6} mol) were added, and the reaction mixture was kept under stirring for 24 h. The product was purified by dialysis against distilled water using a cellulose membrane (cutoff = 6000–8000 g/mol). The solution was lyophilized and an orange solid was recovered (700 mg, 1.63×10^{-5} mol). The content of FITC in the conjugate was measured by UV-vis and the degree of labeling was expressed as the ratio of FITC/DEX molar concentration (labeling 2%).

Chapter III

Pharmaceutical formulations for Cerbios Pharma

III.1 Agreement with Cerbios Pharma

Some active principles have been studied as proposed by Cerbios Pharma within the research project "Production of pharmaceutical formulations for improvement bioavailability using supercritical assisted atomization". The Swiss company Cerbios Pharma funded the research project supporting this Ph.D. work with the aim to invest in a GMP atomization plant for particle engineering using SCFs. As part of the agreement between the company and the Department of Industrial Engineering (DIIN) of the University of Salerno, this part of thesis was focused on the development of formulations based on active principles directly proposed by Cerbios for its world-wide partners, in order to scale up the process for industrialization. This section, due to secrecy agreements, will be presented using acronyms and no further detailed information will be reported.

Investigations and studies were performed on drugs previously tested using traditional techniques by other groups of research with no satisfying results. These drugs were:

- ❖ BRI
- ❖ FUL
- ❖ DAS
- ❖ NAP
- ❖ GPB.

First, for each compound a feasibility study was carried out in order to investigate the applicability of SAA process to different classes of compounds; different solvents and concentrations were investigated. Then, SAA operative conditions was optimized to reach the targets requested by

Cerbios. A series of characterization analyses was performed according to methods suggested by Cerbios Pharma and by our analytical experiences. Finally, grams of powders were produced by SAA and sent to the company for further pharmaceutical considerations.

Materials

Polyvinylpyrrolidone (PVP, Mw: 10,000), dextran from *Leuconostoc mesenteroides* (DEX, average MW 43,000), ethanol (EtOH, purity 99.9%), acetone (Ac, purity 99.8%), tetrahydrofuran (THF, purity >99.9%), dimethyl sulfoxide (DMSO, purity >99.9%), ethyl acetate (AcEt), 1-Methyl-2-pyrrolidinone (NMP, purity 99.5%) were supplied by Sigma Aldrich (Italy). Carbon dioxide (CO₂, 99.9%) was purchased by Morlando Group (Italy) and nitrogen (N₂, 99%) by SOL (Italy).

III.2 Compound #1: BRI

BRI is an alpha adrenergic agonists drug. The objective of this experimentation was to produce BRI crystalline particles, in form of agglomerates with $D_{90} < 1 \mu\text{m}$ and with no residual solvents, thus reaching the desired target for the customers.

III.2.1 Experimental results on BRI

BRI is a crystalline pharmaceutical compound, as shown in Figure III.1, where it is possible to observe long crystals of 30-70 μm . In Table III.1, BRI solubilities in different solvents are summarized.

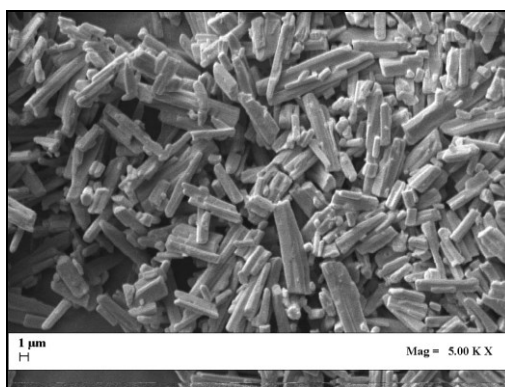
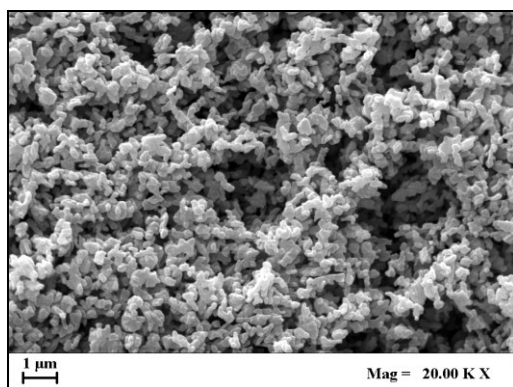


Figure III.1 FESEM image of untreated BRI.

Table III.1 *BRI solubilities in different solvents.*

Solvent	Solubility [mg/mL]
EtOH	0.87
MetOH	0.90
THF	3.00
DMSO	>30

A first set of experiments was performed using methanol as solvent and the process conditions used were: BRI concentration 0.9 mg/mL; GLR of 1.8, injection pressure of 80 bar in the saturator, saturator temperature (T_s) of 60°C and precipitation temperature (T_p) of 70°C. An example of particles obtained is shown in Figure III.2.

**Figure III.2** *FESEM image of SAA BRI powders produced using methanol as solvent at $T_s=60^\circ\text{C}$, $T_p=70^\circ\text{C}$.*

Produced particles were irregular and partly coalescent; moreover, powder collection was very complicated. Therefore, methanol was not a good candidate solvent for this experimentation. Another solvent tested for BRI micronization was THF, in which BRI is soluble up to 3 mg/mL. Operative conditions investigated were: GLR of 1.8 and 2.5, pressure of 80 bar and temperature (T_s) of 60-80°C in the saturator and precipitation temperature (T_p) of 80°C. No powders were collected in these three tests. Ac:DMSO (80:20 v/v), NMP:Ac (80:20 v/v), AcEt:DMSO (80:20 v/v) mixtures were investigated for BRI micronization; however, no satisfactory results were obtained using these mixtures.

BRI micronization was attempted using ethanol as solvent and a drug concentration fixed at 0.87 mg/mL. Trying to take advantage of SAA previous experiences (Liparoti et al., 2015), the process conditions used were: GLR 1.8, injection pressure of 80 bar, saturator (T_s) and precipitation (T_p) temperature varying between 60 and 80°C. Figure III.3 reports some examples of particles obtained at different operating conditions tested.

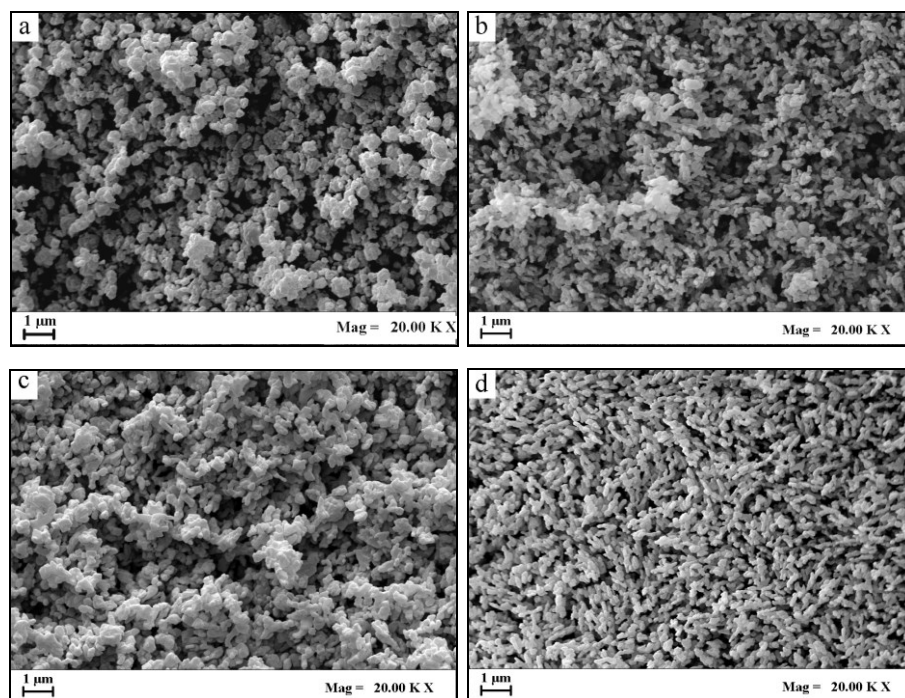


Figure III.3 FESEM images of SAA BRI powders produced at: a) $T_s = T_p = 60^\circ\text{C}$; b) $T_s = 60^\circ\text{C}$, $T_p = 70^\circ\text{C}$; c) $T_s = 60^\circ\text{C}$, $T_p = 80^\circ\text{C}$; d) $T_s = T_p = 80^\circ\text{C}$.

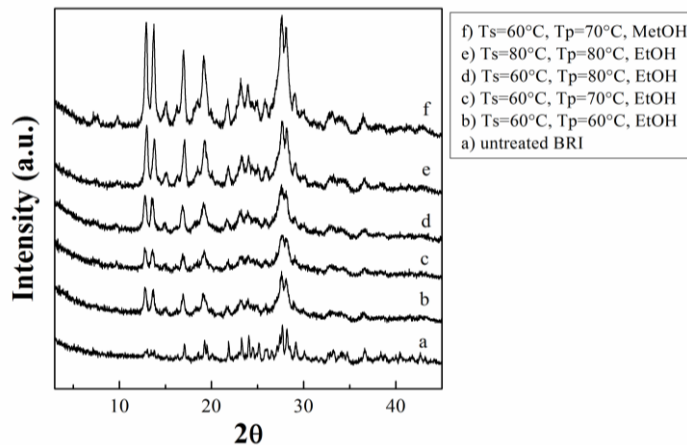
The precipitates were formed by irregular particles; the presence of submicronic/nanometric crystalline particles was evident in all samples, by satisfying the targets of Cerbios Pharma. This is not the typical morphology exhibited by SAA precipitates, which usually show collapsed spherical or spherical particles resulting from droplet evaporation formed during atomization (Liparoti et al., 2015, Adami et al., 2017a, Di Capua et al., 2017b). However, similar morphologies have been observed when a superposition of crystallization processes take place during droplet drying in SAA precipitator (Liparoti et al., 2012, Martin et al., 2013, Reverchon et al., 2005). SAA BRI particles was suspended in heptane and after 10 minutes of sonication analyzed using DLS technique (as indicated by Cerbios). In Table III.2, PSDs values, expressed as d_{10} , d_{50} and d_{90} indicating the diameters at 10th, 50th and 90th percentiles, are reported.

Table III.2 PSD data of BRI particles produced by SAA.

SAA test	d ₁₀ (nm)	d ₅₀ (nm)	d ₉₀ (nm)
T _s =60°C, T _p =60°C	394	672	1036
T _s =60°C, T _p =70°C	162	218	288
T _s =60°C, T _p =80°C	165	204	252
T _s =80°C, T _p =80°C	225	297	396

III.2.2 Characterization of BRI particles

XRPD analyses were carried out to study the crystallization behavior of untreated BRI and SAA powders produced. In Figure III.4, a comparison of spectra obtained on untreated BRI and SAA particles produced at different operative conditions is reported. The analyses showed the crystalline nature of BRI that was preserved also in the micronized particles. These results were confirmed by calorimetry analyses, reported in Figure III.5.

**Figure III.4** XRPD spectra related to SAA particles and untreated BRI.

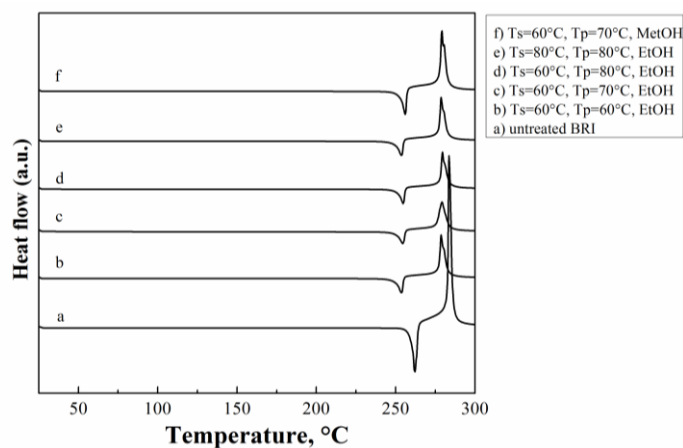


Figure III.5 DSC thermograms related to untreated BRI and SAA particles.

BRI thermogram showed an endothermic peak around 262°C (melting point) and an exothermic peak around 284°C (crystallization temperature). The absence of peaks in the range 80-120°C demonstrated that BRI is not a hygroscopic compound. From all the calorimetric diagrams, it was possible to denote the absence of water in the range 80-110°C. In thermograms related to SAA particles, the characteristic peaks of BRI were confirmed but slightly translated at lower temperatures.

Residual solvent and purity

These analyses were performed to verify the limits requested by customers. Ethanolic samples showed values below 0.04%, whereas methanolic samples did not present residual solvent. Furthermore, SAA process was able to remove all solvent and produced powders preserved BRI purity.

The particles produced satisfied the targets indicated by Cerbios Pharma.

III.3 Compound #2: FUL

FUL is an antiestrogen used to treat the breast cancer in postmenopausal women. The goal to produce sub-microparticles of FUL with mean diameter ranging between 0.3 and 0.7 μm was investigated with the aim to improve its dissolution rate. In literature, only SAS process was used to micronize FUL using DMSO until now; however, no satisfactory results were obtained, as it is possible to observe in Figure III.6.

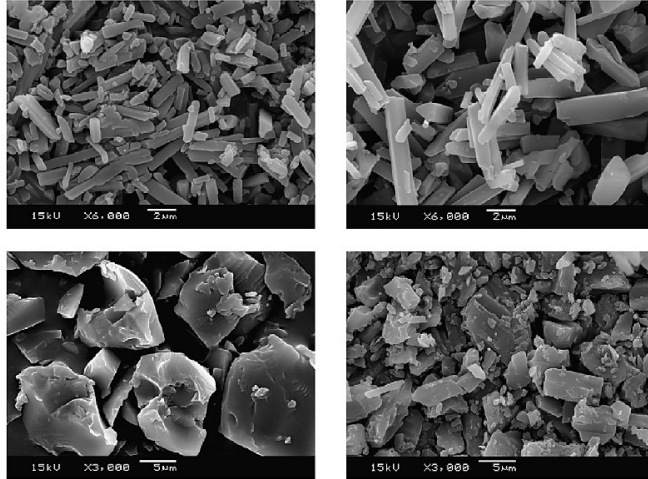


Figure III.6 FESEM images of micronized FUL using SAS technique (article not cited for secrecy agreements).

Irregular crystals with broad distribution were produced using SAS technique. On the basis of the state of the art on FUL micronization, SAA process was attempted to reach Cerbios targets.

III.3.1 Experimental results on FUL

Figure III.7 shows FUL crystalline morphology, in forms of long crystals with size ranging between 10 and 30 μm .

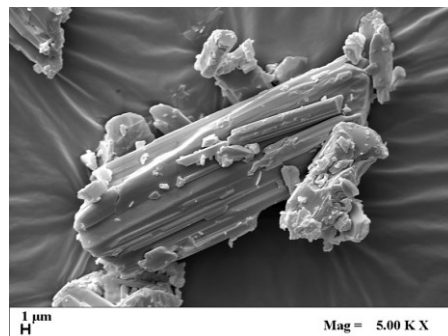


Figure III.7 FESEM image of untreated FUL.

The solvents used for this experimentation were selected based on their boiling temperature, to guarantee the evaporation of the droplets in SAA precipitator. Ethanol and acetone are solvents often used for the SAA tests, and FUL is very soluble in both of them, as summarized in Table III.3.

Table III.3 *FUL solubilities in solvents.*

Solvent	Solubility (mg/mL)
EtOH	>200
Ac	>200

First, FUL micronization was attempted using ethanol as solvent; on the basis of previous experience (Liparoti et al., 2015), the SAA operative conditions studied were: concentration in ethanol ranging between 10 and 50 mg/mL; GLR varying between 0.5 and 1.8, injection pressure around 85-88 bar in the saturator, saturator (T_s) and precipitation (T_p) temperature of 80°C. However, ethanol was not a good solvent to micronize this drug, due to FUL fast tendency to sublime at the temperatures used during SAA tests; no powders, indeed, were produced and all tests failed.

Therefore, acetone was selected to carry out a new set of experiments, since acetone is more volatile than ethanol. This aspect allowed using lower temperature in SAA precipitator and, consequently, to inhibit FUL tendency to sublime. After a set of failed tests using acetone, finally SAA operating conditions optimized were: GLR 2.5, injection pressure around 70 bar in the saturator, saturator temperature 60°C and precipitation temperature 40°C. FUL concentrations in acetone investigated were 20, 40 and 60 mg/mL. The particles produced in these experiments consisted of defined, perfectly spherical submicrospheres, as shown in Figure III.8, where examples of FESEM images at different concentrations are reported.

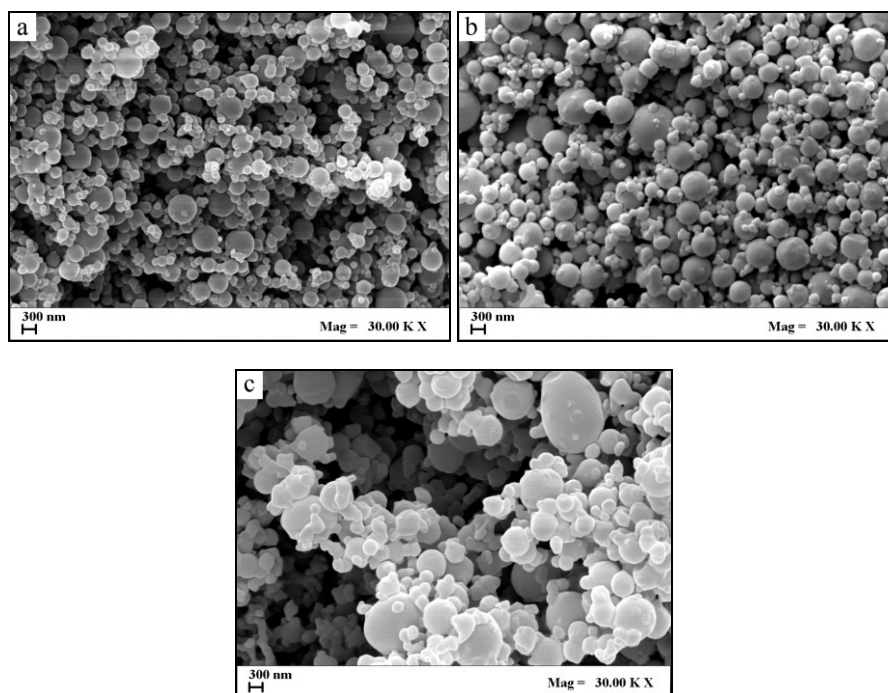


Figure III.8 FESEM images of micronized FUL using SAA technique at a) 20 mg/mL, b) 40 mg/mL and c) 60 mg/mL.

Spherical and non-coalescing microparticles were obtained. As it is possible to observe, increasing FUL concentration up to 60 mg/mL particles were still spherical but a little coalescent. Comparing the PSDs of the microparticles obtained, it was observed that, increasing the concentration, the mean diameter increased and the PSDs enlarged (Figure III.9).

PSDs values related to these three different concentrations are also summarized in Table III.4.

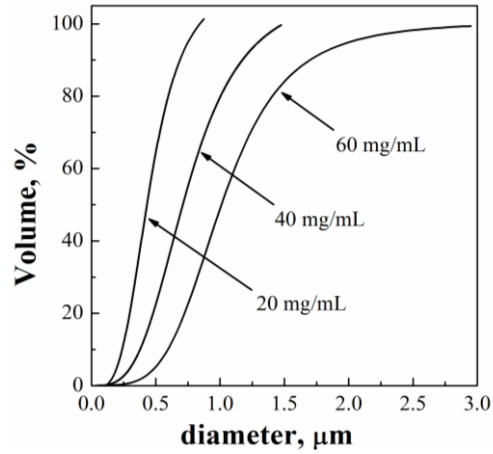


Figure III.9 PSDs of FUL particles obtained at different concentrations.

Table III.4 PSDs data of FUL particles produced by SAA.

C (mg/mL)	d ₁₀ (μm)	d ₅₀ (μm)	d ₉₀ (μm)
20 mg/mL	0.24	0.43	0.67
40 mg/mL	0.37	0.71	1.16
60 mg/mL	0.58	1.00	1.69

This behavior is commonly observed in the SAA results, since increasing the solute concentration, the viscosity of solution increases and larger droplets are formed at the exit of the injector, with the consequent production of larger particles (Liparoti et al., 2015). Using the concentrations 20 and 40 mg/mL, the desired diameters by the customers were obtained.

III.3.2 Dissolution tests

In order to test the effectiveness of FUL precipitates in improving the dissolution rate of the drug, experiments in a physiological solution (0.9% p/v of NaCl in water) were performed. As an example, in Figure III.10, the dissolution profile of micronized FUL by SAA (at 40 mg/mL) is compared with that of the untreated FUL.

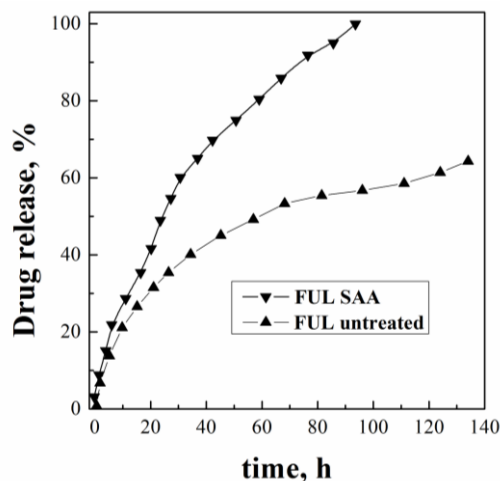


Figure III.10 Dissolution profiles of FUL in physiological solution at 37°C.

It is clearly possible to observe the different dissolution rates comparing the slopes of the two curves reported. In particular, the curve related to the FUL micronized by SAA (40 mg/mL) shows a larger slope and a complete dissolution in about 94 hours. Around 60% of the untreated FUL, instead, is dissolved after 140 hours. This result confirms that FUL dissolution rate is improved 4 times compared to the untreated drug.

The particles produced satisfied the targets indicated by Cerbios Pharma.

III.4 Compound #3: DAS

DAS is a potent inhibitor of multiple oncogenic kinases, classified as an API. It is insoluble in water (0.008 mg/mL), slightly soluble in ethanol (> 4 mg/mL) and very slightly soluble in acetone. The goal of this research was to produce solid dispersions of DAS in a polymeric matrix with the aim to prepare sub-micrometric particles loaded with the drug and to improve its bioavailability.

III.4.1 Experimental results on DAS

Figure III.11 shows native DAS morphology characterized by large flat crystals with size ranging between 10 and 30 μm .

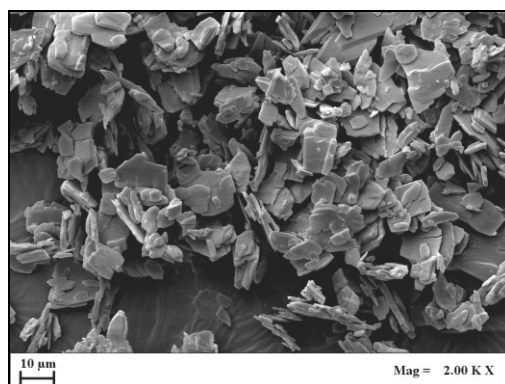


Figure III.11 FESEM image of untreated DAS.

The polymer selected for the coprecipitation is PVP, because it is an ingredient present in a patented pharmaceutical formulations based on DAS. Furthermore, PVP is soluble in water and in organic solvents, a crystal growth inhibitor and approved by FDA (Paradkar et al., 2004). PVP is already micronized in previous studies (Liparoti et al., 2015) using different solvents and operative conditions. Furthermore, it was already verified PVP processability by SAA technique.

PVP micronization

The solvent used for this experimentation was ethanol. First, PVP alone was micronized by SAA using two different process conditions (Table III.5): 60 or 80°C in the saturator; 70 or 80°C in the precipitator; GLR 1.8 or 2.5. These process conditions were selected to assure a good solubility of CO₂ in ethanol (Liparoti et al., 2015, Adami et al., 2017a) and to identify the best results for the following coprecipitation.

Table III.5 summarizes the main tests performed. In Figure III.12 FESEM images of micronized PVP at different operative conditions are reported.

Table III.5 Operating conditions used SAA micronization experiments. (T_s : saturator temperature; T_p : precipitator temperature; P_s : saturator pressure; P_p : precipitator pressure; GLR: gas to liquid ratio).

Test	C (mg/mL)	T_s (°C)	T_p (°C)	P_s (bar)	P_p (bar)	GLR	d_{10} (μm)	d_{50} (μm)	d_{90} (μm)
PVP01	10	60	70	84	1.5	1.8	0.29	0.66	0.99
PVP02	10			90	1.6	2.5	0.17	0.38	0.68
PVP03	10	80	80	88	1.5	1.8	0.37	0.77	1.16
PVP04	20			88	1.5	1.8	0.41	0.79	1.37
PVP05	30			89	1.4	1.8	0.52	0.91	1.57

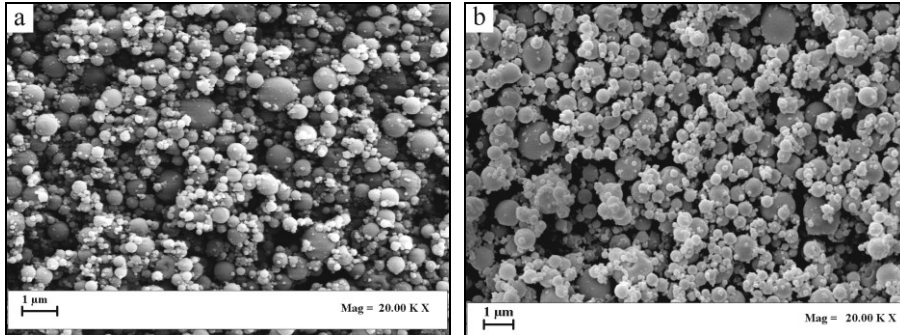


Figure III.12 FESEM images of PVP micronized at a) $T_s=60^\circ\text{C}$, $T_p=70^\circ\text{C}$, $GLR=2.5$, 10 mg/mL ; b) $T_s=80^\circ\text{C}$, $T_p=80^\circ\text{C}$, $GLR=1.8$, 20 mg/mL .

PVP was perfectly micronized by the SAA process, as seen in Figure III.12, obtaining spherical and regular particles for each operative conditions used. The morphology of particles is not influenced by the saturator temperature. However, mean diameter variations were relatively small when the saturator temperature changed (see Table III.5). PSD analyses demonstrated that smaller particles were produced using a GLR of 2.5. This result is typical for SAA micronization (Liparoti et al., 2015) and is due to the increase of the amount of CO_2 dissolved in the liquid solution in the saturator.

PVP-DAS coprecipitation

According to some patents (not cited for secrecy agreements), the recent pharmaceutical formulations contain a quantity of DAS ranging between 10 and 70% (w/w). Therefore, for SAA coprecipitation tests, a fixed DAS concentration was selected (1.5 mg/mL) to assure a complete dissolution in ethanol, and two DAS/PVP mass ratios (R) were investigated (1/20 and 1/5), corresponding to a DAS weight percentage of 5 and 17%, respectively. The SAA tests performed were summarized in Table III.6.

Table III.6 Operating conditions used for SAA coprecipitation experiments; PSD data in terms of volume of particles (T_s : saturator temperature; T_p : precipitator temperature; P_s : saturator pressure; P_p : precipitator pressure; GLR: gas to liquid ratio).

Test	R	T_s ($^\circ\text{C}$)	T_p ($^\circ\text{C}$)	P_s (bar)	P_p (bar)	GLR	d_{10} (μm)	d_{50} (μm)	d_{90} (μm)
DAS01	1/20	60	70	78	>>>3	1.8	-	-	-
DAS02	1/20	60	70	80	>>>3	2.5	-	-	-
DAS03	1/20	80	80	83	1.5	1.8	0.33	0.75	1.38
DAS04	1/5	80	80	83	1.5	1.8	0.39	0.85	1.54

The first experiments on DAS-PVP were performed using a precipitation temperature of 70°C (varying GLR from 1.8 and 2.5). In both cases, the results were not satisfactory, since no material was collected due to drying problems. An increase of precipitator pressure, indeed, did not allow obtaining a complete evaporation of solvent at temperature used. As consequence, the following experiments were performed using higher temperatures in the saturator and in the precipitator ($T_s=80^\circ\text{C}$ and $T_p=80^\circ\text{C}$, $\text{GLR}=1.8$), obtaining dried powders as result. Examples of these precipitates are shown in Figure III.13, where SEM photomicrographs taken at the same enlargement are reported.

Particles produced at $R=1/20$ were spherical and more regular than those obtained at $R=1/5$; this effect was due to the major quantity of PVP used that stabilized DAS compound. Nevertheless, defined and separated particles were produced also increasing R .

PSD diagrams are reported in Figure III.14 and PSD values are summarized in Table III.6. PSD was influenced by DAS/PVP mass ratio; the particles produced at $R=1/5$ resulted smaller than those obtained at $R=1/20$. The mean diameter variations were relatively small by varying R (see Table III.6 and Figure III.14). However, the DAS-PVP coprecipitates diameters were consistent with PVP particles sizes.

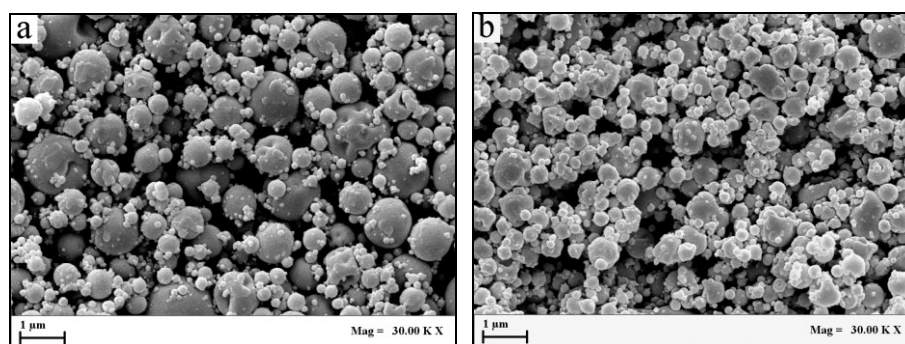


Figure III.13 FESEM images of DAS-PVP particles produced at $T_s=80^\circ\text{C}$, $T_p=80^\circ\text{C}$, $\text{GLR}=1.8$, and at a) $R=1/20$, b) $R=1/5$.

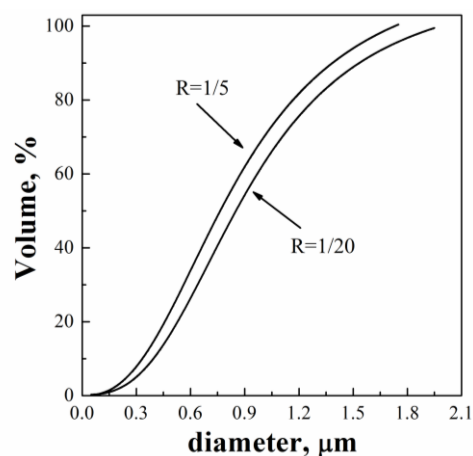


Figure III.14 Cumulative volumetric particle size distribution of DAS-PVP powder obtained by SAA at different R (see Table III.6).

III.4.2 Characterization of DAS-PVP particles

In order to attest DAS presence in SAA particles produced, EDX analyses were performed to give a chemical characterization of powders. In particular, this technique allowed detecting the characteristic elements of DAS (not present in PVP structure): chlorine (Cl) and sulfur (S). Figure III.15 shows an example of EDX diagram for sample R=1/20. These analyses confirmed DAS presence in both coprecipitates produced, since peaks related to S and Cl were clearly evidenced. Furthermore, the key chemical elements were uniformly distributed in the microparticles, confirming the hypothesis that DAS was intimately mixed in each particle at nanometric level, forming microspheres.

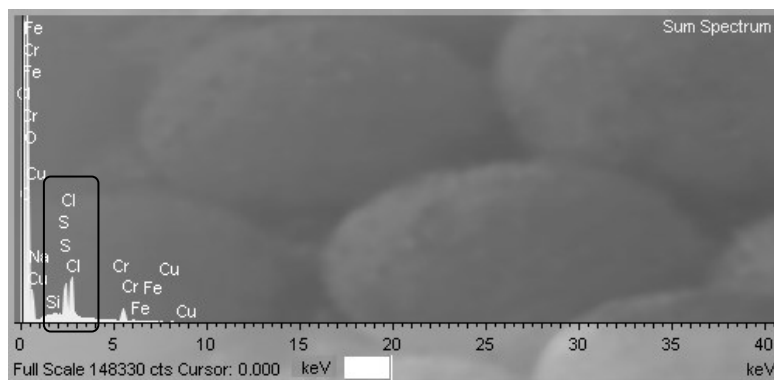


Figure III.15 EDX analyses related to DAS-PVP particles produced at $R=1/20$.

However, EDX analyses is not a quantitative analysis. For this information, DAS-PVP batches were sent to Cerbios Pharma to perform HPLC analyses and further studies, that cannot be reported in this thesis.

The particles produced satisfied the targets indicated by Cerbios Pharma.

III.5 Compound #4: NAP

NAP is a non-steroidal anti-inflammatory drug. It is very soluble in water (200 mg/mL) and ethanol (25 mg/mL). The objective of this experimentation was to identify the optimized process conditions to micronize NAP and to control its crystallization tendency, in order to validate SAA industrial plant purchased by Cerbios Pharma and obtain *SwissMedic authorization* for GMP (*Good Manufacturing Practice*) production. Furthermore, the study aimed at starting the plant to produce powders.

III.5.1 Experimental results on NAP

Figure III.16 shows raw NAP morphology characterized by large flat crystals with size ranging between 10 and 60 μm .

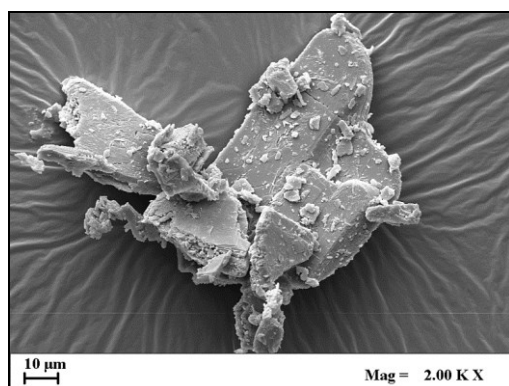


Figure III.16 FESEM image of untreated NAP.

Particles produced using water as solvent

The first part of NAP micronization experiments was performed using water as solvent. SAA operating conditions were: drug concentration in water 15 or 30 mg/mL; GLR varying between 1 and 2.5, injection pressure of about 90 and 100 bar in the saturator, saturator temperature 85°C and precipitation temperature 100°C. These conditions were optimized in a previous works (Adami et al., 2017b). In Table III.7, a list of the main operative conditions investigated in water is reported.

Table III.7 Operating conditions used for SAA experiments on NAP using water; PSD data in terms of volume of particles (C: NAP concentration; GLR: gas to liquid ratio).

C (mg/mL)	GLR	d ₁₀ (μm)	d ₅₀ (μm)	d ₉₀ (μm)
30	2.5	0.6	1.3	2.3
15	1.8	0.8	1.7	2.9
15	1	1.2	2.3	3.6

At the end of all SAA tests using water, foaming materials were found in the saturator. This drawback may be related to an antisolvent precipitation phenomenon. In SAA process the choice of the proper conditions in the plant and the solvent is fundamental to produce microparticles, since SC-CO₂ solubilization in the liquid feed to form an expanded liquid is the key of the technique. However, some compounds may be not completely soluble in this expanded liquid and, consequently, may precipitate in the saturator, as shown in the picture in Figure III.17. This drawback may take place when the system enters into the two-phase region where gas phase coexists with the liquid phase and NAP precipitation may occur from the gas phase (Della Porta et al., 2006).



Figure III.17 Photographs of foaming materials in the saturator.

However, a white powder was collected on the filter located in SAA precipitator and some examples of micronized NAP were shown in Figure III.18. Produced particles were partly spherical with a no smooth surface. NAP tended partially to crystallize: probably the water evaporation rate was comparable to that of drug crystallization.

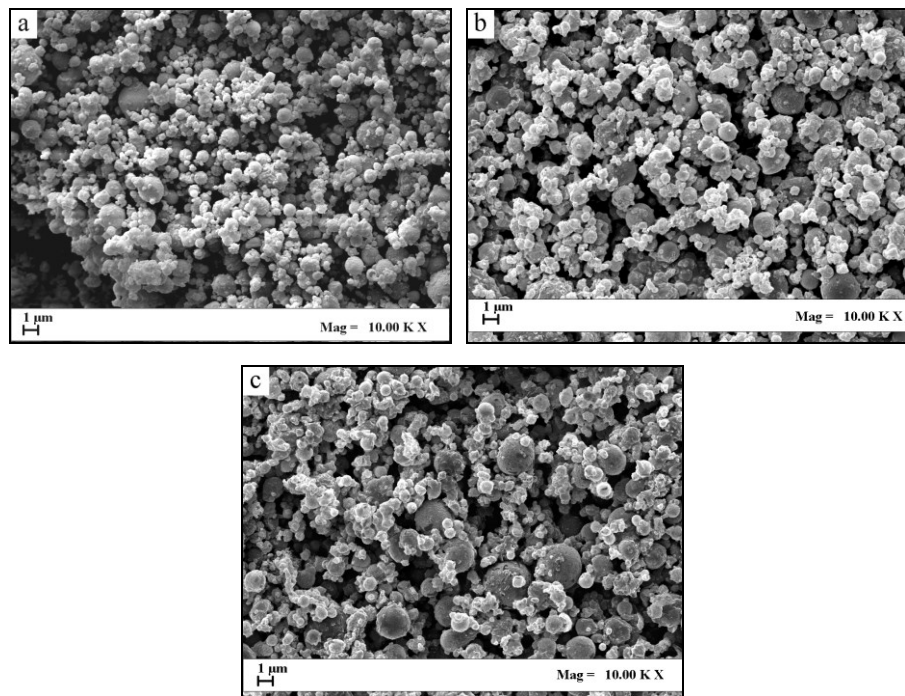


Figure III.18 FESEM images of micronized NAP at a) $T_s=85^\circ\text{C}$, $T_p=100^\circ\text{C}$, $GLR=2.5$, 30 mg/mL; b) $T_s=85^\circ\text{C}$, $T_p=100^\circ\text{C}$, $GLR=1.8$, 15 mg/mL; c) $T_s=85^\circ\text{C}$, $T_p=100^\circ\text{C}$, $GLR=1$, 15 mg/mL.

However, PSD data are summarized in Table III.7. As it is possible to observe, keeping constant NAP concentration (15 mg/mL) and decreasing GLR down to 1, d_{50} increased, as SAA typical result (Liparoti et al., 2015, Adami et al., 2017a). When GLR, indeed, is decreasing, there is a decrease of the amount of CO₂ dissolved in the saturator, hence, of CO₂ content in the liquid system forming the expanded liquid, with the formation of larger droplets in the spray and consequently of particles formed (Adami et al., 2017a). Unfortunately, NAP micronization in water was ineffective, due to the loss of material in the saturator (*antisolvent effect*). In order to overcome these limitations, subsequent tests were performed using ethanol as solvent.

Particles produced using ethanol as solvent

Process conditions investigated using ethanol were: NAP concentration 10 and 20 mg/mL, saturator temperature 60-80°C, precipitator temperature 70-80°C, GLR varying between 1 and 1.8. In Table III.8 process parameters considered are reported.

Table III.8 *Operating conditions used for NAP micronization using ethanol; (C: NAP concentration; T_s: saturator temperature; T_p: precipitator temperature; GLR: gas to liquid ratio).*

C (mg/mL)	T _s (°C)	T _p (°C)	P _s (bar)	GLR
20	80	80	83	1.8
20			72	1.3
20			90	1
10			85	1.8
20	60	70	82	1.8

In Figure III.19, some exemplificative SEM images related to samples of NAP particles produced using ethanol are reported. No material was found in the saturator at the end of SAA tests, as in the previous experiments performed in water. Produced particles were perfectly spherical with smooth surface and no crystallization phenomenon was evidenced from FESEM image in Figure III.19a, when T_s=80°C, T_p=80°C and GLR=1.8 were investigated. These NAP particles showed a relatively narrow distribution, with d_{10} =0.6 μm; d_{50} =1.2 μm; d_{90} =2.0 μm. In Figure III.19 (a, b, c) the influence of GLR on SAA processed NAP can be qualitatively evaluated. In particular, at lower GLR (1.3 and 1) particle coalescence and less regular morphologies were evinced. When operating at lower temperatures in the saturator and in the precipitator (T_s=60°C, T_p=70°C) drug particle recrystallization was observed (Figure III.19d), probably caused by partial solvent re-condensation on the precipitated particles (Della Porta et al., 2006).

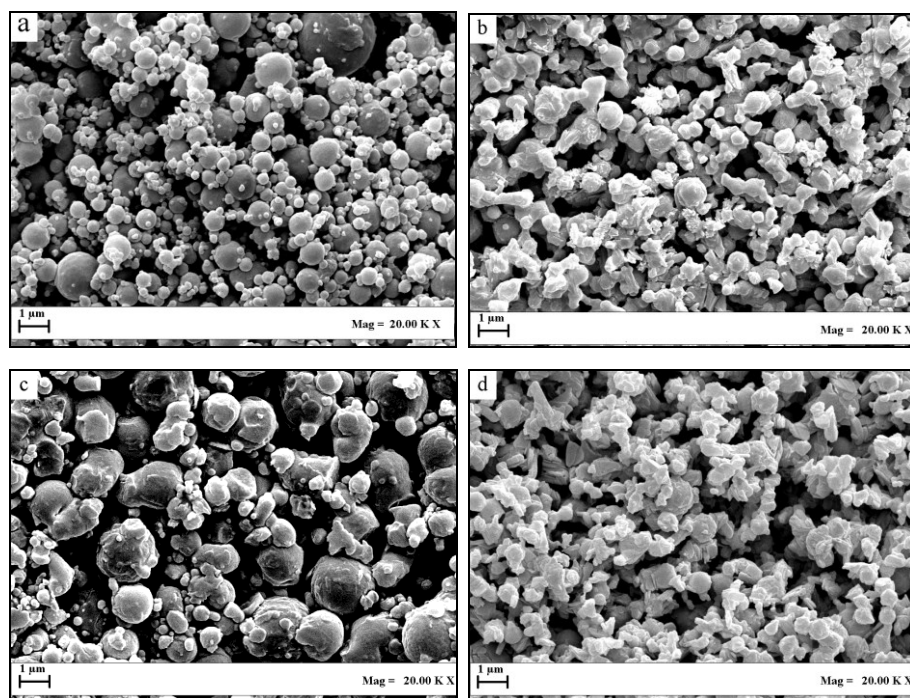


Figure III.19 FESEM images of NAP micronized using ethanol at 20 mg/mL and a) $T_s=T_p=80^\circ\text{C}$, $GLR=1.8$; b) $T_s=T_p=80^\circ\text{C}$, $GLR=1.3$; c) $T_s=T_p=80^\circ\text{C}$, $GLR=1$; d) $T_s=60^\circ\text{C}$, $T_p=70^\circ\text{C}$, $GLR=1.8$.

Therefore, the best results in terms of precipitated particle morphology and size were obtained operating at $T_s=80^\circ\text{C}$, $T_p=80^\circ\text{C}$ and $GLR=1.8$ when ethanol was used as solvent. Similar morphology was obtained using a lower NAP concentration keeping constant the operative conditions (figure not reported). The PSDs in terms of cumulative volumetric percentage showed an effect of concentration that is evidenced in Figure III.20.

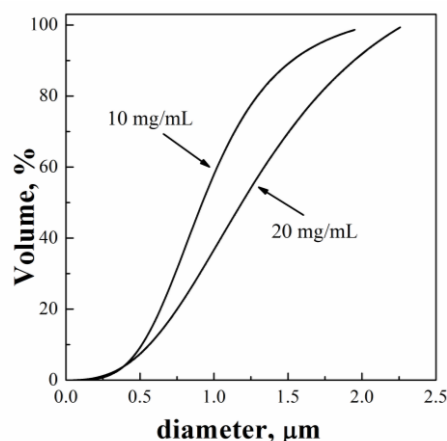


Figure III.20 Comparison of cumulative volumetric PSDs of NAP particles obtained by SAA at different concentrations.

Decreasing the concentration down to 10 mg/mL, smaller particles were produced with d_{50} of about 0.9 μm. This behavior is commonly observed in SAA powders, since decreasing the solute concentration, the viscosity of the injected solution decreases and smaller droplets are formed at the exit of the nozzle, with the consequent formation of smaller microspheres (Liparoti et al., 2015, Di Capua et al., 2018).

All SAA powders were characterized by X-Ray and DSC analyses. Generally speaking the spherical shape of SAA micronized particles may indicate an amorphous solid state. However, for some compounds it has been observed that SAA precipitates are formed by spherical particles constituted by smaller crystals (Della Porta et al., 2006). Therefore, X-Ray and DSC analyses revealed that the micronized NAP is semi-crystalline. As an example, in Figure III.21 X-ray traces of untreated and processed NAP in ethanol are reported.

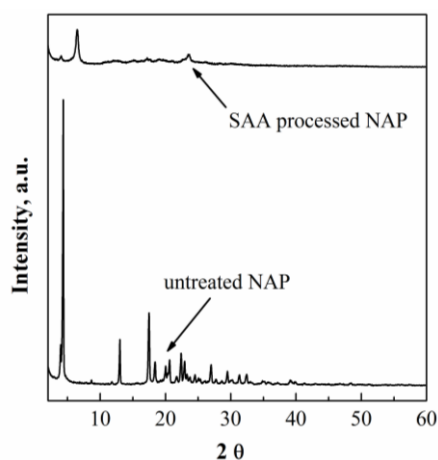


Figure III.21 X-ray traces of untreated NAP and SAA processed NAP.

It can be observed that micronized NAP partially retained the crystalline structure after SAA process. This result was consistent with Cerbios Pharma's targets.

Before NAP experimentation, no atomized powders were produced using the SAA industrial plant (at Cerbios Pharma). This study on NAP micronization was fundamental in order to validate the industrial plant and obtain **SwissMedic authorization** for GMP production on January 2017.

III.6 Compound #5: GPB

GPB is an anticholinergic agent used to treat chronic obstructive pulmonary disease. It is soluble in water (45 mg/mL) and in ethanol (30 mg/mL). The goal of this project was the production of stable particles with d_{90} higher than 3 μm ; this objective was not reached with conventional techniques, as spray drying. GPB is, indeed, very difficult to micronize since it has a very fast crystallization rate and tends quickly to agglomerate.

III.6.1 Experimental results on GPB

GPB shows a morphology characterized by large flat crystals (Figure III.22) with size ranging between 20 and 80 μm . This crystalline behavior was confirmed by DSC analyses (Figure III.23): the raw GPB shows an endothermic peak at about 196°C, due to the fusion of crystalline structure, and another broad endothermic peak ranging between 250 and 300°C.

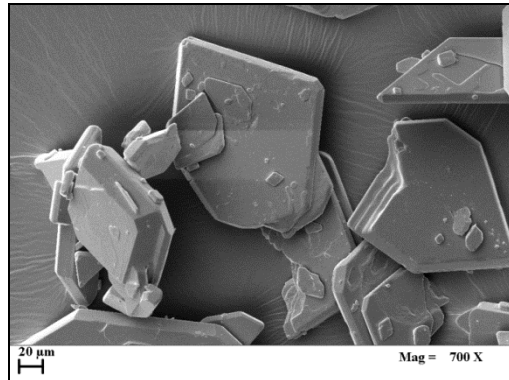


Figure III.22 FESEM image of untreated GPB.

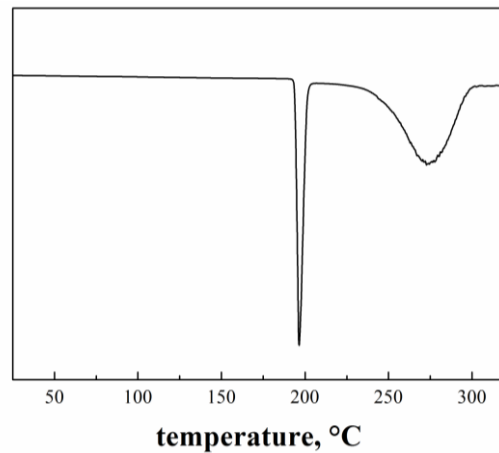


Figure III.23 DSC thermogram related to untreated GPB.

Preliminary SAA tests were performed to precipitate GPB alone, using ethanol and water as solvents that are commonly used for SAA process (Della Porta et al., 2006, Reverchon and Della Porta, 2003). GPB concentration in ethanol was fixed at 25 mg/mL. Process conditions studied were: saturator temperature changing between 40 and 80°C; precipitator temperature between 55 and 70°C; GLR varying between 1.8 and 3. GPB concentration in water was fixed at 20 mg/mL. Process conditions studied were: saturator temperature 85°C; precipitator temperature between 100 and 110°C; GLR set at 1.8. However, no powders were collected both in ethanol and in water, probably due to a fast crystallization phenomenon in the precipitator. In order to reduce the precipitator temperature and inhibit the crystallization phenomenon, a different configuration of SAA plant, using vacuum pumps, was used; however, also in these cases, no powder was collected.

In the literature, patents related to GPB (not cited for secrecy agreement) described dry powder formulations of GPB using for examples dextran, lactose, and magnesium stearate as excipients. For this reason, the research project was continued producing composite systems. First, SAA tests were performed processing suspensions based on GPB and magnesium stearate both in water and in ethanol; however, no powders were still collected as in the previous experiments described. Then, solid dispersions of GPB in carrier able to inhibit drug crystallization and promote the stabilization of powder were explored. Two carriers very soluble in water were proposed to Cerbios Pharma: polyvinylpyrrolidone (PVP) and dextran (DEX) both classified as crystal growth inhibitor and accepted by the Food & Drug Administration (Mehvar, 2000, Kamada et al., 2000).

GPB-PVP particles produced using ethanol

SAA coprecipitation tests were carried out using water and ethanol as solvents. However, SAA tests using water were unsuccessful. Two polymer concentrations and three drug/polymer mass ratios (R, 1/5, 1/3 and 1/2) were investigated. The operative conditions studied, based on the literature, were: GPB concentration 2 and 8 mg/mL, PVP concentration 10-20-40 mg/mL saturator temperature 80°C, precipitator temperature 80°C, GLR 1.8 (Adami et al., 2017a, Adami et al., 2019, Di Capua et al., 2017b). Examples of GPB-PVP particles produced in ethanol are shown in Figure III.24.

Spherical and regular particles were obtained, at R=1/5 and varying PVP concentration from 10 to 40 mg/mL. PSDs in terms of volumetric cumulative percentage showed that no significant differences in size were obtained varying PVP concentration (see Table III.9).

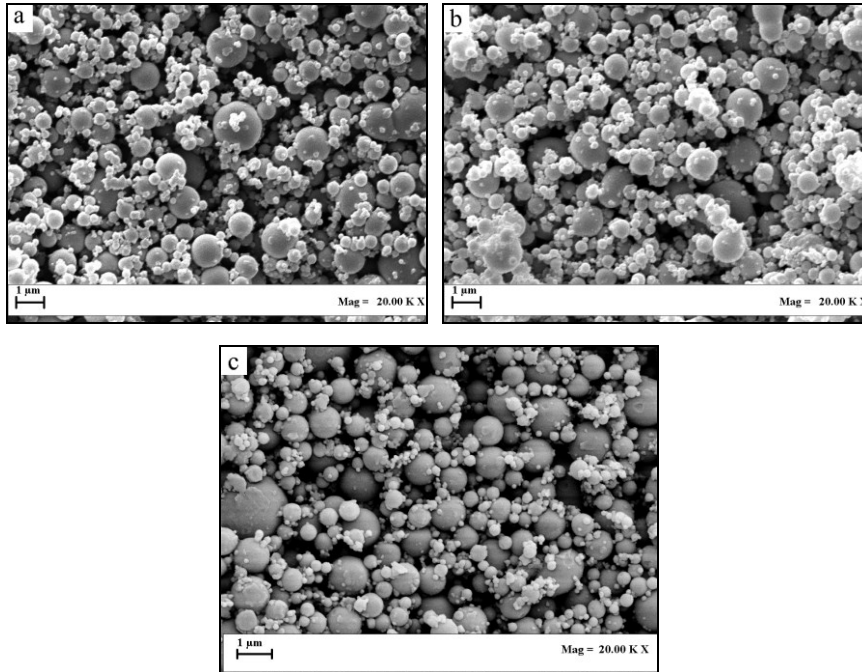


Figure III.24 FESEM images of GPB-PVP particles ($R=1/5$), using a PVP concentration in ethanol of: a) 10 mg/mL; b) 20 mg/mL; c) 40 mg/mL.

Table III.9 Concentrations used for GPB-PVP coprecipitation using ethanol; PSD data in terms of volume of particles (C_{PVP} : PVP concentration; C_{GPB} : GPB concentration; R : GPB/PVP weight ratio w/w).

C_{GPB} (mg/mL)	C_{PVP} (mg/mL)	R	d_{10} (μm)	d_{50} (μm)	d_{90} (μm)
2	10	1/5	0.5	1.0	1.8
4	20	1/5	0.5	1.0	1.7
8	40	1/5	0.5	1.0	1.9

Fixed PVP concentration at 10 mg/mL, two higher R were investigated (1/3 and 1/2) at the same process conditions; these SAA tests produced powders with no regular morphology (Figure III.25), probably due to the lower amount of PVP (in weight percentage) that was not enough to inhibit GPB crystallization/coalescence.

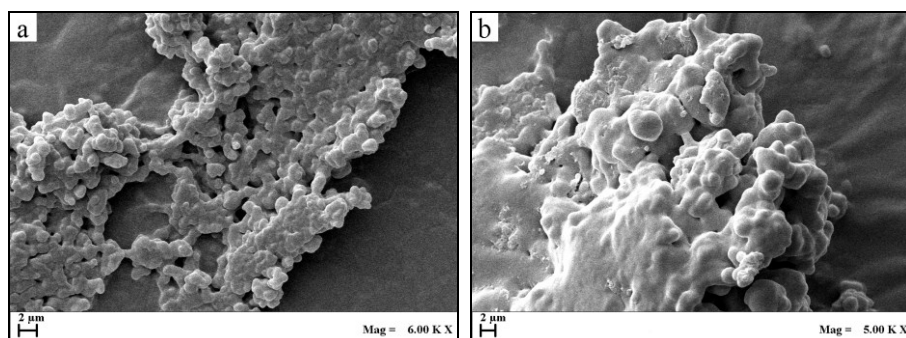


Figure III.25 FESEM images of GPB-PVP particles produced using ethanol and a PVP concentration of 10 mg/mL and: a) $R=1/3$, b) $R=1/2$.

GPB-DEX particles produced using water:ethanol (70:30 v/v)

First, GPB-DEX coprecipitation tests were performed using a mixture of water:ethanol (70:30 v/v) as solvent, on the basis of SAA experiments on DEX (Di Capua et al., 2017a). Three DEX concentrations and three drug/polysaccharide weight ratios (R) were investigated. The operative conditions studied, based on the literature, were: GPB concentration 2 and 8 mg/mL, DEX concentration 10-20-40 mg/mL saturator temperature 85°C, precipitator temperature 100°C, GLR 1.8 (Adami and Reverchon, 2012, Di Capua et al., 2017a). Examples of GPB-DEX particles produced in water:ethanol (70:30 v/v) were shown in Figure III.26.

GPB-DEX coprecipitation in water:ethanol was very promising. Spherical and well-separated particles, using different R weight ratios, were obtained. PSDs in terms of volumetric cumulative percentage showed a significant effect of DEX concentration on particle size (see Table III.10 and Figure III.27).

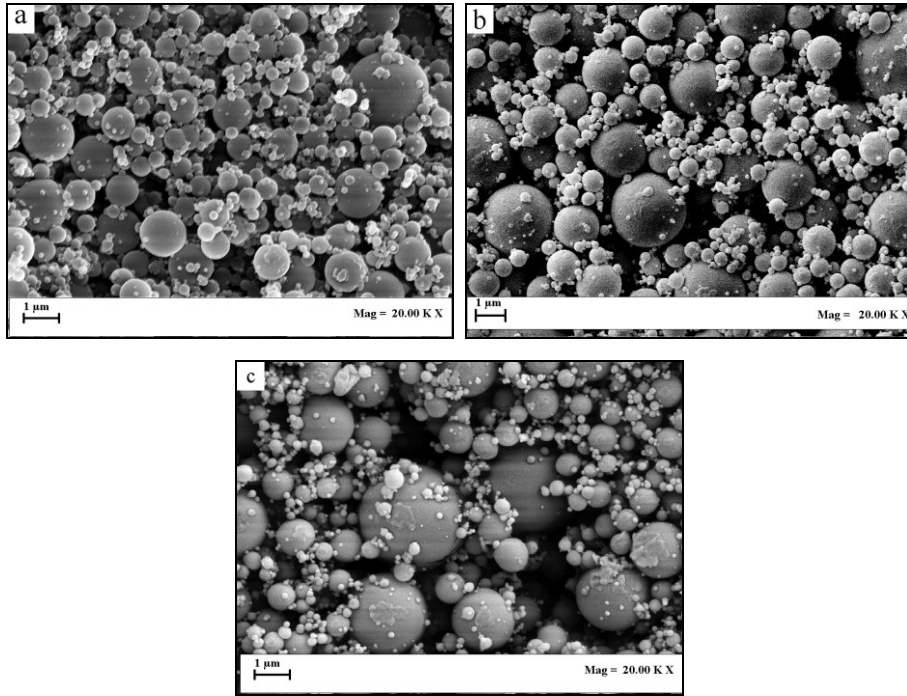


Figure III.26 FESEM images of GPB-DEX particles produced using water:ethanol (70:30 v/v) at $R=1/5$ and a DEX concentration of: a) 10 mg/mL; b) 20 mg/mL; c) 40 mg/mL.

Table III.10 Operating conditions used SAA coprecipitation experiments for GPB-DEX particles produced in water:ethanol (70:30 v/v); PSD data in terms of volume of particles (C_{DEX} : DEX concentration; C_{GPB} : GPB concentration; R : GPB/DEX w/w).

C_{GPB} (mg/mL)	C_{DEX} (mg/mL)	R	d_{10} (μm)	d_{50} (μm)	d_{90} (μm)
2	10	1/5	0.3	0.9	1.3
4	20	1/5	0.6	1.8	3.0
8	40	1/5	0.6	2.1	3.4

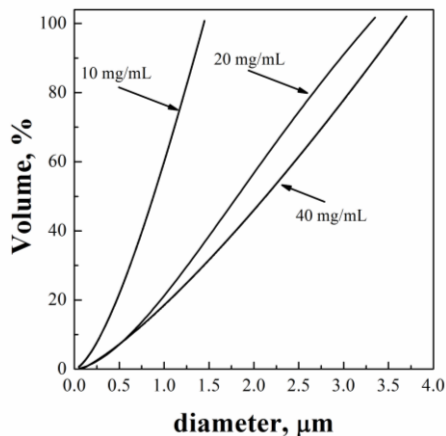


Figure III.27 Comparison of cumulative volumetric PSDs of GPB-DEX particles obtained by SAA at different DEX concentrations in water:ethanol (70:30 v/v).

In order to obtain large particles, DEX concentration was fixed at 40 mg/mL and several R were investigated (1/5, 1/4, 1/2 and 1/1) at the same process conditions. Examples of these produced particles at different drug/DEX weight ratios are shown in Figure III.28.

Regular morphology and perfect particles (Figure III.28) were obtained also increasing drug concentration up to 20 mg/mL, corresponding to a weight ratio of $R=1/2$ (where the mass percentage of active ingredient is 33.3%). Only for $R=1/1$ the coprecipitation test failed, probably due to the low amount of polysaccharide (in weight percentages) that was not able to inhibit GPB crystallization.

PSDs data in terms of volumetric cumulative percentage are summarized in Table III.11.

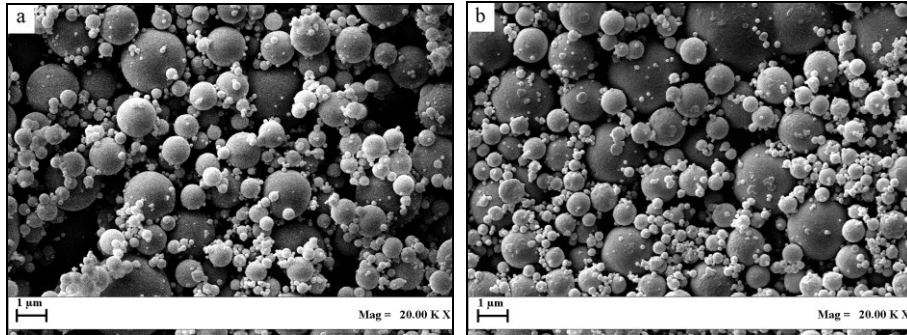


Figure III.28 FESEM images of GPB-DEX particles produced using water:ethanol at DEX concentration of 40 mg/mL and: a) $R=1/4$, $[GPB]=10$ mg/mL, b) $R=1/2$, $[GPB]=20$ mg/mL.

Table III.11 PSD data in terms of volume of particles (C_{DEX} :DEX concentration; C_{GPB} :GPB concentration; R : GPB/DEX w/w); *: no powder produced.

C_{GPB} (mg/mL)	C_{DEX} (mg/mL)	R	d_{10} (μm)	d_{50} (μm)	d_{90} (μm)
8	40	1/5	0.6	2.1	3.4
10	40	1/4	0.6	1.9	3.2
20	40	1/2	0.7	1.6	2.7
40	40	1/1*	-	-	-

PSD data showed that increasing the weight ratio GPB/DEX (hence, increasing GPB concentration in the solution injected during SAA process) up to $R=1/2$, smaller particles were obtained.

GPB-DEX particles produced using water

GPB-DEX coprecipitation tests were performed also using water as solvent and the same operative conditions, on the basis of SAA experiments on DEX (Adami and Reverchon, 2012).

Examples of GPB-DEX particles produced in water were shown in Figure III.29. PSDs data in terms of volumetric cumulative percentage are summarized in Table III.12.

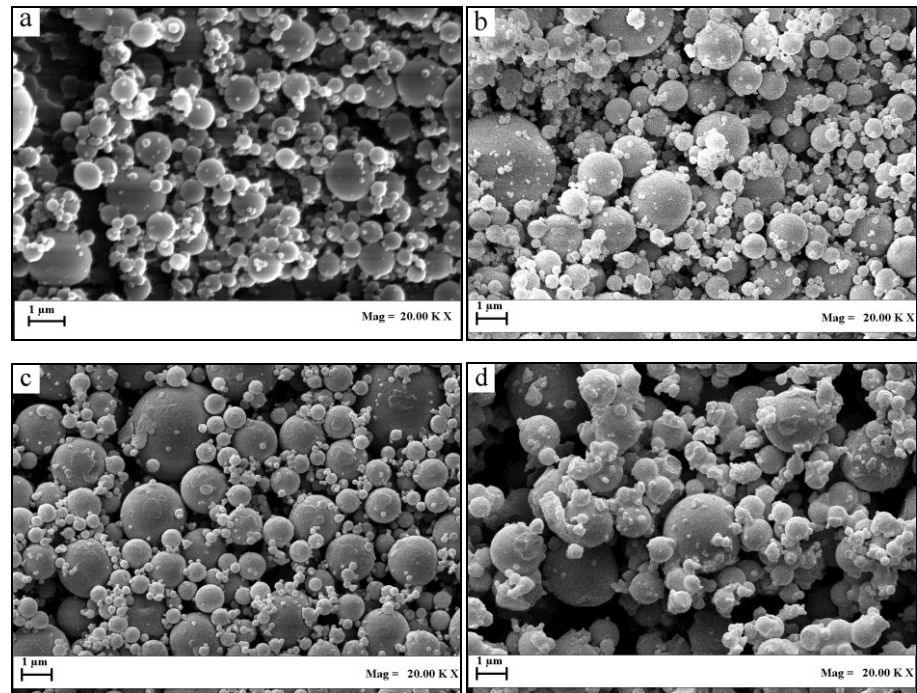


Figure III.29 FESEM images of GPB-DEX particles produced using water at: a) $[DEX]=10$ mg/mL, $R=1/5$; b) $[DEX]=20$ mg/mL, $R=1/5$; c) $[DEX]=40$ mg/mL, $R=1/4$; d) $[DEX]=40$ mg/mL, $R=1/2$.

Table III.12 PSD data in terms of volume of particles (C_{DEX} : DEX concentration; C_{GPB} : GPB concentration; R : GPB/DEX w/w).

C_{GPB} (mg/mL)	C_{DEX} (mg/mL)	R	d_{10} (μm)	d_{50} (μm)	d_{90} (μm)
2	10	1/5	0.3	0.7	1.3
4	20	1/5	0.3	0.7	1.2
10	40	1/4	0.7	2.3	3.6
20	40	1/2	0.6	1.6	2.7

As in the previous study using the mixture water:ethanol (70:30 v/v), it can be observed an effect of R on particle size. In particular, fixed DEX concentration in water, increasing R (hence, increasing GPB concentration) smaller particles were produced.

Characterization of powders

Solid state analyses performed revealed that a homogeneous dispersion of GPB was produced in all SAA powders. Thermograms (figure not reported) did not show the endothermic peak at about 196°C shown in Figure III.23, due to the fusion of crystalline structure, but only the glass transitions of the carriers used. Therefore, GPB coprecipitates were amorphous. Furthermore, FTIR spectra (figure not reported) demonstrated that no chemical interactions were created between the drug and the two carriers investigated.

Stability tests

To demonstrate the absence of recrystallization phenomena, the morphology of the produced coprecipitates GPB-PVP and GPB-DEX was observed for 4 months by scanning electron microscope, as requested by Cerbios Pharma. Examples of the morphology of the coprecipitates at different time of storage are reported in Figure III.30.

FESEM images showed that all SAA powder did not change morphology with time and no aggregation of particles was observed. These results were confirmed by DSC analyses: the thermograms did not present the melting peak related to GPB (at about 196°C) over time.

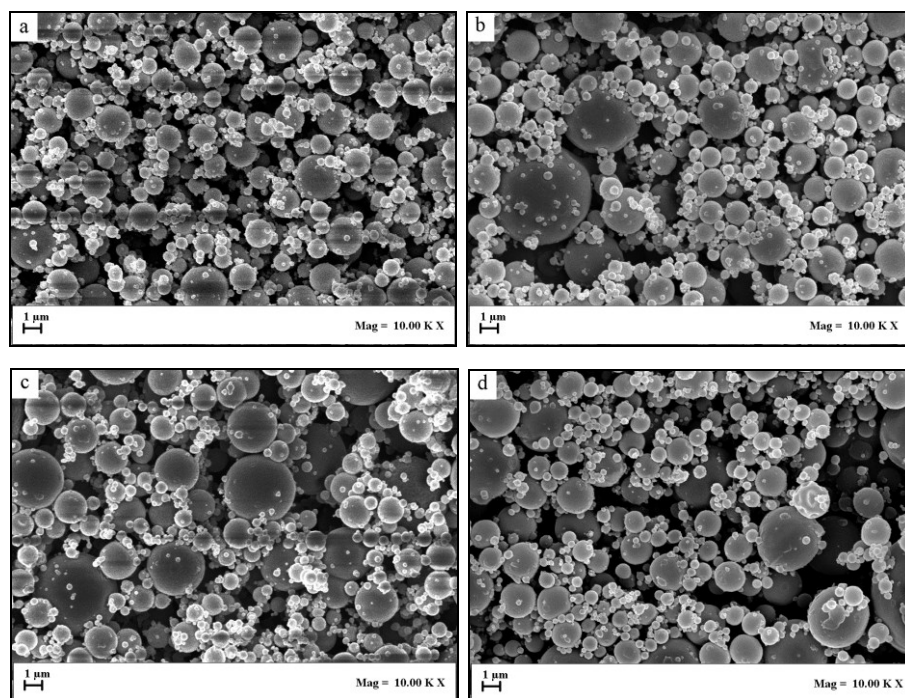


Figure III.30 FESEM images of coprecipitates after 4 months; a) GPB/PVP=1/5; using [DEX]=40 mg/mL in water:ethanol (70:30 v/v) b), GPB/DEX=1/4; c) GPB/DEX=1/2; d) [DEX]=40 mg/mL, GPB/DEX=1/4, using water.

Comparison of the investigated systems

The best results were obtained using DEX as carrier, producing perfect and spherical particles. Furthermore, using the mixture water:ethanol (70:30 v/v) as solvent, the system allowed to produce larger and perfect particles using GPB/DEX weight ratios up to $R=1/2$ (corresponding to a weight percentage of GPB of 33.3%), whereas a starting coalescence was evinced using water. The differences between water and water:ethanol systems were to assign to the different surface tension (droplet diameter), solvents evaporation rate (ethanol is more volatile than water) and solvents solubility in SC-CO₂. These characteristics can influence particle production and size, as demonstrated by the results.

III.7 Conclusions on drugs proposed by Cerbios Pharma

All these compounds were previously unsuccessfully tested using conventional techniques by other research groups. On the contrary, SAA demonstrated to be effective in overcoming these limitations and reaching the specific targets requested by the company. BRI, FUL and NAP were micronized alone, whereas DAS and GPB were dispersed in carrier matrices producing coprecipitates.

In particular, BRI crystalline particles, in form of agglomerates, were produced using ethanol as solvent, with a particle size $d_{90} < 1 \mu\text{m}$ and with non detectable residual solvents, as requested by the customers. Unfortunately, the low solubility did not allow to obtain a good productivity (mL of solute injected per minute), useful in a large-scale production perspective.

FUL micronization in acetone was really successful; amorphous sub-microparticles with d_{50} ranging between 0.4 and 0.7 μm were obtained, by reaching the desired targets. Furthermore, SAA FUL particles showed a 4-fold faster dissolution rate compared to the untreated FUL, demonstrating the improvement of bioavailability.

The experimentation on NAP in ethanol was fundamental in order to validate SAA industrial plant and obtain SwissMedic authorization for GMP (*Good Manufacturing Practice*) production on January 2017.

The production of a SAA solid dispersion of DAS in a matrix consisted of PVP was obtained and confirmed by EDX analyses, demonstrating that DAS was intimately mixed in each particle at nanometric level, forming microspheres.

GPB was a very difficult compound to be processed due to the fast crystallization rate and the high tendency to agglomerate. The production of composite systems using the two different matrices investigated (dextran and PVP) demonstrated to be able to promote the stabilization of the drug on time, by preventing the typical GPB behavior to agglomerate.

For each optimized product, different batches were produced for further analyses, directly performed by Cerbios Pharma.

Chapter IV

Coprecipitation of pharmaceutical compounds using SAA technique

IV.1 Introduction

About 40% of novel drugs on the market is classified as *poorly water-soluble*, according to the Biopharmaceutics Classification System (Lipinski et al., 2001, Bhakay et al., 2018). Among the several approaches mentioned in the Introduction section, particle size reduction approaches to form stable sub-microparticles and nanoparticles have emerged to enhance the bioavailability of poorly water-soluble compounds. Indeed, these particles have larger specific surface areas promoting greater interactions with the solvent and, hence, higher dissolution rates. However, micro and nanoparticles of drug may be affected by aggregation or recrystallization phenomena and are difficult to handle in an industrial perspective. For this reason, the current strategy is the production of composite systems with improved pharmacokinetic behavior and bioavailability (Junyaprasert and Morakul, 2015, Savjani et al., 2012, Khadka et al., 2014). As mentioned in the state of the art, conventional methods are not always suitable or feasible and may show some drawbacks, whereas SC-CO₂-based processes can be used as an alternative to traditional techniques to overcome these limitations (Cocero et al., 2009, Campardelli et al., 2015). The aim of this part of work was to test the applicability of SAA process in the production of coprecipitates able to improve dissolution rates and, hence, the bioavailability of different type of active principles. In particular, investigations and studies were performed on some compounds of natural origin with attested pharmacological properties (curcumin, luteolin, palmitoylethanolamide) and a drug (nifedipine). Three carriers were used in these coprecipitation experiments: polyvinylpyrrolidone, dextran and hydroxypropyl- β -cyclodextrin.

Materials

Polyvinylpyrrolidone (PVP, Mw: 10,000), dextran from *Leuconostoc mesenteroides* (DEX, average MW 43,000), curcumin (CUR, purity 99%), nifedipine (NIF, purity), fluorescein isothiocyanate (FITC isomer I, purity 90%), ethanol (EtOH, purity 99.9%), acetone (Ac, purity 99.8%) were supplied by Sigma Aldrich (Italy). Hydroxypropyl- β -cyclodextrin (HP β CD, 97%) was provided by Acros Organic (Belgium), luteolin (LUT) and palmitoylethanolamide (PEA) were provided by Epitech Group SpA (Italy). Carbon dioxide (CO₂, 99.9%) was purchased by Morlando Group (Italy) and nitrogen (N₂, 99%) by SOL (Italy). All materials were used as received.

IV.2 PEA stabilization

PEA is an endogenous fatty acid amide, belonging to the class of nuclear factor agonists. It has been studied extensively for its anti-inflammatory and neuroprotective action (Skaper et al., 2014, Petrosino et al., 2016). It has recently been demonstrated that PEA exerts neuroprotection in central nervous system pathologies and it significantly reduces inflammatory secondary events associated with spinal cord injury (Andresen et al., 2016). However, the lipidic nature of the molecule and its large particle size in the native state produce limitations in terms of solubilization in aqueous systems and, consequently, reduce its bioavailability. Indeed, native PEA shows a morphology characterized by large flat crystals (Reverchon et al., 2015). The production of particles with micrometric size can overcome the problems related to the low bioavailability; indeed, the dissolution rate of a drug can be enhanced by the increase of exposed surface area (Schifilliti et al., 2014, Andresen et al., 2016, Impellizzeri et al., 2014, Impellizzeri et al., 2015). In previous studies (Reverchon et al., 2015) some SCF techniques were tested in the attempt of reducing PEA particle size and crystallization. The work was only partly successful because PEA shows very fast crystallization rates, interfering with the micronization processes. PEA was also micronized by SAA technique; the best results in terms of powder morphology were obtained using ethanol and isopropanol as liquid solvent; but, irregular particles were produced in the micrometric range, due to PEA tendency to crystallize forming flat particles (Reverchon et al., 2015). Therefore, in this work (Adami et al., 2019) in collaboration with the Italian company Epitech Group, PEA coprecipitation experiments were carried using PVP and LUT, with the aim to reduce PEA tendency to crystallize during SAA micronization and to obtain micrometric composite particles with a regular (spherical) morphology.

IV.2.1 Experimental results

SAA coprecipitation experiments PEA/PVP

The first part of PEA coprecipitation experiments were performed using PVP, selected for its capacity to act as crystallization controller of active principles (Jain and Banga, 2010, Lee et al., 2013, Sekikawa et al., 1978). SAA operating conditions were: total concentration in ethanol 10 or 20 mg/mL, 40°C; *gas to liquid ratio* (mass based, GLR) 2, injection pressure and temperature of about 80 bar and 80°C in the saturator, precipitation temperature 65 or 70°C. These conditions were optimized in a previous paper in which SAA precipitation of PEA alone was attempted (Reverchon et al., 2015). In this work, PEA/PVP weight ratios (R) 1:3, 1:5 and 1:8 w/w were proposed. In Table IV.1, the operating conditions for coprecipitation experiments are summarized. Each experiment was performed in triplicate.

Table IV.1 Operating conditions used for PEA-PVP coprecipitation experiments. (C: total concentration; Q_{CO_2} : CO_2 flow rate; T_p : precipitator temperature).

Solute	C (mg/mL)	Q_{CO_2} (g/min)	T_p (°C)
PEA	10	7.82	65
PEA:PVP 1:8	20	6.64	70
PEA:PVP 1:5	20	7.47	70
PEA:PVP 1:3	20	8.19	65

It is already known that a GLR=2 avoids the precipitation of PEA in the saturator by antisolvent effect (Reverchon et al., 2015). Moreover, previous studies on SAA process showed that decreasing the concentration of the starting solution, smaller droplets/particles were obtained (Liparoti et al., 2015). The first coprecipitation experiments were performed using the 1:3 w/w PEA/PVP ratio. Figure IV.1a reports a SEM image of the particles obtained; the precipitate was formed by irregular, large particles and the presence of flat particles was also evident, that confirms the typical tendency of PEA to crystallize with this morphology. This fact demonstrates that at this PEA/PVP ratio, PVP was not able to block the tendency to fast crystallization typical of PEA and the experiments were substantially unsuccessful.

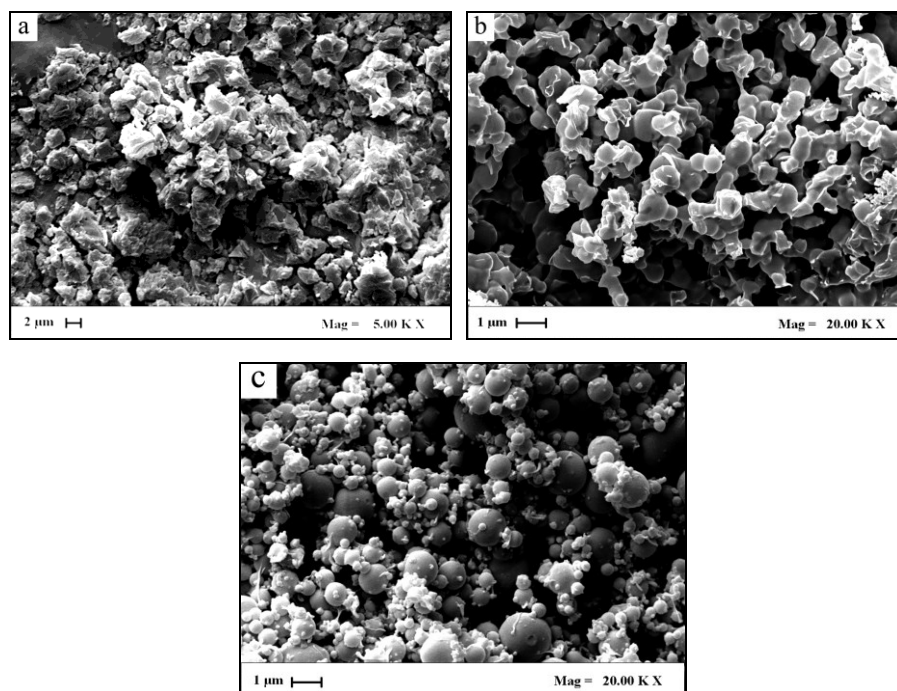


Figure IV.1 FESEM images of SAA powders produced at different weight ratios ($R=PEA/PVP$ w/w): a) $R=1/3$; b) $R=1/5$ and c) $R=1/8$.

Therefore, PVP content was increased to 1:5 wt/wt. In Figure IV.1b, a SEM image is reported of the composite particles obtained by SAA using this composition ratio. They show a quasi-spherical morphology; but, they are still coalescent and not well separated, probably due to PEA incipient crystallization. However, the morphology obtained in this experiment represents an improvement with respect to the one observed in the previous tests. When SAA tests at PEA/PVP ratio 1:8 w/w were performed, particles like the ones reported in Figure IV.1c were obtained. In this case, FESEM image shows perfectly spherical particles with no coalescence, in which PEA has been efficiently blocked, producing a coprecipitate. PSD of coprecipitated PEA/PVP 1:8 w/w was investigated calculating particle diameter from FESEM photomicrographs. PEA/PVP particles showed a relatively narrow distribution, with $d_{10}=0.23\ \mu\text{m}$; $d_{50}=0.40\ \mu\text{m}$; $d_{90}=0.84\ \mu\text{m}$.

IV.2.2 Characterization of coprecipitates PEA-PVP

XRPD analysis (Figure IV.2) showed that untreated PEA has a crystalline structure, with well-defined peaks; SAA micronized PEA using ethanol as solvent shows a different crystalline structure. The coprecipitates PEA/PVP 1:8 and 1:5 w/w do not show the characteristic peaks of PEA.

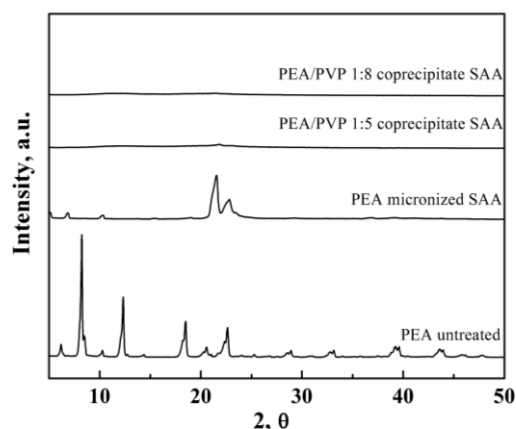


Figure IV.2 XRPD spectra: comparison among SAA coprecipitates PEA-PVP, PEA micronized by SAA and PEA untreated.

A detail of XPRD of coprecipitates PEA/PVP 1:8 and 1:5 w/w (figure not shown) reports the characteristic peak halos of PVP whereas PEA peaks are almost disappeared, except than one at $2\theta=22^\circ$ that is more evident for PEA/PVP 1:5 w/w ratio. Therefore, we can state PEA in these coprecipitates has an amorphous structure.

Loading efficiency tests

To verify the effective coprecipitation of the two compounds, loading measurements were performed. HPLC analyses carried out on SAA coprecipitates showed the presence of 11.1% and 16.7% of PEA for PEA/PVP 1:8 and 1:5 w/w respectively, with very high loading efficiency for all the samples, close to 100%.

SAA coprecipitation experiments PEA/LUT

LUT alone when micronized by SAA, starting from a solution of 20 mg/mL in ethanol, at 81°C and 93 bar in the saturator and 65°C in the precipitator, has a partially irregular morphology, as shown in the FESEM photomicrograph reported in Figure IV.3, with the formation of spherical particles covered by small needles. This result means that, during spherical droplet evaporation, small LUT acicular crystals are formed on particle surface, due to LUT recrystallization. Nevertheless, the original spherical shape is still visible.

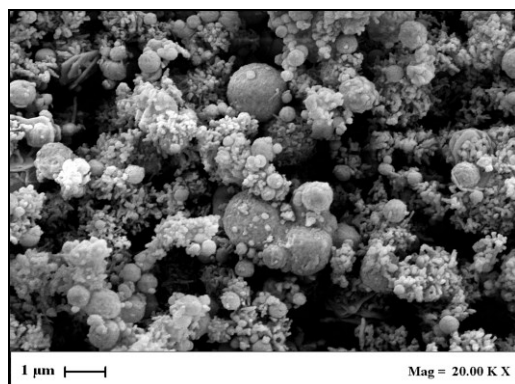


Figure IV.3 FESEM image of LUT micronized by SAA at 81°C and 93 bar in the saturator, 65°C in the precipitator.

Therefore, differently from PVP, whose microparticles produced by SAA are perfectly spherical, luteolin precipitates are relatively less regular. However, it has been reported that the pharmacological association PEA-LUT shows better results than PEA alone and it is currently on the market as *Glialia*® (produced by Epitech Group Spa, Saccolongo, Italy). Therefore, a series of coprecipitation experiments was performed by SAA to try to produce PEA-LUT nanostructured coprecipitates.

Coprecipitation experiments were carried using PEA-LUT weight ratios 10:1, 8:1, 6:1 w/w, solubilizing both compounds in ethanol. SAA operating conditions were: total concentration in ethanol 10 or 20 mg/mL, *gas to liquid ratio* 2, saturator temperature 80°C, precipitation temperature between 55 and 65°C. In Table IV.2, SAA operating conditions, used in this set of experiment, are summarized.

A FESEM photomicrograph of the coprecipitates PEA/LUT 10:1 w/w is reported in Figure IV.4.

Table IV.2 Compositions and operating conditions used to perform PEA-LUT coprecipitation experiments. (*C*: total concentration; *Q*_{CO₂}: CO₂ flow rate; *P*_{sat}: saturator pressure; *T*_p: precipitator temperature).

solute	C (mg/mL)	Q _{CO₂} (g/min)	P _{sat} (bar)	T _p (°C)
LUT	20	7.82	93	65
PEA:LUT 10:1	10	6.75	93	65
PEA:LUT 8:1	10	7.13	80	60
PEA:LUT 6:1	10	7.13	80	55

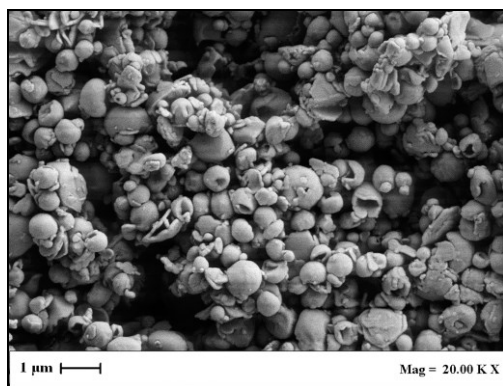


Figure IV.4 FESEM image of SAA PEA-LUT coprecipitate, produced at PEA/LUT=10:1 (w:w) ratio.

A large improvement of the morphology with respect to pure LUT and PEA can be noted; indeed, spherical particles are produced in which the flat crystals characteristic of PEA are no more visible, no acircular crystals are present and particle coalescence is practically absent. However, the microparticles are not perfectly spherical: holes and cavities can be observed: similar morphologies have been previously observed when the start of a crystallization process superimposed to droplet (amorphous) drying (Reverchon et al., 2005, Martin et al., 2013, Adami et al., 2012).

Increasing the amount of luteolin (8:1, 6:1 w/w), keeping constant the total concentration of solutes in ethanol, only small modifications of particle morphology were observed with no more morphological improvements. Therefore, we assumed that the best results in terms of particle morphology were obtained using the highest PEA/LUT ratio (10:1 w/w) and analysed in details these coprecipitates. The particles show a sharp PSD with a d_{50} of 0.97 μm ; i.e., submicronic particles have been successfully produced.

A possible explanation of the success of PEA/LUT coprecipitation is the influence of two scientific aspects: luteolin very efficiently inhibits PEA crystallization process, favourably interacting with it and the use of a lower temperature in the precipitator reduces crystallization rate of precipitates. PEA/LUT 10:1 w/w reproducibility tests were repeated 7 times using the same starting batch; practically the same results in terms of coprecipitate morphology and PSDs were obtained.

IV.2.3 Characterization of coprecipitates PEA-LUT

In Figure IV.5, XRPD analyses of PEA, LUT and their coprecipitates are reported.

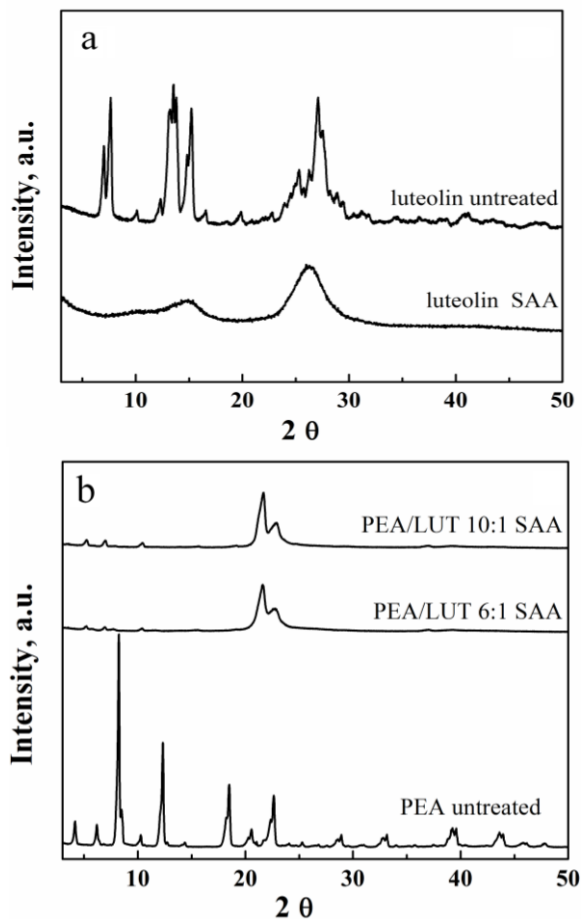


Figure IV.5 XRPD spectra: comparison among a) LUT, untreated and micronized by SAA and b) SAA coprecipitates PEA-LUT and untreated PEA.

It is possible to note that LUT micronized by SAA mainly shows the halos typical of the amorphous structures, confirming FESEM images observations, whereas the untreated compound shows a crystalline structure. These spectra have been used as subtraction reference for the measurement of the crystalline degree of coprecipitates. XRPD analyses showed that PEA in SAA coprecipitates 10:1 w/w has a crystalline degree of 43% when compared to the untreated sample.

The infrared (IR) spectrum of PEA/LUT coprecipitates showed significant changes when compared to the spectra of LUT and PEA alone, as shown in Figure IV.6, where a detail of these spectra in the range 2500-3700 cm^{-1} is reported.

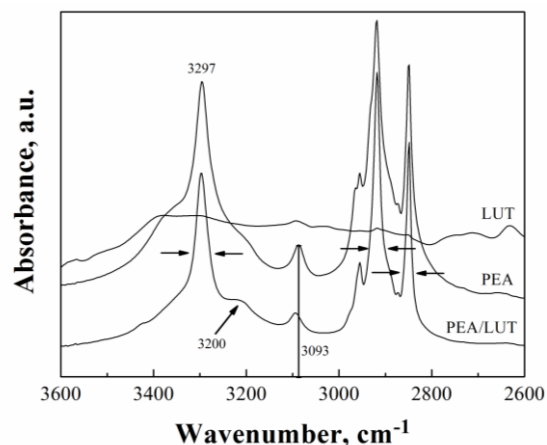


Figure IV.6 FTIR spectra in the 3700-2500 cm^{-1} range: comparison among SAA PEA-LUT coprecipitate (10:1 w:w), untreated LUT and pure PEA.

The coprecipitates show the presence of hydrogen bonding between the two compounds that have a significant influence on the peak shape and intensities in the region of the IR spectrum evidenced. They caused peak broadening and shifts in absorption to lower frequencies. IR traces indicated that there is a smoother band at 3297 cm^{-1} , compared with PEA spectrum; furthermore, a band broadening is present at 3200 cm^{-1} . These two changes can be explained by the breakdown of the intermolecular hydrogen bonding of LUT and the creation of new hydrogen bonds between PEA and LUT (Corredor et al., 2009). The interaction between the two compounds produces also the shift of the PEA peak located at 3093 cm^{-1} , to higher frequencies. In addition, the absorption band at 1284 cm^{-1} in PEA is shifted to 1269 cm^{-1} in PEA/LUT spectrum, due to another interaction between the compounds. These intermolecular bonds and the steric hindrance restrict the molecular mobility of PEA molecules and provide stability to the system (Baghel et al., 2016). As reported in the literature, molecules capable of specifically interacting with an active principle in a dispersion, such as through hydrogen bonding, can inhibit crystallization (Newman et al., 2012). These results substantially confirm the previous observation that LUT efficiency in the partial blocking PEA crystallization should be related to interactions between the two compounds (Lin et al., 2008, Di Capua et al., 2017a, Di Capua et al., 2017b). DSC analyses are reported in Figure IV.7.

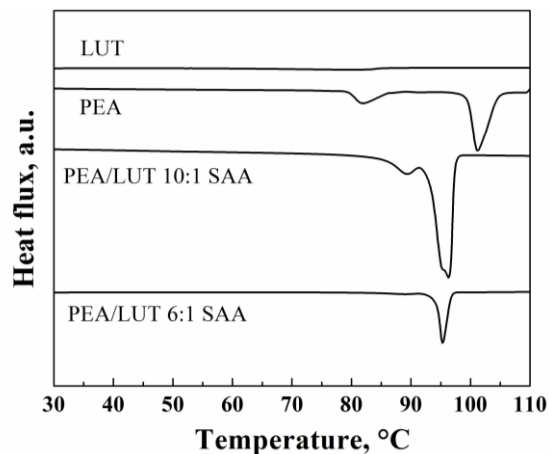


Figure IV.7 DSC thermograms related to PEA, LUT and SAA PEA-LUT coprecipitates.

It is possible to note that PEA-LUT coprecipitated by SAA show a different thermal behavior compared to the untreated materials. In particular, untreated LUT thermogram shows no peaks, indicating that it is amorphous and untreated PEA thermogram shows two melting peaks at 80°C and 100°C, indicating that two crystalline forms are present in the molecule. The thermograms of PEA-LUT coprecipitates show a single melting peak at temperatures between 95°C and 100°C that suggests the presence of a single PEA crystalline form.

The analyses of ethanol residues showed that for all the powders produced by SAA, they are far below the limits stated by US Pharmacopeia (5000 ppm for ethanol) (Levy and Nelson, 1961), and are even below the ones in the starting (untreated) material in the case of LUT, due to solvent extraction during SAA processing (see Table IV.3).

Table IV.3 Solvent residues in the tested materials.

Sample	ppm Ethanol
PEA untreated	2
LUT untreated	435
PEA/LUT 10:1 coprecipitated by SAA	87

Loading efficiency tests

HPLC analyses on the sample PEA/LUT 10:1 w/w, confirms the efficiency of SAA process in producing coprecipitates, showing the presence of 90.5% of PEA, with a loading efficiency of 99.6%.

Stability tests

Stability tests on the coprecipitates PEA/LUT 10:1 w/w SAA processed, have been carried for 23 days, aimed at studying the variation of morphology and PSD of the coprecipitates with time, as required by Epitech Group SpA. The sample was stored in dark and dry conditions, keeping the powder under nitrogen; then, SEM analyses were repeated at different times. An example of the morphology of the coprecipitates after 10 days of storage is reported in Figure IV.8. FESEM photomicrograph shows that the powder did not change morphology with time and no aggregation of particles took place. The same morphology was also observed after 4 months of storage, in a long stability test performed at the end of this study. In Table IV.4 the major characteristics of particles PSD with time are reported. They show very similar characteristic dimensions for d_{10} and d_{50} ; only d_{90} shows a non-negligible increase at the longest storage times.

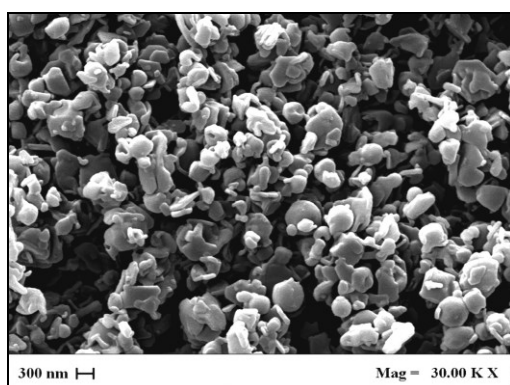


Figure IV.8 FESEM image of PEA-LUT particles (10:1 w/w) coprecipitated by SAA after 10 days of storage.

Table IV.4 Stability analysis of SAA coprecipitates of PEA/LUT 10:1 w/w during 23 days.

day	PSD		
	d_{10} [μm]	d_{50} [μm]	d_{90} [μm]
0	0.4	1.1	12.6
3	0.6	1.4	11.9
7	0.6	1.3	10.1
10	0.6	1.2	11.5
16	0.6	1.3	14.4
23	0.5	1.2	15.8

IV.2.4 Conclusions on PEA-PVP and PEA-LUT systems

This work demonstrated that the solid dispersions obtained by SAA coprecipitation allow to efficiently produce PEA-PVP and PEA-LUT submicroparticles. PEA showed the tendency to precipitate separately from PVP and the control of morphology was incomplete at lower PVP contents; however, increasing PVP content, stable dispersions were obtained for PEA/PVP 1:8 w/w ratio. Spherical particles were obtained without the production of PEA independent crystals and with a PEA loading very similar to the starting formulation value.

The coprecipitation of PEA-LUT also produced spherical submicrometric particles. LUT was efficient in controlling the tendency of PEA to crystallize even at very low LUT contents. This result can be explained by the fact that PEA-LUT interactions are obtained. The ratio PEA/LUT that produces the best control of morphology is 10:1 w/w.

The most relevant difference between the two series of results proposed in this work is the different sensitivity of PEA at the two guest compounds. PEA/PVP 1:8 w/w gives good results in terms of morphology and loading efficiency; however, PEA/LUT 10:1 w/w is an exceptional result: very small quantities of LUT stabilize the coprecipitates; i.e., they are sufficient to modify the crystallization behavior of PEA, using a quantity of the guest compound 80 times smaller than in the case of PVP. The explanation is that PEA-LUT is not a simple coprecipitate and PEA-LUT chemical interactions control the result of the precipitation.

IV.3 Improvement of CUR bioavailability

CUR is contained in large quantities in the roots of *Curcuma longa*; it possesses well-known antioxidant, antimicrobial, anti-inflammatory and anticancer properties (Bansal et al., 2011, Wilken et al., 2011, Chattopadhyay et al., 2004). However, it has a very low solubility in water based systems and, consequently, it shows a poor bioavailability, that represents a great limitation to its use as a powerful pharmaceutical agent. Moreover, CUR is relatively unstable in aqueous solution and undergoes rapid hydrolytic degradation that severely reduces its bioavailability (Shen and Ji, 2012, Paradkar et al., 2004).

Martins et al. (Martins et al., 2013) used spray-drying to prepare microparticles of Curcuma longa extract plus PVP and colloidal silicon dioxide. CUR-PVP microparticles were generally larger than 5 μm with a maximum yield of 53%. Comparison of the dissolution profiles of these microparticles with starting materials and residual solvent analysis were not reported. Paradkar et al. (Paradkar et al., 2004) used the same technique to produce microspheres of CUR in PVP, obtaining irregular and spherical particles of 3-10 μm . Solid dispersions of CUR at different PVP ratios were also prepared. Dissolution studies on CUR and its physical mixtures in 0.1 N HCl (pH 1.2) showed negligible release of CUR (0.25%) after 90 min. During the same time microspheres release up to 1.5% CUR for the 1/10 ratio. Farazuddin et al. (Farazuddin et al., 2014) proposed the encapsulation of CUR in PLGA microparticles to increase its bioavailability and facilitate slow release kinetics. Microparticles were prepared using an oil-in-water emulsion plus solvent evaporation technique. PLGA microparticles showed 17% release of CUR in 48 hours, which increased slowly with time. Khan et al. (Khan and Rathod, 2014) prepared CUR alone nanoparticles via solvent-nonsolvent nanoprecipitation using a spinning disc reactor. CUR particle diameters were in the range 180-220 nm, using PVP as stabilizer. They showed a decrease of crystallinity and displayed larger water dissolution rates than pure CUR. It was observed a complete dissolution in about 50 minutes in water, whereas the starting material in the same time dissolved at no more than 5%. Krausz et al. (Krausz et al., 2015) dissolved CUR and chitosan in methanol with PEG400 and tetramethyl orthosilicate-HCl inducing polymerization. The resulting gel was dried and processed by ball milling cycles to produce uniform particles. They obtained particles with a mean diameter around 220 nm containing CUR at 1% embedded in a porous lattice. An incomplete release (around 80%) of CUR was obtained in 24 hours. CUR loaded in dextran sulphate and chitosan nanoparticles was prepared by simple coarcevation method by Anitha et al. (Anitha et al., 2011). These particles had a spherical morphology with an average size around 200 nm. Drug entrapment efficiency was around 74%. In vitro drug release studies showed a burst release in the first 3 h, followed by a release

of CUR over a period of one week; about 70% of drug was released in this time.

In addition, SCFs based techniques were attempted to produce curcumin delivery systems. For example, Xie et al. (Xie et al., 2015) used SAS process with a coaxial injector and hexafluoroisopropanol as the solvent, to form a silk fibroin plus 0.5-1% CUR solution. These authors produced nanoparticles generally smaller than 100 nm. They obtained low drug loading and encapsulation efficiencies of $12\% \pm 0.62$ and $36\% \pm 1.9$, respectively. In vitro studies in phosphate buffer saline solution showed that 75% of CUR was released from silk-fibroin in about 200 hours. Nanoparticles produced by SAS are formed by nucleation and growth; therefore, the composite nanoparticles can be produced by homogeneous nucleation and/or chemical interactions between the compounds to be coprecipitated. This mechanism can explain the low encapsulation efficiencies they obtained (Reverchon and De Marco, 2011). Zabihi et al. (Zabihi et al., 2014) produced CUR nanoparticles coated by poly(lactic-co-glycolic acid) (PLGA) using a fluidization assisted supercritical anti-solvent process. PLGA solution was sprayed into supercritical CO₂ medium, in which CUR nanoparticles were fluidized by ultrasonic vibration. The loading of particles was enhanced by increasing ultrasound power and fluidizing potential. High anti-solvent flow rate also improved the loading efficiency and size distribution. PLGA-CUR particles were obtained with the average size of 40 nm at the ultrasonic power of 350 W. However, the CUR loading never exceeded 38%. No burst release was observed and after 600 minutes only 31.3% of CUR was released. Pedro et al. (Pedro et al., 2016) used PGSS to process [tristearin/soy phosphatidylcholine]/[CUR/DMSO] mixtures. Various lipid/CUR mixtures were processed. SEM analyses showed that the particles were large and presented an irregular shape in all formulations proposed. For example, mean particle size was between 20 μm and 70 μm . CUR loading ranged between 30 and 87 drug/lipid w/w and strongly decreased, increasing CUR content in the initial mixture. Dissolution studies were not proposed.

Therefore, according to the literature, until now the problem of CUR dissolution rate enhancement has not been resolved. In this work (Adami et al., 2017a), for the first time SAA process was proposed for the production of a biocompatible drug delivery system based on PVP loaded with CUR. Appropriate SAA process parameters and conditions were studied and the effect of polymer/drug ratio on the co-precipitate characteristics is investigated. The precipitates were analyzed in terms of morphology, solid state and loading efficiency. *In-vitro* release studies were performed to measure the increase of CUR release rate.

IV.3.1 Experimental results

Trying to take advantage of these previous experiences (Liparoti et al., 2013, Liparoti et al., 2015), the process conditions used in this study were: saturator pressures ranging between 93 and 99 bar and temperature fixed at 80°C; these conditions assure large solubility of CO₂ in the liquid solution formed by ethanol and CUR. The temperature of the precipitation vessel was fixed at 80°C at a pressure of about 1.50 bar. Different *gas-to liquid ratio* (GLR: mass ratio between CO₂ and liquid solution) were investigated: 0.8, 1.3 and 1.8. Considering these GLR values in the framework of the high-pressure phase equilibria diagram CO₂-ethanol at 80°C, the operating points fall into the two-phase gas-liquid region, as shown in Figure IV.9. The polymer was dissolved in ethanol at a concentration of 10 mg/mL and several drug/polymer weight ratios (R) were investigated, as summarized in Table IV.5.

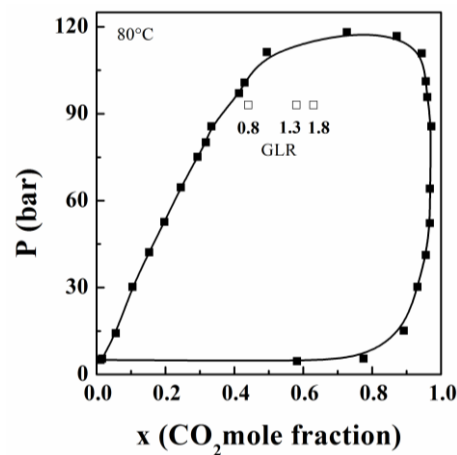


Figure IV.9 Operative points in the phase equilibrium diagram CO₂-ethanol at 80°C.

Table IV.5 Operative conditions used to produce CUR and PVP particles by SAA technique.

Test code	R (w_{cur}/w_{pol})	C (mg/mL)	GLR
PVPC1	1/8	11.25	1.8
PVPC2	1/6	11.66	
PVPC3	1/4	12.50	
PVPC4	1/2	15.00	
PVPC5	1/8	11.25	1.3
PVPC6	1/8	11.25	0.8

The particles produced in these experiments consisted of spherical and/or spherical collapsed submicrospheres, as shown in Figure IV.10, where examples of FESEM images at different R are reported.

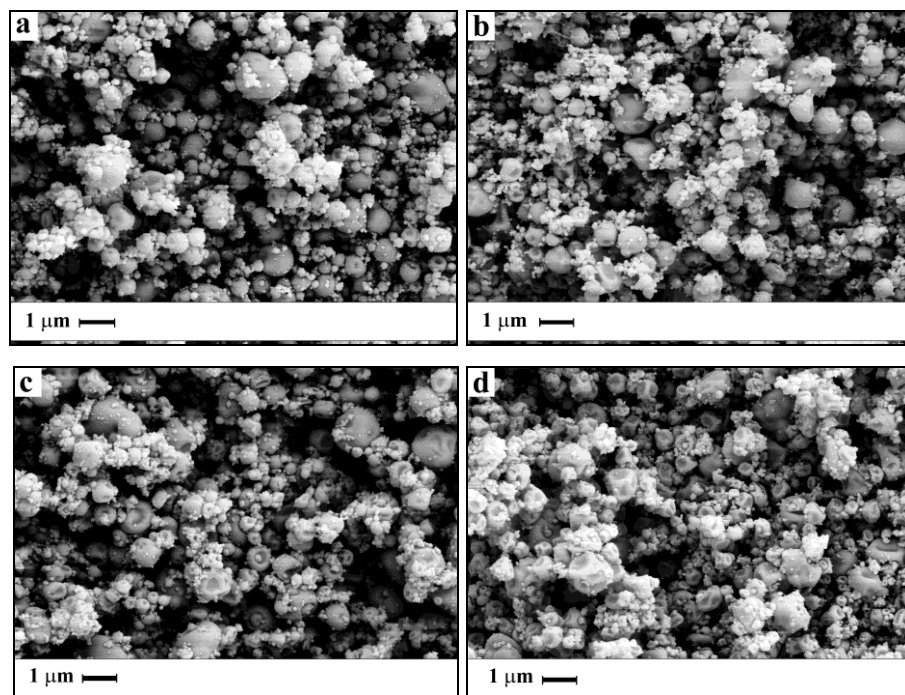


Figure IV.10 FESEM images ($Mag=20\text{ KX}$) of CUR/PVP microparticles, obtained by SAA at different mass ratios R: a) 1/8, b) 1/6, c) 1/4, d) 1/2.

The collapse of microparticles may be due to the fragility of the solid structure formed and can be correlated to the presence of CUR, since PVP alone particles formed by SAA did not show this characteristic (Adami et al., 2017b). The collapse of particles is particularly evident as R increases, confirming that can be correlated to the increase of CUR content. Similar results have sometimes been previously observed in SAA produced microparticles (Adami et al., 2017b, Della Porta et al., 2010), but also in some cases of spray drying, that shows some similarities with the SAA process (Vicente et al., 2013). In both processes, the evaporation of the droplets involves mass and heat transfer mechanisms, influenced by the drying temperature and the solute concentration. During drying, the precipitation of the solid starts from the droplet surface and the thin layer formed can be fragile, depending on the material. If solvent evaporation is fast, due to the high temperature in the precipitator, particles can collapse (Vicente et al., 2013).

PSDs in term of number of particles calculated from FESEM images are reported in Figure IV.11, where the curves obtained at different drug/polymer ratios are compared. Table IV.6 also summarizes PSDs data obtained, in term of number of particles and particle volume. For all CUR/PVP mass ratios studied, the mean particle size ranged between 0.24 and 0.38 μm and a very moderate increase of the mean diameter was observed increasing the amount of CUR. Probably, the presence of CUR implies an increase of viscosity in the starting solution, the generation of larger droplets and an overall result of enlargement of particle size. This effect is more evident for $R=1/2$ and $1/4$; whereas, no large differences can be noted for coprecipitates at $1/6$ and $1/8$. This result is expected for SAA, where parameters such as viscosity and density of the solution can influence the atomization process. Volumetric PSDs data in Table IV.6 confirm that the mean particle size is larger when the distribution is calculated in terms of particle volume: these differences are mainly due to the formation of few larger particles that have a relevant impact on the volumetric distribution.

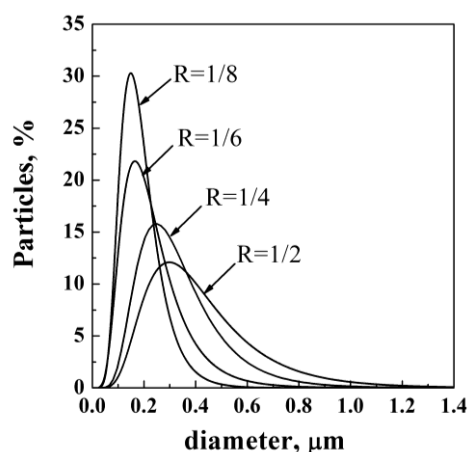


Figure IV.11 PSDs in terms of particles number of CUR/PVP particles at different drug/polymer weight ratios.

Table IV.6 PSDs data based on number and volume of CUR-PVP particles.

	% particles number			% particles volume		
	D ₁₀	D ₅₀	D ₉₀	D ₁₀	D ₅₀	D ₉₀
	[μm]	[μm]	[μm]	[μm]	[μm]	[μm]
R=1/8	0.13	0.24	0.51	0.24	0.54	0.94
R=1/6	0.12	0.22	0.48	0.26	0.53	0.95
R=1/4	0.18	0.31	0.63	0.34	0.64	1.06
R=1/2	0.21	0.38	0.73	0.39	0.76	1.24

GLR depends on the amount of CO₂ dissolved in the saturator, increasing the GLR there is an increase of CO₂ content in the liquid system forming the expanded liquid, smaller droplets are formed in the spray and consequently smaller particles are formed, as summarized in Table IV.7.

Table IV.7 PSDs data based on the volume of CUR/PVP particles at different GLR values, for R=1/8 w/w.

	D ₁₀	D ₅₀	D ₉₀
	[μm]	[μm]	[μm]
GLR=1.8	0.24	0.54	0.94
GLR=1.3	0.24	0.54	0.97
GLR=0.8	0.62	1.43	2.3

IV.3.2 Characterization of coprecipitates

XRPD analyses of all coprecipitates and pure CUR and PVP are reported in Figure IV.12. Untreated drug is crystalline and PVP is amorphous. SAA particles show only the characteristic peak halos of PVP while CUR peaks are not detectable; therefore, CUR in coprecipitates is amorphous. The drug is homogeneously dispersed at nanolevel in PVP matrix; therefore, a nanodispersion of CUR in SAA microparticles can be hypothesized. This result can be also explained by the particle formation mechanism in SAA process: each particle is the result of the drying of a droplet containing dissolved PVP and CUR; as a consequence, a homogeneous solid mixture of the two compounds is expected in the solid particle.

These results are confirmed by DSC analyses, shown in Figure IV.13. CUR alone is crystalline and its fusion temperature is at 174°C, whereas PVP is completely amorphous with a glass transition temperature around 155°C. According to the literature, when only one glass transition temperature, T_g, is observed, a one-phase solid powder is obtained (Aid et al., 2017). In the thermograms of SAA coprecipitates, the peak related to CUR fusion is not present, and the profiles are very similar to the one of PVP. Therefore, all SAA particles are in an amorphous state, and a homogenous CUR dispersion in PVP matrix are obtained by SAA process.

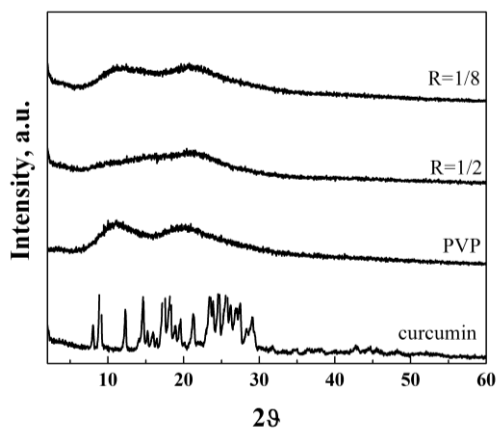


Figure IV.12 XRPD related to the PVP and CUR untreated and all coprecipitates produced by SAA.

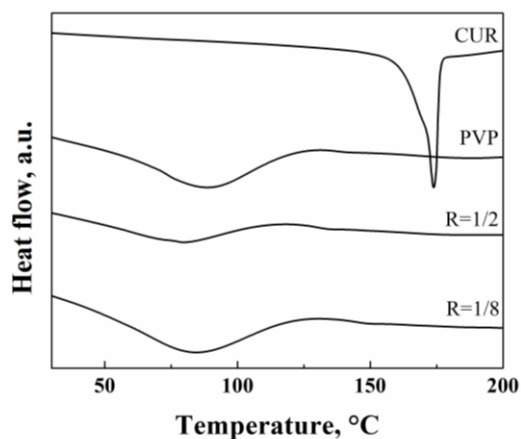


Figure IV.13 DSC analysis related to the PVP and CUR untreated and all coprecipitates produced by SAA.

The FTIR analyses (Figure IV.14) showed that no chemical bonds were formed between CUR and PVP during the coprecipitation. It can be observed, indeed, that the characteristic peaks of CUR ($1000\text{-}750\text{ cm}^{-1}$) are present in all coprecipitates spectra and they are not shifted from the original position.

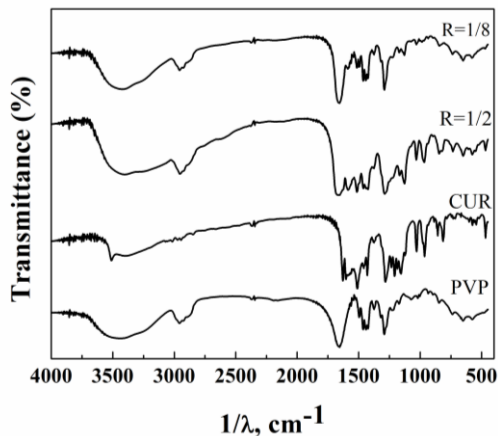


Figure IV.14 FTIR analyses of raw material and SAA coprecipitates.

Loading efficiencies and dissolution tests

A relevant information is the loading efficiency of the process that also indicates if coprecipitation was successful. The UV-vis analyses showed CUR loading efficiencies larger than 94% for all drug/polymer weight ratios studied, up to a maximum of 100%. These high values of loading efficiency correspond to high contents of CUR in SAA coprecipitates: for example, for the particles produced at R=1/2, it was demonstrated the presence of 32.5% of CUR, with a loading efficiency of 97%.

To test the effectiveness of CUR/PVP coprecipitates in improving the dissolution rate of the drug, experiments in PBS at pH 6.5 and 7.4, were performed; standard deviations were about 1.2% for SAA coprecipitates. These different values of pH are similar to those in a tumoral tissue and blood system, respectively. Figure IV.15 shows the dissolution profiles of SAA coprecipitates with respect to a physical mixture at pH 6.5.

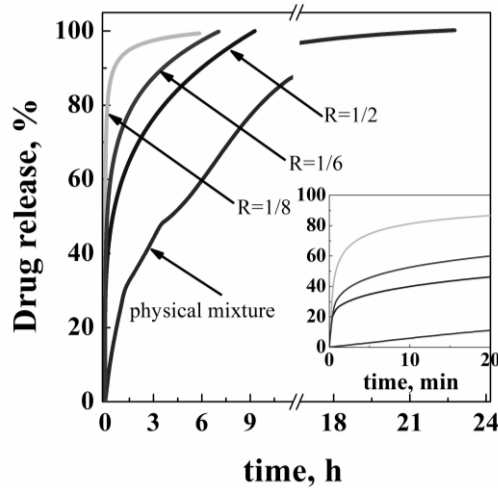


Figure IV.15 Dissolution profiles of CUR in PBS at 37 °C and pH 6.5.

Decreasing drug/polymer mass ratio, larger drug release rates are obtained; probably a more efficient dispersion of CUR in the polymeric matrix can be obtained and this fact allows the improvement of dissolution rate, observed in this study. These results are consistent with the literature: by reducing the particle size and the crystallinity behavior of curcumin, an enhanced dissolution rate resulted (DiNunzio et al., 2008). The physical mixture of the raw materials was realized using $R=1/8$; i.e., the most favorable ratio from the point of view of release rate, used in this study. It releases 100% of CUR in about 23 hours. All SAA coprecipitates show a faster release and the coprecipitates produced at $R=1/8$ show a total dissolution time of about 5.5 hours, that is about 4.5 times faster than the one of the physical mixture. Figure IV.15 also presents an insert with the enlargement of the first 20 minutes of CUR release, that cannot be appreciated in the overall diagram. During these first minutes, large quantities of CUR are released.

The dissolution tests were repeated at pH 7.4 (Figure IV.16), to study the influence of this parameter on the release rate of CUR.

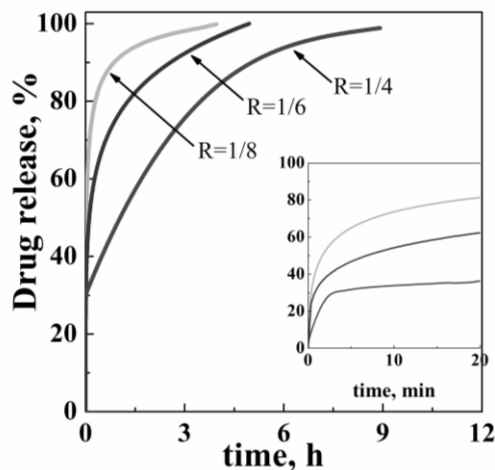


Figure IV.16 Dissolution profiles of CUR in PBS at 37 °C and pH 7.4.

In these experiments we excluded $R=1/2$ that demonstrated in the previous analysis to be the less favorable value from the release rate point of view, and, on the basis of the results obtained for the pH 6.5, we did not repeat the dissolution test on the physical mixture. Standard deviations of these curves were about 1.5% for SAA coprecipitates.

The results of the *in vitro* release of the particles obtained at CUR/PVP weight ratios of 1/8 and 1/6 and 1/4 show similar qualitative profiles as at pH 6.5. However, dissolution times are largely smaller. The full release of CUR occurs in a shorter time for all three coprecipitates. For example, for the coprecipitates at $R=1/8$ the total dissolution time is about 5.5 h at pH 6.5; but, it is 3.8 h at pH 7.4. Also at the higher pH values, the coprecipitates with a CUR/PVP weight ratio at 1/8 remain the most favorable from the point of view of release rate. In the literature, it is reported that a pH increase produces an opposite trend on CUR dissolution rates (Patra and Sleem, 2013, Rahman et al., 2009); i.e., dissolution rate decreases when pH increases. An explanation of our results could be the presence of PVP. Probably dissolution rate of PVP increases when the pH of the medium changes from acidic to mildly basic and can influence the dissolution rate of CUR. This phenomenon has been already observed in the literature and it is due to the increase of PVP swelling at mildly basic pH; this fact can improve the release of the drug entrapped in the polymeric matrix (Mishra et al., 2008).

IV.3.3 Conclusions on CUR-PVP system

SAA process demonstrated to be very efficient in the entrapment (up to 100%) of CUR in a polymeric hydrosoluble matrix in which CUR is dispersed at nanometric level. The dissolution rate of CUR from SAA produced particles was successfully enhanced, when compared to the physical mixture, as confirmed by *in vitro* release results. CUR release is 4.5 times faster for the 1/8 mass ratio with respect to CUR/PVP physical mixture. This result is very relevant from a pharmaceutical point of view, since an enhancement of CUR bioavailability is expected. Furthermore, drug/polymer ratio revealed to be an effective controlling parameter for drug release and the amorphous state of the powders produced by SAA process leads to a faster dissolution of the active principle.

IV.4 Improvement of LUT bioavailability

Flavonoids are naturally occurring polyphenolic compounds found in several kind of fruits, vegetables and medicinal plants (Lotito and Frei, 2004, Zheng and Wang, 2001). Apart from their physiological roles in the plants, flavonoids are relevant for human health because of their pharmacological properties, e.g. antiviral, antibacterial, anti-inflammatory, vasodilatory, anti-ischemic and anticancer (Procházková et al., 2011). They may block proliferation of tumor cells, including metastasis and angiogenesis, by inhibiting kinase, reducing transcription factors, regulating cell cycle and inducing apoptotic cell death (Neuhouser, 2004, Sulaiman, 2015). Luteolin (LUT) is one of the most common flavonoids present in plants, usually used in Chinese traditional medicine to treat a wide variety of diseases, such as hypertension, inflammatory disorders and cancer (Sulaiman, 2015). However, its instability, poor bioavailability and hydrophobicity restricts its clinical applications.

Several conventional micronization processes were used to improve LUT dissolution rate: spray drying, jet milling, coacervation, solvent evaporation. Dang et al. (Dang et al., 2014) prepared solid lipid nanoparticles (SLN) of LUT-soybean lecithin by hot-microemulsion technique at laboratory scale, melting lecithin at 75°C. They obtained nanoparticles with an entrapment efficiency of about 75%, that were tested *in vitro* and *in vivo* on rats, demonstrating an increase of LUT bioavailability of about 4.9 times with respect to LUT suspension in water. Khan et al. (Khan et al., 2014) prepared a laboratory recipe in which LUT was complexed with phospholipids, forming nanoparticles. They demonstrated that a faster dissolution rate of complexed LUT was possible, up to about 2.5 times than pure LUT in water. The LUT complex was also successfully tested in animal studies. Puhl et al. (Puhl et al., 2012) prepared LUT+polymer particles (polycaprolactone (PCL)

and poly(lactic-co-glycolic acid) (PLGA)) by nanoprecipitation at small laboratory scale using, as the organic phase, oils like oleic acid and isodecyl oleate, and obtained high encapsulation efficiencies (larger than 97%). This result is surprising, since, in nanoprecipitation, particles formation is driven by nucleation and growth and only a wrapping activity of the polymer can justify the formation of composite micro/nanoparticles instead of two separate precipitates. The success was possible due to the fact that very small quantities of LUT were used with respect to polymer content; they used 75 mg of polymer against 1.25 mg of LUT: it means a ratio drug/polymer of 1/60 w/w.

Summarizing, the works found in the literature were successful in demonstrating the feasibility of LUT bioavailability increase when coprecipitated and produced at submicro scale. However, reliable, large scale applicable processes have not yet been tested for LUT coprecipitation. Therefore, in this work (Di Capua et al., 2017b) the applicability of SAA process for the production of systems LUT-PVP to produce composite particles with improved bioavailability and stability, is studied.

IV.4.1 Experimental results

First, LUT alone was micronized by SAA to evaluate its processability. The process conditions selected were: 4 mg/mL LUT in ethanol, at 80°C and 95 bar in the saturator and 80°C in the precipitator. The CO₂ flow rate was set at 7.8 g/min and the solvent flow rate was set at 5.4 mL/min, to obtain a gas-to liquid ratio (GLR: mass ratio between CO₂ and liquid solution) in the saturator of 1.8. These process conditions were selected to assure a good solubility of CO₂ in ethanol. The particles obtained showed an irregular morphology, as in the FESEM photomicrograph reported in Figure IV.17, with the formation of spherical particles from which small needles emerge.

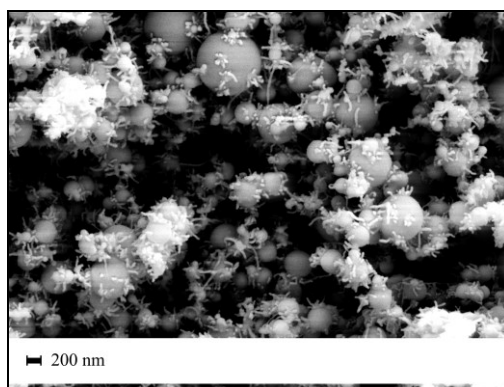


Figure IV.17 FESEM image (*Mag= 35 KX*) of SAA LUT particles.

These results indicate that LUT has a very fast crystallization kinetics and, during the late steps of droplets evaporation, it starts to crystallize. This particular tendency has been previously observed for other SAA processed materials (Martin et al., 2013, Adami et al., 2012). Each microsphere evidences the superposition of amorphous solidification and crystallization processes; therefore, LUT was not a good candidate for SAA micronization but for coprecipitation. The process conditions selected for coprecipitation experiments, were the same used for SAA experiments performed using LUT alone. LUT/PVP weight ratios 1/8, 1/6 and 1/4 w/w were selected to study the influence of this parameter on LUT release rate, using a constant concentration of polymer (10 mg/mL). In Table IV.8, the ratios and concentrations of LUT/PVP used in selected coprecipitation experiments are summarized. Examples of FESEM images of LUT/PVP 1/8 and 1/4 (w/w) samples are reported in Figure IV.18.

Table IV.8 Ratios and concentrations of LUT and PVP used for SAA experiments. (C_{pol} : PVP concentration; C : total concentration; $R=LUT/PVP$ w/w; * superposition of amorphous and crystalline product).

Test code	R (w_{LUT}/w_{PVP})	C_{pol} (mg/mL)	C (mg/mL)	Mean diameter [μm]
LUT01	-	-	4.0	0.34 (± 0.11)*
PVP	-	10	10.0	0.16 (± 0.11)
PVPL01	1/8	10	11.3	0.33 (± 0.12)
PVPL02	1/6	10	11.7	0.23 (± 0.11)
PVPL03	1/4	10	12.5	0.22 (± 0.09)

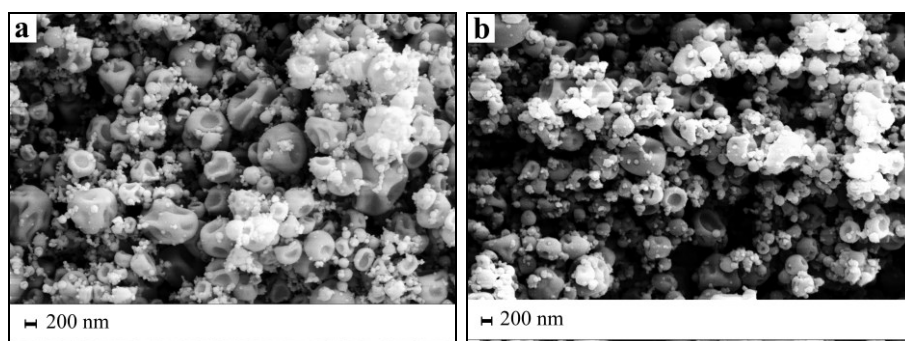


Figure IV.18 FESEM images (Mag=30 KX) of LUT/PVP microparticles produced at a) $R=1/4$ and b) $R=1/8$.

These particles consist of spherical and/or collapsed submicrospheres. This morphology has been sometimes previously observed in SAA processing and can be due to the fragility of the solid structure (Liparoti et al., 2012, Adami et al., 2017a, Adami et al., 2017b). SAA particles are collapsed in a more evident manner as R increases. Since SAA shows many similarities with spray drying, particles collapse can be explained referring to this latter process. The theory of particle formation in spray drying (Vicente et al., 2013, Eslamian et al., 2009) claims that the particle morphology is influenced by drying time, shell flexibility and evaporation rate. When a dilute solution is processed, during drying, a thin layer of solid is formed. This shell can be fragile or flexible and, if the drying temperature is high, the solvent evaporation will be very fast and particles can deflate. This theory can also explain the morphology of LUT-PVP SAA produced particles. Figure IV.19 reports PSDs, in terms of number of particles calculated from FESEM images, where the curves obtained at different LUT/PVP ratios are compared. The mean size of the coprecipitates depends on LUT/PVP weight ratio (R): their mean diameter increases as R decreases. Submicroparticles were consistently obtained; the largest PSD covers the range from 0.1 to about 1.2 μm .

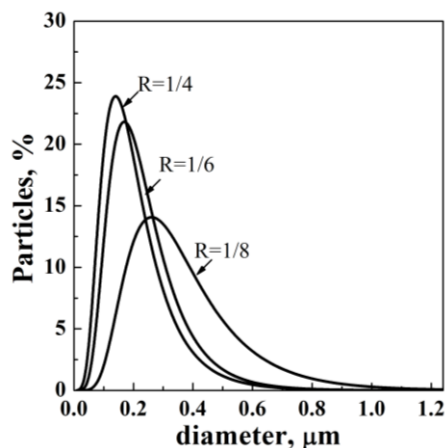


Figure IV.19 PSDs of LUT/PVP composite particles produced by SAA at different drug/polymer weight ratios.

IV.4.2 Characterization of particles

XRPD analysis of coprecipitates and of pure LUT and PVP is reported in Figure IV.20. The analyses revealed that unprocessed LUT has a crystalline structure; whereas, untreated PVP shows the typical halos of an amorphous polymer. LUT processed by SAA, instead, shows only two enlarged peaks, probably due to a partial LUT re-crystallization during droplets evaporation.

This fact could explain the presence of the small needles, as seen in Figure IV.17. The diffractograms of all SAA coprecipitates show only PVP halos, whereas LUT peaks are not present: all coprecipitates show an amorphous structure. This result can be explained by a homogeneous dispersion of LUT in the polymer matrix (Aid et al., 2017).

FT-IR analyses were performed to identify possible interactions between LUT and PVP in the composite particles. In Figure IV.21, FT-IR spectra of unprocessed LUT and PVP, SAA coprecipitates and physical mixture are reported in the range 1750-500 cm^{-1} .

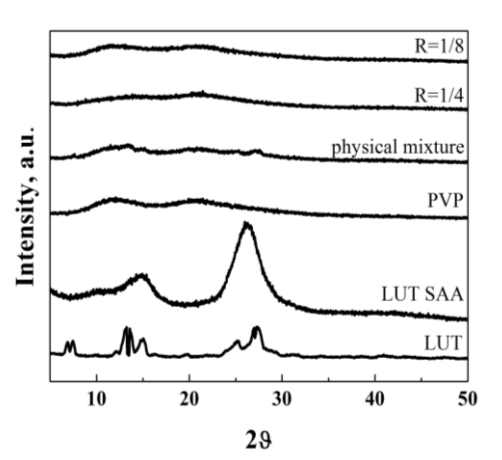


Figure IV.20 XRPD related to the PVP and LUT untreated and SAA coprecipitates.

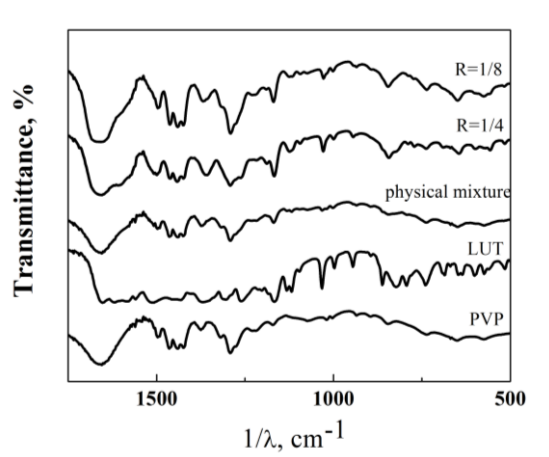


Figure IV.21 FTIR analyses of raw materials and SAA coprecipitates.

PVP spectrum shows a characteristic absorption band at 1653 cm^{-1} , corresponding to the stretching vibration of C=O groups, a C-H stretching vibration at 2875 cm^{-1} and a -OH stretching vibration at 3469 cm^{-1} . The spectrum of untreated LUT shows characteristic absorption bands at 1656 cm^{-1} that suggests the stretching vibration of carbonyl group, at 1166 cm^{-1} related to C-O-C stretching vibration and at 1266 cm^{-1} related to phenolic hydroxyl groups bend. The spectrum of the physical mixture LUT/PVP shows the superimposition of the characteristic bands of LUT and PVP. All SAA coprecipitates show the presence of hydrogen bonding between the two compounds that have a significant influence on peak shape and intensities. The interaction between the two compounds produces the shift of the LUT peak located at 1036 cm^{-1} to lower frequencies. Also, the absorption peak at 1377 cm^{-1} in PVP spectrum is shifted to 1371 and 1361 cm^{-1} in LUT/PVP spectrum, respectively for $R=1/8$ and $R=1/4$, due to another interaction between drug and polymer. Furthermore, there are two peaks broadening towards 1600 and 1260 cm^{-1} in the composite particles spectra, more evident at $R=1/4$. These two changes in LUT/PVP spectrum can be explained by the breakdown of the intermolecular hydrogen bonding of LUT and the creation of new hydrogen bonds between PVP and LUT. Therefore, higher R values lead to more hydrogen bonds and to more marked shifts of characteristic peaks of LUT.

DSC analyses (Figure IV.22) were performed to determine the changes in thermal behavior of drug and polymer in the coprecipitates LUT-PVP. These thermograms confirmed that untreated LUT is crystalline and its fusion temperature is 340°C . Furthermore, LUT is a hygroscopic compound, as proved by the broad endothermic peak ranging from 90 - 100°C . Unprocessed PVP shows a broad endothermic peak ranging between 50 - 130°C , due to the loss of water; as previously demonstrated, it is an amorphous polymer. SAA processed LUT-PVP particles do not present any crystalline peak and their DSC thermograms are very similar to the one of PVP. According to the literature, when only one glass transition temperature, T_g , is observed, a one-phase solid powder is obtained (Aid et al., 2017).

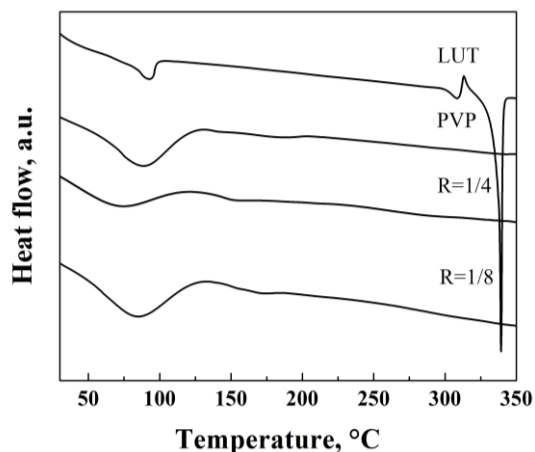


Figure IV.22 DSC analyses of untreated materials and SAA coprecipitates.

Summarizing, all solid state analyses suggest that drug is homogeneously dispersed in the PVP matrix, since each particle is the result of the drying of a droplet containing LUT and PVP. The success of SAA coprecipitation in inhibiting the formation of crystals is the mutual influence of two factors: a favorable interaction between drug and carrier, and the use of low temperatures in the precipitator that reduce crystallization rates of precipitates. In particular, the interactions drug-carrier play a role in stabilizing the composite particles, due to the hydrogen bonding and the steric hindrance that restrict the molecular mobility of LUT molecules. Therefore, the ability of PVP to inhibit crystallization can be linked to its T_g and its capacity to interact with the drug (Baghel et al., 2016).

LUT loading efficiency and dissolution tests

The loading efficiency of LUT in the SAA particles was measured by UV-vis analyses and was over 99% for all weight ratios: an effective loading ranging between 11.1% (for $R=1/8$) and 20% (for $R=1/4$) of LUT with respect to the mass of polymer in the SAA particles, is obtained. This result is not surprising, since the mechanism of SAA microparticles formation is atomization of the solution and droplets drying; therefore, the components of the starting solution tend to remain together in the final particles. This result is particularly relevant since practically all LUT is entrapped in the final product; perhaps, the interactions LUT-PVP, evidenced in the previous analysis, play a role in further stabilizing the composite particles. Therefore, all analytical indications converge towards the conclusion that coprecipitated submicroparticles LUT-PVP were efficiently produced. Dissolution tests were performed to evaluate the improvement of the dissolution rate of LUT in PBS at pH 7.4 (Figure IV.23); this pH simulates blood system.

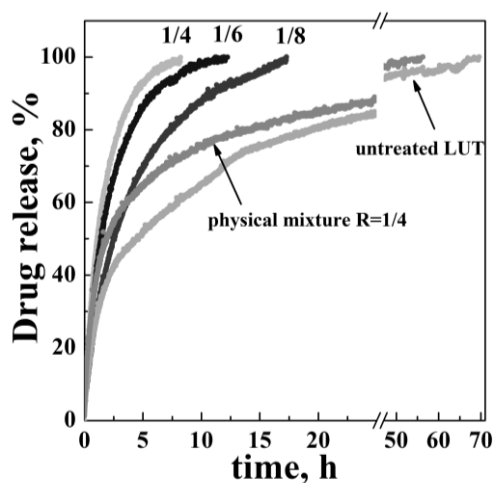


Figure IV.23 Dissolution profiles of LUT in PBS at 37°C and pH 7.4.

It is possible to observe that untreated LUT and the physical mixture at $R=1/4$ show a complete dissolution time in about 70 and 57 hours, respectively. The coprecipitate produced at $R=1/8$ w/w totally dissolves in 17 hours; whereas, the one produced at $R=1/4$ w/w completely dissolves in about 8 hours: 9 times faster than untreated LUT.

The dissolution rate of SAA produced microparticles increases with the increase of drug/polymer weight ratio and all SAA coprecipitates show a faster release than the ones of untreated LUT. This result confirms that drug bioavailability is influenced by several factors, like reduction of particle size, morphology and solid state of material (Adami et al., 2017a, Martín and Cocero, 2008). Increasing the drug/polymer weight ratio, larger drug release rates are obtained. This trend seems unusual when compared to other coprecipitated systems tested by SAA, in which the dissolution rate increases when the relative quantity of polymer decreases (Adami et al., 2017a). This behavior was expected also in this case, since PVP is highly water soluble and at higher polymer contents, smaller LUT nanoparticles should be formed inside the coprecipitate. Several parameters usually influence drug release from coprecipitates. Our hypothesis, to explain the trend of LUT-PVP dissolution behavior, is that the main role is taken by the interactions between the two compounds that reduce the dissolution rate of PVP and, consequently, the release rate of LUT is slower in the liquid medium. These results were expected since the reduced sizes of LUT that is uniformly dispersed in PVP microparticles, as demonstrated by the solid state analyses.

IV.4.3 Conclusions on LUT-PVP system

This work showed that it is possible to improve LUT dissolution rate and bioavailability preparing by SAA process LUT-PVP submicroparticles: the corresponding dissolution rate was up to 9 times faster than untreated drug. Dissolution time was reduced from the scale of days to only several hours. An unexpected result was that small quantities of PVP were enough to obtain excellent results for coprecipitation and for the increase of release rate. The formation of bonds LUT-PVP gives an account of the apparently anomalous trend of the drug release rate curves, showing that LUT release rate increased reducing the PVP percentage used in the coprecipitate, up to the largest drug/polymer ratio tested in this work (R=1/4 w/w).

IV.5 Fluorescent microspheres based on DEX, FITC and LUT

Polysaccharide-based microparticles are used as loading or conjugating imaging and therapeutic agents (Saravanakumar et al., 2012, Swierczewska et al., 2016), to provide a faster, less invasive and accurate way to obtain information about the state of biological systems, to locate tumors and to track drug delivery, its biodistribution and efficacy in the body. DEX is a polysaccharide synthesized from sucrose by lactic-acid bacteria (as *Leuconostoc mesenteroides* and *Streptococcus mutans*) (Wasiak et al., 2016). It is a very simple substance since it is a combination of glucose molecules; but, it is widely used in the medical field for several aspects: reduction of blood viscosity, prevention of blood clots. Fluorescein-isothiocyanate-dextran (FITC-DEX) (de Belder and Granath, 1973) allows to study the permeability changes of cells using an electron microscope (Thorball, 1981) and used to evidence cellular damages (Dvorak et al., 1988) and to monitor and guide the surgical resection of tumors *in vivo* (Piquer et al., 2014). Furthermore, DEX is FDA approved and its application as drug delivery system is used to improve bioavailability of poorly water soluble compounds and to increase the half-life of therapeutic substances (Mehvar, 2000). Among the several applications, the production of targeted delivery systems consisting in DEX and anticancer drug (for example doxorubicin and paclitaxel) for solid tumor therapy are the most relevant (Wasiak et al., 2016, Sagnella et al., 2014). The combination of the potential of DEX as drug delivery agent for anticancer drugs and of DEX-FITC as probe for permeability studies can lead to the production of a fluorescent carrier, to detect the drug transport in *in vitro* and *in vivo*. The addition of FITC to a system carrier+active principle allows to follow the distribution of the fluorescent materials and to track the drug delivery inside the cells (Feng et al., 2010).

In the last decades, researchers are increasingly focusing on the development of formulations based on natural compounds found in vegetables, fruits and plant extracts that have several pharmacological properties: antioxidant, anti-inflammatory, antiseptic, antibiotic (Amin et al., 2009). Compounds of natural origin can lead to new, innovative therapeutic agents for cancer, since they may benefit in cancer prevention and promote human health without recognizable side effects. Therefore, recent studies are shifting their attention from chemically synthetic drugs to natural ones (Amin et al., 2009). As previously reported, LUT is a flavon that exists in many types of vegetables (broccoli, onion leaves, carrots peppers); it exhibits a wide variety of pharmacological properties ranging from anti-inflammation to anticancer effects. Researchers have shown that LUT has antitumor activities in several types of cancer, such as lung cancer, head and neck cancer, prostate, breast, colon, liver and skin cancer (Sulaiman, 2015).

The aim of this work (Di Capua et al., 2017a) was to develop for the first time by SAA a fluorescent system that acts as a carrier for an active molecule and, at the same time, as a probe to identify the distribution and permeability of drug in cells. Two different approaches are used to produce fluorescent DEX. The first one consists of dissolving DEX and FITC in a solution that is processed by SAA. The second method is based on a labeling technique that leads to the production of a DEX chemical conjugated to FITC as described in details in Chapter II, then micronized by SAA to produce microparticles. To confirm that there is no interference of FITC on the system carrier-drug and to study the effectiveness of this fluorescent system, LUT was chosen as model drug.

IV.5.1 Experimental results

In this work, a mixture water:ethanol was used as liquid solvent, because LUT is a poorly water soluble compound, whereas DEX is soluble in aqueous solutions. Solubility of LUT and DEX was measured in different water/ethanol solutions; these tests indicated that DEX did not dissolve in aqueous mixtures containing more than ~35% (v/v) of ethanol (Antoniou et al., 2010). The best compromise was a mixture water:ethanol (70:30 v/v).

Production of LUT/DEX+FITC microparticles

DEX+FITC (0.01 mg/mL) micronization was performed at the following process conditions: mixture water:ethanol (70:30 v/v), injection pressure 92 bar, saturator temperature 85°C and a precipitator temperature 100°C. The CO₂ mass flow rate was set at 7.3 g/min and the one of liquid solvent at 4 mL/min, to obtain a mass flow ratio (GLR, *gas to liquid ratio*) of 1.8. The effect of the concentration of DEX in water:ethanol (70:30 v/v) mixtures from 5 to 20 mg/mL was studied. SAA processing was successful; an

example of FESEM image of DEX+FITC (DF) particles and the PSDs in terms of particle percentages are reported in Figure IV.24.

Spherical and non-coalescing microparticles were obtained, in the submicrometric range. When a concentration of 8 mg/mL was used, well separated microparticles with a mean diameter of about 0.4 μm were obtained, as shown in Figure IV.24a. Comparing the PSDs of the microparticles obtained at 5, 8 and 20 mg/mL, it was observed that, increasing the concentration, the mean diameter increased and the PSDs enlarged (Figure IV.24b). PSDs value related to these three different concentrations are summarized in Table IV.9.

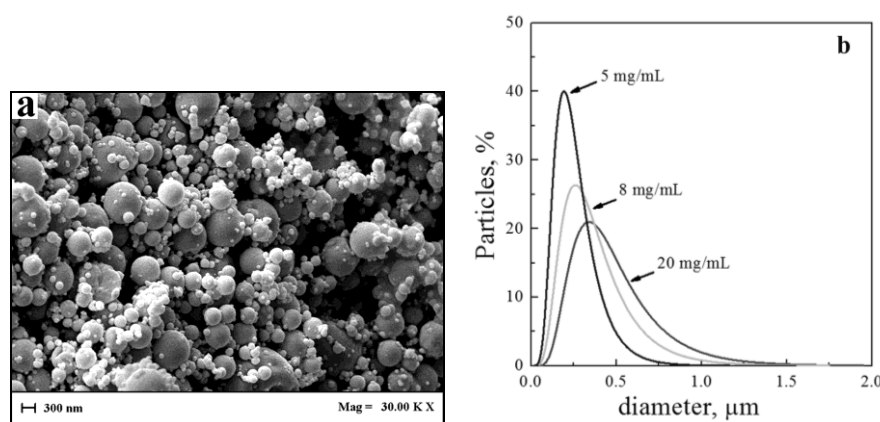


Figure IV.24 a) FESEM image of DF particles at concentration of 8 mg/mL; b) PSDs of DF particles obtained at different DEX concentration.

Table IV.9 Composition and PSD data of LUT/DEX microparticles produced by SAA (C_{FITC} : FITC concentration; C_{tot} : total concentration; C_{DEX} : carrier concentration; C_{LUT} : LUT concentration; $R = LUT/DEX$ w/w, $w_{LUT} = LUT$ weight, $w_{DEX} = DEX$ weight; DF: DEX+FITC; DF*: DEX labeled FITC; DLF: DEX+LUT+FITC; DFL*: DEX labeled FITC + LUT).

# test	C_{FITC} (mg/mL)	R	C_{DEX} (mg/mL)	C_{LUT} (mg/mL)	d_{10} (μm)	d_{50} (μm)	d_{90} (μm)
DF01	0.01	-	5	-	0.11	0.16	0.77
DF02	0.01	-	8	-	0.22	0.34	0.81
DF03	0.01	-	20	-	0.25	0.44	0.90
DF*	labeled	-	20	-	0.24	0.42	0.88
DLF01	0.01	1/8	10	1.25	0.27	0.41	0.76
DLF02	0.01	1/8	8	1.00	0.21	0.32	0.68
DLF03	0.01	1/8	5	0.70	0.12	0.20	0.41
DLF04	0.01	1/10	8	0.80	0.24	0.35	0.77
DLF05	0.01	1/6	8	1.33	0.20	0.23	0.63
DFL*	labeled	1/6	8	1.33	0.19	0.24	0.64

This behavior is commonly observed in SAA, since increasing the solute concentration, the viscosity of solution increases and larger droplets are formed at the exit of the injector, with the consequent production of larger particles.

SAA experiments on LUT alone, using water:ethanol as solvent, were not successful: LUT precipitated as irregular particles (figure not reported). LUT shows a fast crystallization rate; probably, using a water:ethanol as solvent and a temperature of 100°C, the crystallization and agglomeration of LUT was very fast. A similar result was obtained in a previous work using pure ethanol (Di Capua et al., 2017b). Coprecipitation experiments were performed dissolving DEX, FITC and LUT in the water:ethanol mixture, at LUT/DEX weight ratio $R=1/8$ (w/w) and at three different polymer concentrations: 5, 8 and 10 mg/mL. In all cases, spherical and well-separated microparticles were produced; an exemplificative FESEM image is reported in Figure IV.25a. PSDs are reported and compared in Figure IV.25b.

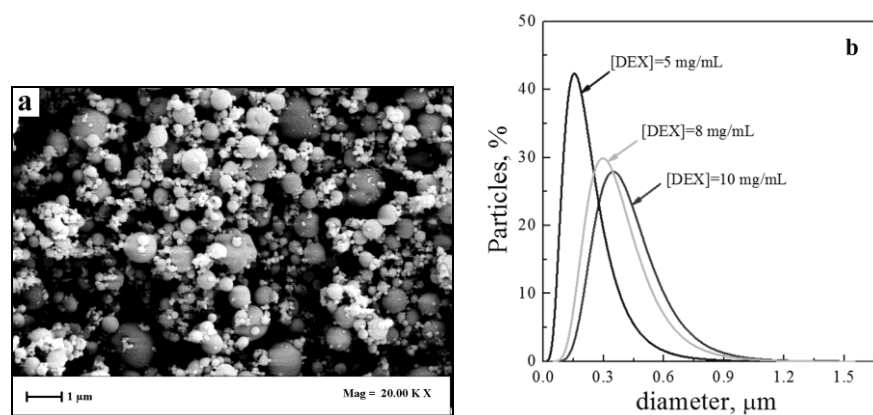


Figure IV.25 FESEM images of LUT/DEX+FITC coprecipitates at $R=1/8$ w/w and DEX concentration of 10 mg/mL; PSDs of LUT/DEX $R=1/8$ w/w coprecipitates obtained at different DEX concentration.

It is possible to observe that, according to the previous results on DEX alone, decreasing DEX concentration from 10 to 5 mg/mL, the mean diameter of particles reduces from 0.4 to 0.2 µm.

Coprecipitated microparticles produced at DEX concentration of 8 mg/mL ($R=1/8$) showed a sharp PSD and a mean diameter 0.3 µm, that can satisfy the desired target of producing micro/nanoparticles for biomedical applications. Therefore, this concentration was used for all the further experiments in this work. Three different LUT/DEX mass ratios (1/6, 1/8 and 1/10) at DEX concentration of 8 mg/mL (and FITC concentration of 0.01 mg/mL) were also selected to perform SAA tests. In Table IV.9, concentration and PSD values are summarized. Examples of FESEM images of LUT/DEX samples are shown in Figure IV.26.

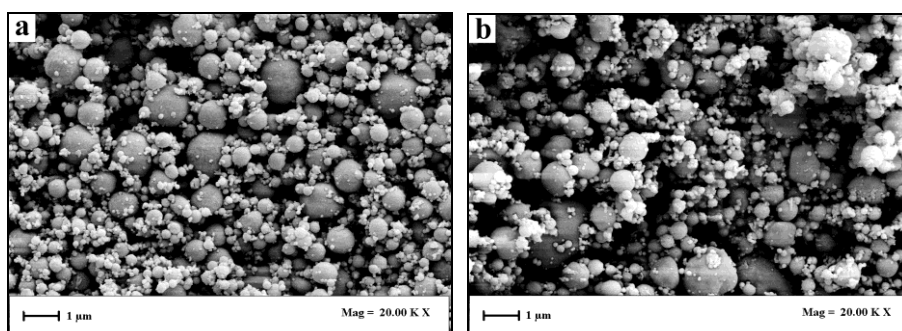


Figure IV.26 FESEM images of coprecipitates produced at a) $R=1/6$ (DLF05), b) $R=1/6$ (DFL*, using DEX labeled FITC).

Again, SAA produced particles are spherical and well separated and the mean size is influenced by the drug-polymer weight ratio (R): when R is increased, the mean size of particles slightly decreases, as shown in Figure IV.27. SAA micronization tests were also performed using a DEX labeled with FITC (DF*) in a mixture of water:ethanol at 20 mg/mL. The particles produced were perfectly spherical and comparable to those obtained in the case of DEX not labeled with FITC. The PSD values are reported in Table IV.9. Then, a mixture containing DEX-FITC conjugate and LUT at $R=1/6$ (test DFL*) weight ratio was processed producing spherical and well-separated particles, as shown in Figure IV.26b. The PSD of DFL* particles is perfectly comparable to that of DLF05 (Figure IV.27): this fact means that chemical conjugation between DEX and FITC does not influence particle size and morphology.

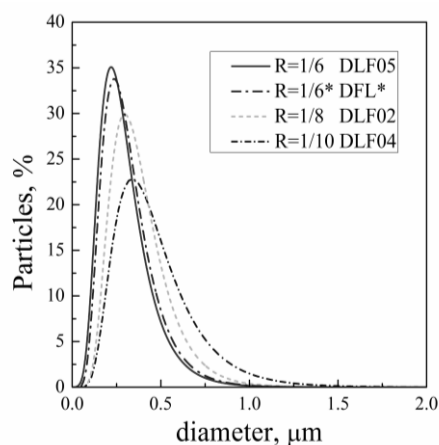


Figure IV.27 PSDs of LUT/DEX micronized by SAA, in terms of number of particle percentage; *: DEX labeled FITC.

Fluorescence microscope and FITC content

FM analyses of SAA processed coprecipitates were performed to study FITC dispersion in the powders and to verify the applicability of SAA microparticles as polymeric probe. Some exemplificative FM images are reported in Figure IV.28, where the blue fluorescence indicates the presence of FITC. The analyses indicated a homogenous FITC distribution into the polysaccharide matrix for all SAA coprecipitates. To visualize the fluorescence of SAA powders, an ultraviolet lamp was used. SAA coprecipitates containing DEX, LUT and FITC are yellow; when these powders are struck by ultraviolet rays, they produce a bright fluorescence. An exemplificative photograph of this behavior is reported in Figure IV.29.

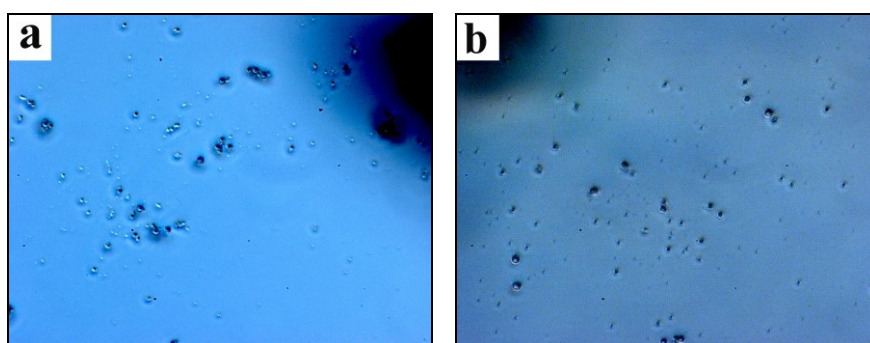


Figure IV.28 FM images related to a) $R=1/6$ DLF05; b) $R=1/6$ DFL*, test using DEX labeled with FITC.

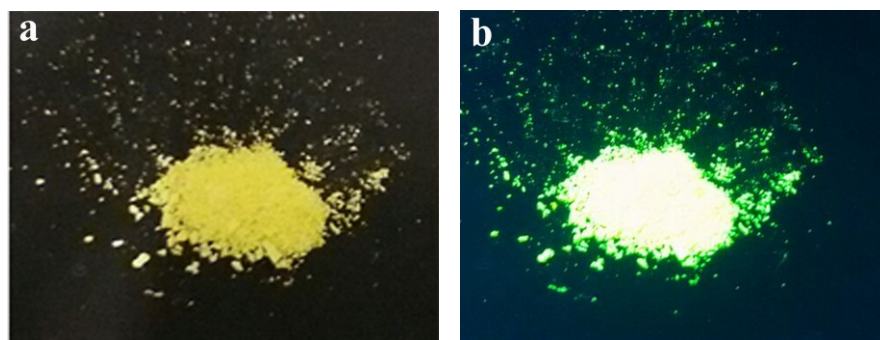


Figure IV.29 a) SAA powder under visible light; b) SAA powder under UV lamp.

To obtain quantitative information about the FITC amount in the produced powders, UV-vis analyses were performed. All SAA coprecipitates obtained using non-linked FITC showed a FITC loading efficiency ranging between 60 and 80%. Using the same analytical technique on the

coprecipitate DFL* produced, instead, using DEX labeled FITC, it was possible to confirm that all FITC labeled DEX before SAA test is present after the process: therefore SAA process does not influence chemical conjugation between FITC and DEX.

IV.5.2 Characterization of particles

XRPD analyses were carried out to study the crystallization behavior of LUT/DEX; the patterns related to the untreated compounds and SAA coprecipitates are shown in Figure IV.30. Untreated DEX and DEX labeled FITC are amorphous, as shown by the single *halo* present in their spectrum. Untreated LUT is crystalline, also in the physical mixture (R=1/6), with the characteristic peaks of the drug. For all SAA coprecipitates, the spectra are similar to the one of DEX, alone showing the *halo* typical of the polysaccharide, it means that all coprecipitated powders are amorphous.

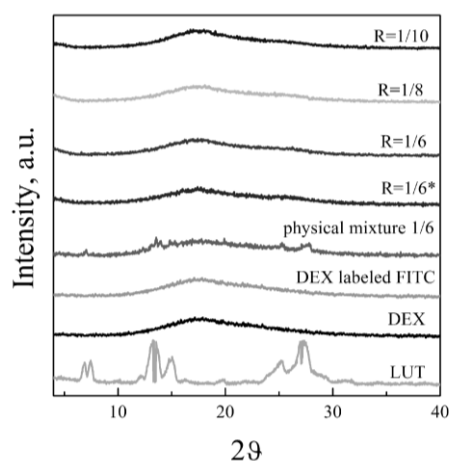


Figure IV.30 XRPD spectra: comparison among untreated compound and microspheres produced by SAA; *test using DEX labeled FITC+LUT (DFL*).

DSC analyses were performed on untreated drug and polymer and on SAA coprecipitates, to determine the changes in the thermal behavior of LUT and DEX in SAA powders. In Figure IV.31, some spectra are reported. LUT thermogram exhibited the profile of a crystalline compound with an endothermic peak at 340°C, due to a fusion phenomenon; unprocessed DEX shows a large endothermic peak between 50 and 150°C, due to the elimination of water. A glass transition of DEX is observed around 220°C that indicates no crystalline DEX are present and confirms the amorphous structure of the polymer, seen in X-Ray patterns. DEX degradation is noted

around 320°C, where a broad endothermic peak is present (Stenekes et al., 2001, Amin et al., 2015). DEX processed with FITC by SAA has a smaller endothermic peak compared to that of untreated DEX and shifted to 305°C, probably due to some changes in polysaccharide chains during the atomization process. The physical mixture shows two endothermic peaks at 275 and 312°C, indicating that the drug-polymer mixture generates some changes in the thermal behavior. In the thermograms of coprecipitates, the same loss of water noted for untreated DEX is observed, furthermore the endothermic peaks of DEX and LUT are both present, but shifted to lower temperatures and have smaller intensities. It is relevant to note that the intensity of the peak related to LUT increases when R increases. The shift of these two peaks, associated to the endothermic phenomenon of the loaded LUT and of DEX, could be related to the formation of chemical complex between the drug and the polysaccharide.

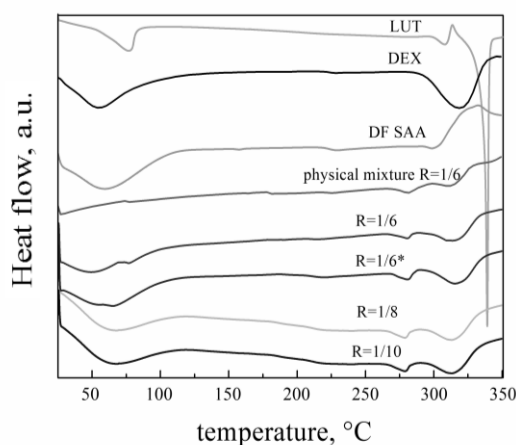


Figure IV.31 DSC thermographs related to DEX, LUT and SAA coprecipitates; DF: DEX+FITC; * test using DEX labeled FITC (DFL*).

This hypothesis is confirmed by FTIR analyses, performed to get information about the presence of some specific interactions between the drug and the polysaccharide. The spectra for unprocessed materials and SAA coprecipitates are shown in Figure IV.32, in the wavenumber range of interest (where the characteristic peaks are present). DEX spectrum shows a band in the region of 3400 cm^{-1} that is related to $-\text{OH}$ stretching vibration of the of the polysaccharide. The band in the region of 2920 cm^{-1} is attributed to C-H stretching vibration and the band in the region of 1642 cm^{-1} is due to carboxyl group. The absorption peak at 906 cm^{-1} indicates the existence of α -glycosidic bond. Peaks at 1151 cm^{-1} are due to vibrations of C-O-C bond and glycosidic bridge; the band at 1100 and 1044 cm^{-1} are due to the C-O

bond of glucose (Purama et al., 2009). The spectrum related to physical mixture of DEX and FITC (not reported) perfectly overlaps that of DEX. Untreated LUT spectrum shows: a broad peak at 3420 cm^{-1} that is attributed to the stretching vibration of the hydroxyl group (-OH); characteristic absorption bands at 1656 cm^{-1} , related to the stretching vibration of carbonyl group, at 1266 cm^{-1} , due to the bending of the phenolic hydroxyl groups, and at 1166 cm^{-1} , related to C-O-C stretching vibration (Lin et al., 2008). In all SAA coprecipitates spectra, DEX characteristic bands are confirmed. However, some changes with respect to the LUT spectrum are present. For example, it is possible to note some adsorption bands at 1656 , 1610 and 945 cm^{-1} that confirm the presence of LUT in the microparticles; these peaks are shifted to lower frequencies compared to those of LUT spectrum; this result can be explained by an interaction between the drug and the polysaccharide. The smoother peak at (1538 - 1490 cm^{-1}), compared with LUT spectrum (1541 - 1477 cm^{-1}), reveals another interaction between the two compounds. In FTIR studies peak shape and intensities have a great importance to understand which kind of interactions is created between compounds. Our hypothesis is that DEX and LUT interact each other, leading to the creation of new hydrogen bonds between the drug and the polysaccharide; probably these interactions could be related to the carbonyl or a hydroxyl group in DEX molecule and a -OH group in LUT molecule. This kind of interactions has been already observed for LUT-PVP coprecipitated by SAA (Di Capua et al., 2017b). These interactions are more evident as higher R values (higher LUT content) are considered. The same considerations can be extended for the coprecipitate DFL*, where the chemical conjugation DEX-FITC is not easily visible, since FITC is labeled on DEX attacking a -OH bond.

As already observed in previous works, the hydrogen bonding and the steric hindrance between the two compounds can allow to restrict the molecular mobility of LUT molecules and to provide stability to the system (Baghel et al., 2016).

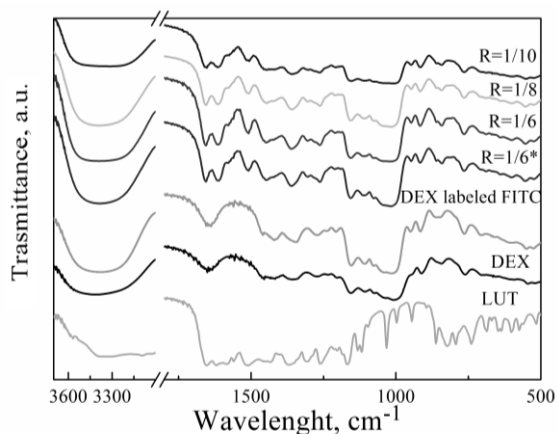


Figure IV.32 FTIR spectra of untreated compounds and SAA coprecipitates; *test using DEX labeled FITC (DFL*).

LUT loading and dissolution tests

The amount of LUT for each LUT/DEX weight ratio was measured by UV-vis spectroscopy. The loading efficiency ranged between 98.7% and 100%, with LUT content ranging between 8.9% (for R=1/10) and 14.3% (for R=1/6) with respect to the mass of polymer. All the active principle processed is practically loaded in the polysaccharide matrix, as it frequently occurs during SAA particles formation (Adami et al., 2017a, Di Capua et al., 2017b), due to the droplets drying mechanism.

To verify the improvement of LUT dissolution rate when loaded in SAA microparticles, LUT release behavior was monitored using a dialysis bag in PBS pH 7.4, following the recommendation of US Pharmacopeia. The analyses were performed on the untreated compounds (physical mixture of DEX, LUT and FITC) and SAA coprecipitates in triplicates. The curves practically overlapped, for this reason, standard deviation reported in the diagram in Figure IV.33 is very small.

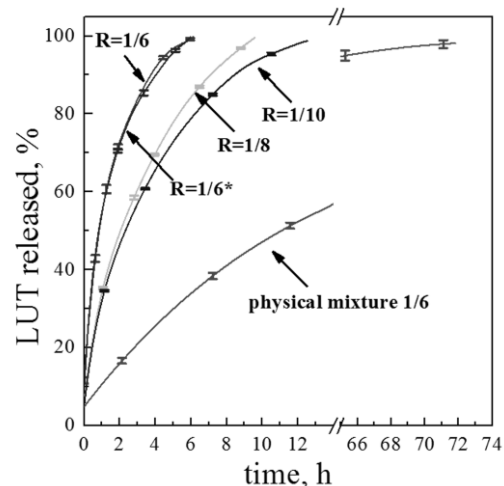


Figure IV.33 Release profiles of LUT in PBS at pH 7.4 and 37°C; * test using DEX labeled FITC (DFL*).

The dissolution profiles related to the physical mixture and some SAA coprecipitates are compared by plotting the percentage of released LUT as a function of time. The physical mixture of untreated compounds ($R=1/6$), completely dissolved in 72 hours (3 days). The release of LUT from DEX coprecipitates was faster at all R values and was controlled by LUT/DEX ratio. The coprecipitates produced at $R=1/10$ and $1/8$ totally dissolved in 12 and 10 hours respectively; whereas, the one produced at $R=1/6$ achieve the fastest release: the 100% release in about 6 hours. Therefore, in this case the dissolution rate of LUT is about 12 times faster than the one of physical mixture. The same result was obtained for the coprecipitate ($R=1/6^*$) produced using DEX labeled FITC: the dissolution curves overlapped (see Figure IV.33). This result confirms that the presence of FITC in the coprecipitates does not influence their overall behavior. Increasing the drug/polymer ratio, LUT content increases and leads to a larger drug release rate; this result is uncommon for SAA coprecipitates (Adami et al., 2017a, Liparoti et al., 2013), where the dissolution rate of the drug increases by increasing the relative amount of polymer. However, a similar result was obtained in a previous work (Di Capua et al., 2017b), where LUT was coprecipitated with PVP. Besides the diameter of microparticles, another relevant aspect that influences the dissolution rate is related to chemical interactions between the compounds, that can control the drug release from the polymeric matrix. In case of LUT/DEX coprecipitates, the presence of these interactions, evidenced in the FTIR spectra, decreases the dissolution rate of DEX and, as a result, LUT release is slower (Di Capua et al., 2017b). The effect of LUT is in some way similar to the influence of the charge

distribution in weak polyelectrolytes on the formation of hydrogen bond (Mella et al., 2015).

IV.5.3 Conclusions on LUT-DEX-FITC system

Complex multifunctional coprecipitates were successfully produced by SAA: microparticles with a mean diameter down to 350 nm were produced, formed by DEX, LUT and FITC. The free fluorescent material was encapsulated with efficiencies up to 80% and did not influence the overall behavior of the powders. SAA process did not affect also the chemical conjugation between DEX and FITC. The best results were obtained in correspondence of the largest drug/polymer weight ratio tested ($R=1/6$) with an increase of LUT dissolution rate up to 12 times with respect to the physical mixture.

A possible perspective of this work might be to investigate the potential of SAA produced fluorescent microparticles for cells drug delivery and imaging carriers.

IV.6 Improvement of NIF bioavailability

Nifedipine (NIF) is a 1,4-dihydropyridine calcium channel blocking activity with a high photosensitivity and poor solubility in water resulting in low and irregular bioavailability. It is indeed a Class II drug in accordance with Biopharmaceutics Classification System (BCS) (Khadka et al., 2014). When a drug is administered orally, as in the case of NIF, it has to dissolve in intestinal fluids, permeate the gut membrane and reach the blood system (Baghel et al., 2016). Bioavailability of poorly water soluble drugs that undergo dissolution rate-limited gastrointestinal absorption can be improved using chemical strategies, such as complexation (Brewster and Loftsson, 2007, Adeoye et al., 2018, Taupitz et al., 2013) and salt formations, and physical ones, such as micronization and drug dispersions in carrier matrix (Kogermann et al., 2013). Most of the literature on the improvement of NIF bioavailability is based on the production of solid dispersions, for example using polyethylene glycol (Emara et al., 2002), mannitol (Zajc et al., 2005), poly(vinyl caprolactam-co-vinyl acetate-co-ethylene glycol) (Soulaïrol et al., 2015), hydroxypropylmethylcellulose (HPMC) (Cilurzo et al., 2002), Eudragit and mesoporous silica from rice husks (Sriamornsak et al., 2016, Weerapol et al., 2017) as carriers. β -cyclodextrin, 2-hydroxypropyl- β -cyclodextrin (HP β CD) (Jagdale et al., 2012, Beig et al., 2013) are instead used frequently to produce complexes with NIF.

Solid dispersions of NIF and mannitol at different concentrations were prepared by hot melt method (Zajc et al., 2005); however, no regular particles are produced but only crystalline agglomerates up to 200 μm .

Soularoil et al (Soulaïrol et al., 2015) prepared solid dispersions of NIF and poly(vinyl caprolactam-co-vinyl acetate-co-ethylene glycol) using spray drying technique by dissolving the compounds in ethanol in different weight ratios. Irregular and amorphous particles were produced with average particle size between 0.8 and 1.7 μm . No interactions between drug and polymer were created and an improved dissolution rate compared to original NIF was obtained. Cilurzo et al. (Cilurzo et al., 2002) used the same technique to prepare NIF-HPMC in different weight ratios using methylene chloride:ethanol 90/10 v/v as solvent; however, no particles are showed in the work and the organic solvent used is classified as a Class 2 solvent (Schlosser et al., 2015, Pacheco et al., 2016) that should be limited in pharmaceutical products because of their inherent toxicity. Vippagunta et al. (Vippagunta et al., 2002) dispersed NIF (33.3% w/w) in a polymer matrix consisting of Pluronic F68 (33.3% w/w) and Gelucire (33.3% w/w) using melt method at 70°C. No results in terms of morphology are reported in this work; solid state analyses demonstrated that NIF is crystalline in the produced particles. Solid dispersions of NIF in Eudragit and mesoporous silica from rice husks were investigated by Sriamornsak et al. (Sriamornsak et al., 2016) and Weerapol et al. (Weerapol et al., 2017) by dissolving the compounds in different weight ratios and with some adsorbents in methylene chloride (Class 2); then, the solvent was removed by evaporation. No particles but agglomerates were formed in all cases studied. Summarizing, the works found in the literature were in part successful in demonstrating the improvement of NIF dissolution rate; however, the conventional techniques show the well-known drawbacks, such as the use of heavy and toxic organic solvents (as methylene chloride) with residual solvents in the produced powders, thermal degradation due to high temperatures used, difficulty in controlling recrystallization and particle size distribution.

The aim of this work was the production of solid dispersions of NIF using HP β CD as carrier by SAA coprecipitation process, in order to improve NIF bioavailability avoiding the use of heavy solvents and the complexation steps. HP β CD was successfully precipitated by SAA in previous works, using water (Reverchon and Antonacci, 2006b) and a water:ethanol (30:70 v/v) mixture as solvent (Di Capua et al., 2018), obtaining in both cases regular and spherical particles. The coprecipitation experiments for the production of NIF-HP β CD particles were performed using ethanol as solvent in which NIF and HP β CD are both soluble; however, until now neither of them were processed in ethanol by SAA.

IV.6.1 Experimental results

Preliminary studies were performed processing NIF alone to verify the feasibility of SAA process for this drug, investigating three different solvents: acetone, methanol and ethanol, since NIF is very soluble in these

solvents. Acetone-NIF solutions with concentrations ranging between 10 and 40 mg/mL were tested by SAA operating the saturator at 75 bar and 40°C and the precipitator at 1 bar and 30°C, with a GLR of 3.5. These operative conditions were optimized to assure the evaporation of the solvent using two vacuum pumps (DVP mod. ZA100P) operating downstream the precipitator (Liparoti et al., 2012). Examples of morphologies obtained are shown in Figure IV.34.

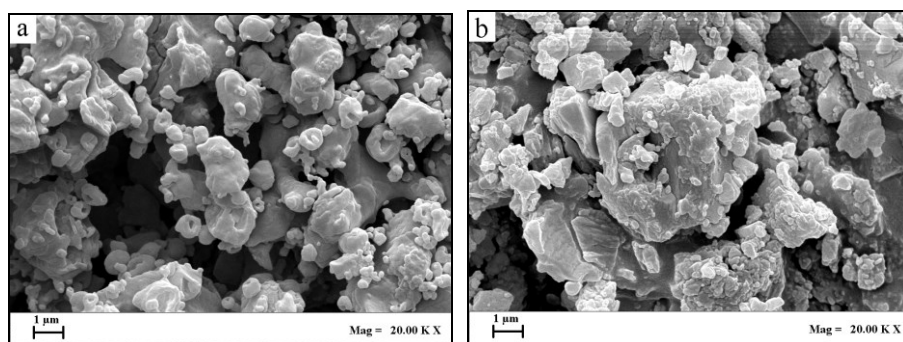


Figure IV.34. FESEM images of NIF micronized by SAA technique, using acetone as solvent at: a) 10 mg/mL, b) 40 mg/mL.

As it is possible to observe, non-regular particles were formed but a partial spherical structure is present using low NIF concentration (Figure IV.34a). Increasing the amount of NIF dissolved in acetone, instead, some agglomerates were produced (Figure IV.34b). Other SAA tests were performed using methanol and ethanol: the results were unsatisfactory.

SAA coprecipitation experiments NIF-HP β CD

NIF coprecipitation experiments were performed using HP β CD, a water soluble cyclodextrin selected for its capacity to act as crystallization controller of active principles and to improve the bioavailability of some active compounds (Di Capua et al., 2017a). The coprecipitation experiments were performed in ethanol that was the best compromise since the carrier was not soluble in acetone and the drug was not soluble in water. SAA operating conditions were: HP β CD concentration in ethanol 10 mg/mL; gas to liquid ratio 1.8 (mass based, defined as GLR), injection pressure of about 80-83 bar, saturator temperature 80°C and precipitation temperature 80°C. These conditions were optimized in a set of experiments.

A first set of SAA tests was carried out to test HP β CD alone in ethanol. These experiments were performed operating at a solute concentration of 10 mg/mL and at the operating conditions previously reported. HP β CD precipitated in form of non-coalescing with shrinkage cavities (Figure IV.35).



Figure IV.35. FESEM image of HP β CD micronized by SAA technique.

This morphology was sometimes observed in the SAA particles (Di Capua et al., 2017b, Martin et al., 2013) and can be due to the fragility of the solid structure during the drying in the precipitator. This result can be related to a series of aspects, such as drying time, shell flexibility, evaporation rate, as described and evidenced by the theory of particle formation in spray drying (Eslamian et al., 2009), since this process shows many similarities with the SAA technique. When a dilute solution is processed, during drying a thin layer of solid is formed. This shell can be fragile or flexible and, if the drying temperature is high, the solvent evaporation will be very fast and particles can deflate.

In this work, NIF/HP β CD weight ratios 1:2, 1:3, 1:4 and 1:8 w/w were proposed. In Table IV.10, a list of some experiments, with the indication of particle size distribution values (in terms of volume of particles) are summarized. Each experiment was performed in duplicate. The effect of NIF/HP β CD weight ratio (R, w/w) on morphology, mean size and particle size distribution was investigated. The influence of R on SAA NIF/HP β CD particles morphology can be semi-qualitatively observed in Figure IV.36, where some examples of particles produced at different R are reported.

Table IV.10 Composition and PSD data of NIF/HP β CD particles produced by SAA (R=NIF/HP β CD w/w; C_{NIF} : NIF concentration; C_{tot} : total concentration; *loss of carrier into the saturator).

Test code	R	C_{NIF} (mg/mL)	C_{tot} (mg/mL)	d_{10} (μ m)	d_{50} (μ m)	d_{90} (μ m)	Loading Efficiency (%)
#01	1/8	1.25	11.3	0.08	0.14	0.24	>100*
#02	1/4	2.50	12.5	0.11	0.24	0.48	>100*
#03	1/3	3.33	13.3	0.15	0.28	0.52	>100*
#04	1/2	5.00	15.0	0.18	0.37	0.73	>100*

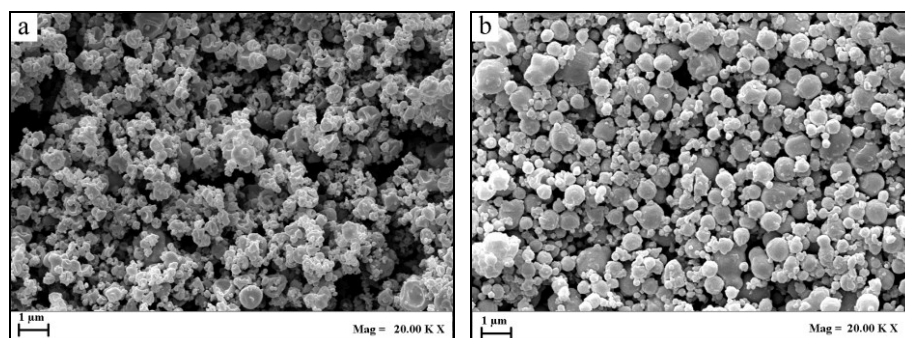


Figure IV.36. FESEM images of NIF-HP β CD precipitated, at different weight ratios R: a) 1/4, b) 1/2.

The produced particles at R=1/8 w/w (figure not reported) showed a morphology similar to that of SAA HP β CD (reported in Figure IV.35). When R increases up to 1/2, more defined spherical particles were produced, as shown in Figure IV.36. A comparison of the volumetric PSDs at different R are shown in Figure IV.37 and summarized in Table IV.10. The mean size of the coprecipitates depended on NIF/HP β CD weight ratio (R): increasing the amount of NIF in the injected solution, the mean diameter of the particles increases and PSD enlarged. The presence of the drug in solution influenced the viscosity and the density of the starting solution, generating larger droplets and consequently larger microparticles, during the atomization (Adami et al., 2017a).

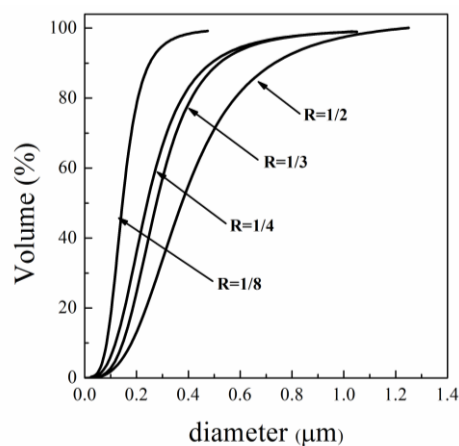


Figure IV.37 Volumetric cumulative particle size distributions of NIF/HP β CD, at different weight ratios R.

IV.6.2 Characterization of particles

In order to study the solid state of produced powders X-ray diffractometry and IR spectroscopy were performed on untreated compounds and SAA particles. X-Ray analyses are reported in Figure IV.38.

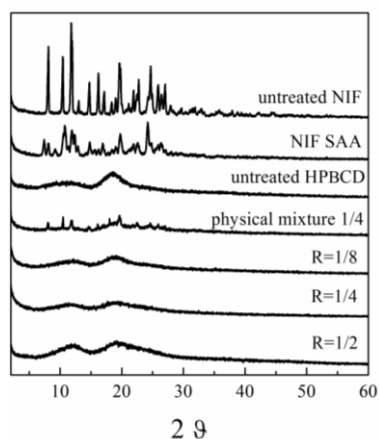


Figure IV.38 X-Ray spectra of NIF/HP β CD: comparison among raw materials and SAA coprecipitated microspheres.

The diffraction pattern of HP β CD shows two broad *halos* at 11° and 18°, thus confirming its amorphous structure. Pure NIF shows characteristic peaks at 8.2°, 10.5°, 11.9°, 14.9°, 17.1°, 20°, 22.6°, 24.7° and 27.2°, distinctive of X-ray scattering from crystalline structure. In the diffractogram of NIF processed by SAA, not all of these peaks are confirmed, whereas new peaks are evidenced at 7.5°, 9.2° and 12.4°: this might be related to the partial loss of crystalline degree or to a recrystallization of NIF in a new crystalline form, as described in literature (Chan et al., 2004). The physical mixture (R=1/4) shows the most important peaks related to NIF with low intensities. The diffractograms related to the SAA produced particles retain the pattern of the cyclodextrin with its typical two *halos*, confirming that the coprecipitated powders are amorphous.

FT-IR spectroscopy allows studying the possible interactions between NIF and HP β CD in SAA particles. FT-IR spectra (in the range of 4000-500 cm^{-1}) of unprocessed NIF and cyclodextrin, and some SAA particles are reported in the transmittance mode in Figure IV.39.

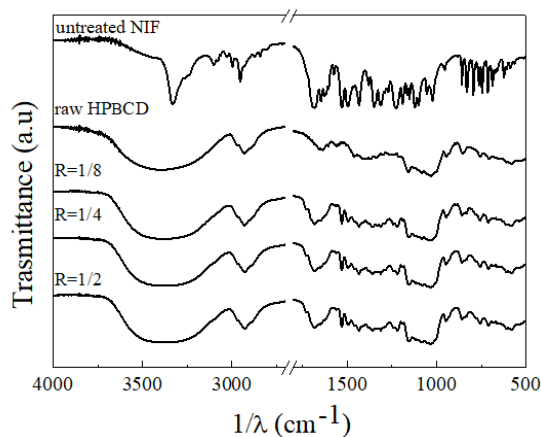


Figure IV.39 FT-IR spectra of NIF/HP β CD: comparison among raw materials and SAA coprecipitated microspheres.

The spectrum of untreated NIF indicates a characteristic absorption bands –NH stretching at 3330 cm^{-1} and the absorption bands at 3245.8 and 2996.5 cm^{-1} can be assigned to the stretching vibrations of –CH aromatic. At 2844 cm^{-1} is evidenced the band related to the stretching of the group –CH₃; the characteristic band –C=O stretching vibration of ester group is present at 1686.7 cm^{-1} whereas those of pyridine group at 1642.8 and 1618.5 cm^{-1} . In NIF spectrum, –NH bending (1534 cm^{-1}), –CH bending (1497.9 cm^{-1}), –CN symmetrical bending (1309 cm^{-1}), –CO stretching (1224.2 cm^{-1}) are highlighted. In the range between 830 and 700 cm^{-1} , –CN stretching of aryl-nitro group and –CH bending of aromatic group are evidenced (Blajovan and Modra, 2013). The FT-IR spectrum of HP β CD indicates a prominent absorption bands between 3300 and 3500 cm^{-1} (for –OH stretching vibration) and at 2926 cm^{-1} (for C–H stretching vibration) and 1159.1 cm^{-1} , 1086 cm^{-1} (–CH, –CO stretching vibration) (Lin et al., 2010). In all SAA coprecipitates spectra, HP β CD characteristic bands are confirmed; furthermore, the major peaks related to NIF are also present in all SAA patterns, such as for example at 830 cm^{-1} , 862 cm^{-1} , 1497.9 cm^{-1} , 1534 cm^{-1} . Particularly, increasing R the peaks related to NIF characteristic bands are more defined and deeper in terms of intensity due to the presence of higher amounts of drug. No new or shifted peaks are evidenced in all SAA spectra; therefore, the absence of interactions created between carrier and drug is verified.

Loading efficiencies and dissolution tests

Qualitatively, SAA powders are light yellow in color that is a compromise between that of HP β CD (white) and NIF (dark yellow). Quantitatively, NIF content in SAA samples for each weight ratio was

measured by UV-vis analyses. Table IV.10 summarizes these results. All NIF/HP β CD particles show high loading efficiencies, higher than 100%. These high values are due to the loss of small quantity of HP β CD into the saturator, due to an anti-solvent effect. This result is not new, indeed, this effect was previously observed in SAA processing (Martin et al., 2013). Indeed, the addition of carbon dioxide can induce the precipitation of small quantities of cyclodextrin from the feed solution.

In order to verify the improvement of NIF dissolution rate, dissolution tests were performed in PBS pH 7.4 to simulate blood conditions. The drug release was monitored by UV-vis spectrophotometer and replicated for each sample. Dissolution tests were performed on untreated NIF and SAA coprecipitates (Figure IV.40). The untreated NIF dissolved completely in about 110 hours (more than 4 days), due to its poor solubility in water. The analyses on SAA coprecipitates revealed that the powders of NIF-HP β CD show a faster release than raw NIF for all weight ratios tested. The best result was obtained for the coprecipitate produced at $R=1/8$ that shows a total dissolution time around 3 times lower than the untreated NIF. The powders produced at $R=1/4$ and at $R=1/2$ dissolved completely in about twice times faster than raw drug. Furthermore, the dissolution rate was controlled by NIF/HP β CD ratio: decreasing drug/cyclodextrin mass ratio, indeed, larger drug release rates were obtained.

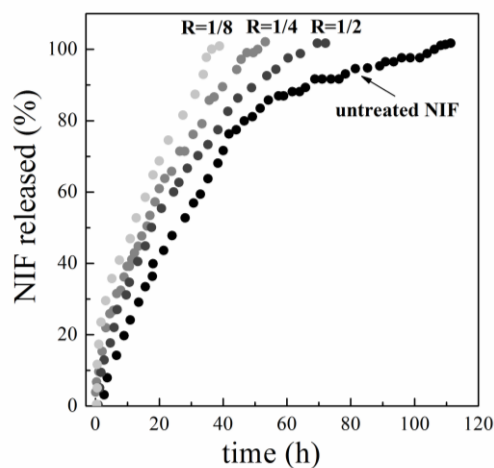


Figure IV.40 Release profiles of NIF in PBS at 37°C and pH 7.4.

This result is common for SAA coprecipitates produced at fixed carrier concentration: the dissolution rate of the drug increases by increasing the relative quantity of carrier. The drug bioavailability is indeed influenced by several aspects, as explained in literature: particle size, solid state, chemical interactions between compounds (Adami et al., 2017a, Di Capua et al., 2017a, Di Capua et al., 2017b, Adami et al., 2017b). These results are consistent with the literature: by reducing the particle size and the efficient dispersion of NIF in the cyclodextrin, an enhanced dissolution rate resulted (DiNunzio et al., 2008).

IV.6.3 Conclusions on HP β CD-NIF system

SAA process demonstrated to be very efficient in the entrapment (up to 100%) of NIF in the cyclodextrin selected as carrier, obtaining more regular and spherical particles by increasing NIF weight percentage in the solution injected. The dissolution rate of NIF related to the SAA produced particles was successfully enhanced up to 3 times faster for the 1/8 weight ratio when compared with the physical mixture. Furthermore, NIF/HP β CD mass ratio revealed to be an effective controlling parameter for drug release.

Chapter V

Coprecipitation of nutraceutical compounds using SAA technique

V.1 Introduction

Nowadays, a significant interest in incorporating several kinds of micronutrients into functional food and beverage products to benefit human health and wellness through diet. These bioactive compounds include vitamins, polyphenols, antioxidants, carotenoids, flavors, prebiotics; most of them are essential for human wellbeing (such as vitamins), whereas other substances derived from food sources provide health benefits in addition to their diet (*nutraceuticals*) (Joye et al., 2014, Handford et al., 2014). These compounds are usually labile molecules, highly affected by light, oxygen, heat; they cannot be incorporated into commercial food products in their pure form due to their low solubility in oil and/or water and to their easy physical and chemical degradation during food processing, transport or preparation. Therefore, the microencapsulation can be useful tool to improve the delivery of bioactive compounds into food (Joye et al., 2014, Champagne and Fustier, 2007) and overcome all limitations. Different delivery systems may be based on food grade biopolymers that include polyelectrolyte complexes, polymer particles and hydrogel particles.

The aim of this part of work was to test for the first time the applicability of SAA process in the incorporation of bioactive compounds in polymeric matrices able to stabilize and protect the bioactive compound from environmental conditions and to enhance their bioavailability (Di Capua et al., 2018, Joye and McClements, 2013, Champagne and Fustier, 2007). In particular, investigations and studies were performed on beta-carotene and an ethanolic extract from propolis. Two carriers were used in these coprecipitation experiments: polyvinylpyrrolidone and hydroxypropyl- β -cyclodextrin.

Materials

Polyvinylpyrrolidone (PVP, Mw: 10,000), ethanol (EtOH, purity 99.9%), acetone (Ac, purity 99.8%), Trolox and 2,2-Diphenyl-1-picrylhydrazyl (DPPH), β -carotene (BC, purity >93%) were supplied by Sigma Aldrich (Italy). Acros Organic (Belgium) provided Hydroxypropyl- β -cyclodextrin (HP β CD, 97%). A propolis sample is an ethanolic extract of propolis (EEP) and was purchased from a local beekeeper from the center of Chile; specifically located in northern part of the Valparaiso region, and was collected from the beehive in 2015. Sodium carbonate, Gallic Acid and Folin-Ciocalteu reagent were purchased from Merck Millipore (Darmstadt, Germany). Carbon dioxide (CO₂, 99.9%) was purchased by Morland Group (Italy) and nitrogen (N₂, 99%) by SOL (Italy). All materials were used as received.

V.2 Stabilization and protection of Chilean propolis

Propolis is a natural resinous mixture collected by honeybees from plant resins, leaves, buds and barks. Propolis mainly consists of resin, vegetable balsam, essential oils, waxes, pollen; it appears as a hard and fragile material at room temperature and it becomes gummy and very sticky when heated. The composition of propolis depends on the geographic origin and from the vegetation of the area in which bees live and feed (Wagh, 2013). Therefore, different kinds of propolis are present all over the world, from Venezuela, Brazil, Chile, Bulgaria, Italy, Argentina, Egypt, etc; each propolis is chemically different and has specific properties and applications (Russo et al., 2004). For thousands of years, it has been largely used in traditional medicine: researchers demonstrated the great pharmacological potential of propolis in many fields: it can be used as antimicrobial, anti-inflammatory, antiviral, antioxidant, antibacterial, antiseptic, antibiotic and anti-carcinogenic; it is used also in cosmetic and food industries (Wagh, 2013, Russo et al., 2004, Krol et al., 2013, Khurshid et al., 2017). The major properties of propolis have to be attributed to its polyphenol content.

Several procedures have been used to extract the bioactive components of propolis and to remove compounds such as waxes and hive detritus, using conventional techniques, such as maceration, ultrasonic extraction, microwave assisted extraction (Trusheva et al., 2007) and supercritical fluid extraction and fractionation (Machado et al., 2015, Paviani et al., 2012, Biscaia and Ferreira, 2009, De Zordi et al., 2014). The application of propolis extracts as a food ingredient or in the cosmetic and pharmaceutical industries is limited by their strong and unpleasant taste and aroma, and alcohol residues in the case of conventional extraction techniques. Propolis encapsulation can be an option to overcome these negative aspects, succeeding at the same time to protect bioactivity against oxidation of active

compounds. Encapsulation and dispersion in a water soluble matrix allow to increase propolis bioavailability in pharmaceutical formulations (Bruschi et al., 2003). Some several conventional processes have been proposed for this purpose: spray drying (Bruschi et al., 2003, Busch et al., 2017), emulsion/evaporation solvent (de Souza Ferreira et al., 2014), coacervation (Nori et al., 2011), inclusion complexation (Kalogeropoulos et al., 2009, Rocha et al., 2012), nanoprecipitation (do Nascimento et al., 2016).

Busch et al. (2017) (Busch et al., 2017) encapsulated an Argentine alcohol free propolis in different maltodextrin matrices using spray drying, with production yields around 65%. The spray dried powders showed deformed spherical shape, due to the shrinkage of the particles during the drying process, with an encapsulation degree of quercetin and cinnamic acid of 40%. A high antioxidant activity was achieved, with a polyphenol encapsulation of around 89%. Kalogeropoulos et al. (Kalogeropoulos et al., 2009) proposed the inclusion of propolis ethanol extract in β -cyclodextrin (β CD) cavity by sonication of propolis suspensions in aqueous solution containing β CD, followed by filtration and freeze-drying. Encapsulation efficiencies of flavonoids were around 4 and 10%, whereas encapsulation yield of polyphenols ranges between 3 and 20%. The inclusion complex of Brazilian propolis with HP β CD was prepared by Rocha et al. (Rocha et al., 2012). Amorphous complexes were obtained with low antioxidant activity compared to the extract, due to the loss of phenolic compounds that were not encapsulated in the HP β CD. Do Nascimento et al. (do Nascimento et al., 2016) developed polymeric nanoparticles loaded with Brazilian propolis extract with a combination of poly- ϵ -caprolactone and pluronic using nanoprecipitation method. Produced dried particles were irregular and coalescent, with size ranging between 200 and 960 nm. The mean encapsulation efficiency of flavonoids was 75% and the DPPH studies demonstrated a high antioxidant activity.

SCF based techniques have been proposed as a successful alternative to conventional processes in several fields, such as extraction and fractionation (Machado et al., 2015, Paviani et al., 2012, Biscaia and Ferreira, 2009, De Zordi et al., 2014, Catchpole et al., 2004) and micronization/encapsulation (Wu et al., 2009) of propolis. SC-CO₂ extraction of propolis tincture has been used by Catchpole et al. (Catchpole et al., 2004) to obtain flavonoids and essential oils fraction and to remove high molecular weight components by antisolvent precipitation. The process was optimized at laboratory and pilot scale, demonstrating a successful scale up and obtaining a flavonoid concentration in the ethanolic extract around 25-30%. The best results for extraction were obtained using ethanol as co-solvent (Machado et al., 2015) (or by supercritical antisolvent fractionation (Catchpole et al., 2004). Wu et al. (Wu et al., 2009) and Yang et al. (Yang et al., 2014) adopted SAS process to micronize propolis and to encapsulate it in polyethylene glycol, respectively. They obtained sticky irregular particles. Therefore, the

coprecipitation was substantially unsuccessful. No analyses on total polyphenol content were performed. In conclusion, the works found in the literature demonstrated the feasibility of propolis processing by SC-CO₂, but irregular morphologies and agglomerates were produced that can hinder the practical (industrial) application of the products in the case of coprecipitates.

Therefore, in this work (Di Capua et al., 2018) in collaboration with Chilean Institute of Fraunhofer, propolis coprecipitation was attempted by SAA to assess the feasibility and efficiency of the process to load and protect phenolic compounds contained in a propolis ethanolic extract. Experiments were carried using HP β CD and PVP as *carriers*, with the aim to obtain micrometric particles, to prevent oxidation and to improve its bioavailability.

V.2.1 Experimental results

The propolis solution used for the experiments was a mother tincture of water:ethanol 30:70 (v/v) that is the typical preservation technique for propolis in the Chilean area. HP β CD and PVP were used as *carrier*; they are selected based on their suitable chemical and physical properties, including good solubility in the water:ethanol 30:70 (v/v) solution used in this work, possible protection ability, possible enhancement of the bioavailability of bioactive compounds (Kanaze et al., 2010, Jun et al., 2007).

These two carriers were successfully precipitated by SAA in previous works: HP β CD from water (Reverchon and Antonacci, 2006) and PVP from ethanol, water, and mixtures of water/acetone (Liparoti et al., 2015); but, they were never processed in a water:ethanol 30:70 (v/v) solution that is required in this case since the starting material is present in this solution. Therefore, a first set of experiments was performed testing each *carrier* alone, using a solute concentration of 20 mg/mL for each *carrier*. To assure large solubility of CO₂ in the liquid solution (Adami et al., 2017a, Di Capua et al., 2017b, Liparoti et al., 2013), the process conditions used were: pressure of about 90 bar and temperature of 80°C in the saturator, temperature of 90°C in the precipitation vessel; CO₂ mass flow rate was set at 9 g/min and the one of liquid solvent at 5 g/min, to obtain a mass flow ratio (GLR, *gas to liquid ratio*) of 1.8. HP β CD and PVP precipitated in form of non-coalescing, regular spheres (Figure V.1).

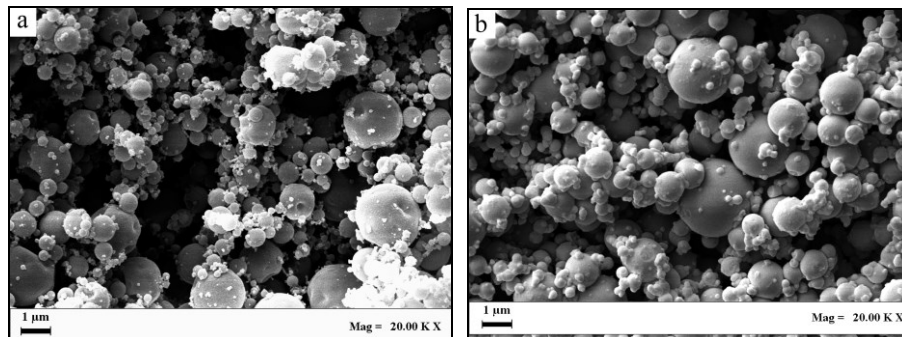


Figure V.1 FESEM images related to a) HP β CD and b) PVP, micronized by SAA alone at 20 mg/mL in water:ethanol 30:70 (v/v) solution.

A simple representation of the whole process of coprecipitation and SAA precipitator with the aim to give an overview of the whole experimental procedure is reported in Figure V.2.

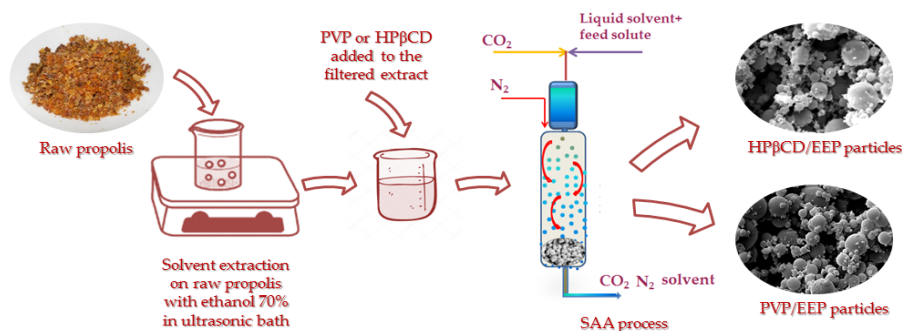


Figure V.2 A simple representation of the whole process and SAA precipitator.

Table V.1 reports a list of the coprecipitation experiments performed to study the effect of the total concentration and of the EEP/*carrier* mass ratio (R , w/w) for both *carriers* investigated, with the indications of concentration, and PSD values (in terms of number of particles) expressed as d_{10} , d_{50} and d_{90} indicating the diameters at 10th, 50th and 90th percentile.

Table V.1 Composition and PSDs data of EEP-carrier microparticles produced by SAA ($R = EEP/carrier$ w/w; C_{tot} : total concentration; C_{EEP} : EEP concentration; C_{car} : carrier concentration).

Test code	R	C_{tot} (mg/mL)	C_{EEP} (mg/mL)	C_{car} (mg/mL)	d_{10} (μm)	d_{50} (μm)	d_{90} (μm)
HP β CD							
#01	1/2	30	10	20	---	---	---
#02	1/3		7	23	0.21	0.37	1.03
#03	1/5		5	25	0.20	0.28	0.80
#04	1/8		3	27	0.14	0.20	0.71
#05	1/5	60	10	50	0.27	0.44	1.31
PVP							
#06	1/2	30	10	20	---	---	---
#07	1/3		7	23	0.34	0.50	1.26
#08	1/5		5	25	0.32	0.43	1.11
#09	1/8		3	27	0.16	0.23	0.50
#10	1/5	60	10	50	0.28	0.41	1.23

Effect of EEP/carrier (R, w/w)

For each *carrier*, the effect of EEP/*carrier* ratio (R, w/w) on morphology, mean size and particle size distribution was investigated at a total concentration of 30 mg/mL in solution. The influence of R on SAA EEP-HP β CD particles morphology can be semi-qualitatively observed in Figure V.3, in which some FESEM images obtained at different R are reported. When $R=1/2$ was processed, coalescing microparticles were observed (Figure V.3a); therefore, the powder could not be characterized in terms of PSD. At the ratio R 1/3 (image not reported) and at the same operating process conditions, particles were still partly coalescing. When R was decreased down to 1/5 and 1/8, well defined spherical particles were produced; Figure V.3b reports, for example a FESEM image of the particles obtained at $R=1/5$.

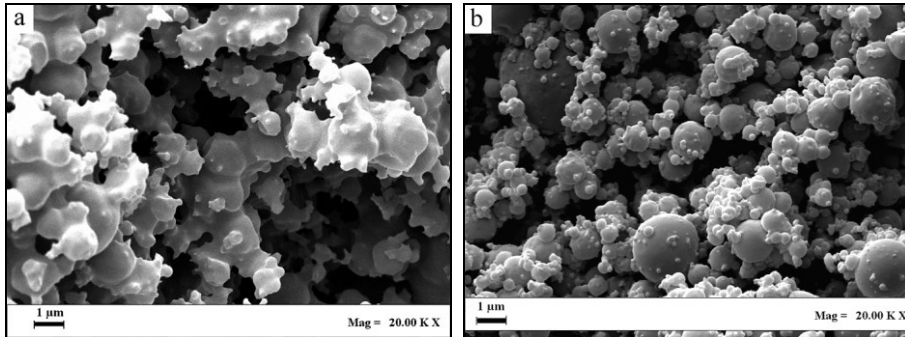


Figure V.3 FESEM images related to SAA test a) #01 ($R=1/2$), b) #03 ($R=1/5$).

A comparison of the PSDs on the basis of number of particles at different R are shown in Figure V.4. Increasing the amount of EEP in the injected solution, the mean diameter of the particles increases and PSD enlarges (Figure V.4 and Table V.1). A possible explanation of the effect of R on particle size and distribution can be related to the increase of viscosity of the starting solution due to a higher concentration of EEP. Since viscosity is a cohesive force, its increase tends to produce larger droplets and consequently larger microparticles, during the atomization.

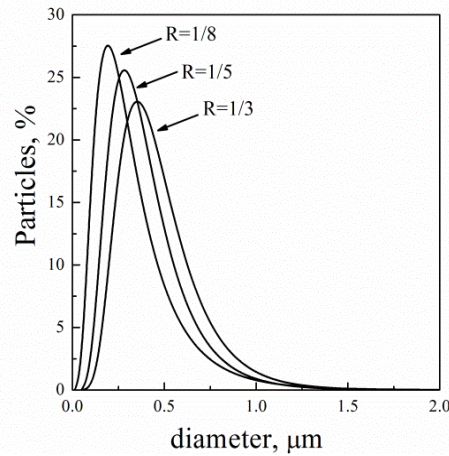


Figure V.4 Comparison of PSDs related to EEP-HP β CD particles precipitated at a concentration of 30 mg/mL (tests #02, #03, #04).

Also PVP was tested, with EEP/PVP mass ratios ranging between 1/2 and 1/8 at a fixed total concentration of 30 mg/mL. Using PVP as *carrier*, in the case of $R=1/2$ coalescing microparticles were obtained; consequently, it was not possible to evaluate the PSD. Operating at the same operating conditions and decreasing R down to 1/3 or lower, well separated and spherical particles were produced, as shown in Figure V.5, where FESEM images are reported, for $R=1/3$ and $R=1/8$, respectively. Lower amounts of PVP compared to HP β CD are necessary to obtain regular particles.

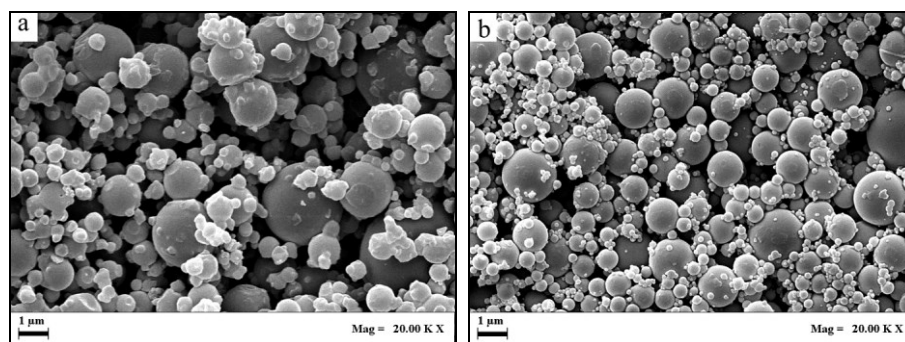


Figure V.5 FESEM images related to SAA test a) #07 ($R=1/3$ w/w), b) #09 ($R=1/8$ w/w).

PSDs are summarized in Figure V.6 and Table V.1. Also for EEP-PVP system, increasing the percentage of EEP in the injected solution, the mean diameter of the particles increases and PSD enlarges. Also in this case, increasing R , the viscosity of the solution injected increases and larger particles are obtained. Looking at the overall results (Table V.1), the effect of R on the PS is more pronounced in the system EEP-PVP compared to EEP-HP β CD and EEP-PVP particles are slightly larger than those produced using HP β CD as *carrier* at each R tested.

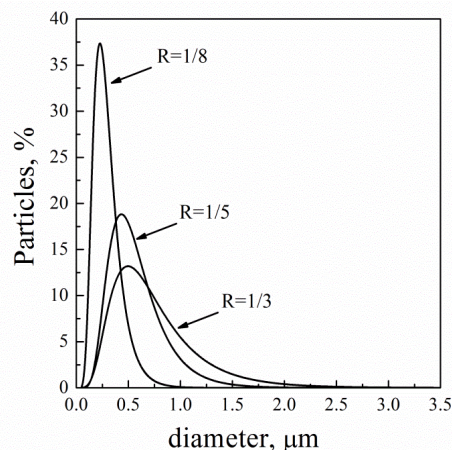


Figure V.6 Comparison of PSDs related to EEP-PVP particles precipitated at a concentration of 30 mg/mL (tests #07, #08, #09).

Effect of total concentration

The effect of the total concentration in water:ethanol was investigated for both systems at $R=1/5$, varying the overall concentration (EEP+carrier) from 30 to 60 mg/mL (Table V.1). The PSDs in terms of number of particle percentage at different concentrations show very similar mean diameters for both carriers. However, if the PSD is remeasured in terms of volumetric cumulative, the comparison between the results at different concentration are more emphasized. Using an overall concentration of 30 mg/mL for the system EEP-HP β CD (test #03) and EEP-PVP (test #08), spherical microparticles are produced, with a mean diameter in terms of volumetric cumulative of about 1 μm and 1.4 μm , respectively. Increasing the concentration to 60 mg/mL (test #05 and #10), regular microparticles were still obtained, but larger particles were obtained with a mean size of about 1.7 μm and 1.8 μm . This behavior is commonly observed in SAA powders, since increasing the solute concentration, the viscosity of the injected solution increases and larger droplets are formed at the exit of the nozzle, with the consequent formation of larger microspheres.

Particles of EEP-PVP are larger than those produced in the case of EEP-HP β CD; whereas the effect of the overall concentration on PSD is less significant for EEP-PVP particles compared to those of EEP-HP β CD.

V.2.2 Characterization of particles

Differential Scanning Calorimetry (DSC) and X-Ray analyses were performed on unprocessed materials and on SAA processed EEP-carrier, to evaluate potential changes in the thermal and the crystallization behavior of EEP and the carriers in the coprecipitates, respectively. DSC thermograms of both system are reported in Figure V.7. DSC thermogram of the unprocessed EEP show different endothermic phenomena at temperatures of 85, 95, 102 and 125°C (do Nascimento et al., 2016). Broad endothermic peaks ranging between 85 and 102°C are due to the water loss, whereas the other endothermic peaks can be related to the melting of phenolic compounds (several compounds) that are present in the EEP. DSC of untreated HP β CD reveals that the carrier is amorphous with a broad endothermic peak ranging from 40 to 100°C, related to water loss. Thermal decomposition occurs after 300°C. As already reported in previous works, PVP is an amorphous and hygroscopic polymer. The thermal profiles of SAA EEP-HP β CD and SAA EEP-PVP particles are close to that of pure HP β CD and PVP, respectively: these curves reveal only the broad endothermic peak associated with the release of water from the samples. The absence of melting peaks suggests that EEP-HP β CD and EEP-PVP coprecipitates are in an amorphous and homogeneous solid state (Aid et al., 2017).

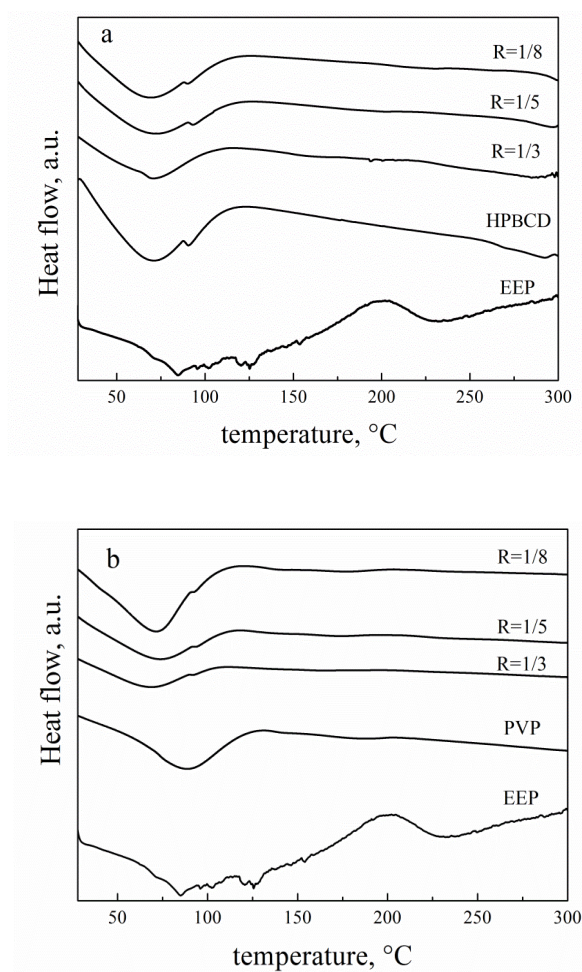


Figure V.7 DSC analyses of a) HP β CD, EEP and EEP-HP β CD coprecipitates b) PVP, EEP and EEP-PVP coprecipitates.

A further supporting indication was obtained from the powder X-Ray diffraction patterns. XRDPs of both EEP-carrier system are reported in Figure V.8.

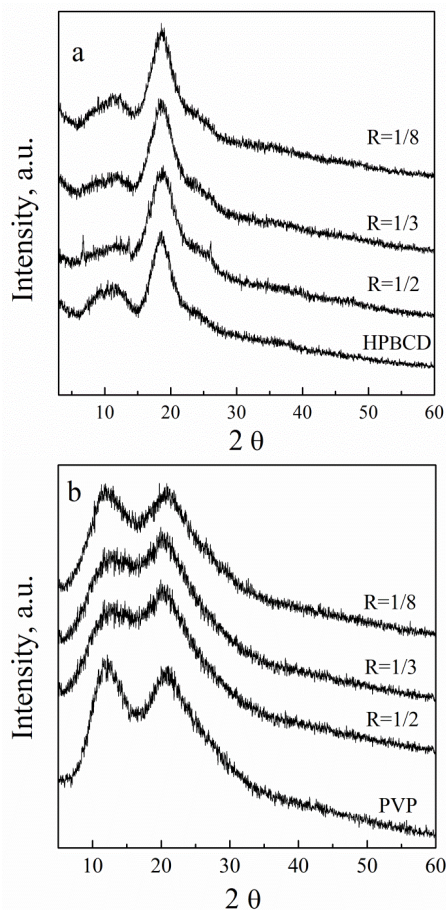


Figure V.8 XPRD related to a) HP β CD and EEP-HP β CD coprecipitates b) PVP and EEP-PVP coprecipitates.

Pure EEP was not tested by this technique because of its status: EEP is in form of concentrated slurry and becomes very sticky when heated. Untreated HP β CD shows an amorphous structure: in the pattern, two broad peaks around 11.7° and 18.8° are identified. SAA EEP-HP β CD coprecipitates have only the broad peaks related to the carrier: this fact suggests that propolis is finely dispersed in the HP β CD matrix. A similar result was observed in Figure V.8b for EEP-PVP produced microparticles: also in this case, a homogeneous dispersion of the EEP in polymer matrix was obtained.

Summarizing, all solid state analyses suggest that EEP is homogeneously dispersed in the two matrices used for coprecipitation tests. The success of SAA coprecipitation in inhibiting the formation of crystals is due to the use of low temperatures in the precipitator, that reduce crystallization rates of precipitates, and the production of a one-phase dispersion (Aid et al., 2017)

EEP-carrier, related to the glass transition temperatures of PVP and HP β CD (Baghel et al., 2016).

V.2.3 Antioxidant activity

The antioxidant activity of coprecipitates obtained by SAA was studied using as reference the total concentration of polyphenols (expressed in mg of Gallic Acid Equivalents (GAE) per gram of powder) and DPPH free radical scavenging activity, as described in Chapter II (equation (2)). DPPH assay is widely used to measure the ability of the particles to act as free radical scavengers; this method is fast, easy and reliable since it does not require a special reaction and device. All results are summarized in Table V.2.

Table V.2 Antioxidant activity of propolis coprecipitates: total polyphenol content; scavenging activity (IC_{50}) by DPPH method (R: EEP/carrier w/w; GA: Gallic Acid; Eff: polyphenol loading efficiency).

# test code	R	% EEP	% carrier	$\frac{mg_{GA}}{g_{powder}}$	Eff. (%)	IC_{50} ($\mu g/mL$)
HP β CD						
#01	1/2	33.3	66.7	99.7 \pm 6.3	100.0	17.2 \pm 2.8
#02	1/3	25.0	75.0	71.2 \pm 7.3	98.6	19.0 \pm 1.3
#03	1/5	16.7	83.3	47.6 \pm 7.2	98.4	38.8 \pm 0.3
#04	1/8	11.1	88.9	32.0 \pm 7.2	98.7	56.6 \pm 0.3
PVP						
#06	1/2	33.3	66.7	91.3 \pm 6.0	93.6	17.3 \pm 1.0
#07	1/3	25.0	75.0	68.4 \pm 7.7	96.0	25.2 \pm 0.4
#08	1/5	16.7	83.3	43.0 \pm 7.8	87.9	30.2 \pm 1.0
#09	1/8	11.1	88.9	29.3 \pm 8.1	90.2	67.2 \pm 0.3

Total polyphenol content increases in SAA particles as the amount of EEP in the starting solution, that corresponds to a higher EEP-to-carrier mass ratio increases. Polyphenol-rich particles are obtained for both carrier used and their loading efficiency is calculated as the percentage of total polyphenol in the dried powder compared to the total polyphenol in EEP (Table V.2). Total polyphenol content reaches values around 100 and 96.0% for HP β CD coprecipitates and for PVP coprecipitates, respectively, therefore, the encapsulation efficiency in SAA particles is very high, confirming that the SAA coprecipitation mechanism, based on droplet drying, allows the effective coprecipitation and preservation of the active principles contained in the native EEP. SAA demonstrated to be an alternative technique to overcome the results obtained using conventional processes. The homogeneous dispersion of EEP in the two matrices made by

SAA process, indeed, improve the quality of powders obtaining an highest polyphenol loading efficiency up to 30 times larger than those reported in literature by Kalogeropoulos et al. (Kalogeropoulos et al., 2009).

In Table V.2, DPPH results are summarized and expressed as the half maximum inhibitory concentration of DPPH radicals (IC_{50}), in $\mu\text{g/mL}$. The antioxidant activity obviously increases with EEP content in the starting solution. Results suggest that there are no significant differences in the inhibition of radicals by the particles obtained with both carriers. The IC_{50} values of free radical scavenging activity ranged between 56.6 and 17.2 $\mu\text{g/mL}$ for HP β CD and 67.2 and 17.3 $\mu\text{g/mL}$ for PVP; whereas, the IC_{50} of EEP alone is 17.1 $\mu\text{g/mL}$. A lower IC_{50} means a higher free radical scavenging activity of the compounds. For both systems studied, the best results were obtained in the case of EEP-*carrier* at R=1/2 w/w (tests #01 and #06), where IC_{50} values are close to the one of EEP alone. The homogeneous dispersion of EEP in the two matrixes provides the retention of polyphenols in the coprecipitates and both HP β CD and PVP are good carriers to preserve the antioxidant properties. They can inhibit the crystallization and reduce the chemical degradation rate of the active ingredient, since the areas of EEP exposed to the external environment are reduced in SAA particles, thereby contributing to increase the shelf life of the loaded EEP. It is known in literature, that the entrapment in a matrix allows to stabilize the active compounds because the carrier acts as a physical barrier for oxygen and small molecules inhibiting chemical and enzymatic degradation; consequently, the shelf life of the loaded products could be prolonged (Wang et al., 2009, Reksamunandar et al., 2017, Machado et al., 2018). In case of EEP, the oxidation prevention is demonstrated by the IC_{50} values for both studied systems, that show that in case of coprecipitates produced at R=1/2 and R=1/5 the antioxidant activity is preserved. Therefore, the coprecipitation of EEP-*carrier* and the size reduction may allow to maintain a good quality of the scavenging activity of untreated EEP (Meneses et al., 2015): this fact could be an interesting added value for the production of nutraceutical and functional products.

V.2.4 Conclusions on EEP solid dispersions

SAA technique revealed to be a good alternative to conventional processes for EEP-*carriers* coprecipitation. In this study, SAA was successfully used to load and protect bioactive compounds, such as polyphenols in an ethanolic extract of propolis, using two *carriers*: HP β CD and PVP. Not all the mass ratios EEP/*carrier* were suitable for successful coprecipitation of non-coalescing microparticles, but starting from R=1/5 for EEP-HP β CD and R=1/3 for EEP-PVP the process is successful. The product obtained was a dry powder formed by microparticles containing up to 100% of the total polyphenol content present in the EEP and with a preserved

antioxidant power due to the homogeneous EEP dispersion in the used carriers.

As a result, the polyphenol-rich particles produced using SAA could be very promising, as a source of natural antioxidants, and for food supplies. Indeed the suggested *carriers* allow improving the handling of the product and simplifying its storage.

V.3 Stabilization and protection of beta-carotene

BC is one of the most common and abundant carotenes in nature; it is a strongly orange-colored pigment (Fiedor and Burda, 2014, Gul et al., 2015) and is the major carotenoid in human diet. It has several biological activities, like high antioxidant activity and high pro-vitamin A activity. Clinical studies demonstrated that BC may reduce the risk of some chronic diseases, such as lung cancer, cardiovascular and heart diseases, colorectal adenomas and can protect against cutaneous photodamage (Grune et al., 2010, Fiedor and Burda, 2014, Goralczyk, 2009). The application of BC to food systems, nutraceutical products is limited because of its poor water solubility, low bioavailability, lipophilic and crystalline nature and instability in presence of light, heat and oxygen (Fiedor and Burda, 2014, Gul et al., 2015). Since carotenoid particles alone with a very small size are more sensitive to degradation, its incorporation in polymeric matrices can represent a suitable method to stabilize and protect it from environmental conditions (Champagne and Fustier, 2007, Di Capua et al., 2018).

Traditional approaches used to try to incorporate BC are spray drying (Loksuwan, 2007, Coronel-Aguilera and San Martín-González, 2015) and emulsion/solvent evaporation (Tan and Nakajima, 2005). For examples, using spray drying, BC were loaded in carriers, such as starch, tapioca starch and native starch and Arabic gum, obtaining particles with irregular morphologies, wide particle size distributions and BC content ranging between 47 and 82%, depending on the carrier. Moreover, no studies on dissolution rates of encapsulated BC were performed, to verify the enhancement of bioavailability. Analyses on BC antioxidant activity were not performed (Loksuwan, 2007, Coronel-Aguilera and San Martín-González, 2015). The application of SC-CO₂ techniques to the precipitation of BC alone and to the production of formulations based on BC and biopolymers, using SAS technique (Cocero et al., 2009, Mattea et al., 2009) and SAILA (Campardelli et al., 2012) was already studied. For example De Paz et al. (de Paz et al., 2012) studied a system formed by BC and poly-(ϵ -caprolactones), using SAS technique. Produced particles were irregular and agglomerated, with very low BC content. BC has been coprecipitated with poly(3-hydroxybutyrate-co-hydroxyvalerate) (Priamo et al., 2011, Franceschi

et al., 2008) or polyethylene glycol (He et al., 2007) by SAS, with loading efficiencies lower than 50% and irregular particle shapes. Prosapio et al. (Prosapio et al., 2015) proposed SAS to prepare coprecipitates of BC and PVP from an acetone:ethanol (70:30 v/v) mixture. Spherical and amorphous microparticles in the range 1-2.4 μm were obtained; dissolution analyses showed a vitamin dissolution rate 10 times faster than untreated BC.

Therefore, in this study (Di Capua et al., 2019) in collaboration with the Laboratory of Mechanics, Modeling & Clean Processes of University of Marseille, BC coprecipitation experiments were carried using PVP, aimed at reducing BC tendency to crystallize, obtaining micrometric particles with spherical morphology and enhanced BC bioavailability. Two liquid solutions were used, ethanol and acetone:ethanol (70:30 v/v), to compare their performance in giving coprecipitates.

V.3.1 Experimental results

In previous studies, PVP was precipitated by SAA using ethanol, water, and water:acetone mixtures (Liparoti et al., 2013, Liparoti et al., 2015, Adami et al., 2017a); but, it was never processed using acetone:ethanol (70:30 v/v) mixtures. Therefore, first experiments were performed to test SAA polymer behavior in ethanol as reference point and in acetone:ethanol (#06) at a concentration of 10 mg/mL. SAA operating conditions were: GLR 1.8, injection pressure of about 85 bar, saturator and precipitation vessel temperature 80°C; they were based on previous SAA studies (Adami et al., 2017a, Di Capua et al., 2017b, Di Capua et al., 2018). PVP precipitated in form of spherical, separated microparticles from both solvents; in Figure V.9, two SEM images are reported that, qualitatively, confirm this statement. However, using the mixture acetone:ethanol, smaller PVP particles were obtained. In Table V.3, PSDs values, expressed in percentiles as d_{10} , d_{50} and d_{90} , are summarized.

BC alone processed by SAA, at high concentrations, showed a marked antisolvent effect in the saturator producing an undesired precipitation. For this reason in the SAA coprecipitation experiments only a low BC concentration (0.5 mg/mL) was used.

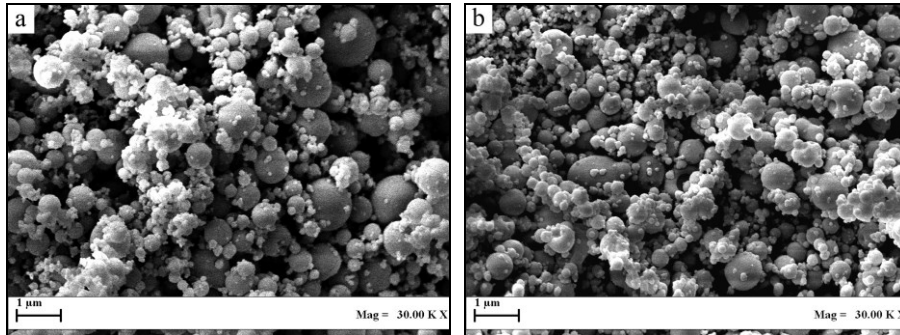


Figure V.9 FESEM images of PVP precipitated from a) ethanol and b) acetone/ethanol 70/30 (v/v) (#06).

Table V.3 Composition and PSD data of BC-PVP SAA particles ($R=BC/polymer$ w/w; C_{tot} : total concentration; C_{PVP} : PVP concentration).

Test code	R	C_{PVP} (mg/mL)	C_{tot} (mg/mL)	d_{10} (μm)	d_{50} (μm)	d_{90} (μm)
<i>ethanol</i>						
#01	-	10	10	0.37	0.78	1.18
#02	1/4	2	2.5	0.20	0.42	0.70
#03	1/6	3	3.5	0.22	0.49	0.83
#04	1/10	5	5.5	0.36	0.70	1.18
#05	1/20	10	10.5	0.43	0.84	1.33
<i>acetone/ethanol 70/30 (v/v)</i>						
#06	-	10	10	0.25	0.53	0.85
#07	1/4	2	2.5	0.16	0.28	0.42
#08	1/6	3	3.5	0.19	0.39	0.63
#09	1/10	5	5.5	0.25	0.43	0.69
#10	1/20	10	10.5	0.25	0.48	0.80

SAA coprecipitation experiments BC-PVP using ethanol

Keeping constant BC amount in ethanol (0.5 mg/mL) and varying the polymer concentration, a set of experiments was performed, to study the effect of BC/PVP weight ratio (R); in particular, $R=1/4$, $1/6$, $1/10$ and $1/20$ wt/wt were investigated (Table V.3). A SAA test using $R=1/2$ was also performed, but, it is not reported since particles produced showed a partially coalescent morphology. All produced powders showed an homogeneous orange color (Figure V.10a), intermediate between that of PVP (white) and BC (deep orange). The amount of powder obtained for all coprecipitation experiments ranges between about 70 and 80% of all solutes injected since part of the material produced was difficult to recover from the internal

surfaces of the precipitator. An example of SEM image of coprecipitated BC-PVP particles is reported in Figure V.10b.

Spherical microparticles with a homogeneous morphology were produced. A significant increase in particle size was observed when the total concentration moved from 2.5 to 10.5 mg/mL, with d_{50} varying between 0.42 and 0.84 μm (Table V.3). A graphical comparison between volumetric cumulative particle size distributions of BC-PVP microspheres obtained from ethanol is reported in Figure V.11. All particles were smaller than about 1.6 μm and a decrease of d_{50} was observed when R increased.

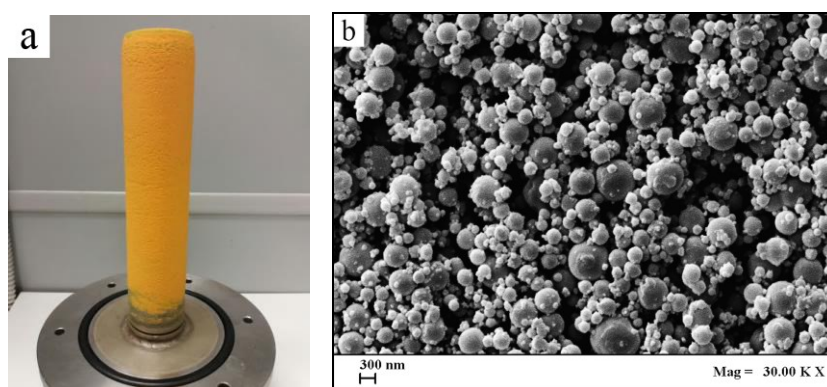


Figure V.10 a) Picture of the filter covered by coprecipitated powder; SEM image of BC-PVP precipitated from ethanol at $R=1/6$ (#03).

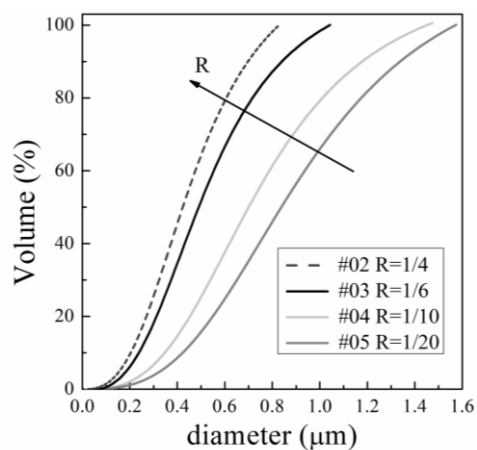


Figure V.11 Volumetric cumulative PSD of BC-PVP in ethanol, at different weight ratios R (w/w).

BC/PVP coprecipitation experiments using acetone:ethanol 70/30 v/v

A second set of experiments was performed dissolving BC and PVP in a mixture of acetone:ethanol (70:30 v/v). Concentrations and BC/PVP weight ratios used in these SAA tests are summarized in Table V.3 and the operating conditions were the same of the previous set of experiments. Homogeneous and orange powders were produced also in this case. Spherical and well-defined microparticles were obtained, as shown, for example, in the SEM image reported Figure V.12a in the case of $R=1/20$. When R increased, particles produced were smaller and morphologies obtained were less regular (Figure V.12b). Volumetric PSDs were compared and shown in Figure V.13: all particles were smaller than about $1.1\ \mu\text{m}$ and, also in this case, a decrease of d_{50} was observed when R increased.

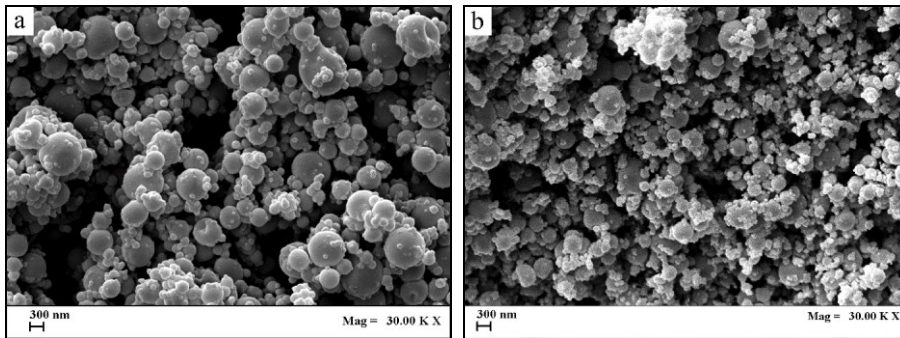


Figure V.12 FESEM images of BC-PVP precipitated from acetone/ethanol 70/30 (v/v) at different R , a) $1/20$ and b) $1/6$ (#08).

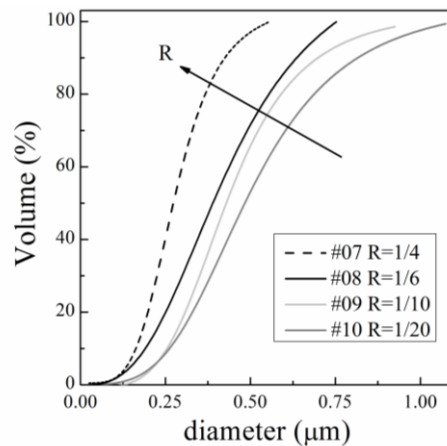


Figure V.13 Volumetric cumulative particle size distribution of BC-PVP in the mixture acetone:ethanol, at different R .

Summarizing, the particles obtained using ethanol are more regular and larger than those produced using the mixture acetone:ethanol (70:30 v/v). As a general comment, SAA particles obtained in this work showed a markedly more regular morphology compared to those obtained by spray drying and SAS technique (Prosapio et al., 2015, Franceschi et al., 2008, Priamo et al., 2011), also using BC/PVP weight ratios up to 1/4. The production of more regular morphologies and the absence of aggregates can be an indication of a successful coprecipitation process. Until now, only Prosapio et al. (Prosapio et al., 2015) obtained reasonably microparticles, using SAS technique and BC/PVP lower than 1/10 w/w. Generally speaking, SAS coprecipitation is frequently not successful since at nanoparticles level the two compounds (polymer+active principle) tend to precipitate separately.

V.3.2 Characterization of BC-PVP coprecipitates

DSC analyses were performed on untreated compounds, physical mixture BC/PVP and SAA processed BC-PVP, to study the changes in the thermal behavior of the active principle and polymer in the coprecipitates. In Figure V.14 the thermograms related to two coprecipitates (produced at R=1/6 and 1/20) and raw materials are reported. Raw BC shows a broad endothermic peak ranging between 50 and 100°C, due to the evaporation of bond water, and a second endothermic peak at about 170°C, due to the fusion of crystalline structure. Unprocessed PVP shows only the removal of water between 50 and 130°C; the physical mixture (at R=1/6) shows both the polymer and BC peaks (the intensity of this last peak is lower than that of raw BC). In thermograms of all SAA processed BC-PVP, obtained both in ethanol and in the mixture, the melting peak of BC is not present, indicating that the BC entrapped in the microspheres is in an amorphous state. The thermograms of SAA coprecipitates are very similar to the one of PVP. According to the literature, when only one glass transition temperature, T_g , is observed, a one-phase solid powder is obtained and the production of a homogeneous dispersion is produced (Aid et al., 2017).

These results were confirmed by X-Ray analyses that give informations about the solid state of materials (Figure V.15).

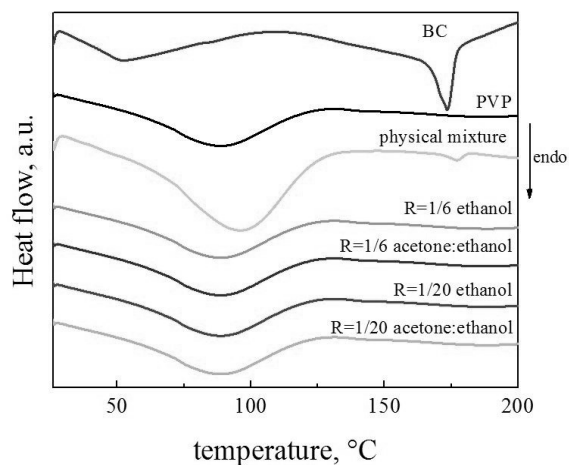


Figure V.14 DSC thermograms of BC-PVP: comparison among raw materials and SAA coprecipitates.

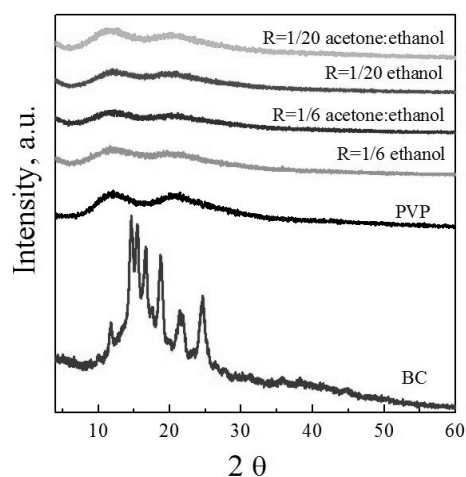


Figure V.15 X-Ray spectra of BC/PVP: comparison among raw materials and SAA coprecipitated microspheres.

Untreated BC has a spectrum typical of crystalline form, whereas PVP shows the *halos* typical of amorphous form. As an example, in Figure V.15, the spectra of coprecipitates produced at R=1/6 and R=1/20, obtained in ethanol and in the mixture acetone:ethanol, are reported and showed the same behavior. The patterns of these coprecipitated powders show a complete amorphous solid state, with no characteristic BC peak.

FT-IR analyses were performed to identify possible interactions between the active principle and the polymer in the coprecipitates. FT-IR spectra (in the range of $4000\text{-}500\text{ cm}^{-1}$) of unprocessed BC and PVP, SAA processed BC-PVP coprecipitates, obtained in ethanol and in the mixture acetone:ethanol at $R=1/6$ and $R=1/20$, as an example, are reported in Figure V.16. In the spectrum of BC, the broad peak at 3411 cm^{-1} represents the presence of -OH stretching of the hydroxyl group. The peaks at 2929 and 2869 cm^{-1} are related to the CH_2 asymmetry and symmetric stretching, respectively. The most intense peak in the spectrum is the one at about 1000 cm^{-1} , that is the trans-conjugated-alkenes CH out of the plane deformation mode (Yi et al., 2015). In the FT-IR spectrum of PVP, the broad peak in the range of $3550\text{-}3200\text{ cm}^{-1}$ is related to the OH stretching of the hydroxyl group. The sharp peak at 1656 cm^{-1} indicates the presence of carbonyl group, whereas the peak at 1291 and 1440 cm^{-1} are due to the stretching of amide group and C-H deformation of CH_2 group, respectively (Laot et al., 1999). FT-IR spectra of all coprecipitates show the same behavior: the peaks related to the active principle are present, but not very marked. No shifts or broadening of peaks related to BC and PVP are present in these spectra and this suggests that no new bonds are formed between BC and PVP.

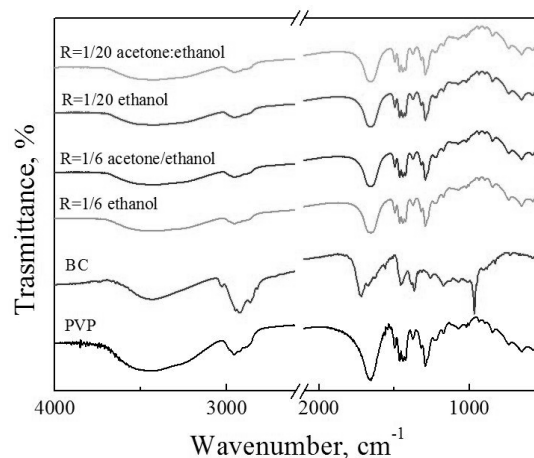


Figure V.16 FT-IR spectra: comparison among raw materials and SAA coprecipitated microspheres.

Loading efficiencies and dissolution tests

Qualitatively, BC presence in SAA produced microparticles is easy to demonstrate, since powders are orange, as already reported (Figure V.10a). Quantitatively, BC content in SAA powders for each BC/PVP weight ratio was measured using an UV-vis spectrophotometer, to ascertain the effective presence and the quantity of this compound in coprecipitates. BC content in

Coprecipitation of nutraceutical compounds using SAA technique

SAA powders can give an indication about the success of coprecipitation process. The loading efficiency, expressed as the amount of BC in SAA powder vs its amount in the starting solution, ranged between about 73% and 93% for BC-PVP coprecipitates obtained in ethanol and between about 63 and 94% for BC-PVP coprecipitates obtained from the acetone:ethanol mixture, as summarized in Table V.4.

Table V.4 BC loading efficiency in SAA coprecipitates; antioxidant activity of SAA powders by DPPH method. R= BC/PVP w/w.

Test Code	R	Theoretical loading (%)	Effective loading (%)	Loading efficiency (%)	SA (%)	$\frac{\mu\text{mol}_{\text{Trolox}}}{\text{g}_{\text{powder}}}$
untreated BC	-		-	-	9.4	730.2±1.5
<i>Ethanol</i>						
#02	1/4	20.0	18.5	92.6	10.5	901.2±1.0
#03	1/6	14.3	10.7	75.0	11.3	963.2±1.2
#04	1/10	9.0	6.6	73.2	14.6	1194.8±0.8
#05	1/20	4.7	3.4	73.2	20.8	1741.1±1.3
<i>acetone/ethanol 70/30 (v/v)</i>						
#08	1/6	14.3	13.5	94.4	8.2	623.0±0.9
#09	1/10	9.0	5.7	63.4	9.6	752.3±1.0
#10	1/20	4.7	3.1	66.0	15.9	1305.8±1.6

During SAA tests, very small quantities of BC precipitated in the saturator; therefore, loading efficiencies lower than in previous studies were obtained (Adami et al., 2017a, Di Capua et al., 2017b). In particular, loading efficiencies decrease with the increasing amount of polymer; probably, when PVP at large concentrations was used a larger antisolvent effect, though at a limited value, could be added in the saturator, reducing BC content also. However, these values are much higher than those reported in the literature, where BC loading efficiencies obtained, for example using SAS technique, are lower than 50% (Franceschi et al., 2008, Priamo et al., 2011).

To verify the improvement of BC bioavailability when loaded in PVP matrix, dissolution tests were performed using a dialysis bag in PBS pH 7.4, simulating conditions of the small intestine. The dissolution profiles, obtained fixed an equivalent amount of BC (5 ppm) for each BC/PVP weight ratio, for particles obtained from ethanol and the mixture acetone:ethanol (70:30 v/v) are reported in Figure V.17.

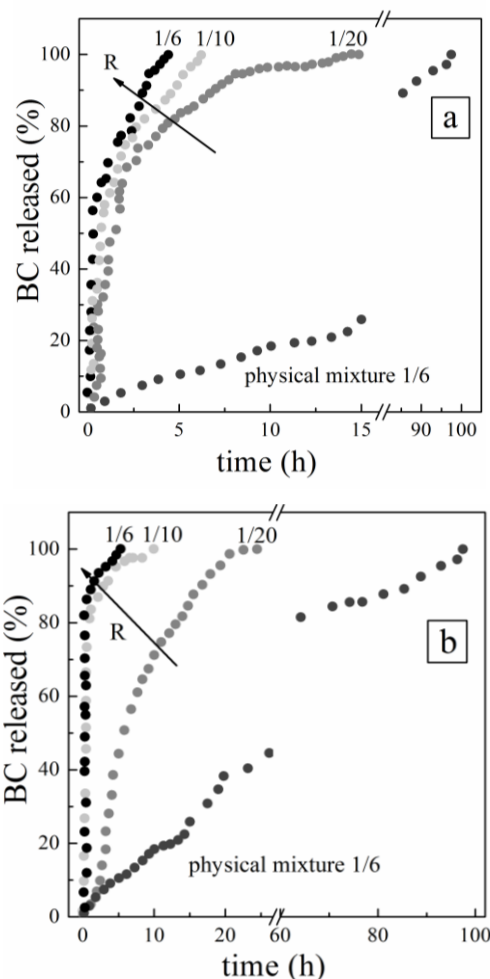


Figure V.17 Release profiles of BC in PBS at 37°C and pH 7.4: BC-PVP particles obtained using a) EtOH and b) Ac:EtOH (70:30 v/v) as solvent.

The physical mixture of the raw materials was prepared at $R=1/6$; it released 100% of BC in about 100 hours (more than 4 days), due to its poor solubility in water. The analyses on SAA coprecipitates confirmed that the powders of BC-PVP show a faster release than physical mixture. In Figure V.17a, the coprecipitate at $R=1/6$ shows a total dissolution time of about 4.5 hours, that is about 22 times faster than the one of the physical mixture, overcoming the best results (10 times) found in literature (Prosapio et al., 2015). The coprecipitates produced using ethanol at $R=1/10$ and $1/20$ totally dissolved in 6 and 15 hours, respectively. Furthermore, the release was controlled by BC/PVP weight ratio: increasing R , larger drug release rates were obtained. This trend is unusual when compared to other coprecipitated

systems tested by SAA, in which the dissolution rate increases when R decreases (Adami et al., 2017a). However, in those cases, particles were produced keeping constant polymer concentration in the liquid and changing active principle concentration and the produced particle size increased with R (Adami et al., 2017a). In this work, instead, particles are produced fixing BC concentration and varying PVP concentration and particle size decreases with R. As a general comment, the dissolution behavior of coprecipitates is affected by several parameters: interactions between compounds, particle size, solid state. Our hypothesis to explain the trend of BC-PVP dissolution behavior, is that the main role is taken by particle size: smaller particles are produced at higher R and, consequently, larger surface areas are available for dissolution in the aqueous medium and faster dissolution rates are obtained.

In the dissolution curves related to particles obtained using the mixture acetone:ethanol, particularly in the case of higher BC/PVP weight ratios, the release profiles showed different behaviors from those obtained using ethanol (Figure V.17b). This fact might be due, again, to the differences of the two liquid solutions injected in SAA apparatus and more specifically to the different drying/solidification rates of droplets in SAA precipitator. Droplets drying is, indeed, a fundamental step during SAA process that can influence the distribution of the active compound in the carrier. Parameters including temperature, initial droplet size, droplet number density influence particle formation (Eslamian et al., 2009, Mezhericher et al., 2007, Wang et al., 2005). Furthermore, a very fast evaporation of the solvent may affect the dispersion of the active principle in the carrier that can be more concentrated on particle surface. Only the coprecipitate at $R=1/20$ (Figure V.17b) showed a dissolution curve similar to those obtained using the ethanolic system, with a 4-fold faster dissolution rate compared to the physical mixture. The most intriguing results are that BC dissolution rate largely depends not only by BC/PVP ratio, but also on the solvent/solvent mixture used. A possible explanation of this result can be found looking at the precipitation mechanism that forms microparticles. SAA microparticles are formed from liquid droplets and their subsequent transformation in microparticles by solvent evaporation. Different solvent/solvent mixtures are characterized by different surface tension (droplet diameter), solvents evaporation rate (acetone is more volatile than ethanol) and solvents solubility in SC-CO₂. These last two characteristics can produce different particle arrangements at nanometric level that, in turn, can induce different BC release rates.

V.3.3 Antioxidant activity

In the works found in the literature and reported in the Introduction (section V.3) , none of authors proposed the study of BC antioxidant activity before and after the process; however, to demonstrate the preservation of this feature is fundamental. Antioxidant activity of untreated BC was measured

using DPPH assay, as described in Materials and Methods. The scavenging activity related to the untreated BC is 9.4%. Analyses on SAA coprecipitates showed a general enhancement of the inhibition capacity with respect to BC. The SA (%) values found in ethanol were between 10.5 and 20.8% for BC-PVP particles obtained using ethanol and between 8.2 and 15.9% for BC-PVP particles obtained using acetone:ethanol (Table V.4). A higher SA value indicates a higher free radical scavenging activity of the compounds dissolved: this means that a lower concentration is required to quench DPPH radical. The antioxidant capacity of SAA powders were also expressed in terms of Trolox equivalent (TE) by gram of powder, where higher value means higher antioxidant power. The values found for each sample were reported in Table V.4. The results indicate that SAA coprecipitates show a good preservation of BC antioxidant power. The highest SA values were achieved for samples produced at R=1/20: the coprecipitate #05 (obtained using ethanol) shows a SA of 20.8% and the coprecipitate #10 (obtained using acetone:ethanol) a SA of 15.9%. As reported in literature (Desai and Jin Park, 2005, Reksamunandar et al., 2017), the dispersion of an active compound in polymeric matrices may provide a better preservation of the active ingredient creating a barrier with the external environment.

Furthermore, all SAA formulations showed larger SA compared to untreated BC. This unexpected result might be due to several issues. Some researchers demonstrated that reduced size of a pure active principle can improve free radical scavenging activity, due to the enhanced dissolution rate of the compound (Kakran et al., 2012, Meneses et al., 2015). Furthermore, another aspect to be considered, to explain the enhanced antioxidant activity of complex systems, is the chemical structure of the compounds in the formulations. Both compounds are good hydrogen and electron donors and contribute to the quenching of DPPH radical. As a support to this hypothesis, both BC and PVP have many protons in their structures that can reduce DPPH radical in solution.

V.3.4 Conclusions on BC-PVP system

Coprecipitates formed by PVP and BC were successfully produced using SAA technique: microparticles with loading efficiencies up to 94% and an enhanced BC dissolution rate up to 22 times with respect to the physical mixture largely overcoming the best result in the literature (10 times using SAS technique) (Prosapio et al., 2015).

An unexpected result was that very small quantities of PVP were enough to improve BC release rate and protect it from chemical degradation. Another interesting result is that changing the organic solvent, and leaving all the other processed conditions unmodified, different arrangements can be obtained inside the microparticles (at nanometric level) that can largely influence BC release rate.

Chapter VI

Recovery and protection of antioxidants from bio-residues

VI.1 Saffron petals as sources of antioxidants

Interest in natural antioxidants is increasing due to concerns by consumers over safety of synthetic antioxidants that may potentially cause health problems (Carocho et al., 2015, Wojcik et al., 2010). Antioxidants are mainly used in food to prevent off-flavors by oxidation of fats; however, they play a role also in the prevention and treatment of several chronic diseases, such as asthma, cardiovascular problems and cancer (Sardas, 2003). Due to their highly profitable properties, the extraction of these antioxidant compounds from plants and flowers and their incorporation in our diet as nutraceutical ingredients is growing.

Crocus Sativus, most known as saffron, is a perpetual plant used to produce the typical spice in our kitchens. Only stigmas (the red part of the flower) are collected, dried and used as a culinary spice; whereas, the remaining part of saffron flowers is considered as a waste (Righi et al., 2015). Floral bio-residues are the major by-product (around 90% of total weight of saffron) composed by tepals, stamens and styles. Mechanization of flower collection and spice production have led to an increase of productive capacity, expanding also the amount of waste materials (Serrano-Díaz et al., 2013). These floral bioresidues are rich of carotenoid derivates (such as crocetin, crocin and lutein diesters), carbohydrates (glucose, fructose, mannitol), monoterpenoids (picrocrocin, crocusatins), flavonoids and their glycoside derivates and anthocyanins (Serrano-Díaz et al., 2013, Tuberoso et al., 2016). These substances can be used in food, pharmaceutical and/or cosmetic industries due to their natural colorant, antioxidant and therapeutic properties (Ahmad et al., 2018). Flavonoids in saffron flowers are mainly represented by kaempferol and quercetin and their glycosides (Hadizadeh et al., 2010, Righi et al., 2015, Tuberoso et al., 2016, Zeka et al., 2015,

Termentzi and Kokkalou, 2008), with kaempferol 3-O-sophoroside being the most abundant (around 84%) (Zeka et al., 2015, Babaei et al., 2014). Researchers have demonstrated that saffron petal extracts show biological, antioxidant, antifungal and antiradical activities, cytotoxic effect and metal chelant properties (Tuberoso et al., 2016). They may induce malignant cell death, slow skin aging by inhibiting a variety of enzymes that degrade the extracellular matrix, prevent arteriosclerosis and heart diseases (Hadizadeh et al., 2010). The major properties of saffron flower extracts have to be attributed to its kaempferol content (Tuberoso et al., 2016).

Some procedures have been used to extract bioactive components from saffron petals, such as maceration, ultrasound assisted extraction (Ahmad et al., 2018, Khazaei et al., 2016, Lotfi et al., 2015) and, more recently, using supercritical fluid processes (Ahmadian-Kouchaksaraie et al., 2016b, Ahmadian-Kouchaksaraie and Niazmand, 2017, Ahmadian-Kouchaksaraie et al., 2016a). Conventional methods are mainly based on a solid-liquid extraction using organic solvents, like ethanol, water, and mixtures water:ethanol (Zeka et al., 2015, Ahmadian-Kouchaksaraie et al., 2016b, Ahmadian-Kouchaksaraie and Niazmand, 2017, Khazaei et al., 2016). Ahmadian-Kouchaksaraie et al. (Ahmadian-Kouchaksaraie et al., 2016b, Ahmadian-Kouchaksaraie and Niazmand, 2017) investigated green extraction technologies, such as supercritical carbon dioxide and subcritical water extraction of antioxidants from saffron petals. These innovative technologies allowed increasing the extraction capacity both in phenolic compounds and anthocyanins compared to conventional extractions. In particular, using supercritical CO₂ and subcritical water extraction the amount of flavonoids extracted was 2 and 3 times higher compared to conventional extraction results, respectively.

Nevertheless, the effectiveness of these extracted bioactive compounds depends on preserving their stability against heat, light and oxygen (Ahmad et al., 2018, Machado et al., 2018, Guamán-Balcázar et al., 2019) and the bioactivity and bioavailability of active principles. Furthermore, the strong and unpleasant taste and aroma sometimes can limit the direct application of these extracted compounds in food products (Di Capua et al., 2018). The current challenge is to protect such promising molecules from deterioration and loss of their activity. The encapsulation of extracted compounds from saffron petals is still poorly investigated. In the literature, very few works have focused their attention on the encapsulation of saffron petal extracts. For example, Ahmad et al. (2018) loaded anthocyanins extracted from saffron petals using ethanol acidified at pH=2 in two different carrier: β -glucan and β -cyclodextrin, using spray drying technique. In Figure VI.1, examples of particles produced by Ahmad et al. are reported (Ahmad et al., 2018).

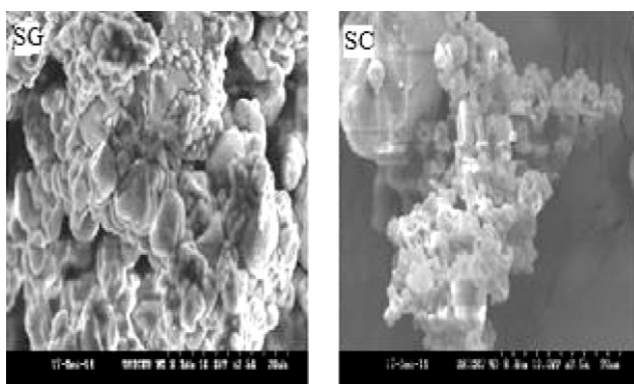


Figure VI.1 SEM images of samples produced using: SG) β -glucan and SC) β -cyclodextrin (Ahmad et al., 2018).

As it is possible to observe, produced powders were irregular and coalescent agglomerates, difficult to be characterized in terms of particle size. Loading efficiencies were very low, ranging between 45 and 63%, respectively using β -glucan and β -cyclodextrin. Mahdavee Khazaei et al. (Mahdavee Khazaei et al., 2014) studied the microencapsulation of saffron petal's anthocyanins using maltodextrin and gum Arabic as carrier and the freeze drying as technique. Also in this case, powders produced consisted of very irregular and flat crystals; however, no results in terms of loading efficiencies were reported, whereas a stability study demonstrated a preservation of anthocyanins encapsulated. In recent years, the encapsulation by SC-CO₂-based processes is demonstrated to be an efficient alternative for natural products preservation, due to the use of low temperatures, to reduce organic solvent consumption and to control PSD (Cocero et al., 2009). Several investigations have obtained successful results using PVP as carrier, for examples in the case of mango leaves (Guamán-Balcázar et al., 2019) and blackberry residues (Machado et al., 2018). Indeed, PVP is a common polymer, often used as carrier to enhance the dissolution rate of hydrophobic compounds; it is readily soluble in water, non-toxic, biocompatible and accepted by FDA (Kamada et al., 2000, Guamán-Balcázar et al., 2019). In this thesis work, SAA demonstrated to be effective in the production of coprecipitates in which bioactive compounds, such as propolis ethanolic extract and beta-carotene, were dispersed in PVP matrix (Di Capua et al., 2018) preserving antioxidant power of the active compounds investigated.

Therefore, the first aim of this work was to optimize extraction parameters (temperature, flower maceration time, solvent) in order to maximize the amount of kaempferol and quercetin glycosides extracted. Then, the optimized extracts were processed by SAA technique in order to stabilize these glycosides through their dispersion in PVP matrix. The objective was to produce stable particles able to preserve glycoside

antioxidant activity and to extend their shelf life. Analyses of solid state, morphology, PSD, glycosides content in the formulations and antioxidant activity analyses on time were performed, to assess the efficiency of SAA process on the production of glycoside-rich powders and on the preservation of floral bio-residues.

Materials

Polyvinylpyrrolidone (PVP, M_w : 10,000), ethanol (EtOH, purity 99.9%), 2,2-Diphenyl-1-picrylhydrazyl (DPPH) and methanol (MetOH, purity >99.9%) were supplied by Sigma Aldrich. *Crocus Sativus* bulbs were from Holland; they were collected in Magnano in Riviera (Udine, Italy). The floral residues, obtained after the separation of the stigma, were stored in a dark, dry place, under vacuum conditions. Carbon dioxide (CO₂, 99.9%) was purchased by Morland Group (Italy) and nitrogen (N₂, 99%) by SOL (Italy). All materials were used as received.

VI.1.1 Extraction from saffron petals

The polyphenols extraction was obtained by conventional solid-liquid extraction from saffron petals (Figure VI.2), as described in literature with minor modifications (Ahmadian-Kouchaksaraie and Niazmand, 2017, Ahmadian-Kouchaksaraie et al., 2016a, Ahmadian-Kouchaksaraie et al., 2016b, Zeka et al., 2015).



Figure VI.2 *Saffron petals.*

Saffron petals (2.5 g) were mixed with 75 mL of solvent; the extraction was carried under dark and continuous stirring (Ahmadian-Kouchaksaraie et al., 2016a). Four different solvents (pure ethanol, aqueous ethanol (59% v/v), ethanol acidified with HCl (pH=2), aqueous ethanol (59% v/v) acidified with HCl (pH=2) were investigated for extraction, at room temperature. Furthermore, different intervals of time extraction were investigated ranging

between 3 and 24 hours. After extraction, each sample was filtered through filter paper; 20 mL of each extract was then evaporated under vacuum at 30°C. The dried extract was weighted to evaluate the extract concentration; then, each dried extract was dissolved in methanol and analyzed by HPLC to estimate the amount of glycosides of kaempferol and quercetin extracted.

First, saffron petals extractions using ethanol and a mixture of water:ethanol (41:59 v/v) were performed. Examples of extracts produced varying the time of maceration and solvents are reported in Figure VI.3.

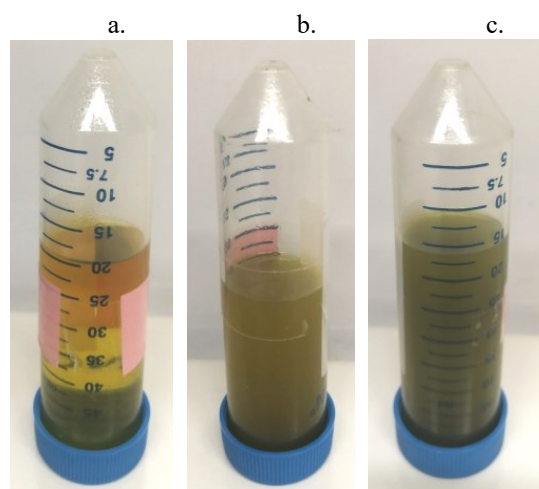


Figure VI.3 Extracts obtained using ethanol as solvent at room temperature after a) 3 h; b) 6h; c) 24h.

A gradient of color is easily observable in Figure VI.3, where ethanolic extracts at different time of flower maceration are reported. In particular, the extract obtained after 3 hours of extraction was clear yellow; however, increasing the time of infusion (6 and 24 h), the extracts were less clear and greenish. A similar trend is possible to note also in the case of extracts obtained using a mixture of water:ethanol (41:59 v/v), in Figure VI.4.

As shown in Figure VI.4, extracts obtained in water:ethanol mixture were increasingly dark, varying the time of flower maceration between 3 and 24 hours.

A second set of extraction experiments was carried out using the same solvents (ethanol, water:ethanol 41:59 v/v) acidified with HCl at pH=2 (Khazaei et al., 2016, Ahmad et al., 2018). Examples of extracts produced after 6 hours of flower maceration and solvents are reported in Figure VI.5.

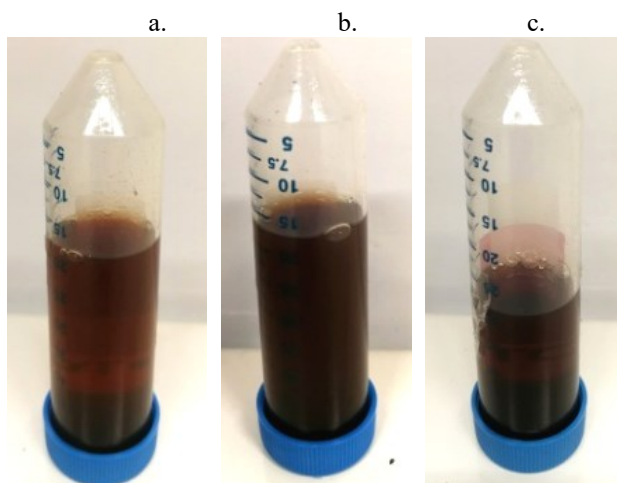


Figure VI.4 Extracts obtained using water:ethanol (41:59 v/v) as solvent at room temperature after a) 3 h; b) 6h; c) 24h.

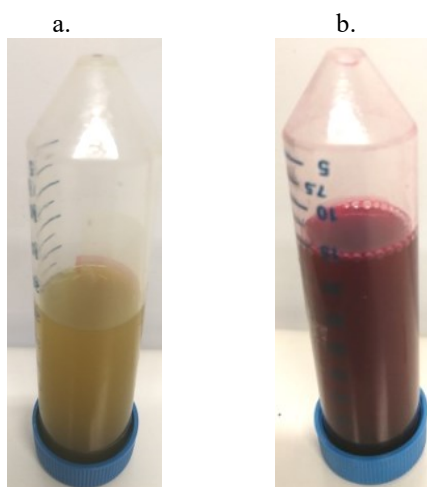


Figure VI.5 Extracts obtained at room temperature after 6 hours of flower maceration, using a) ethanol at pH=2; b) water:ethanol (41:59 v/v) at pH=2.

As it is possible to observe in Figure VI.5a, the extract obtained in ethanol at pH=2 was opaque and yellow/greenish; it was really similar to the color obtained using the solvent not acidified (Figure VI.3b). The extract produced using the mixture water:ethanol (41:59 v/v) at pH=2, instead, was dark with shades of purple, as shown in Figure VI.5b. This particular color was due to the extraction of compounds like anthocyanins that are water-

soluble pigments belonging to flavonoid family, used as food supplements (Ahmad et al., 2018, Khazaei et al., 2016, Mahdavee Khazaei et al., 2014).

Another extraction parameter considered was the temperature. On the basis of literature (Ahmadian-Kouchaksaraie et al., 2016a), two different temperatures were investigated: 25 and 66°C. However, a real effect of temperature was not verified, indeed the results obtained at 25°C were similar to those at 66°C (not reported); hence, a lower temperature was preferred to avoid the degradation of active compounds in solution.

Quantification of kaempferol and quercetin glycosides in extracts

This study focused mainly in two antioxidant compounds: kaempferol and quercetin glycosides. These compounds were identified and quantified using HPLC analyses, as described in Chapter II. In Figure VI.6 and Figure VI.7, histograms represent the areas under the peaks identified in HPLC chromatograms as quercetin (elution time 2 min) and kaempferol (elution time 7 min) glycosides, for extracts obtained using ethanol and water:ethanol (41:59 v/v), respectively, varying the time of flower maceration.

As it is possible to observe in Figure VI.6, the amount of kaempferol and quercetin glycosides in the extract obtained in ethanol increases as increasing the time of flower maceration. However, the increase of extracted compounds obtained from 6 to 24 hours was limited. Figure VI.7 shows the extraction capacity of mixture water:ethanol (41/59 v/v).

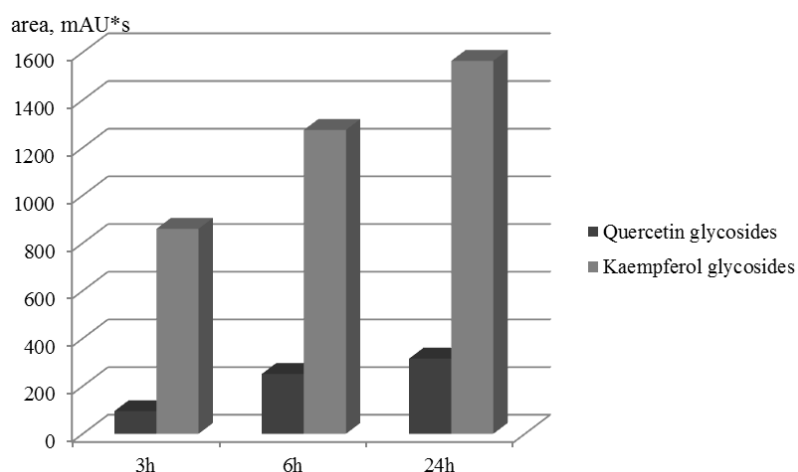


Figure VI.6 Areas under peaks related to the glycosides of kaempferol and quercetin in the HPLC chromatograms of the extracts obtained in ethanol, at 25°C and different times of flower maceration.

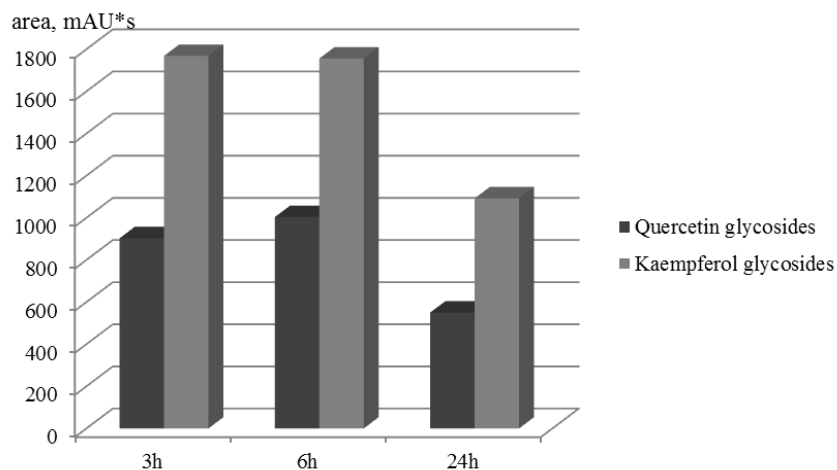


Figure VI.7 Areas under peaks related to the glycosides of kaempferol and quercetin in the HPLC chromatograms of the extracts obtained in water:ethanol (41:59 v/v), at 25°C and different times of flower maceration.

The amount of extracted compounds was practically unchanged increasing the time of flower infusion up to 6 hours, whereas after 24 hours, HPLC analyses demonstrated a reduction of kaempferol and quercetin glycosides, due to a partial degradation of extracted compounds. However, the mixture water:ethanol (41:59 v/v) shows a highest extraction power in terms of kaempferol and quercetin glycosides compared to ethanol, as resulted by the comparison of the results summarized in Figure VI.6 and Figure VI.7. On the basis of results obtained both in ethanol and in the mixture water:ethanol, a flower maceration of 6 hours was the best compromise to perform extraction experiments, avoiding compounds degradation and obtaining a good amount of quercetin and kaempferol glycosides extracted.

The results obtained using solvents acidified at pH=2 are summarized in histograms reported in Figure VI.8, where it is possible to observe the areas related to an extraction after 6 hours of flower maceration.

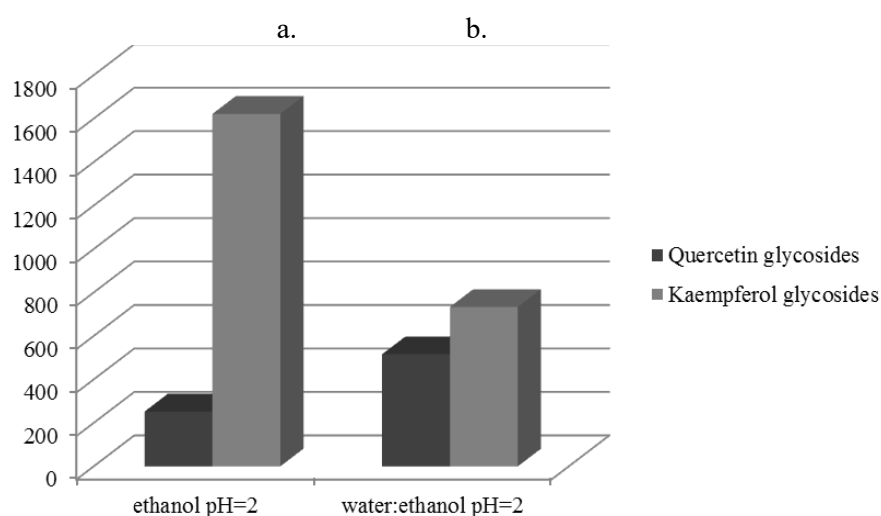


Figure VI.8 Areas under peaks related to the glycosides of kaempferol and quercetin in the HPLC chromatograms of the extracts obtained in ethanol and water:ethanol (41:59 v/v) at pH=2 and 6 hours of flower maceration.

By comparing the results obtained using acidified ethanol and pure ethanol, quercetin glycoside was practically extracted in the same quantity, whereas the amount of kaempferol glycoside increased at pH=2 (Figure VI.8a); a similar result is obtained also by Yi et al. (Yi et al., 2016) from *Gynura medica*. Using the mixture water:ethanol (41:59 v/v) at pH=2, instead, HPLC analyses demonstrated a reduction of both kaempferol and quercetin glycosides (Figure VI.8b).

In Table VI.1 results of extractions performed at 6 hours of flowers maceration are summarized, in terms of total yield of extraction (expressed as mg of dried extract/g of saffron petals), total extract concentration (C_{ext}) and kaempferol (C_K) and quercetin (C_Q) concentrations evaluated from HPLC chromatograms of the extracts produced after 6 hours of flower maceration.

Table VI.1 Extraction results obtained after 6 hours using ethanol and water:ethanol (41:59 v/v); (C_{ext} : extract concentration; C_K : kaempferol concentration; C_Q : quercetin concentration; SA: Scavenging Activity).

Solvent	$\frac{\text{mg}_{\text{dried extract}}}{\text{g}_{\text{petal}}}$	C_{ext} (mg/mL)	C_K (mg/mL)	C_Q (mg/mL)	SA (%)	SA reduction (%)
EtOH	405.0	13.5	5.5	1.0	55.0	30.4
EtOH (pH=2)	344.7	11.5	7.4	0.6	36.1	27.0
H ₂ O:EtOH	723.0	24.1	12.4	4.6	76.8	35.1
H ₂ O:EtOH (pH=2)	868.2	28.9	5.7	1.9	83.8	32.5

From Table VI.1, it can be clearly noted that the higher levels of quercetin and kaempferol extracted were obtained using water:ethanol (41:59 v/v). After 6 hours, about 165 mg of kaempferol glycoside and 30 mg of quercetin glycoside per g of dried petals were extracted using ethanol, whereas, about 370 mg of kaempferol glycoside and 137 mg of quercetin glycoside per g of dried petals using water:ethanol (41:59 v/v). These results overcome the yields of extraction obtained, for examples, by Zeka et al. (Zeka et al., 2015) where 126 mg of kaempferol aglycone for g dried petals were extracted using methanol in 16 hours. In Table VI.1, antioxidant activities related to extracts (at $t=0$, i.e. time of preparation) are also reported; Scavenging Activity (SA) results were consistent with the total extract concentrations. It was observed, indeed, that SA related to aqueous extracts is higher than those evaluated for ethanol extracts; therefore, SA showed a strong dependence on the solvent used for the extraction. After 3 months, the extracts stored in a dark and dry place were analyzed afresh; as detailed in Table VI.1, it was verified a SA reduction ranged between 27 and 30% for ethanol extracts and between 32 and 35% for aqueous extracts.

Preparation of saffron petals extracts and polymer solutions

Produced extracts were characterized by different concentrations, depending on the solvents used (Table VI.1). For the precipitation experiments, firstly extracts were processed as produced, dissolving PVP directly into the extracts, at different R=extract/PVP weigh ratios (1/3, 1/5). A second set of experiments were performed after extract dilution down to 2 mg/mL and using the same extract/PVP weight ratios.

VI.1.2 SAA coprecipitation experiments

Identified the best extraction conditions, the produced extracts have been treated using SAA technique to produce particles consisting in a polymeric matrix (PVP) in which the active compounds extracted from the petals can be finely dispersed (Ahmad et al., 2018, Mahdavee Khazaei et al., 2014). PVP was already precipitated by SAA in form of spherical, separated microparticles, using ethanol, water, and water:acetone and acetone:ethanol mixtures (Liparoti et al., 2015, Liparoti et al., 2013, Di Capua et al., 2018, Adami et al., 2017a, Di Capua et al., 2019). Therefore, since PVP behavior in ethanol, and water:ethanol mixture was well known, SAA operating conditions were optimized in previous studies. For ethanol system, SAA process conditions were: GLR 1.8, injection pressure of about 80-83 bar, saturator and precipitation vessel temperature 80°C. For water:ethanol system, SAA process conditions were: GLR 1.8, injection pressure of about 80-85 bar, saturator temperature of 80°C and precipitator temperature of 90°C (Adami et al., 2017a).

By using the produced extracts as they were obtained (total extract concentrations summarized in Table VI.1) in SAA coprecipitation tests, a clear coalescence was observed in the particles produced; moreover, for water:ethanol extracts at pH=2, irregular and non-uniform in color particles were obtained. Therefore, the best compromise was to decrease extract concentrations (2 and 4 mg/mL) to promote the production of regular and homogeneous particles. Table VI.2 reports a list of coprecipitation experiments, concentrations and PSD values (in terms of volume particles) expressed as d_{10} , d_{50} and d_{90} . Keeping constant extract concentration and varying polymer concentration, a set of experiments was performed for each system, to study the effect of extract/polymer weight ratios R (w/w).

Table VI.2 Composition and PSD data of extract-PVP particles produced by SAA (R =extract/PVP w/w; C_{ext} : total extract concentration; C_{PVP} : PVP concentration; T_s = saturator temperature; T_p = precipitator temperature).

Test Code	R	C_{PVP} (mg/mL)	C_{ext} (mg/mL)	T_s (°C)	T_p (°C)	d_{10} (μ m)	d_{50} (μ m)	d_{90} (μ m)
<i>ethanol</i>								
#ZAF01	1/5	10	2	80	80	0.20	0.42	0.67
#ZAF02	1/3	6				0.19	0.33	0.55
<i>ethanol pH=2</i>								
#ZAF03	1/5	10	2	80	80	0.16	0.29	0.51
#ZAF04	1/3	6				0.13	0.24	0.44
<i>water:ethanol (41:59 v/v)</i>								
#ZAF05	1/5	10	2	80	90	0.34	0.76	1.32
#ZAF06	1/3	6				0.26	0.59	0.99
<i>water:ethanol (41:59 v/v) pH=2</i>								
#ZAF08	1/5	10	2	80	90	0.38	0.76	1.20
#ZAF09	1/3	6				0.25	0.56	1.00

A picture of SAA powders and some examples of FESEM images related to particles produced from extracts based on ethanol with PVP are reported in Figure VI.9 and Figure VI.10. Qualitatively all SAA produced powders are homogeneously colored and resulted in a color intermediate between that of PVP (white) and processed extract. In particular, the powders produced from both ethanol extracts were clear yellow (Figure VI.9a, Figure VI.10a) and completely uniform in color.

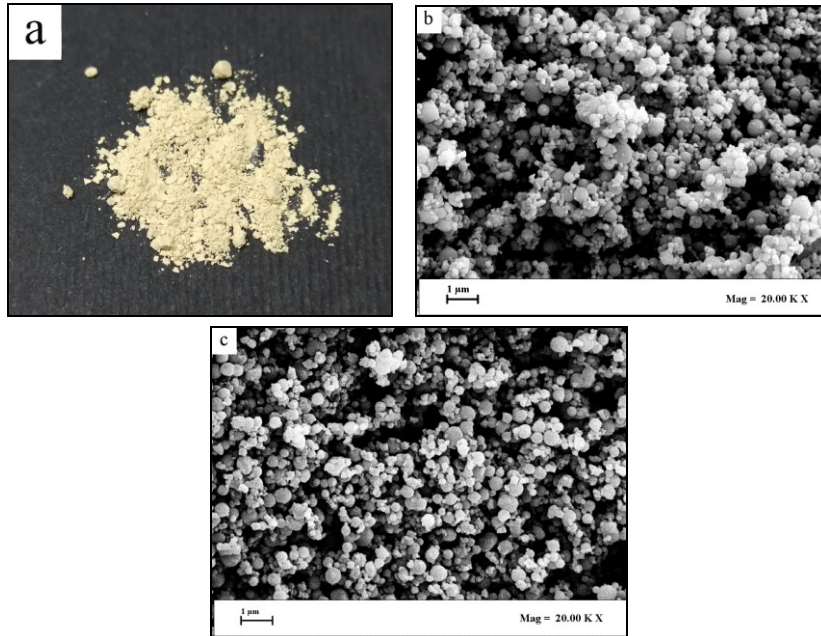


Figure VI.9 a) SAA powder obtained from EtOH extract with PVP; FESEM images related to SAA tests performed at b) $R=1/5$, c) $R=1/3$.

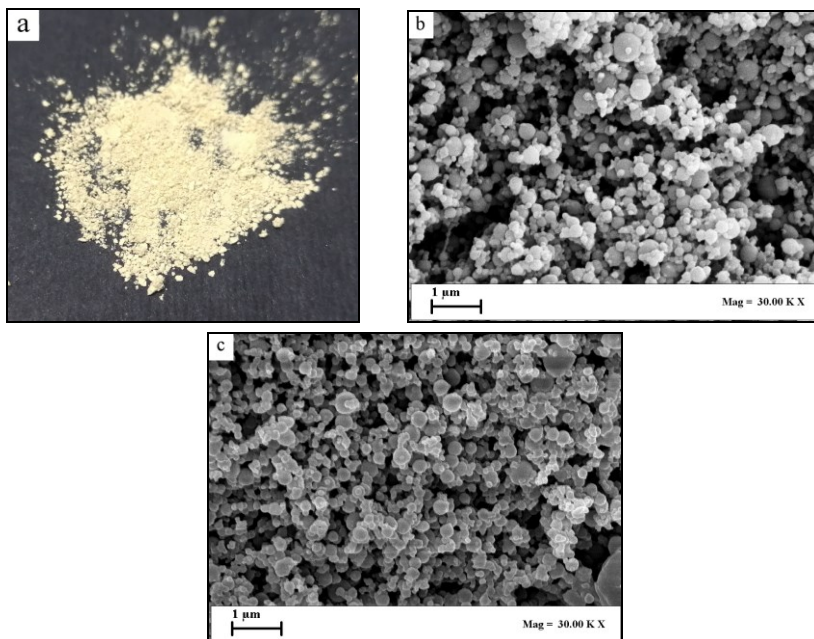


Figure VI.10 a) SAA powders from EtOH extract at pH=2 with PVP; FESEM images related to SAA tests performed at b) $R=1/5$, c) $R=1/3$.

The particles produced were spherical and well separated at all R investigated. In Figure VI.11, a comparison of PSDs related to extract-PVP particles precipitated from ethanol extract (pink) and from ethanol extract at pH=2 (blue) at different R is reported (PSD values are reported also in Table VI.2). As it is possible to observe, there is an effect due to the presence of HCl on SAA particle size. Indeed, particles obtained from ethanol extracts at pH=2 resulted smaller than those produced without HCl. Moreover, an increase of d_{50} was observed when R decreased (hence, increasing PVP concentration) due to the higher viscosity of the solution injected, as summarized also in Table VI.2 (Di Capua et al., 2017a, Di Capua et al., 2018).

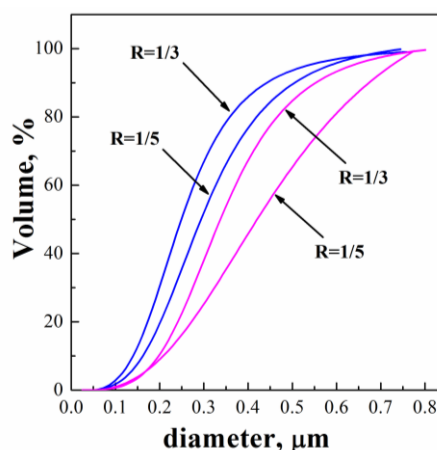


Figure VI.11 Comparison of PSDs related to extract-PVP particles precipitated from ethanol extract (pink) and from ethanol extract at pH=2 (blue) at different R (w/w).

Also extracts based on the water:ethanol (41:59 v/v) were tested by SAA; exemplificative FESEM images with enlargement of 20 KX are proposed in Figure VI.12 and Figure VI.13.

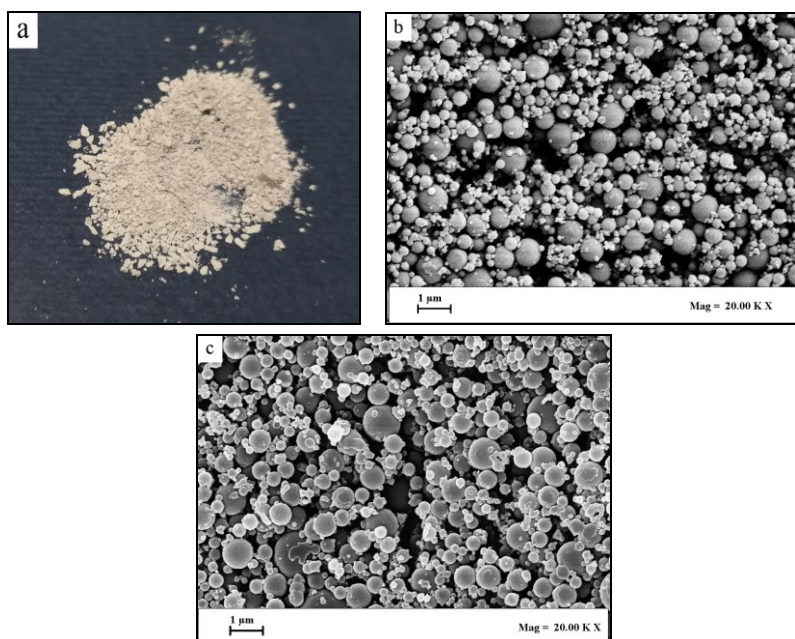


Figure VI.12 a) SAA powder from $H_2O:EtOH$ (41:59 v/v) extract with PVP; FESEM images of samples obtained at: b) $R=1/5$, c) $R=1/3$.

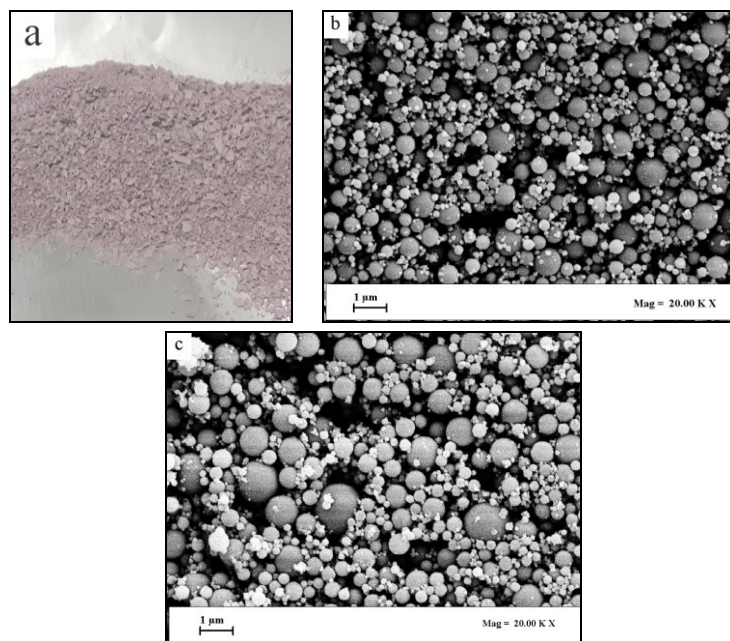


Figure VI.13 a) SAA powder from $H_2O:EtOH$ (41:59 v/v) extract at $pH=2$ with PVP; FESEM images of samples obtained at b) $R=1/5$, c) $R=1/3$.

As the photographs showed, the powders obtained from water:ethanol extracts (41:59 v/v) were clear brown in color (Figure VI.12); whereas, pink powders were collected when the extracts based on water:ethanol (41:59 v/v) at pH=2 were processed (Figure VI.13). However, when an extract concentration of 2 mg/mL was used for the coprecipitation tests, homogeneous powders consisted of spherical and well-defined particles were obtained regardless of the pH of solution injected (Figure VI.12b and c, Figure VI.13b and c). A SAA test was performed processing a higher concentration of extract (4 mg/mL) and using R=1/3: in this case, a partial coalescence was observed in SAA particles produced (figure not reported). In Table VI.2, PSD data are summarized: there is no effect related to the pH of the water:ethanol extract, but smaller particles were obtained increasing R (Di Capua et al., 2017a, Di Capua et al., 2018). Looking at overall results (Table VI.2), the particles produced using water:ethanol (41:59 v/v) extracts were larger and more perfectly spherical than those produced in ethanol.

VI.1.3 Characterization of extract-PVP coprecipitates

DSC (Figure VI.14) and X-Ray (Figure VI.15) analyses were performed to study the solid state and the crystallization behavior of extracts-PVP coprecipitates.

In Figure VI.14, the thermograms related to coprecipitates produced at R=1/3 for each kind of extract and PVP are reported. In literature, kaempferol and quercetin glycosides show melting point around 276-278°C and 316°C, respectively (Har Bhajan and Bharati, 2014). In Figure VI.14, the unprocessed PVP shows only the removal of water between 50 and 130°C, due to its amorphous nature. In thermograms of SAA processed extract-PVP particles reported, patterns similar to that of PVP can be observed, and no peaks are detectable. Therefore, a nanodispersion of extracted compounds in SAA particles can be hypothesized. These results were confirmed by X-Ray analyses; in Figure VI.15, the diffractograms related to the coprecipitates obtained from ethanol and water:ethanol at different extract/PVP weight ratios.

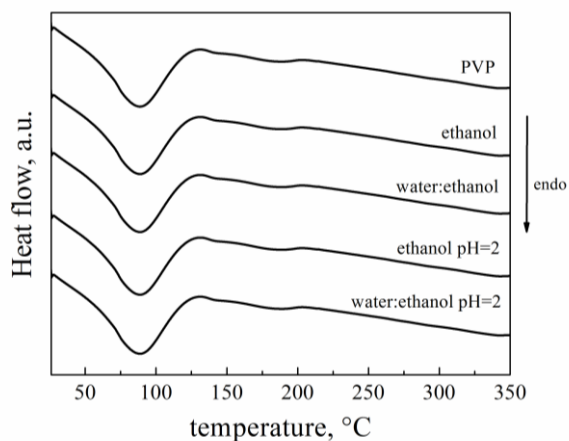


Figure VI.14 DSC thermograms of extract-PVP coprecipitates.

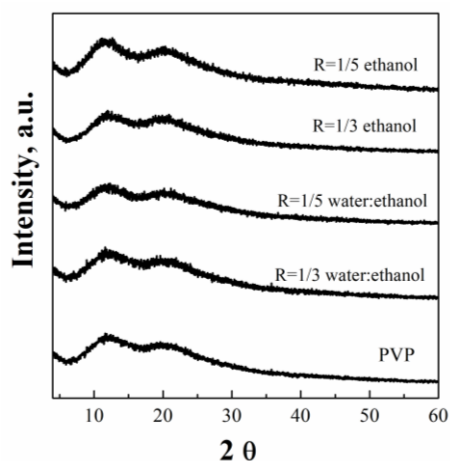


Figure VI.15 XPRD related to coprecipitates obtained from ethanol extract and from water:ethanol (41:59 v/v) with PVP, at different R (extract/PVP w/w).

Untreated PVP shows the typical halos due to its amorphous structure: in the pattern, two broad peaks around 11.5° and 20.5° are identified. SAA extract-PVP coprecipitates show only the broad peaks related to the carrier, regardless of the extract type processed and the weight ratio R. These analyses suggested that extracted compounds were finely dispersed in the PVP matrix (Aid et al., 2017). This is a typical result for SAA coprecipitates when compared to other coprecipitated systems tested by SAA; for example, the homogeneous dispersion of the active principle in polymer matrix obtained in this work can be found also in the coprecipitates based on beta-

carotene and PVP (Di Capua et al., 2019), propolis extract and PVP or hydroxypropyl- β -cyclodextrin (Di Capua et al., 2018), curcumin and PVP (Adami et al., 2017a), LUT and dextran (Di Capua et al., 2017a), dexamethasone and PVP (Liparoti et al., 2013). Similar results were obtained for the particles produced from extracts at pH=2.

Loading efficiencies and antioxidant activity in SAA particles

The loading efficiencies of quercetin and kaempferol glycosides in SAA powder were calculated using HPLC calibration curves; the resulted values are summarized in Table VI.3.

Table VI.3 *Loading efficiencies of quercetin and kaempferol glycosides and antioxidant activity of powders (R: extract/PVP w/w; C_{ext}: extract concentration; Q: quercetin glycoside; K: kaempferol glycoside; SA reduction: Scavenging Activity reduction after 3 months).*

Test code	R	C _{ext} (mg/mL)	Q loading efficiencies (%)	K loading efficiencies (%)	SA reduction (%)
<i>ethanol</i>					
#ZAF01	1/5	2	90.0	75.2	24.1
#ZAF02	1/3		88.0	74.0	22.0
<i>ethanol pH=2</i>					
#ZAF03	1/5	2	89.9	89.8	23.8
#ZAF04	1/3		85.1	83.1	26.4
<i>water:ethanol (41:59 v/v)</i>					
#ZAF05	1/5	2	~100	~100	7.9
#ZAF06	1/3		~100	~100	1.4
<i>water:ethanol (41:59 v/v) pH=2</i>					
#ZAF08	1/5	2	88.5	89.6	1.0
#ZAF09	1/3		92.8	95.0	18.2

Looking at the particles produced from ethanol extracts, quercetin loading efficiencies ranged between about 85% and 90%, whereas kaempferol loading efficiencies between about 74 and 90%. Also the particles obtained from water:ethanol extracts exhibited high loading efficiencies both for quercetin and kaempferol glycosides. In particular, particles precipitated from water:ethanol extracts showed loading efficiencies up to 100%. These results were very promising, mainly compared to encapsulation efficiencies found in literature ranging between 45 and 63% (Ahmad et al., 2018).

In Table VI.3, the antioxidant activities related to SAA powders (at t=0, i.e. time of powder preparation) were consistent with the corresponding

extracts. Indeed, the SA values related to powders obtained from aqueous extracts were higher than those measured from particles precipitated from ethanol extracts. However, the most relevant aspect to be considered was the SA reductions over time. After 3 months in a dry and dark place, it was verified a SA reduction ranged between 22 and 24% for powders produced from ethanol extracts and between 1 and 8% for powders produced from water:ethanol extracts (see Table VI.3). Values slightly higher were found for powders produced from the extracts at pH=2. An excellent result was obtained, since SA reductions were greatly reduced compared to the raw extracts results (see Table VI.1). Particularly, after 3 months, the SA values were practically confirmed for the coprecipitates produced from water:ethanol extracts, and reduced by 35% for raw saffron extracts.

Therefore, the incorporation of these glycosides into PVP matrix allowed stabilizing the active compounds since the polymer acts as a barrier against oxygen and small molecules promoting the shelf life of the loaded products. In particular, PVP has been demonstrated a carrier recommendable to enhance precipitate stability and integrity mainly starting from water:ethanol extracts. This fact can be probably due to the larger particle diameters and the more regular morphologies obtained using water:ethanol extract that proved to be the best starting solution to prepare stable coprecipitated particles using SAA process.

VI.1.4 Conclusions on extract-PVP systems

The process proposed in this work was effective for the protection of valuable compounds obtained from saffron residues by solid-liquid extractions. SAA product obtained was a dry powder formed by particles containing up to 100% of compounds extracted, using a water:ethanol mixture (41:59 v/v). An excellent result is that small quantities of PVP are enough to preserve their antioxidant activity over time; these results could be used as evidence of the effective protection role of PVP. After three months, the values of scavenging activity were practically confirmed for SAA coprecipitates and reduced by 35% for raw saffron extracts

Therefore, the SAA process was efficient in producing stable particles with remarkable antioxidant capacity, which can be applied in the food and nutraceutical industry.

Conclusions

The aim of this Ph.D. work was the development of new and stable formulations consisting of microparticles with improved bioavailability, using supercritical assisted processes for pharmaceutical and nutraceutical applications. The SAA process has revealed to be very efficient in the improvement of the bioavailability of several active principles, producing nano and microparticles of pure drugs and coprecipitates, as well as in the case some compounds to be difficultly processed by conventional methods.

The SAA process was successfully applied both in pharmaceutical and nutraceutical fields, demonstrating to be attractive and available from an industrial point of view.

In the framework of the pharmaceutical formulations, five drugs were investigated, as part of the agreement between Cerbios Pharma and the Department of Industrial Engineering (DIIN) of the University of Salerno. Differently from the conventional techniques, the SAA process was able to reach the specific targets requested by the Company. In particular, BRI, FUL and NAP were micronized alone, whereas DAS and GPB were dispersed in carrier matrices producing coprecipitates. This study eventually allowed obtaining the validation of the SAA industrial plant in the Cerbios Pharma facility of Lugano, and achieving the SwissMedic authorization for GMP production, on January 2017.

Selected carriers (PVP, DEX and HP β CD) demonstrated to be very able to produce well-separated and amorphous microspheres with diameters lower than 1.8 μm and high active principle loading efficiencies, up to 100% in most of the performed studies. In particular, they were very valuable in controlling the tendency of active principles to crystallize and agglomerate, by producing SAA particles stable over time. Dissolution tests confirmed that the produced composite particles showed drug dissolution rates much faster with respect to the corresponding physical mixtures, thus improving their bioavailability up to 12 times. In particular, the achieved results allow

concluding that the active principle/carrier weight ratio and the chemical interactions revealed to be controlling parameters for dissolution rate.

Definitely, the particle size reduction and the production of amorphous composite systems demonstrated to be crucial in achieving the Ph.D. goals using the SAA technique. The SAA amorphous formulations have proved to be homogeneous dispersions of a drug in a carrier matrix since each particle is the result of the fast drying of a droplet containing the two compounds. These SAA composite systems show higher dissolution rates: the water-soluble carrier fastly dissolves and releases the micronized drug molecules. The smaller drug particles show larger surface area to volume ratios thus obtaining higher interactions with the aqueous medium; whereas, the disordered arrangements, typical of an amorphous solid, lead to faster dissolutions since no energy is required to break up the crystal lattice. Therefore, the mutual influence of these two factors positively affects the final dissolution rates of the active principles. The success of the SAA technique in the stabilization of active principles is related to the ability to develop some one-phase amorphous solid dispersions, and to the interactions between active substance and carrier, mostly attributed to the formation of hydrogen bonding and the steric hindrance resulting from the kind of carrier structure.

Finally, the SAA technique revealed to be a reliable alternative to conventional processes also in the unexplored field of nutraceuticals. For the first time, SAA composite systems based on the dispersion in different carriers of bioactive compounds, such as carotenoids, polyphenols and flavonoids, were successfully produced. Defined, spherical and amorphous particles with high loading efficiencies up to 94-100% and with preserved antioxidant activity were obtained. Particularly, the study on saffron petals, normally considered as industrial wastes, demonstrated that SAA produced particles, using PVP as carrier, were able to preserve the antioxidant power over time. After three months, the antioxidant activity was confirmed for the SAA coprecipitates and reduced by 35% for crude saffron extracts. As an overall result, the antioxidant-rich particles produced can be used as source of natural antioxidants and for food supplements. Moreover, the suggested carriers allowed improving the handling of the product and simplifying its storage.

References

- ADAMI, R., DI CAPUA, A. & REVERCHON, E. 2017a. Supercritical Assisted Atomization for the production of curcumin-biopolymer microspheres. *Powder Technology*, 305, 455-461.
- ADAMI, R., LIPAROTI, S., DELLA PORTA, G., DEL GAUDIO, P. & REVERCHON, E. 2017b. Lincomycin hydrochloride loaded albumin microspheres for controlled drug release, produced by Supercritical Assisted Atomization. *The Journal of Supercritical Fluids*, 119, 203-210.
- ADAMI, R., LIPAROTI, S., DI CAPUA, A., SCOGNAMIGLIO, M. & REVERCHON, E. 2019. Production of PEA composite microparticles with polyvinylpyrrolidone and luteolin using Supercritical Assisted Atomization. *The Journal of Supercritical Fluids*, 143, 82-89.
- ADAMI, R., LIPAROTI, S., IZZO, L., PAPPALARDO, D. & REVERCHON, E. 2012. PLA-PEG copolymers micronization by supercritical assisted atomization. *The Journal of Supercritical Fluids*, 72, 15-21.
- ADAMI, R., LIPAROTI, S. & REVERCHON, E. 2011. A new supercritical assisted atomization configuration, for the micronization of thermolabile compounds. *Chemical Engineering Journal*, 173, 55-61.
- ADAMI, R., OSSEO, L. S. & REVERCHON, E. 2009. Micronization of lysozyme by supercritical assisted atomization. *Biotechnol Bioeng*, 104, 1162-70.
- ADAMI, R. & REVERCHON, E. 2012. Composite polymer-Fe₃O₄ microparticles for biomedical applications, produced by Supercritical Assisted Atomization. *Powder Technology*, 218, 102-108.
- ADAMI, R., SCHUSTER, J., LIPAROTI, S., REVERCHON, E., LEIPERTZ, A. & BRAEUER, A. 2013. A Raman spectroscopic method for the determination of high pressure vapour liquid equilibria. *Fluid Phase Equilibria*, 360, 265-273.
- ADEOYE, O., COSTA, C., CASIMIRO, T., AGUIAR-RICARDO, A. & CABRAL-MARQUES, H. 2018. Preparation of ibuprofen/hydroxypropyl- γ -cyclodextrin inclusion complexes using supercritical CO₂-assisted spray drying. *The Journal of Supercritical Fluids*, 133, 479-485.
- AHMAD, M., ASHRAF, B., GANI, A. & GANI, A. 2018. Microencapsulation of saffron anthocyanins using beta glucan and beta cyclodextrin: Microcapsule characterization, release behaviour & antioxidant potential during in-vitro digestion. *Int J Biol Macromol*, 109, 435-442.
- AHMADIAN-KOUCHAKSARAIE, Z. & NIAZMAND, R. 2017. Supercritical carbon dioxide extraction of antioxidants from Crocus

References

- sativus petals of saffron industry residues: Optimization using response surface methodology. *The Journal of Supercritical Fluids*, 121, 19-31.
- AHMADIAN-KOUCHAKSARAIE, Z., NIAZMAND, R. & NAJAF NAJAFI, M. 2016a. Optimization of extraction conditions of bioactive components from saffron petal using response surface method (RSM). *JRIFST*, 5, 39-54.
- AHMADIAN-KOUCHAKSARAIE, Z., NIAZMAND, R. & NAJAFI, M. N. 2016b. Optimization of the subcritical water extraction of phenolic antioxidants from *Crocus sativus* petals of saffron industry residues: Box-Behnken design and principal component analysis. *Innovative Food Science & Emerging Technologies*, 36, 234-244.
- AID, S., EDDHAHAK, A., ORTEGA, Z., FROELICH, D. & TCHARKHTCHI, A. 2017. Experimental study of the miscibility of ABS/PC polymer blends and investigation of the processing effect. *Journal of Applied Polymer Science*, 134.
- ALIAKBARIAN, B., PAINI, M., ADAMI, R., PEREGO, P. & REVERCHON, E. 2017. Use of Supercritical Assisted Atomization to produce nanoparticles from olive pomace extract. *Innovative Food Science & Emerging Technologies*, 40, 2-9.
- ALONZO, D. E., ZHANG, G. G. Z., ZHOU, D., GAO, Y. & TAYLOR, L. S. 2010. Understanding the Behavior of Amorphous Pharmaceutical Systems during Dissolution. *Pharmaceutical Research*, 27, 608-618.
- ALSHAMSAN, A. 2014. Nanoprecipitation is more efficient than emulsion solvent evaporation method to encapsulate cucurbitacin I in PLGA nanoparticles. *Saudi Pharm J*, 22, 219-22.
- AMIN, A. R. M. R., KUCUK, O., KHURI, F. R. & SHIN, D. M. 2009. Perspectives for Cancer Prevention With Natural Compounds. *Journal of Clinical Oncology*, 27, 2712-2725.
- AMIN, M., HUSSAIN, M. A., SHAHWAR, D. & HUSSAIN, M. 2015. Thermal Analysis and Degradation Kinetics of Dextran and Highly Substituted Dextran Acetates. *Journal of the Chemical Society of Pakistan*, 37, 673-679.
- ANDRESEN, S. R., BING, J., HANSEN, R. M., BIERING-SØRENSEN, F., JOHANNESSEN, I. L., HAGEN, E. M., RICE, A. S. C., NIELSEN, J. F., BACH, F. W. & FINNERUP, N. B. 2016. Ultramicronized palmitoylethanolamide in spinal cord injury neuropathic pain: a randomized, double-blind, placebo-controlled trial. *PAIN*, 157, 2097-2103.
- ANITHA, A., DEEPAGAN, V. G., DIVYA RANI, V. V., MENON, D., NAIR, S. V. & JAYAKUMAR, R. 2011. Preparation, characterization, in vitro drug release and biological studies of curcumin loaded dextran sulphate-chitosan nanoparticles. *Carbohydrate Polymers*, 84, 1158-1164.

- ANTONIOU, E., THEMISTOU, E., SARKAR, B., TSIANOU, M. & ALEXANDRIDIS, P. 2010. Structure and dynamics of dextran in binary mixtures of a good and a bad solvent. *Colloid and Polymer Science*, 288, 1301-1312.
- AQUINO, R. P., AURIEMMA, G., MENCHERINI, T., RUSSO, P., PORTA, A., ADAMI, R., LIPAROTI, S., DELLA PORTA, G., REVERCHON, E. & DEL GAUDIO, P. 2013. Design and production of gentamicin/dextran microparticles by supercritical assisted atomisation for the treatment of wound bacterial infections. *Int J Pharm*, 440, 188-94.
- BABAEI, A., ARSHAMI, J., HAGHPARAST, A. & DANESH MESGARAN, M. 2014. Effects of saffron (*Crocus sativus*) petal ethanolic extract on hematology, antibody response, and spleen histology in rats. *Avicenna Journal of Phytomedicine*, 4, 103-109.
- BAGHEL, S., CATHCART, H. & O'REILLY, N. J. 2016. Polymeric Amorphous Solid Dispersions: A Review of Amorphization, Crystallization, Stabilization, Solid-State Characterization, and Aqueous Solubilization of Biopharmaceutical Classification System Class II Drugs. *Journal of Pharmaceutical Sciences*, 105, 2527-2544.
- BALASUNDRAM, N., SUNDRAM, K. & SAMMAN, S. 2006. Phenolic compounds in plants and agri-industrial by-products: Antioxidant activity, occurrence, and potential uses. *Food Chemistry*, 99, 191-203.
- BALDINO, L., CARDEA, S., DE MARCO, I. & REVERCHON, E. 2014a. Chitosan scaffolds formation by a supercritical freeze extraction process. *The Journal of Supercritical Fluids*, 90, 27-34.
- BALDINO, L., CARDEA, S. & REVERCHON, E. 2014b. Supercritical assisted enzymatic membranes preparation, for active packaging applications. *Journal of Membrane Science*, 453, 409-418.
- BANSAL, S. S., GOEL, M., AQIL, F., VADHANAM, M. V. & GUPTA, R. C. 2011. Advanced drug delivery systems of curcumin for cancer chemoprevention. *Cancer Prev Res (Phila)*, 4, 1158-71.
- BEIG, A., MILLER, J. M. & DAHAN, A. 2013. The interaction of nifedipine with selected cyclodextrins and the subsequent solubility-permeability trade-off. *Eur J Pharm Biopharm*, 85, 1293-9.
- BETANCOURT, T., BROWN, B. & BRANNON-PEPPAS, L. 2007. Doxorubicin-loaded PLGA nanoparticles by nanoprecipitation: preparation, characterization and in vitro evaluation. *Nanomedicine (Lond)*, 2, 219-32.
- BHAKAY, A., RAHMAN, M., DAVE, R. & BILGILI, E. 2018. Bioavailability Enhancement of Poorly Water-Soluble Drugs via Nanocomposites: Formulation-Processing Aspects and Challenges. *Pharmaceutics*, 10, 86.

References

- BISCAIA, D. & FERREIRA, S. R. S. 2009. Propolis extracts obtained by low pressure methods and supercritical fluid extraction. *The Journal of Supercritical Fluids*, 51, 17-23.
- BLAJOVAN, R. & MODRA, D. 2013. THE STUDY SYNTHESIS OF NIFEDIPINE-CALCIUM ANTAGONIST. *New Frontiers in Chemistry*, 22, 47.
- BRAND-WILLIAMS, W., CUVELIER, M. E. & BERSET, C. 1995. Use of a free radical method to evaluate antioxidant activity. *LWT - Food Science and Technology*, 28, 25-30.
- BREWSTER, M. E. & LOFTSSON, T. 2007. Cyclodextrins as pharmaceutical solubilizers. *Adv Drug Deliv Rev*, 59, 645-66.
- BRUSCHI, M. L., CARDOSO, M. L., LUCCHESI, M. B. & GREMIAO, M. P. 2003. Gelatin microparticles containing propolis obtained by spray-drying technique: preparation and characterization. *Int J Pharm*, 264, 45-55.
- BUSCH, V. M., PEREYRA-GONZALEZ, A., ŠEGATIN, N., SANTAGAPITA, P. R., POKLAR ULRIH, N. & BUERA, M. P. 2017. Propolis encapsulation by spray drying: Characterization and stability. *LWT*, 75, 227-235.
- CAI, M.-Q., GUAN, Y.-X., YAO, S.-J. & ZHU, Z.-Q. 2008. Supercritical fluid assisted atomization introduced by hydrodynamic cavitation mixer (SAA-HCM) for micronization of levofloxacin hydrochloride. *The Journal of Supercritical Fluids*, 43, 524-534.
- CAMPARDELLI, R., ADAMI, R. & REVERCHON, E. 2012. Preparation of Stable Aqueous Nanodispersions of β -Carotene by Supercritical Assisted Injection in a Liquid Antisolvent. *Procedia Engineering*, 42, 1493-1501.
- CAMPARDELLI, R., BALDINO, L. & REVERCHON, E. 2015. Supercritical fluids applications in nanomedicine. *The Journal of Supercritical Fluids*, 101, 193-214.
- CAPUTO, G., LIPAROTI, S., ADAMI, R. & REVERCHON, E. 2012. Use of Supercritical CO₂ and N₂ as Dissolved Gases for the Atomization of Ethanol and Water. *Industrial & Engineering Chemistry Research*, 51, 11803-11808.
- CAROCHO, M., MORALES, P. & FERREIRA, I. C. F. R. 2015. Natural food additives: Quo vadis? *Trends in Food Science & Technology*, 45, 284-295.
- CATCHPOLE, O. J., GREY, J. B., MITCHELL, K. A. & LAN, J. S. 2004. Supercritical antisolvent fractionation of propolis tincture. *The Journal of Supercritical Fluids*, 29, 97-106.
- CHAMPAGNE, C. P. & FUSTIER, P. 2007. Microencapsulation for the improved delivery of bioactive compounds into foods. *Current Opinion in Biotechnology*, 18, 184-190.

- CHAN, K. L. A., FLEMING, O. S., KAZARIAN, S. G., VASSOU, D., CHRYSSIKOS, G. D. & GIONIS, V. 2004. Polymorphism and devitrification of nifedipine under controlled humidity: a combined FT-Raman, IR and Raman microscopic investigation. *Journal of Raman Spectroscopy*, 35, 353-359.
- CHATTOPADHYAY, I., BISWAS, K., BANDYOPADHYAY, U. & BANERJEE, R. K. 2004. Turmeric and curcumin: Biological actions and medicinal applications. *Current Science*, 87, 44-53.
- CHEN, H., KHEMTONG, C., YANG, X., CHANG, X. & GAO, J. 2011. Nanonization strategies for poorly water-soluble drugs. *Drug Discov Today*, 16, 354-60.
- CHIOU, A. H.-J., CHENG, H.-C. & WANG, D.-P. 2006. Micronization and microencapsulation of felodipine by supercritical carbon dioxide. *Journal of Microencapsulation*, 23, 265-276.
- CHOW, S.-C. 2014. Bioavailability and Bioequivalence in Drug Development. *Wiley interdisciplinary reviews. Computational statistics*, 6, 304-312.
- CILURZO, F., MINGHETTI, P., CASIRAGHI, A. & MONTANARI, L. 2002. Characterization of nifedipine solid dispersions. *Int J Pharm*, 242, 313-7.
- COCERO, M. J., MARTÍN, Á., MATTEA, F. & VARONA, S. 2009. Encapsulation and co-precipitation processes with supercritical fluids: Fundamentals and applications. *The Journal of Supercritical Fluids*, 47, 546-555.
- CORONEL-AGUILERA, C. P. & SAN MARTÍN-GONZÁLEZ, M. F. 2015. Encapsulation of spray dried β -carotene emulsion by fluidized bed coating technology. *LWT - Food Science and Technology*, 62, 187-193.
- CORREDOR, C., TESLOVA, T., CAÑAMARES, M. V., CHEN, Z., ZHANG, J., LOMBARDI, J. R. & LEONA, M. 2009. Raman and surface-enhanced Raman spectra of chrysin, apigenin and luteolin. *Vibrational Spectroscopy*, 49, 190-195.
- DANG, H., MENG, M. H. W., ZHAO, H., IQBAL, J., DAI, R., DENG, Y. & LV, F. 2014. Luteolin-loaded solid lipid nanoparticles synthesis, characterization, & improvement of bioavailability, pharmacokinetics in vitro and vivo studies. *Journal of Nanoparticle Research*, 16, 2347.
- DE BELDER, A. N. & GRANATH, K. 1973. Preparation and properties of fluorescein-labelled dextrans. *Carbohydrate Research*, 30, 375-378.
- DE CICCO, F., REVERCHON, E., ADAMI, R., AURIEMMA, G., RUSSO, P., CALABRESE, E. C., PORTA, A., AQUINO, R. P. & DEL GAUDIO, P. 2014. In situ forming antibacterial dextran blend hydrogel for wound dressing: SAA technology vs. spray drying. *Carbohydr Polym*, 101, 1216-24.

References

- DE PAZ, E., MARTÍN, Á., DUARTE, C. M. M. & COCERO, M. J. 2012. Formulation of β -carotene with poly-(ϵ -caprolactones) by PGSS process. *Powder Technology*, 217, 77-83.
- DE SOUZA FERREIRA, S. B., DE ASSIS DIAS, B. R., OBREGON, C. S., GOMES, C. C., DE ARAUJO PEREIRA, R. R., RIBEIRO GODOY, J. S., ESTIVALET SVIDZINSKI, T. I. & BRUSCHI, M. L. 2014. Microparticles containing propolis and metronidazole: in vitro characterization, release study and antimicrobial activity against periodontal pathogens. *Pharm Dev Technol*, 19, 173-80.
- DE SOUZA SIMÕES, L., MADALENA, D. A., PINHEIRO, A. C., TEIXEIRA, J. A., VICENTE, A. A. & RAMOS, Ó. L. 2017. Micro- and nano bio-based delivery systems for food applications: In vitro behavior. *Advances in Colloid and Interface Science*, 243, 23-45.
- DE ZORDI, N., CORTESI, A., KIKIC, I., MONEGHINI, M., SOLINAS, D., INNOCENTI, G., PORTOLAN, A., BARATTO, G. & DALL'ACQUA, S. 2014. The supercritical carbon dioxide extraction of polyphenols from Propolis: A central composite design approach. *The Journal of Supercritical Fluids*, 95, 491-498.
- DELLA PORTA, G., ADAMI, R., DEL GAUDIO, P., PROTA, L., AQUINO, R. & REVERCHON, E. 2010. Albumin/gentamicin microspheres produced by supercritical assisted atomization: optimization of size, drug loading and release. *J Pharm Sci*, 99, 4720-9.
- DELLA PORTA, G., ERCOLINO, S. F., PARENTE, L. & REVERCHON, E. 2006. Corticosteroid Microparticles Produced by Supercritical-Assisted Atomization: Process Optimization, Product Characterization, and "in Vitro" Performance. *Journal of Pharmaceutical Sciences*, 95, 2062-2076.
- DESAI, K. G. H. & JIN PARK, H. 2005. Recent Developments in Microencapsulation of Food Ingredients. *Drying Technology*, 23, 1361-1394.
- DI CAPUA, A., ADAMI, R., COSENZA, E., JALABER, V., CRAMON, C., BADENS, E. & REVERCHON, E. 2019. β -Carotene/PVP microspheres produced by Supercritical Assisted Atomization. *Powder Technology*, 346 (2019), 228-236.
- DI CAPUA, A., ADAMI, R., IZZO, L. & REVERCHON, E. 2017a. Luteolin/dextran-FITC fluorescent microspheres produced by supercritical assisted atomization. *The Journal of Supercritical Fluids*, 130, 97-104.
- DI CAPUA, A., ADAMI, R. & REVERCHON, E. 2017b. Production of Luteolin/Biopolymer Microspheres by Supercritical Assisted Atomization. *Industrial & Engineering Chemistry Research*, 56, 4334-4340.
- DI CAPUA, A., BEJARANO, A., ADAMI, R. & REVERCHON, E. 2018. Preparation and characterization of Chilean propolis coprecipitates

- using Supercritical Assisted Atomization. *Chemical Engineering Research and Design*, 136, 776-785.
- DINUNZIO, J. C., MILLER, D. A., YANG, W., MCGINITY, J. W. & WILLIAMS, R. O. 2008. Amorphous Compositions Using Concentration Enhancing Polymers for Improved Bioavailability of Itraconazole. *Molecular Pharmaceutics*, 5, 968-980.
- DO NASCIMENTO, T. G., DA SILVA, P. F., AZEVEDO, L. F., DA ROCHA, L. G., DE MORAES PORTO, I. C., LIMA, E. M. T. F., BASILIO-JUNIOR, I. D., GRILLO, L. A., DORNELAS, C. B., FONSECA, E. J., DE JESUS OLIVEIRA, E., ZHANG, A. T. & WATSON, D. G. 2016. Polymeric Nanoparticles of Brazilian Red Propolis Extract: Preparation, Characterization, Antioxidant and Leishmanicidal Activity. *Nanoscale Res Lett*, 11, 301.
- DU, Z., TANG, C., GUAN, Y.-X., YAO, S.-J. & ZHU, Z.-Q. 2013. Bioactive insulin microparticles produced by supercritical fluid assisted atomization with an enhanced mixer. *International Journal of Pharmaceutics*, 454, 174-182.
- DVORAK, H. F., NAGY, J. A., DVORAK, J. T. & DVORAK, A. M. 1988. Identification and characterization of the blood vessels of solid tumors that are leaky to circulating macromolecules. *The American Journal of Pathology*, 133, 95-109.
- EMARA, L. H., BADR, R. M. & ELBARY, A. A. 2002. Improving the dissolution and bioavailability of nifedipine using solid dispersions and solubilizers. *Drug Dev Ind Pharm*, 28, 795-807.
- ESLAMIAN, M., AHMED, M. & ASHGRIZ, N. 2009. Modeling of Solution Droplet Evaporation and Particle Evolution in Droplet-to-Particle Spray Methods. *Drying Technology*, 27, 3-13.
- FAHIM, T. K., ZAIDUL, I. S. M., ABU BAKAR, M. R., SALIM, U. M., AWANG, M. B., SAHENA, F., JALAL, K. C. A., SHARIF, K. M. & SOHRAB, M. H. 2014. Particle formation and micronization using non-conventional techniques- review. *Chemical Engineering and Processing: Process Intensification*, 86, 47-52.
- FARAZUDDIN, M., DUA, B., ZIA, Q., KHAN, A. A., JOSHI, B. & OWAIS, M. 2014. Chemotherapeutic potential of curcumin-bearing microcells against hepatocellular carcinoma in model animals. *Int J Nanomedicine*, 9, 1139-52.
- FENG, X., LV, F., LIU, L., TANG, H., XING, C., YANG, Q. & WANG, S. 2010. Conjugated polymer nanoparticles for drug delivery and imaging. *ACS Appl Mater Interfaces*, 2, 2429-35.
- FIEDOR, J. & BURDA, K. 2014. Potential Role of Carotenoids as Antioxidants in Human Health and Disease. *Nutrients*, 6, 466-488.
- FRANCESCHI, E., DE CESARO, A. M., FEITEN, M., FERREIRA, S. R. S., DARIVA, C., KUNITA, M. H., RUBIRA, A. F., MUNIZ, E. C., CORAZZA, M. L. & OLIVEIRA, J. V. 2008. Precipitation of β -

References

- carotene and PHBV and co-precipitation from SEDS technique using supercritical CO₂. *The Journal of Supercritical Fluids*, 47, 259-269.
- FU, Q., MA, M., LI, M., WANG, G., GUO, M., LI, J., HOU, Y. & FANG, M. 2017. Improvement of oral bioavailability for nisoldipine using nanocrystals. *Powder Technology*, 305, 757-763.
- GORALCZYK, R. 2009. Beta-carotene and lung cancer in smokers: review of hypotheses and status of research. *Nutr Cancer*, 61, 767-74.
- GRUNE, T., LIETZ, G., PALOU, A., ROSS, A. C., STAHL, W., TANG, G., THURNHAM, D., YIN, S. A. & BIESALSKI, H. K. 2010. Beta-carotene is an important vitamin A source for humans. *J Nutr*, 140, 2268s-2285s.
- GUAMÁN-BALCÁZAR, M. C., MONTES, A., PEREYRA, C. & MARTÍNEZ DE LA OSSA, E. 2019. Production of submicron particles of the antioxidants of mango leaves/PVP by supercritical antisolvent extraction process. *The Journal of Supercritical Fluids*, 143, 294-304.
- GUL, K., TAK, A., SINGH, A. K., SINGH, P., YOUSUF, B. & WANI, A. A. 2015. Chemistry, encapsulation, and health benefits of β -carotene - A review. *Cogent Food & Agriculture*, 1, 1018696.
- GUPTA, S., KESARLA, R. & OMRI, A. 2013. Formulation Strategies to Improve the Bioavailability of Poorly Absorbed Drugs with Special Emphasis on Self-Emulsifying Systems. *ISRN Pharmaceutics*, 2013, 16.
- HADIZADEH, F., KHALILI, N., HOSSEINZADEH, H. & KHAIR-ALDINE, R. 2010. Kaempferol from Saffron Petals. *Iranian Journal of Pharmaceutical Research*, Volume 2, 251-252.
- HANCOCK, B. C. & PARKS, M. 2000. What is the True Solubility Advantage for Amorphous Pharmaceuticals? *Pharmaceutical Research*, 17, 397-404.
- HANDFORD, C. E., DEAN, M., HENCHION, M., SPENCE, M., ELLIOTT, C. T. & CAMPBELL, K. 2014. Implications of nanotechnology for the agri-food industry: Opportunities, benefits and risks. *Trends in Food Science & Technology*, 40, 226-241.
- HAR BHAJAN, S. & BHARATI, K. A. 2014. 6 - Enumeration of dyes. In: HAR BHAJAN, S. & BHARATI, K. A. (eds.) *Handbook of Natural Dyes and Pigments*. Woodhead Publishing India.
- HE, W., SUO, Q., HONG, H., SHAN, A., LI, C., HUANG, Y., LI, Y. & ZHU, M. 2007. Production of natural carotene-dispersed polymer microparticles by SEDS-PA co-precipitation. *Journal of Materials Science*, 42, 3495-3501.
- HIJAZI, N., RODIER, E., LETOURNEAU, J.-J., LOUATI, H., SAUCEAU, M., LE MOIGNE, N., BENEZET, J.-C. & FAGES, J. 2014. Chitosan nanoparticles generation using CO₂ assisted processes. *The Journal of Supercritical Fluids*, 95, 118-128.
- HOYER, H., SCHLOCKER, W., KRUM, K. & BERNKOP-SCHNÜRCH, A. 2008. Preparation and evaluation of microparticles from thiolated

- polymers via air jet milling. *European Journal of Pharmaceutics and Biopharmaceutics*, 69, 476-485.
- HUANG, Q., YU, H. & RU, Q. 2010. Bioavailability and Delivery of Nutraceuticals Using Nanotechnology. *Journal of Food Science*, 75, R50-R57.
- IMPELLIZZERI, D., BRUSCHETTA, G., CORDARO, M., CRUPI, R., SIRACUSA, R., ESPOSITO, E. & CUZZOCREA, S. 2014. Micronized/ultramicronized palmitoylethanolamide displays superior oral efficacy compared to nonmicronized palmitoylethanolamide in a rat model of inflammatory pain. *J Neuroinflammation*, 11, 136.
- IMPELLIZZERI, D., CAMPOLO, M., DI PAOLA, R., BRUSCHETTA, G., DE STEFANO, D., ESPOSITO, E. & CUZZOCREA, S. 2015. Ultramicronized palmitoylethanolamide reduces inflammation in a Th1-mediated model of colitis. *European Journal of Inflammation*, 13, 14-31.
- ISHWARYA, S. P., ANANDHARAMAKRISHNAN, C. & STAPLEY, A. G. F. 2015. Spray-freeze-drying: A novel process for the drying of foods and bioproducts. *Trends in Food Science & Technology*, 41, 161-181.
- JAGDALE, S. C., JADHAV, V. N., CHABUKSWAR, A. R. & KUCHEKAR, B. S. 2012. Solubility enhancement, physicochemical characterization and formulation of fast-dissolving tablet of nifedipine- β -cyclodextrin complexes. *Brazilian Journal of Pharmaceutical Sciences*, 48, 131-145.
- JAIN, P. & BANGA, A. K. 2010. Inhibition of crystallization in drug-in-adhesive-type transdermal patches. *International Journal of Pharmaceutics*, 394, 68-74.
- JANISZEWSKA-TURAK, E. 2017. Carotenoids microencapsulation by spray drying method and supercritical micronization. *Food Res Int*, 99, 891-901.
- JOYE, I. J., DAVIDOV-PARDO, G. & MCCLEMENTS, D. J. 2014. Nanotechnology for increased micronutrient bioavailability. *Trends in Food Science & Technology*, 40, 168-182.
- JOYE, I. J. & MCCLEMENTS, D. J. 2013. Production of nanoparticles by anti-solvent precipitation for use in food systems. *Trends in Food Science & Technology*, 34, 109-123.
- JUN, S. W., KIM, M.-S., KIM, J.-S., PARK, H. J., LEE, S., WOO, J.-S. & HWANG, S.-J. 2007. Preparation and characterization of simvastatin/hydroxypropyl- β -cyclodextrin inclusion complex using supercritical antisolvent (SAS) process. *European Journal of Pharmaceutics and Biopharmaceutics*, 66, 413-421.
- JUNYAPRASERT, V. B. & MORAKUL, B. 2015. Nanocrystals for enhancement of oral bioavailability of poorly water-soluble drugs. *Asian Journal of Pharmaceutical Sciences*, 10, 13-23.

References

- KAKRAN, M., SAHOO, N. G., TAN, I.-L. & LI, L. 2012. Preparation of nanoparticles of poorly water-soluble antioxidant curcumin by antisolvent precipitation methods. *Journal of Nanoparticle Research*, 14, 757.
- KALEPU, S. & NEKKANTI, V. 2015. Insoluble drug delivery strategies: review of recent advances and business prospects. *Acta Pharmaceutica Sinica B*, 5, 442-453.
- KALOGEROPOULOS, N., KONTELES, S., MOURTZINOS, I., TROULLIDOU, E., CHIOU, A. & KARATHANOS, V. T. 2009. Encapsulation of complex extracts in beta-cyclodextrin: an application to propolis ethanolic extract. *J Microencapsul*, 26, 603-13.
- KAMADA, H., TSUTSUMI, Y., YAMAMOTO, Y., KIHARA, T., KANEDA, Y., MU, Y., KODAIRA, H., TSUNODA, S. I., NAKAGAWA, S. & MAYUMI, T. 2000. Antitumor activity of tumor necrosis factor-alpha conjugated with polyvinylpyrrolidone on solid tumors in mice. *Cancer Res*, 60, 6416-20.
- KANAZE, F. I., KOKKALOU, E., NIOPAS, I., BARMPALEXIS, P., GEORGARAKIS, E. & BIKIARIS, D. 2010. Dissolution rate and stability study of flavanone aglycones, naringenin and hesperetin, by drug delivery systems based on polyvinylpyrrolidone (PVP) nanodispersions. *Drug Dev Ind Pharm*, 36, 292-301.
- KAWABATA, Y., WADA, K., NAKATANI, M., YAMADA, S. & ONOUE, S. 2011. Formulation design for poorly water-soluble drugs based on biopharmaceutics classification system: Basic approaches and practical applications. *International Journal of Pharmaceutics*, 420, 1-10.
- KHADKA, P., RO, J., KIM, H., KIM, I., KIM, J. T., KIM, H., CHO, J. M., YUN, G. & LEE, J. 2014. Pharmaceutical particle technologies: An approach to improve drug solubility, dissolution and bioavailability. *Asian Journal of Pharmaceutical Sciences*, 9, 304-316.
- KHAN, J., ALEXANDER, A., AJAZUDDIN, SARAF, S. & SARAF, S. 2014. Luteolin-phospholipid complex: preparation, characterization and biological evaluation. *J Pharm Pharmacol*, 66, 1451-62.
- KHAN, W. H. & RATHOD, V. K. 2014. Process intensification approach for preparation of curcumin nanoparticles via solvent-nonsolvent nanoprecipitation using spinning disc reactor. *Chemical Engineering and Processing: Process Intensification*, 80, 1-10.
- KHAZAEI, K. M., JAFARI, S. M., GHORBANI, M., KAKHKI, A. H. & SARFARAZI, M. 2016. Optimization of Anthocyanin Extraction from Saffron Petals with Response Surface Methodology. *Food Analytical Methods*, 9, 1993-2001.
- KHURSHID, Z., NASEEM, M., ZAFAR, M. S., NAJEEB, S. & ZOHAIB, S. 2017. Propolis: A natural biomaterial for dental and oral healthcare.

- Journal of Dental Research, Dental Clinics, Dental Prospects*, 11, 265-274.
- KOGERMANN, K., PENKINA, A., PREDBANNIKOVA, K., JEEGER, K., VESKI, P., RANTANEN, J. & NAELAPÄÄ, K. 2013. Dissolution testing of amorphous solid dispersions. *International Journal of Pharmaceutics*, 444, 40-46.
- KRAUSZ, A. E., ADLER, B. L., CABRAL, V., NAVATI, M., DOERNER, J., CHARAFEDDINE, R. A., CHANDRA, D., LIANG, H., GUNTHER, L., CLENDANIEL, A., HARPER, S., FRIEDMAN, J. M., NOSANCHUK, J. D. & FRIEDMAN, A. J. 2015. Curcumin-encapsulated nanoparticles as innovative antimicrobial and wound healing agent. *Nanomedicine*, 11, 195-206.
- KROL, W., BANKOVA, V., SFORCIN, J. M., SZLISZKA, E., CZUBA, Z. & KUROPATNICKI, A. K. 2013. Propolis: properties, application, and its potential. *Evid Based Complement Alternat Med*, 2013, 807578.
- LABUSCHAGNE, P. W., ADAMI, R., LIPAROTI, S., NAIDOO, S., SWAI, H. & REVERCHON, E. 2014. Preparation of rifampicin/poly(D,L-lactide) nanoparticles for sustained release by supercritical assisted atomization technique. *The Journal of Supercritical Fluids*, 95, 106-117.
- LAFKA, T.-I., SINANOGLU, V. & LAZOS, E. S. 2007. On the extraction and antioxidant activity of phenolic compounds from winery wastes. *Food Chemistry*, 104, 1206-1214.
- LAOT, C. M., MARAND, E. & OYAMA, H. T. 1999. Spectroscopic characterization of molecular interdiffusion at a poly(vinyl pyrrolidone)/vinyl ester interface. *Polymer*, 40, 1095-1108.
- LEE, S. Y., YU, G. & KIM, I. W. 2013. Effects of Polymeric Additives on the Crystallization and Release Behavior of Amorphous Ibuprofen. *Journal of Nanomaterials*, 2013, 7.
- LEVY, G. & NELSON, E. 1961. United States Pharmacopeia and National Formulary standards, Food and Drug Administration regulations, and the quality of drugs. *N Y State J Med*, 61, 4003-8.
- LIN, S. Y., HSU, C. H. & SHEU, M. T. 2010. Curve-fitting FTIR studies of loratadine/hydroxypropyl-beta-cyclodextrin inclusion complex induced by co-grinding process. *J Pharm Biomed Anal*, 53, 799-803.
- LIN, Y., SHI, R., WANG, X. & SHEN, H. M. 2008. Luteolin, a flavonoid with potential for cancer prevention and therapy. *Curr Cancer Drug Targets*, 8, 634-46.
- LIPAROTI, S., ADAMI, R., CAPUTO, G. & REVERCHON, E. 2013. Supercritical Assisted Atomization: Polyvinylpyrrolidone as Carrier for Drugs with Poor Solubility in Water. *Journal of Chemistry*, 2013, 5.
- LIPAROTI, S., ADAMI, R. & REVERCHON, E. 2012. PEG micronization by supercritical assisted atomization, operated under reduced pressure. *The Journal of Supercritical Fluids*, 72, 46-51.

References

- LIPAROTI, S., ADAMI, R. & REVERCHON, E. 2015. Supercritical Assisted Atomization: effect of operative conditions on PVP microparticle size and morphology. *The Journal of Supercritical Fluids*, 97, 31-35.
- LIPINSKI, C. A., LOMBARDO, F., DOMINY, B. W. & FEENEY, P. J. 2001. Experimental and computational approaches to estimate solubility and permeability in drug discovery and development settings. Original article: S0169-409X(96)00423-1. The article was originally published in *Advanced Drug Delivery Reviews* 23 (1997) 3–25. *Advanced Drug Delivery Reviews*, 46, 3-26.
- LOH, Z. H., SAMANTA, A. K. & SIA HENG, P. W. 2015. Overview of milling techniques for improving the solubility of poorly water-soluble drugs. *Asian Journal of Pharmaceutical Sciences*, 10, 255-274.
- LOKSUWAN, J. 2007. Characteristics of microencapsulated β -carotene formed by spray drying with modified tapioca starch, native tapioca starch and maltodextrin. *Food Hydrocolloids*, 21, 928-935.
- LOTFI, L., KALBASI-ASHTARI, A., HAMED, M. & GHORBANI, F. 2015. Effects of sulfur water extraction on anthocyanins properties of tepals in flower of saffron (*Crocus sativus* L.). *Journal of Food Science and Technology*, 52, 813-821.
- LOTITO, S. B. & FREI, B. 2004. Relevance of apple polyphenols as antioxidants in human plasma: contrasting in vitro and in vivo effects. *Free Radical Biology and Medicine*, 36, 201-211.
- MACHADO, A. P. D. F., RUEDA, M., BARBERO, G. F., MARTÍN, Á., COCERO, M. J. & MARTÍNEZ, J. 2018. Co-precipitation of anthocyanins of the extract obtained from blackberry residues by pressurized antisolvent process. *The Journal of Supercritical Fluids*, 137, 81-92.
- MACHADO, B. A., BARRETO GDE, A., COSTA, A. S., COSTA, S. S., SILVA, R. P., DA SILVA, D. F., BRANDAO, H. N., DA ROCHA, J. L., NUNES, S. B., UMSZA-GUEZ, M. A. & PADILHA, F. F. 2015. Determination of Parameters for the Supercritical Extraction of Antioxidant Compounds from Green Propolis Using Carbon Dioxide and Ethanol as Co-Solvent. *PLoS One*, 10, e0134489.
- MAHDAVEE KHAZAEI, K., JAFARI, S. M., GHORBANI, M. & HEMMATI KAKHKI, A. 2014. Application of maltodextrin and gum Arabic in microencapsulation of saffron petal's anthocyanins and evaluating their storage stability and color. *Carbohydrate Polymers*, 105, 57-62.
- MARTÍN, A. & COCERO, M. J. 2008. Micronization processes with supercritical fluids: Fundamentals and mechanisms. *Advanced Drug Delivery Reviews*, 60, 339-350.
- MARTIN, L., LIPAROTI, S., DELLA PORTA, G., ADAMI, R., MARQUÉS, J. L., URIETA, J. S., MAINAR, A. M. & REVERCHON,

- E. 2013. Rotenone coprecipitation with biodegradable polymers by supercritical assisted atomization. *The Journal of Supercritical Fluids*, 81, 48-54.
- MARTINS, R. M., PEREIRA, S. V., SIQUEIRA, S., SALOMÃO, W. F. & FREITAS, L. A. P. 2013. Curcuminoid content and antioxidant activity in spray dried microparticles containing turmeric extract. *Food Research International*, 50, 657-663.
- MATTEA, F., MARTÍN, Á., MATÍAS-GAGO, A. & COCERO, M. J. 2009. Supercritical antisolvent precipitation from an emulsion: β -Carotene nanoparticle formation. *The Journal of Supercritical Fluids*, 51, 238-247.
- MEHVAR, R. 2000. Dextrans for targeted and sustained delivery of therapeutic and imaging agents. *J Control Release*, 69, 1-25.
- MELLA, M., MOLLICA, L. & IZZO, L. 2015. Influence of charged intramolecular hydrogen bonds in weak polyelectrolytes: A Monte Carlo study of flexible and extendible polymeric chains in solution and near charged spheres. *Journal of Polymer Science Part B: Polymer Physics*, 53, 650-663.
- MENESES, M. A., CAPUTO, G., SCOGNAMIGLIO, M., REVERCHON, E. & ADAMI, R. 2015. Antioxidant phenolic compounds recovery from *Mangifera indica* L. by-products by supercritical antisolvent extraction. *Journal of Food Engineering*, 163, 45-53.
- MERISKO-LIVERSIDGE, E. & LIVERSIDGE, G. G. 2011. Nanosizing for oral and parenteral drug delivery: a perspective on formulating poorly-water soluble compounds using wet media milling technology. *Adv Drug Deliv Rev*, 63, 427-40.
- MEZHERICHER, M., LEVY, A. & BORDE, I. 2007. Theoretical Drying Model of Single Droplets Containing Insoluble or Dissolved Solids. *Drying Technology*, 25, 1025-1032.
- MISHRA, R. K., DATT, M. & BANTHIA, A. K. 2008. Synthesis and Characterization of Pectin/PVP Hydrogel Membranes for Drug Delivery System. *AAPS PharmSciTech*, 9, 395-403.
- MOSHARRAF, M. & NYSTRÖM, C. 1995. The effect of particle size and shape on the surface specific dissolution rate of microsized practically insoluble drugs. *International Journal of Pharmaceutics*, 122, 35-47.
- MURTHY, P. S. & NAIDU, M. M. 2012. Recovery of Phenolic Antioxidants and Functional Compounds from Coffee Industry By-Products. *Food and Bioprocess Technology*, 5, 897-903.
- NEUHOUSER, M. L. 2004. Dietary flavonoids and cancer risk: evidence from human population studies. *Nutr Cancer*, 50, 1-7.
- NEWMAN, A., KNIPP, G. & ZOGRAFI, G. 2012. Assessing the performance of amorphous solid dispersions. *Journal of Pharmaceutical Sciences*, 101, 1355-1377.

References

- NORI, M. P., FAVARO-TRINDADE, C. S., MATIAS DE ALENCAR, S., THOMAZINI, M., DE CAMARGO BALIEIRO, J. C. & CONTRERAS CASTILLO, C. J. 2011. Microencapsulation of propolis extract by complex coacervation. *LWT - Food Science and Technology*, 44, 429-435.
- NYKAMP, G., CARSTENSEN, U. & MÜLLER, B. W. 2002. Jet milling—a new technique for microparticle preparation. *International Journal of Pharmaceutics*, 242, 79-86.
- O'DONNELL, P. B. & MCGINITY, J. W. 1997. Preparation of microspheres by the solvent evaporation technique. *Advanced Drug Delivery Reviews*, 28, 25-42.
- PACHECO, C., MAGALHÃES, R., FONSECA, M., SILVEIRA, P. & BRANDÃO, I. 2016. Accidental intoxication by dichloromethane at work place: Clinical case and literature review. *Journal of Acute Medicine*, 6, 43-45.
- PARADKAR, A., AMBIKE, A. A., JADHAV, B. K. & MAHADIK, K. R. 2004. Characterization of curcumin–PVP solid dispersion obtained by spray drying. *International Journal of Pharmaceutics*, 271, 281-286.
- PATRA, D. & SLEEM, F. 2013. A new method for pH triggered curcumin release by applying poly(L-lysine) mediated nanoparticle-congregation. *Anal Chim Acta*, 795, 60-8.
- PAVIANI, L. C., SAITO, E., DARIVA, C., MARCUCCI, M. C., SÁNCHEZ-CAMARGO, A. P. & CABRAL, F. A. 2012. Supercritical CO₂ extraction of raw propolis and its dry ethanolic extract. *Brazilian Journal of Chemical Engineering*, 29, 243-251.
- PEDRO, A. S., VILLA, S. D., CALICETI, P., MELO, S. A. B. V. D., ALBUQUERQUE, E. C., BERTUCCO, A. & SALMASO, S. 2016. Curcumin-loaded solid lipid particles by PGSS technology. *The Journal of Supercritical Fluids*, 107, 534-541.
- PETROSINO, S., SCHIANO MORIELLO, A., CERRATO, S., FUSCO, M., PUIGDEMONT, A., DE PETROCELLIS, L. & DI MARZO, V. 2016. The anti-inflammatory mediator palmitoylethanolamide enhances the levels of 2-arachidonoyl-glycerol and potentiates its actions at TRPV1 cation channels. *British Journal of Pharmacology*, 173, 1154-1162.
- PIQUER, J., LLÁCER, J. L., ROVIRA, V., RIESGO, P., RODRIGUEZ, R. & CREMADES, A. 2014. Fluorescence-Guided Surgery and Biopsy in Gliomas with an Exoscope System. *BioMed Research International*, 2014, 6.
- PRIAMO, W. L., DE CEZARO, A. M., BENETTI, S. C., OLIVEIRA, J. V. & FERREIRA, S. R. S. 2011. In vitro release profiles of β -carotene encapsulated in PHBV by means of supercritical carbon dioxide micronization technique. *The Journal of Supercritical Fluids*, 56, 137-143.

- PROCHÁZKOVÁ, D., BOUŠOVÁ, I. & WILHELMOVÁ, N. 2011. Antioxidant and prooxidant properties of flavonoids. *Fitoterapia*, 82, 513-523.
- PROSAPIO, V., REVERCHON, E. & DE MARCO, I. 2015. Coprecipitation of Polyvinylpyrrolidone/ β -Carotene by Supercritical Antisolvent Processing. *Industrial & Engineering Chemistry Research*, 54, 11568-11575.
- PUHL, A. C., FAGUNDES, M., DOS SANTOS, K. C., POLIKARPOV, I., DA SILVA, M. F. D. G. F., FERNANDES, J. B., VIEIRA, P. C. & FORIM, M. R. 2012. Preparation and characterization of polymeric nanoparticles loaded with the flavonoid luteolin, by using factorial design. *2012*, 3, 16.
- PULIGUNDLA, P., MOK, C., KO, S., LIANG, J. & RECHARLA, N. 2017. Nanotechnological approaches to enhance the bioavailability and therapeutic efficacy of green tea polyphenols. *Journal of Functional Foods*, 34, 139-151.
- PURAMA, R. K., GOSWAMI, P., KHAN, A. T. & GOYAL, A. 2009. Structural analysis and properties of dextran produced by *Leuconostoc mesenteroides* NRRL B-640. *Carbohydrate Polymers*, 76, 30-35.
- RAHMAN, S. M. H., TELNY, T. C., RAVI, T. K. & KUPPUSAMY, S. 2009. Role of Surfactant and pH in Dissolution of Curcumin. *Indian Journal of Pharmaceutical Sciences*, 71, 139-142.
- RECHARLA, N., RIAZ, M., KO, S. & PARK, S. 2017. Novel technologies to enhance solubility of food-derived bioactive compounds: A review. *Journal of Functional Foods*, 39, 63-73.
- REKSAMUNANDAR, R. P., EDIKRESNHA, D., MUNIR, M. M., DAMAYANTI, S. & KHAIRURRIJAL 2017. Encapsulation of β -carotene in poly(vinylpyrrolidone) (PVP) by Electrospinning Technique. *Procedia Engineering*, 170, 19-23.
- REVERCHON, E. 2002. Supercritical-Assisted Atomization To Produce Micro- and/or Nanoparticles of Controlled Size and Distribution. *Industrial & Engineering Chemistry Research*, 41, 2405-2411.
- REVERCHON, E. & ADAMI, R. 2006. Nanomaterials and supercritical fluids. *The Journal of Supercritical Fluids*, 37, 1-22.
- REVERCHON, E. & ADAMI, R. 2013. Supercritical assisted atomization to produce nanostructured chitosan-hydroxyapatite microparticles for biomedical application. *Powder Technology*, 246, 441-447.
- REVERCHON, E., ADAMI, R., CAMPARDELLI, R., DELLA PORTA, G., DE MARCO, I. & SCOGNAMIGLIO, M. 2015. Supercritical fluids based techniques to process pharmaceutical products difficult to micronize: Palmitoylethanolamide. *The Journal of Supercritical Fluids*, 102, 24-31.

References

- REVERCHON, E., ADAMI, R. & CAPUTO, G. 2007. Production of cromolyn sodium microparticles for aerosol delivery by supercritical assisted atomization. *AAPS PharmSciTech*, 8, E114-E114.
- REVERCHON, E., ADAMI, R., CARDEA, S. & PORTA, G. D. 2009. Supercritical fluids processing of polymers for pharmaceutical and medical applications. *The Journal of Supercritical Fluids*, 47, 484-492.
- REVERCHON, E., ADAMI, R., MARCO, I. D., LAUDANI, C. G. & SPADA, A. 2005. Pigment Red 60 micronization using supercritical fluids based techniques. *The Journal of Supercritical Fluids*, 35, 76-82.
- REVERCHON, E., ADAMI, R., SCOGNAMIGLIO, M., FORTUNATO, G. & DELLA PORTA, G. 2010. Beclomethasone Microparticles for Wet Inhalation, Produced by Supercritical Assisted Atomization. *Industrial & Engineering Chemistry Research*, 49, 12747-12755.
- REVERCHON, E. & ANTONACCI, A. 2006a. Chitosan Microparticles Production by Supercritical Fluid Processing. *Industrial & Engineering Chemistry Research*, 45, 5722-5728.
- REVERCHON, E. & ANTONACCI, A. 2006b. Cyclodextrins micrometric powders obtained by supercritical fluid processing. *Biotechnol Bioeng*, 94, 753-61.
- REVERCHON, E. & ANTONACCI, A. 2007a. Drug-polymer microparticles produced by supercritical assisted atomization. *Biotechnology and Bioengineering*, 97, 1626-1637.
- REVERCHON, E. & ANTONACCI, A. 2007b. Polymer microparticles production by supercritical assisted atomization. *The Journal of Supercritical Fluids*, 39, 444-452.
- REVERCHON, E. & DE MARCO, I. 2011. Mechanisms controlling supercritical antisolvent precipitate morphology. *Chemical Engineering Journal*, 169, 358-370.
- REVERCHON, E. & DELLA PORTA, G. 2003. Micronization of antibiotics by supercritical assisted atomization. *The Journal of Supercritical Fluids*, 26, 243-252.
- REVERCHON, E., DELLA PORTA, G., SPADA, A. & ANTONACCI, A. 2004. Griseofulvin micronization and dissolution rate improvement by supercritical assisted atomization. *J Pharm Pharmacol*, 56, 1379-87.
- REVERCHON, E., LAMBERTI, G. & ANTONACCI, A. 2008. Supercritical fluid assisted production of HPMC composite microparticles. *The Journal of Supercritical Fluids*, 46, 185-196.
- REVERCHON, E., PORTA, G. D. & SPADA, A. 2003. Ampicillin micronization by supercritical assisted atomization. *Journal of Pharmacy and Pharmacology*, 55, 1465-1471.
- REVERCHON, E. & SPADA, A. 2004a. Crystalline Microparticles of Controlled Size Produced by Supercritical-Assisted Atomization. *Industrial & Engineering Chemistry Research*, 43, 1460-1465.

- REVERCHON, E. & SPADA, A. 2004b. Erythromycin micro-particles produced by supercritical fluid atomization. *Powder Technology*, 141, 100-108.
- RIGHI, V., PARENTI, F., TUGNOLI, V., SCHENETTI, L. & MUCCI, A. 2015. Crocus sativus Petals: Waste or Valuable Resource? The Answer of High-Resolution and High-Resolution Magic Angle Spinning Nuclear Magnetic Resonance. *J Agric Food Chem*, 63, 8439-44.
- ROCHA, B. A., RODRIGUES, M. R., BUENO, P. C. P., DE MELLO COSTA-MACHADO, A. R., DE OLIVEIRA LIMA LEITE VAZ, M. M., NASCIMENTO, A. P., BARUD, H. S. & BERRETTA-SILVA, A. A. 2012. Preparation and thermal characterization of inclusion complex of Brazilian green propolis and hydroxypropyl- β -cyclodextrin. *Journal of Thermal Analysis and Calorimetry*, 108, 87-94.
- RODRIGUEZ-ALLER, M., GUILLARME, D., VEUTHEY, J.-L. & GURNY, R. 2015. Strategies for formulating and delivering poorly water-soluble drugs. *Journal of Drug Delivery Science and Technology*, 30, 342-351.
- RUSSO, A., CARDILE, V., SANCHEZ, F., TRONCOSO, N., VANELLA, A. & GARBARINO, J. A. 2004. Chilean propolis: antioxidant activity and antiproliferative action in human tumor cell lines. *Life Sci*, 76, 545-58.
- SAGNELLA, S. M., DUONG, H., MACMILLAN, A., BOYER, C., WHAN, R., MCCARROLL, J. A., DAVIS, T. P. & KAVALLARIS, M. 2014. Dextran-Based Doxorubicin Nanocarriers with Improved Tumor Penetration. *Biomacromolecules*, 15, 262-275.
- SARAVANAKUMAR, G., JO, D. G. & PARK, J. H. 2012. Polysaccharide-based nanoparticles: a versatile platform for drug delivery and biomedical imaging. *Curr Med Chem*, 19, 3212-29.
- SARDAS, S. 2003. The Role of Antioxidants in Cancer Prevention and Treatment. *Indoor and Built Environment*, 12, 401-404.
- SAVJANI, K. T., GAJJAR, A. K. & SAVJANI, J. K. 2012. Drug Solubility: Importance and Enhancement Techniques. *ISRN Pharmaceutics*, 2012, 10.
- SCHIFILLITI, C., CUCINOTTA, L., FEDELE, V., INGEGNOSI, C., LUCA, S. & LEOTTA, C. 2014. Micronized Palmitoylethanolamide Reduces the Symptoms of Neuropathic Pain in Diabetic Patients. *Pain Research and Treatment*, 2014, 849623.
- SCHLOSSER, P. M., BALE, A. S., GIBBONS, C. F., WILKINS, A. & COOPER, G. S. 2015. Human Health Effects of Dichloromethane: Key Findings and Scientific Issues. *Environmental Health Perspectives*, 123, 114-119.
- SEKIKAWA, H., NAKANO, M. & ARITA, T. 1978. Inhibitory Effect of Polyvinylpyrrolidone on the Crystallization of Drugs. *CHEMICAL & PHARMACEUTICAL BULLETIN*, 26, 118-126.

References

- SERRANO-DÍAZ, J., SÁNCHEZ, A. M., ALVARRUIZ, A. & ALONSO, G. L. 2013. Preservation of saffron floral bio-residues by hot air convection. *Food chemistry*, 141, 1536-1543.
- SHARMA, M., SHARMA, R. & JAIN, D. K. 2016. Nanotechnology Based Approaches for Enhancing Oral Bioavailability of Poorly Water Soluble Antihypertensive Drugs. *Scientifica (Cairo)*, 2016, 8525679.
- SHEN, L. & JI, H. F. 2012. The pharmacology of curcumin: is it the degradation products? *Trends Mol Med*, 18, 138-44.
- SHEN, Y.-B., DU, Z., WANG, Q., GUAN, Y.-X. & YAO, S.-J. 2014. Preparation of chitosan microparticles with diverse molecular weights using supercritical fluid assisted atomization introduced by hydrodynamic cavitation mixer. *Powder Technology*, 254, 416-424.
- SHEN, Y.-B., GUAN, Y.-X. & YAO, S.-J. 2015. Supercritical fluid assisted production of micrometric powders of the labile trypsin and chitosan/trypsin composite microparticles. *International Journal of Pharmaceutics*, 489, 226-236.
- SIGFRIDSSON, K., LUNDQVIST, A. J. & STRIMFORS, M. 2009. Particle size reduction for improvement of oral absorption of the poorly soluble drug UG558 in rats during early development. *Drug Dev Ind Pharm*, 35, 1479-86.
- SINGLETON, V. L. & ROSSI, J. A. 1965. Colorimetry of Total Phenolics with Phosphomolybdic-Phosphotungstic Acid Reagents. *American Journal of Enology and Viticulture*, 16, 144-158.
- SINHA, S., ALI, M., BABOOTA, S., AHUJA, A., KUMAR, A. & ALI, J. 2010. Solid dispersion as an approach for bioavailability enhancement of poorly water-soluble drug ritonavir. *AAPS PharmSciTech*, 11, 518-527.
- SKAPER, S. D., FACCI, L., FUSCO, M., DELLA VALLE, M. F., ZUSSO, M., COSTA, B. & GIUSTI, P. 2014. Palmitoylethanolamide, a naturally occurring disease-modifying agent in neuropathic pain. *Inflammopharmacology*, 22, 79-94.
- SOULAIROL, I., TARLIER, N., BATAILLE, B., CACCIAGUERRA, T. & SHARKAWI, T. 2015. Spray-dried solid dispersions of nifedipine and vinylcaprolactam/vinylacetate/PEG6000 for compacted oral formulations. *International Journal of Pharmaceutics*, 481, 140-147.
- SRIAMORNSAK, P., KONTHONG, S., LIMMATVAPIRAT, S. & SUTTIRUENGWONG, S. 2016. Dissolution improvement by solid dispersions composed of nifedipine, Eudragit® E and silica from rice husk. *Asian Journal of Pharmaceutical Sciences*, 11, 195-196.
- STELLA, V. J. & HE, Q. 2008. Cyclodextrins. *Toxicol Pathol*, 36, 30-42.
- STENEKES, R. J. H., TALSMA, H. & HENNINK, W. E. 2001. Formation of dextran hydrogels by crystallization. *Biomaterials*, 22, 1891-1898.

- SULAIMAN, G. M. 2015. In vitro study of molecular structure and cytotoxicity effect of luteolin in the human colon carcinoma cells. *European Food Research and Technology*, 241, 83-90.
- SUN, J., WANG, F., SUI, Y., SHE, Z., ZHAI, W., WANG, C. & DENG, Y. 2012. Effect of particle size on solubility, dissolution rate, and oral bioavailability: evaluation using coenzyme Q₁₀ as naked nanocrystals. *International journal of nanomedicine*, 7, 5733-5744.
- SWIERCZEWSKA, M., HAN, H. S., KIM, K., PARK, J. H. & LEE, S. 2016. Polysaccharide-based nanoparticles for theranostic nanomedicine. *Adv Drug Deliv Rev*, 99, 70-84.
- TAN, C. P. & NAKAJIMA, M. 2005. β -Carotene nanodispersions: preparation, characterization and stability evaluation. *Food Chemistry*, 92, 661-671.
- TAUPITZ, T., DRESSMAN, J. B., BUCHANAN, C. M. & KLEIN, S. 2013. Cyclodextrin-water soluble polymer ternary complexes enhance the solubility and dissolution behaviour of poorly soluble drugs. Case example: itraconazole. *Eur J Pharm Biopharm*, 83, 378-87.
- TEPELLI, F. 2018. Perspectives on the use of supercritical particle formation technologies for food ingredients. *The Journal of Supercritical Fluids*, 134, 244-251.
- TERMENTZI, A. & KOKKALOU, E. 2008. LC-DAD-MS (ESI+) analysis and antioxidant capacity of crocus sativus petal extracts. *Planta Med*, 74, 573-81.
- THORBALL, N. 1981. FITC-dextran tracers in microcirculatory and permeability studies using combined fluorescence stereo microscopy, fluorescence light microscopy and electron microscopy. *Histochemistry*, 71, 209-33.
- TRUSHEVA, B., TRUNKOVA, D. & BANKOVA, V. 2007. Different extraction methods of biologically active components from propolis: a preliminary study. *Chemistry Central Journal*, 1, 13-13.
- TUBEROSO, C. I., ROSA, A., MONTORO, P., FENU, M. A. & PIZZA, C. 2016. Antioxidant activity, cytotoxic activity and metabolic profiling of juices obtained from saffron (*Crocus sativus* L.) floral by-products. *Food Chem*, 199, 18-27.
- VANDANA, K. R., PRASANNA RAJU, Y., HARINI CHOWDARY, V., SUSHMA, M. & VIJAY KUMAR, N. 2014. An overview on in situ micronization technique – An emerging novel concept in advanced drug delivery. *Saudi Pharmaceutical Journal*, 22, 283-289.
- VASCONCELOS, T., SARMENTO, B. & COSTA, P. 2007. Solid dispersions as strategy to improve oral bioavailability of poor water soluble drugs. *Drug Discovery Today*, 12, 1068-1075.
- VEHRING, R. 2008. Pharmaceutical particle engineering via spray drying. *Pharmaceutical research*, 25, 999-1022.

References

- VICENTE, J., PINTO, J., MENEZES, J. & GASPAR, F. 2013. Fundamental analysis of particle formation in spray drying. *Powder Technology*, 247, 1-7.
- VIPPAGUNTA, S. R., MAUL, K. A., TALLAVAJHALA, S. & GRANT, D. J. W. 2002. Solid-state characterization of nifedipine solid dispersions. *International Journal of Pharmaceutics*, 236, 111-123.
- WAGH, V. D. 2013. Propolis: A Wonder Bees Product and Its Pharmacological Potentials. *Advances in Pharmacological Sciences*, 2013, 11.
- WANG, B., ZHANG, W., ZHANG, W., MUJUMDAR, A. S. & HUANG, L. 2005. Progress in Drying Technology for Nanomaterials. *Drying Technology*, 23, 7-32.
- WANG, Q., GUAN, Y.-X., YAO, S.-J. & ZHU, Z.-Q. 2010. Microparticle formation of sodium cellulose sulfate using supercritical fluid assisted atomization introduced by hydrodynamic cavitation mixer. *Chemical Engineering Journal*, 159, 220-229.
- WANG, Q., GUAN, Y.-X., YAO, S.-J. & ZHU, Z.-Q. 2011. Controllable preparation and formation mechanism of BSA microparticles using supercritical assisted atomization with an enhanced mixer. *The Journal of Supercritical Fluids*, 56, 97-104.
- WANG, Y., LU, Z., LV, F. & BIE, X. 2009. Study on microencapsulation of curcumin pigments by spray drying. *European Food Research and Technology*, 229, 391-396.
- WASIAK, I., KULIKOWSKA, A., JANCZEWSKA, M., MICHALAK, M., CYMERMAN, I. A., NAGALSKI, A., KALLINGER, P., SZYMANSKI, W. W. & CIACH, T. 2016. Dextran Nanoparticle Synthesis and Properties. *PLOS ONE*, 11, e0146237.
- WEERAPOL, Y., LIMMATVAPIRAT, S., NUNTHANID, J., KONTHONG, S., SUTTIRUENGWONG, S. & SRIAMORNSAK, P. 2017. Development and characterization of nifedipine-amino methacrylate copolymer solid dispersion powders with various adsorbents. *Asian Journal of Pharmaceutical Sciences*, 12, 335-343.
- WILKEN, R., VEENA, M. S., WANG, M. B. & SRIVATSAN, E. S. 2011. Curcumin: A review of anti-cancer properties and therapeutic activity in head and neck squamous cell carcinoma. *Mol Cancer*, 10, 12.
- WOJCIK, M., BURZYNSKA-PEDZIWIATR, I. & WOZNIAK, L. A. 2010. A review of natural and synthetic antioxidants important for health and longevity. *Curr Med Chem*, 17, 3262-88.
- WU, H.-T., HUANG, S.-C., YANG, C.-P. & CHIEN, L.-J. 2015. Precipitation parameters and the cytotoxicity of chitosan hydrochloride microparticles production by supercritical assisted atomization. *The Journal of Supercritical Fluids*, 102, 123-132.

- WU, H.-T. & YANG, M.-W. 2011. Precipitation kinetics of PMMA sub-micrometric particles with a supercritical assisted-atomization process. *The Journal of Supercritical Fluids*, 59, 98-107.
- WU, H.-T., YANG, M.-W. & HUANG, S.-C. 2014. Sub-micrometric polymer particles formation by a supercritical assisted-atomization process. *Journal of the Taiwan Institute of Chemical Engineers*, 45, 1992-2001.
- WU, J.-J., SHEN, C.-T., JONG, T.-T., YOUNG, C.-C., YANG, H.-L., HSU, S.-L., CHANG, C.-M. J. & SHIEH, C.-J. 2009. Supercritical carbon dioxide anti-solvent process for purification of micronized propolis particulates and associated anti-cancer activity. *Separation and Purification Technology*, 70, 190-198.
- XIE, M.-B., LI, Y., ZHAO, Z., CHEN, A.-Z., LI, J.-S., HU, J.-Y., LI, G. & LI, Z. 2015. Solubility enhancement of curcumin via supercritical CO₂ based silk fibroin carrier. *The Journal of Supercritical Fluids*, 103, 1-9.
- YANG, S.-J., WU, J.-J., WANG, Y.-C., HUANG, C.-F., WU, T.-M., SHIEH, C.-J. & CHANG, C.-M. J. 2014. Encapsulation of propolis flavonoids in a water soluble polymer using pressurized carbon dioxide anti-solvent crystallization. *The Journal of Supercritical Fluids*, 94, 138-146.
- YI, J., LAM, T. I., YOKOYAMA, W., CHENG, L. W. & ZHONG, F. 2015. Beta-carotene encapsulated in food protein nanoparticles reduces peroxy radical oxidation in Caco-2 cells. *Food Hydrocolloids*, 43, 31-40.
- YI, X., ZUO, J., TAN, C., XIAN, S., LUO, C., CHEN, S., YU, L. & LUO, Y. 2016. KAEMPFEROL, A FLAVONOID COMPOUND FROM GYNURA MEDICA INDUCED APOPTOSIS AND GROWTH INHIBITION IN MCF-7 BREAST CANCER CELL. *African Journal of Traditional, Complementary, and Alternative Medicines*, 13, 210-215.
- ZABIHI, F., XIN, N., LI, S., JIA, J., CHENG, T. & ZHAO, Y. 2014. Polymeric coating of fluidizing nano-curcumin via anti-solvent supercritical method for sustained release. *The Journal of Supercritical Fluids*, 89, 99-105.
- ZAJC, N., OBREZA, A., BELE, M. & SRČIČ, S. 2005. Physical properties and dissolution behaviour of nifedipine/mannitol solid dispersions prepared by hot melt method. *International Journal of Pharmaceutics*, 291, 51-58.
- ZEKA, K., RUPARELIA, K. C., CONTINENZA, M. A., STAGOS, D., VEGLIO, F. & ARROO, R. R. J. 2015. Petals of *Crocus sativus* L. as a potential source of the antioxidants crocin and kaempferol. *Fitoterapia*, 107, 128-134.
- ZHENG, W. & WANG, S. Y. 2001. Antioxidant activity and phenolic compounds in selected herbs. *J Agric Food Chem*, 49, 5165-70.

List of Symbols

AC	Acetone
AcEt	Ethyl acetate
BC	β -carotene
C	Concentration
CO ₂	Carbon dioxide
CUR	Curcumin
DEX	Dextran
DLS	Dynamic laser scattering
DMSO	Dimethyl sulfoxide
DPPH	2,2-Diphenyl-1-picrylhydrazyl
EEP	Ethanolic extract of propolis
EtOH	Ethanol
FITC	Fluorescein isothiocyanate
FTIR	Fourier Transform infrared
GLR	Gas to liquid ratio
HP β CD	Hydroxypropyl- β -cyclodextrin
HPLC	High Performance Liquid Chromatography
LUT	Luteolin
MetOH	Methanol
M _w	Molecular weight
N ₂	Nitrogen
NIF	Nifedipine
NMP	1-Methyl-2-pyrrolidinone
P	Pressure
P _m	Pressure mixer
PEA	Palmitoylethanolamide
PGSS	Precipitation from Gas Saturated Solution
PSD	Particle Size Distribution
PVP	Polyvinylpyrrolidone
RESS	Rapid Expansion of Supercritical Solutions
SA	Scavenging Activity
SAA	Supercritical Assisted Atomization
SAILA	Supercritical Assisted Injection in a Liquid Antisolvent
SAS	Supercritical Antisolvent
SC-CO ₂	Supercritical carbon dioxide
SCF	Supercritical fluid
SEDS	Solution Enhanced Dispersion by Supercritical Fluid
THF	Tetrahydrofuran
T _p	Temperature precipitator
T _s	Temperature saturator

